PEDECIBA

BIOLOGIA CELULAR Y MOLECULAR

Tesis de Doctorado

La célula de Schwann como fuente alternativa de los ARNs axonales.

Mag. Lucía Canclini

Departamento de Proteínas y Acidos Nucleicos

Director: Dr. José Roberto Sotelo

Co-director: Dra. Alejandra Kun

Tribunal: Dr. Angel Caputti

Dra. Beatriz Garat

Dra. Silvia Chiflet

El formato que hemos elegido para presentar los resultados de la presente tesis está basado en las comunicaciones científicas generadas en el transcurso de la misma. Presentaremos los trabajos publicados agrupados por unidades temáticas en tres capítulos. Los artículos presentados serán precedidos de un breve resumen de los hallazgos más importantes comunicados en cada uno y serán discutidos en la discusión general. Los trabajos publicados que se enumerarán a continuación serán referidos en el texto por el numeral romano correspondiente (trabajos I a IX).

Trabajo I: Canclini, L., Kun, A., Calliari, A., Mercer, J. A., Sotelo, J. R., Sotelo-Silveira, J. R. The axonal transcriptome: RNA localization and function. Current Chemical Biology, 5, 99-107, 2011. Revisión bibliográfica.

Trabajo II: Sotelo J. R.; Canclini L.; Kun A.; Sotelo-Silveira, J.R.; Xu, L.; Wallrabe, H.; Calliari, A.; Rosso G.; Cal K.; Mercer, J.A. Myosin-Va-Dependent Cell-To-Cell Transfer of RNA from Schwann Cells to Axons. PLoS ONE, 8 (4), e61905, 2013.

Trabajo III: Canclini L.; Wallrabe, H.; Di Paolo, P.; Kun A.; Calliari, A.; Sotelo-Silveira, J.R; Sotelo J. R. Association of Myosin Va and Schwann Cells-derived RNA in mammal myelinated axons, analyzed by immunocytochemistry and confocal FRET microscopy. Methods, 66, 153-161, 2014.

Trabajo IV: Canclini, L., Di Paolo, A., Farias J., Wallrabe, H., Kun, A., Sotelo-Silveira, J. R., Sotelo, J. R. Microtubule-based transport of Schwann cell-derived axonal RNAs. Manuscrito enviado.

Trabajo V: Calliari, A., Farias, J., Puppo, A., Canclini, L., Mercer, J. A., Munroe, D., Sotelo, J. R., Sotelo-Silveira, J. R. Myosin Va associates with mRNA in Ribonucleoprotein Particles present in myelinated Peripheral Axons and in the Central Nervous System. Developmental Biology, 74 (3), 382-396, 2014.

Trabajo VI: Kun A.; Canclini L.; Rosso G.; Bresque, M.; Romeo C.; Hanusz, A.; Cal K.; Calliari, A.; Sotelo-Silveira, J.R.; Sotelo J. R. F-actin distribution at nodes of Ranvier and Schmidt-Lanterman incisures in mammalian sciatic nerves. Cytoskeleton, 69, 486-495, 2012.

Trabajo VII: Sotelo, J. R., Canclini, L., Kun, A., Sotelo-Silveira, J. R., Calliari, A., Cal, K., Bresque, M., Di Paolo, A., Farias, J., Mercer, J. A. Glia to axon RNA transfer. Developmental Biology, 74 (3), 292-302, 2014. Revisión bibliográfica.

Trabajo VIII: Kun A., Rosso G., Canclini L., Bresque, M., Romeo C., Cal K., Calliari, A., Hanuzs, A., Sotelo-Silveira, J.R., Sotelo J. R. The Schwann cell-axon link in normal condition or neuro-degenerative diseases: an immunocytochemical approach. Applications of immunocytochesmistry, 249-266, InTech. 2012. Capítulo de libro.

Trabajo IX: Sotelo-Silveira, J.R.; Calliari, A.; Kun A., Elizondo V., Canclini L., Sotelo J. R. Localization of mRNA in vertebrate axonal compartments by *in situ* hybridization. RNA detection and visualization, 714, 125-138, Humana Press. 2011. Capítulo de libro.

INDICE

1. RESUMEN

En las células eucariotas, gran parte de los ARNm se localizan y traducen en dominios celulares específicos, donde las proteínas así sintetizadas cumplirán su función. Este concepto ha sido comprobado en los diferentes territorios neuronales, y en particular en el dominio axonal. En contraposición con las bases del dogma clásico, que sostenía que los axones carecían de síntesis local de proteínas, en la actualidad se sabe que los ARNm son transportados hacia su lugar de síntesis, por proteínas motoras específicas. Durante su transporte, los ARNm forman parte de ribonucleoproteínas (integradas por motores moleculares y otras proteínas, muchas de ellas aún desconocidas). El transporte de los ARNm empaquetados en forma de ribonucleoproteínas, no sólo aumenta su vida media, sino que además inhibe su traducción. Estos ARNm presentes en los axones del Sistema Nervioso Periférico pueden provenir del soma neuronal, pero también pueden ser provistos por una fuente alternativa: la célula de Schwann. En experimentos de inmunomicroscopía electrónica se han observado estructuras vesiculares que contienen ribosomas, protruyendo desde la célula de Schwann hacia el axón, sugiriendo un evento de exo-endocitosis. Éste puede ser uno de los mecanismos por medio de los cuales los ribosomas y los ARNm son transferidos al axón. El objetivo de la presente tesis fue demostrar que la célula de Schwann representa una fuente local, complementaria y alternativa de ARNs para las necesidades axonales, en condiciones normales y/o en respuesta a una lesión (regeneración). Para ello, utilizamos bromouridina para marcar los ARN neosintetizados (ARN-BrU) en las células de Schwann de nervios ciáticos desomatizados (normales y en regeneración). Encontramos, mediante inmunomicroscopía confocal, que los ARN-BrU se observan en el citoplasma de la célula de Schwann y también en los axones de las fibras mielínicas. Estos ARN-BrU proceden de transcripción nuclear, dado que al inhibir la ARN polimerasa II (enzima que transcribe los ARNm nucleares) observamos que su cantidad disminuye aproximadamente a la mitad. Además, observamos que la señal de los ARN-BrU co-localiza escasamente con las mitocondrias axonales. Por tanto, dado que los núcleos neuronales no están

presentes durante la marcación con BrU (desomatización), los ARN-BrU que encontramos en los axones sólo pueden provenir de la célula de Schwann, por transferencia célula-célula. Hemos encontrado que la transferencia célula de Schwann-axón de los ARN-BrU ocurre principalmente a través de los nodos de Ranvier y las incisuras de Schmidt-Lantermann, de forma dependiente del citoesqueleto de actina y su motor molecular asociado, la miosina Va. Mientras que el citoesqueleto de actina está involucrado en la transferencia de ARNs en el límite entre la célula de Schwann y el axón, hemos observado que los microtúbulos están implicados en el transporte de los ARNs desde el núcleo de la célula de Schwann hacia el mencionado límite. Dentro del dominio axonal, pudimos establecer que los microtúbulos también están implicados en el transporte de los ARN-BrU, por medio del motor molecular KIF5B. Culminando nuestro trabajo, determinamos la identidad de los ARN neosintetizados en la célula de Schwann, pudiendo establecer que entre ellos se encuentran varios ARNm que codifican proteínas de expresión específica neuronal.

2. INTRODUCCIÓN

2.1. Sistema Nervioso Periférico: glías y axones

El sistema nervioso periférico (SNP) comprende las estructuras localizadas fuera del cerebro y la médula espinal, incluyendo los nervios periféricos y sus ganglios asociados. Los nervios periféricos están compuestos por conjuntos de fibras nerviosas rodeadas por tejido conjuntivo. Las fibras se pueden clasificar en motoras o sensitivas, en mielínicas o amielínicas o también según su diámetro. Cada nervio puede contener varias clases de fibras, organizadas en haces de tamaños variables y separadas entre sí por una red de tejido conjuntivo que forma el epineuro, perineuro, y endoneuro. En particular, cada fibra mielínica del SNP está formada por la asociación de múltiples células de Schwann que rodean un único axón a lo largo de su recorrido. No existe ningún sector del axón que no esté cubierto por las células de Schwann. La región entre dos células de Schwann contiguas se conoce como nodo de Ranvier (figura 1.1). El nodo de Ranvier está cubierto por extensiones del citoplasma de la célula de Schwann, conocidas como *microvilli* (Poliak and Peles, 2003). En esa zona, las *microvilli* de dos células de Schwann adyacentes se intercalan entre sí en una relación íntima y cubren completamente el axón subyacente. La región entre dos nodos de Ranvier adyacentes se conoce como internodo. En el SNP, las fibras mielínicas poseen una direccionalidad longitudinal dada por la interposición de un nodo de Ranvier, un internodo y el siguiente nodo de Ranvier (Peles and Salzer, 2000; Poliak and Peles, 2003; Salzer, 2003; Sherman and Brophy, 2005; Salzer *et al.*, 2008). Esta organización de la fibra mielínica es crítica para la conducción rápida y eficiente del impulso nervioso (Salzer, 1997). Los nodos están enriquecidos en canales de sodio voltaje dependiente, con una densidad 25 veces mayor que el internodo, lo que explica que estos sean los sitios donde se regenera el potencial de acción (Salzer *et al.*, 2008; Buttermore *et al.*, 2013). El internodo, la región más extensa de la fibra mielínica, comprende la zona del axón cubierta de mielina.

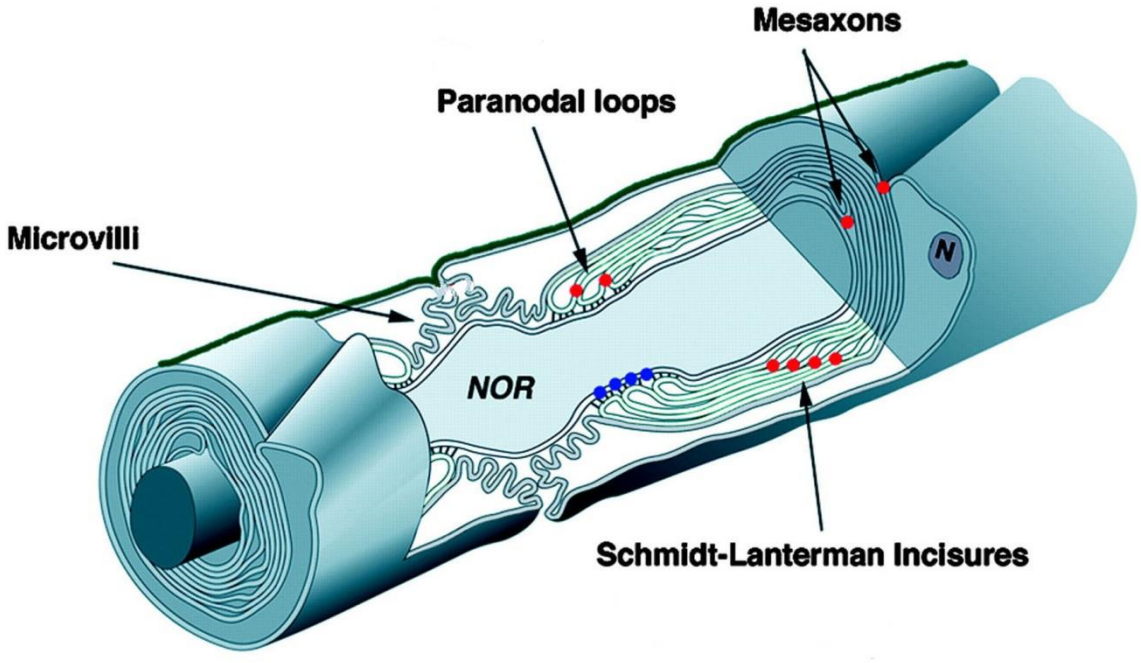

Figura 1.1. Representación esquemática de una fibra mielínica del Sistema Nervioso Periférico. NOR:*node of Ranvier* (nodo de Ranvier), N: núcleo de la célula de Schwann. Los puntos azules indican las uniones especializadas entre la célula de Schwann y el axón en el paranodo. *Modificado de Poliak et. al., 2002.*

El internodo puede ser dividido en dos regiones, la mielina compacta y la mielina laxa (Scherer and Arroyo, 2002). La mielina compacta, formada por capas superpuestas de membrana plasmática de la célula de Schwann, carente de citoplasma, es la forma de mielina mayoritaria del internodo. La mielina laxa, puede encontrarse en dos regiones específicas: los paranodos y las incisuras de Schmidt-Lanterman (Li, 2008). Los paranodos se encuentran inmediatamente adyacentes hacia los lados de cada nodo. Están constituidos por digitaciones de cada una de las células de Schwann que constituyen el nodo, las cuales físicamente invaginan el axolema (Salzer, 2003; Thaxton and Bhat, 2009; Buttermore *et al.*, 2013). Son ricos en uniones especializadas que promueven la adhesión entre la glia y el axón y son responsables de proveer una barrera que mantiene la composición molecular de las membranas axonales del nodo y el internodo (Ching *et al.*; Rios *et al.*, 2003; Rosenbluth *et al.*, 2003, 2013; Salzer *et al.*, 2008). Las incisuras de Schmidt-Lanterman son conductos citoplasmáticos en forma de espiral que conectan el citoplasma externo de la célula de Schwann (abaxonal) con aquel que se encuentra más

próximo al axón. Están localizadas a intervalos a lo largo del internodo y su número por internodo es específico de cada especie (Poliak and Peles, 2003; Li, 2008). Se ha propuesto que el rol de las incisuras de Schmidt-Lantermann es proveer un camino a través del cual los materiales (proteínas, ARNs, etc.) pueden llegar hacia la mielina y las porciones citoplasmáticas más internas de la célula de Schwann (Ghabriel and Allt, 1979, 1980, 1981; Li, 2008). Además de la polaridad longitudinal, las fibras mielínicas del SNP poseen una polaridad radial (Poliak and Peles, 2003; Sherman and Brophy, 2005; Li, 2008), debido a la presencia de dos superficies de membrana muy diferentes en la célula de Schwann: una membrana interna en contacto con el axón (adaxonal), y una superficie externa en contacto con la lámina basal (abaxonal). Tanto la región abaxonal como adaxonal son ricas en citoplasma, al contrario de lo observado en la región entre ambas superficies (la mielina compacta) (Li, 2008).

La interacción entre las células de Schwann y los axones en el SNP no sólo es esencial para la formación y función de la fibra nerviosa periférica, sino que es fundamental durante la regeneración axonal. Inmediatamente luego de una lesión, en el SNP los cabos proximal y distal generados se retraen y las membranas dañadas colapsan. De aquí en adelante los cabos proximal y distal sufrirán procesos completamente diferentes. El cabo distal sufrirá un proceso conocido como degeneración Walleriana, que incluye la degeneración axonal y la de-diferenciación de las células de Schwann mielinizantes quienes comienzan a proliferar (Salzer and Bunge, 1980; Bishop, 1982). Cuando sea posible, las células de Schwann en proliferación formarán un canal, la banda de Bungner, que guiará el axón en regeneración hacia su blanco (Bunge, 1994; Son and Thompson, 1995a; b). En el cabo proximal emergerán varias ramificaciones del axón, principalmente en el primer nodo de Ranvier anterior a la lesión (Friede and Bischhausen, 1980). Algunas de estas ramificaciones se retraerán, pero una de ellas puede seguir creciendo a través de la banda de Bungner, hasta alcanzar su blanco (Bishop, 1982). El proceso de regeneración axonal se atribuye actualmente a: 1) cambios en la expresión de genes de las neuronas lesionadas, que dan lugar al desarrollo de un fenotipo regenerante de las mismas; y 2) modificaciones en las células de Schwann del cabo distal, las cuales generarán los caminos por los que crecerán los axones y a factores neurotróficos generados por las mismas (Terenghi, 1999; Scheib and Höke,

2013). Sin embargo, el rol de las células de Schwann del cabo proximal en el proceso de regeneración axonal ha sido hasta ahora poco explorado.

2.2. Síntesis local de proteínas en el axón

Mientras que las dimensiones de la mayoría de las células está en el rango de las diez micras, las células nerviosas, en particular las del SNP, tienen axones que pueden medir un metro o más en humanos y otros grandes vertebrados. La anatomía de las neuronas determina, como consecuencia, una logística específica respecto al abastecimiento de proteínas al axón. Este abastecimiento no sólo es necesario para el mantenimiento y viabilidad de la masa axoplásmica en el estado estacionario, sino también para satisfacer los requerimientos necesarios en procesos tales como la regeneración (Alvarez *et al.*, 2000). ¿Cómo se suministran las moléculas requeridas para la función del axón? Si bien muchas proteínas axonales provienen del soma neuronal (Black and Lasek, 1979, 1980; Brown, 2003), muchas son sintetizadas localmente en el propio axón (Campenot and Eng; Benech *et al.*, 1982; Sotelo *et al.*, 1992; Koenig and Giuditta, 1999; Eng *et al.*, 1999; Alvarez *et al.*, 2000; Sotelo-Silveira *et al.*, 2000, 2006; Alvarez, 2001; Brittis *et al.*, 2002; Calliari *et al.*, 2002; Giuditta *et al.*, 2002, 2008; Piper and Holt, 2004; Kaplan *et al.*, 2009; Natera-Naranjo *et al.*, 2012; Kar *et al.*, 2013; Crispino *et al.*, 2014). Los componentes principales de la maquinaria traduccional y de la síntesis activa de proteínas (ARNm, ARNr, ARNt, ribosomas, proteínas involucradas en la traducción y factores reguladores de la misma) han sido reportados tanto en axones de invertebrados (Black and Lasek, 1977; Giuditta *et al.*, 1977, 1980, 1991, 2008; Rapallino *et al.*, 1988; Kaplan *et al.*, 1992; Crispino *et al.*, 1993; Gioio *et al.*, 1994; Chun *et al.*, 1997; Sotelo *et al.*, 1999), como de vertebrados (Koenig, 1979; Weiner *et al.*, 1996; Koenig and Martin, 1996; Sotelo-Silveira *et al.*, 2000, 2006, 2008; Kun *et al.*, 2007; Giuditta *et al.*, 2008; Taylor *et al.*, 2009; Zivraj *et al.*, 2010; Gumy *et al.*, 2011; Minis *et al.*, 2014; Sasaki *et al.*, 2014).

Si bien se conoce la existencia de síntesis local de proteínas en el axón, no se ha determinado aún si esta ocurre en regiones específicas del dominio axonal, o bien ocurre todo a lo largo del axoplasma. En 1996, Koenig y Martin describieron por primera vez la presencia de dominios ribosomales

periaxoplásmicos o “Placas Periaxoplásmica Ribosomales” (PPARs) en axones de fibras de Mauthner de pez dorado. Estos dominios son visibles en la zona cortical axonal luego de la tinción con YOYO-1 (colorante de alta afinidad por el ARN), y desaparecen por medio de la digestión con ARNasa. Se evidenció también que las PPARs son ricas en poli-ribosomas y se encuentran en una íntima asociación con la actina-F cortical (Koenig and Martin, 1996). Posteriormente, se describieron PPARs en axones motores y sensoriales de ratas y conejos (Koenig *et al.*, 2000). Los hallazgos descritos señalaron a las PPARs como posible sitios donde podría ocurrir la síntesis local de proteínas (Koenig *et al.*, 2000; Sotelo-Silveira *et al.*, 2004, 2008).

2.3. ARNs en el axón

Todos los tipos de ARNs citosólicos han sido descritos en el dominio axonal, incluyendo ARNs ribosomales, ARNs mensajeros y ARNs pequeños (Black and Lasek, 1977; Sotelo-Silveira *et al.*, 2000, 2008; Willis *et al.*, 2007, 2005; Kaplan *et al.*, 2009; Taylor *et al.*, 2009; Zivraj *et al.*, 2010; Natera-Naranjo *et al.*, 2010; Gumy *et al.*, 2011; Minis *et al.*, 2014; Sasaki *et al.*, 2014). En particular, con respecto a los ARNm, en los últimos años, principalmente durante el transcurso de la presente tesis de Doctorado, varios grupos han publicado trabajos donde se estudió el transcriptoma axonal a gran escala (Taylor *et al.*, 2009; Zivraj *et al.*, 2010; Gumy *et al.*, 2011; Minis *et al.*, 2014). Estos estudios fueron realizados en axones y conos de crecimiento derivados de diversas neuronas utilizando microarreglos (Taylor *et al.*, 2009; Zivraj *et al.*, 2010; Gumy *et al.*, 2011) o secuenciación masiva (Minis *et al.*, 2014). Entre los grupos más representados se encuentran los ARNm que codifican para proteínas ribosomales, y otras proteínas implicadas en la traducción, así como de los componentes del citoesqueleto, proteínas implicadas en el transporte intracelular y proteínas mitocondriales codificadas por el genoma nuclear.

Los resultados sobre el transcriptoma axonal reseñados fueron obtenidos a partir de neuronas en cultivo. Esto implica que se analizaron transcriptomas de axones que no pueden crecer hasta sus dimensiones reales *in vivo*. Además, en estos cultivos, las neuronas se encuentran aisladas, es decir, los axones están desprovistos de glías. Todas estas condiciones, si bien

útiles en una primera aproximación, no necesariamente reflejan la realidad, dejando abierta la pregunta de cuál es el transcriptoma de los axones mielínicos maduros, donde se mantiene la relación axo-glial. Para adaptarse a esta situación, nuestro grupo realizó la micro-disección de axones *in toto*, libres de mielina (Koenig, 1979) y la secuenciación masiva de los ARNm obtenidos de dicha muestra (resultados obtenidos en la Tesis de Maestría de Joaquina Farías). Estos experimentos reconocieron unos 600 ARNm diferentes en axones mielínicos maduros. Al comparar los resultados de Farías con aquellos de otros autores (Zivraj *et al.*, 2010; Gumy *et al.*, 2011; Minis *et al.*, 2014), se observan muchas coincidencias, así como también algunas diferencias con respecto a la identidad de los ARNm presentes en el axón. El 60% de los ARNm identificados por Farías fueron descritos en al menos uno de los trabajos realizados con axones en cultivo. Por el contrario, el 40% restante sólo fueron identificados en nuestras condiciones. Por otra parte, existen numerosos ARNm descritos por el grupo que también utilizó secuenciación masiva (Minis *et al.*, 2014) que no fueron identificados en axones maduros. Estas diferencias sugieren que el transcriptoma axonal es distinto según el contexto biológico y funcional del axón estudiado.

2.4. Origen de los ARNs axonales

Los ARN hallados en el compartimento axonal, presentados anteriormente (Taylor *et al.*, 2009; Zivraj *et al.*, 2010; Gumy *et al.*, 2011; Minis *et al.*, 2014), son sintetizados en el soma neuronal, dado que estos transcriptomas fueron determinados a partir de cultivos de neuronas disociadas, donde no hay ningún otro tipo celular presente y los axones poseen sólo unas cien micras de longitud, en promedio. Sin embargo, el soma neuronal puede no ser el único origen de los ARNs descritos en el axón. La transferencia de ARNs desde la glía al axón fue propuesta por primera vez por Singer y Green en 1968, luego de una inyección intraperitoneal de uridina tritiada, detectando los ARNs neosintetizados utilizando autoradiografía del cabo distal (separado por lo tanto de los somas neuronales de origen) de nervios ciáticos seccionados de salamandra (Singer and Green, 1968).

La primer evidencia de síntesis local de ARN y su transferencia se obtuvo mediante marcado metabólico con uridina radioactiva en el axón gigante de calamar (Fischer *et al.*, 1969; Cutillo *et al.*, 1983; Giuditta *et al.*, 2008). En estos experimentos, las fibras gigantes, en ausencia de soma, pero conservando su capa de células gliales, e incubadas con precursores de ARN fueron perfundidas, recuperándose ARN radiomarcado del axoplasma. Los ARNs encontrados en el dominio axonal fueron posteriormente identificados como ARNr, ARNt y ARNm (Rapallino *et al.*, 1988). En este modelo, se demostró que la transferencia glio-axonal de ARNs es modulada por una comunicación entre ambas células, que involucra neurotransmisores (Giuditta *et al.*, 2002; Eyman *et al.*, 2007).

En vertebrados (ratas), la síntesis local de ARN fue demostrada *in vivo*, mediante autoradiografía seriada cuantitativa de nervios ciáticos lesionados (Benech *et al.*, 1982). Por otra parte, el ARNm que codifica para la subunidad liviana de los neurofilamentos (NF-L), un ARN específico neuronal ha sido detectado en el axón y además en el citoplasma de la célula de Schwann mielinizante en nervios ciáticos de rata (Sotelo-Silveira *et al.*, 2000). Estos experimentos demostraron también que los ARNm de las tres subunidades de los neurofilamentos (NF-L, NF-M y NF-H) están presentes en nervios ciáticos normales y seccionados. Por otra parte, sus niveles se incrementan luego de una lesión. La expresión de otro ARNm "neuronal" (β-tubulina clase II) también se ha observado en células de Schwann de nervios en desarrollo o lesionados (Roberson *et al.*, 1992). En conjunto, esta información sugiere que en vertebrados, la célula de Schwann puede ser una fuente local de ARNm axonales.

También se ha demostrado la transferencia de ribosomas desde la célula de Schwann al axón. Las evidencias experimentales para esta transferencia fueron reunidas utilizando diferentes aproximaciones experimentales, tales como microscopía electrónica (Li *et al.*, 2005a; b), inmunomicroscopía electrónica (utilizando un suero policlonal generado contra ribosomas) (Kun *et al.*, 2007) y proteínas ribosomales marcadas con GFP (Court *et al.*, 2008, 2011).

2.5. Mecanismos de transporte de los ARNs

La primera evidencia de que los ARNs no se distribuyen al azar dentro de una célula sino que se localizan en regiones específicas de la misma fue aportada por Lawrence y Singer, quienes demostraron que el ARNm de β-actina se localiza específicamente en el frente de avance en fibroblastos (Lawrence and Singer, 1986). Esta localización y la traducción local del ARNm de β-actina (Rodriguez *et al.*, 2006) es fundamental para el movimiento de la célula (Kislauskis *et al.*, 1997). De aquí se desprende naturalmente el razonamiento: si la localización específica y traducción local de un ARNm es fundamental para la función de una célula de dimensiones regulares, como lo es un fibroblasto, ¿no lo será más aún en una célula de grandes proporciones, como lo es una neurona? (Sotelo-Silveira *et al.*, 2006, 2008).

La localización de los ARNm en regiones específicas y su traducción local requieren de una regulación sofisticada, la cual se logra mediante múltiples mecanismos. Secuencias específicas, llamadas comúnmente elementos en *cis* (o también conocidos como *zipcodes*), incluidas en la propia secuencia de los ARNm se localizan en las regiones no traducidas 5’ o 3’. Las mismas interactúan con una variedad de factores proteicos que actúan en *trans* (TAFs, del inglés *trans-acting factors*) (Bassell *et al.*, 1999; Buchan, 2014). Estos factores, pueden ser clasificados de acuerdo a su función en proteínas de unión a los elementos en *cis* (variando el número de las mismas para cada ARNm particular) que se unen a los motores moleculares que trasladarán al mensajero a la región celular donde debe ser traducido (Bassell *et al.*, 1999). Los ARNm se asocian con estas proteínas ensamblándose en partículas de apariencia granular, conocidas como partículas ribonucleoproteicas (RNPs, del inglés *ribonucleoprotein particles*). El transporte de las RNPs dentro de una célula y en particular dentro de las neuronas es dependiente de los microtúbulos y los filamentos de actina (Gumy *et al.*, 2014). Mientras que el transporte de largo alcance involucraría los microtúbulos, los filamentos de actina parecen estar vinculados al transporte local y/o el anclaje de macromoléculas (Provance *et al.*, 2008; Holt and Bullock, 2009; Hirokawa *et al.*, 2010; Gumy *et al.*, 2014).

Ciertos motores moleculares han sido descritos como componentes de RNPs o se han vinculado al transporte de ARNm específicos, incluyendo miembros de la familia de las kinesinas (Ohashi *et al.*, 2002; Kanai *et al.*, 2004; Sotelo-Silveira *et al.*, 2004; Dictenberg *et al.*, 2008; Lyons *et al.*, 2009), de la familia de las dineínas (Amrute-Nayak and Bullock, 2012) y de la familia de las miosinas (Ohashi *et al.*, 2002; Sotelo-Silveira *et al.*, 2004; Yoshimura *et al.*, 2006). Sin embargo, aún se conoce muy poco acerca de la identidad de los motores moleculares que dirigen el transporte de los ARNm en los axones (Donnelly *et al.*, 2010).

La presente tesis de Doctorado comenzó con la publicación de un trabajo de revisión (trabajo I) donde se realizó un examen del estado del arte al momento, con respecto al tema que abordamos. En el mismo, justificamos cómo la presencia axonal de ARNm y su traducción local se demostró en varios modelos experimentales, diferentes tipos neuronales y bajo distintas condiciones fisiológicas. Esto implica que la traducción local de ARNm presentes en el axón sería un proceso que ocurre normalmente. Sin embargo, la mayoría de los experimentos fueron realizados en neuronas disociadas *in vitro*, lo cual ha sido usado como modelo de un axón diferenciado, pero en realidad es muy diferente al compartimiento original en cuanto a su organización y tamaño. Más aún, es importante hacer énfasis en las diferencias entre un modelo *in vitro* y uno *in vivo*, sobre todo teniendo en cuenta las interacciones que se establecen *in vivo* entre el axón y la célula de Schwann que lo envaina. El concepto actual de síntesis proteica local, y la autonomía axonal con respecto al soma que se desprende del mismo, implica que las regiones periféricas neuronales son capaces de responder a cambios locales de una manera más rápida y eficiente que si sólo dependieran del soma (normalmente ubicado a distancias magno-celulares de los extremos axonales). En el mismo sentido, la existencia de una fuente alternativa local de ARN que fueran transcritos en la glia y transferidos posteriormente hacia el axón, pondría nuevamente en evidencia la compleja relación entre ambas células y su modulación en diferentes condiciones como el desarrollo, el crecimiento dirigido, el mantenimiento, la regeneración y las patologías originadas cuando se alteran los mecanismos normales.

2.6. TRABAJO I

Canclini, L., Kun, A., Calliari, A., Mercer, J. A., Sotelo, J. R., Sotelo-Silveira, J. R. The axonal transcriptome: RNA localization and function. Current Chemical Biology, 5, 99-107, 2011. Revisión bibliográfica.

The Axonal Transcriptome: RNA Localization and Function

Lucía Canclini[1], Alejandra Kun[1,2], Aldo Calliari[1,3], John A. Mercer[4], José R. Sotelo[1] and José R. Sotelo-Silveira*[,5,6].

[1]Departamento de Proteínas y Ácidos Nucleicos, Instituto de Investigaciones Biológicas Clemente Estable, Av. Italia 3318, CP 11600, Montevideo, Uruguay; [2]Sección Bioquímica, Departamento de Biología Celular y Molecular, Facultad de Ciencias, Universidad de la República, Iguá 4225, CP 11400, Montevideo, Uruguay; [3]Departamento de Biología Molecular y Celular, Facultad de Veterinaria, A. Lasplaces 1550, CP 11600, Montevideo, Uruguay; [4]McLaughlin Research Institute, 1520 23rd Street South, Great Falls, MD, 59415; [5]Departamento de Genética, Instituto de Investigaciones Biológicas Clemente Estable, Av Italia 3318, CP 11600, Montevideo, Uruguay; [6]Departamento de Biología Celular y Molecular, Facultad de Ciencias, Universidad de la República, Iguá 4225, CP 11400, Montevideo, Uruguay.

Abstract: Neurons are highly polarized cells, often with very long processes, which can comprise up to 95% of the cytoplasm. This raises the issue of transporting and turnover of proteins transport. In addition to fast axonal transport, axonal translation has been proposed to be responsible for producing at least some axonal proteins. In multiple experimental models, local synthesis of several proteins has been demonstrated in axons, growth cones, and nerve terminals. Multiple lines of evidence are consistent with the existence of axonal rRNAs, mRNAs, tRNAs, and micro RNAs and micro RNA regulatory proteins (RISC complex). Multiple signalling pathways, including mTOR, may regulate axonal translation. The origin of axonal RNAs is often attributed to transport from the neuronal soma, but evidence supporting cell-to-cell transport from Schwann cells to axons as a source of at least some axonal RNAs is emerging. This intercellular transport will be discussed in the context of normal and regenerative conditions.

Keywords: Axon, local translation, miRNAs, mRNAs, mTOR, transcriptome, UTR.

RNA IN THE AXONAL DOMAIN: BRIEF HISTORICAL OVERVIEW

The presence of RNA in axons has been thoroughly documented, in both vertebrate and invertebrate axons [1-4]. However, for many years the functionals and source of these RNAs have been controversial issues. In the first papers about the subject, some authors concluded that only tRNA [5-7] and mitochondrial RNA [8] could be found in the axonal domain and that these molecules were involved in mitochondrial protein synthesis and/or post-translational axonal modifications [8, 9]. However, more recent findings have suggested additional mechanisms.

Since the first report of RNA [10] and rRNA [11] in the axoplasm, an extensive body of evidence supporting axonal protein synthesis has been published. The presence of ribosomes inside axons was demonstrated in several publications [3, 4, 12-18], in addition to the presence of mRNA [1, 19-29]. The local synthesis of proteins in axons also was demonstrated in both vertebrate and invertebrate axons [3, 12, 15, 17, 30, 31]; considering the entire axonal volume is taken, axonal translation may be 50-fold higher than in the perikaryon [32].

*Address correspondence to this autor at the Departamento de Genética, Instituto de Investigaciones Biológicas Clemente Estable, Av Italia 3318, CP 11600, Montevideo, Uruguay Tel: 5982 4871616 ext 112;
Fax: 5982 487 5461; E-mail: sotelojos@gmail.com

1872-3136/11 $58.00+.00

The targeting of specific RNAs to specific parts of the cell, which has attracted great research interest in recent years, can control regional functional specialization in the cell [33, 34]. Even in fibroblasts, the archetype of a simple cell, RNA targeting is ubiquitous. In the best studied case, β-actin mRNA is transported and locally translated in lamellipodia, where actin subunits would be best positioned to contribute to polymerization [33]. In the case of long neurons, targeting of mRNA and its local translation should allow the utilization of proteins with relatively short half-lives.

The local synthesis of proteins in axons is likely to play important roles in axonal growth, maintenance, regeneration, learning, and memory processes [4, 17, 35-37] Extensive work has also demonstrated that local protein synthesis is involved in axonal growth cone turning [38-40]. In the following sections, we will address the identities of axonal RNAs, transport mechanisms, translational regulation, and the axonal transcriptome origin in the context of function.

STRUCTURAL BASIS OF TRANSLATION IN VERTEBRATE AXONS

The polarity, geometry, and small diameter of the axon have been obstacles to efforts to localize translational machinery. Initially, classical ultrastructural approaches misled the field to conclude that myelinated adult axons were devoid of ribosomes [41]. However, it was relatively easy to find ribosomes in chicken axons during development [42-44], rabbit embryonic spinal ganglia [45, 46], cultured rat sympathetic neurons [47], during postnatal development

sympathetic neurons [47], during postnatal development in rat [48] and in the initial segments of mature mammalian axons [49-53].

It took exhaustive observations by Zelena [54-56] to document the first evidence of ribosome-like structures in rat adult sensory myelinated axons. These studies revealed the presence of units of 4-5 axonal ribosomes, decreasing in density distally, with accumulations in regions near nodes of Ranvier, Schmidt-Lanterman clefts, and in axonal domains near Schwann-cell nuclei. Recently, serial sectioning and conventional electron microscopy confirmed the presence of ribosome-like structures in internodal regions of rat motor axons [57, 58]. Interestingly, Zelena also noted the proximity between ribosomes and transport systems like microtubules, an observation later confirmed by Bassell and coworkers [23].

The initial conclusions of a lack of ribosomes in axons also were contradicted by the pioneering work of Edward Koenig using whole-mount preparations of axoplasm stained with YOYO-1, a high-affinity nucleic acid-binding dye [13]. This approach allowed the Koenig and coworkers to survey large, continuous stretches of axoplasm by confocal microscopy, identifying structures they named periaxoplasmic ribosomal plaques (PARPs). PARPs have a high content of RNA and ribosome-like particles when analyzed by energy-filtered transmission EM (EFTEM), a technique that also was used to find ribosomes in squid giant axons [59, 60]. More important was the extension of these findings to mammalian adult myelinated axons [61]. Both studies showed the presence of translational machinery at the ultrastructural level at discrete locations along the cortex of the axon embedded in a matrix of still unknown properties [13, 61]. As it will be discussed below, further immunocytochemical approaches confirmed the presence of ribosomes and extended the results to molecular motors, mRNA and RNA-binding proteins [2]. Interestingly, Kun and coworkers showed both the presence of ribosome-containing particles in the axonal core and PARPs-like ribosome accumulations in adult myelinated axons from sciatic nerve [18] using a combination of both immunohistochemical and ultrastructural approaches (Fig. **1**). Axoplasmic ribosomes are likely functional, since multiple reports have demonstrated axonal protein synthesis both *in vitro* and *in vivo* [12, 15, 28, 31, 62, 63].

THE AXONAL TRANSCRIPTOME

Every major type of RNA has been observed in the vertebrate axonal domain. Multiple mRNAs have been found in axons using different experimental models and approaches, including mRNAs coding for proteins with multiple functions. The mRNAs encoding all three neurofilament (NF) subunits were detected by RT-PCR in axons of normal and injured (proximal and distal stumps) mammalian peripheral nerves [1]. *In situ* hybridization analysis of rat sciatic nerves showed NF-L [1] and NF-H (Kun *et al*, unpublished) mRNAs not only in the axonal domain but also in the surrounding Schwann cell. In addition, local translation of NF subunits was demonstrated in normal and severed sciatic nerves [1, 64]. The expression level of NF mRNAs is upregulated after injury in the peripheral nervous system [1]. Similar results have been shown in cultures of cortical and hippocampal dissociated neurons using a compartmentalized microfluidic chamber. Here, intermediate filament mRNA expression is upregulated in the axonal domain after axotomy, while levels of other cytoskeletal mRNAs decreased [29].

Actin and other cytoskeletal components were believed to only be transported from the perikaryon by slow axonal transport [65]. However, β-actin mRNA was found in the growth cone of immature and regenerating axons *in vitro* [23, 25, 66, 67]. *In vivo*, β-actin mRNA also was found in the axoplasm of myelinated mature axons [28] (Fig. **2**). In addition, axonal synthesis of this protein was demonstrated in the Mauthner axon, as well as in rodent dorsal and ventral root axons [30]. β-actin mRNA is one of the axonal mRNAs whose expression has been found to be regulated by neurotrophins (NGF, BDNF, NT-3), myelin associated glycoprotein (MAG), and semaphorin 3A, which promote and inhibit axon growth, respectively. This regulation not only impacts mRNA levels but also mRNA localization [25, 27, 68, 69]. The proper localization of β-actin mRNA in the axonal growth cone and its local translation seems to be essential for axonal growth and growth cone guidance [70, 71]. Injury also alters the translation of other mRNAs. In particular, it has been reported that axonal injury upregulates the axonal translation of Ran GTPase, a retrograde injury signal regulator that activates repair mechanisms [72]. Likewise, the increased levels of myosin Va an actin-based molecular motor, is another example of response to nerve injury [73].

Alpha- and beta-tubulin, microtubule-associated proteins and microtubule-based motor mRNAs were also found in axons of cultured neurons [27, 29, 66, 67], with their expression decreased in injured conditioned dorsal-root ganglia cultures [29]. In the case of β-tubulin, its mRNA in the axonal domain was shown to be functional, since its translation has been demonstrated in microdissected motor axons [30], sympathetic cultured neurons [63], and DRG embryonic axons [66].

It is known that mitochondria move by fast axonal transport from the perikaryon to the axonal terminal. It is important to note that mitochondria transport rely on cytoplasmic protein synthesis for 95% of their structural and functional components, since the mitochondrial genome only encodes 5% of mitochondrial proteins. The half-lives of axonal mitochondrial proteins have yet to be determined, but it is known that mitochondrial activity requires the continuous import of nuclear-encoded proteins [74]. It is therefore not surprising that nuclear-encoded mRNAs coding for mitochondrial proteins are also found in the axoplasm, and the local translation and transport across the mitochondrial membranes of these proteins is a requisite for mitochondrial activity [74]. Moreover, inhibition of axonal protein synthesis reduces mitochondrial function, changing mitochondrial membrane potential and the capability to restore axonal ATP levels after depolarization [75]. The proper localization of mitochondrial nuclear-encoded mRNAs to the axonal domain also was shown to play a role in axonal growth *in vitro*. For example, suppression of cytochrome c oxidase subunit IV local translation by inhibition of mRNA translocation to the axon causes a reduction of axonal growth in neuronal cultures

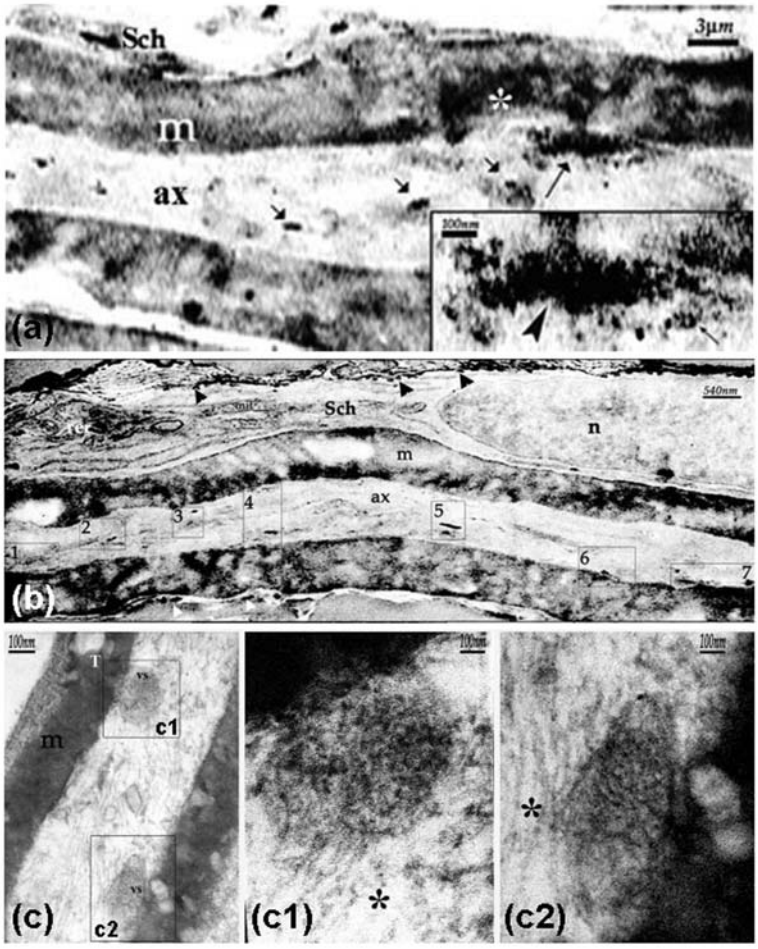

Fig. (1). Ribosomes at the ultrastructural EM level in rat myelinated axons from sciatic nerves. (a) longitudinal profile of a myelinated axon showing ribosome immunoreactivity in a PARP-like distribution (long arrow) together with scattered small ribosomal clusters in the axonal core (short arrows). Similar immunoreactivity was present in the Schwann cell (Sch) and its myelin sheath (white asterisk). (b) Ribosome distribution in a panoramic longitudinal view of a myelinated axon. Schwann cell rough endoplasmic reticulum (rer) is labeled as positive control of the immunoreaction for ribosomes. Ribosome containing particles and/or RNP-like immunoreactivity in the axon core are shown (insets 1–5) and near the axolemma (insets 6 and 7). (c) Myelinated fiber longitudinally sectioned showing vesicle-like structures (vs, c1 and c2) containing ribosome immunoreactivity protruding from myelin into the axon. The two vesicle-like structures are seen in opposite sides of the axon and enlarged in (c1) and (c2). The content is clearly immunostained. Around the vesicle can be seen immunostained ribosomes in the axoplasm. a, b and c are showing HRP staining from secondary antibodies, counterstained briefly (20sec) with lead citrate. Modified from Kun *et al* 2007[18]

[76]. The presence of nuclear-encoded mitochondrial mRNAs was also confirmed in axons and growth cones of DRG and retinal ganglion cells (RGCs) [66, 67]. Interestingly, mRNAs encoding transmembrane proteins also have been found in axons [27]. Ultrastructural analysis of neurons has only detected endoplasmic reticulum and Golgi in perikaryon and dendrites. However, recent findings have shown that markers for these organelles, as well as the secretory traffic of newly synthesized proteins, are present in axons [77].

Very recently, using compartmentalized cultures or laser-capture microdissection combined with genome-wide analysis of gene expression, the groups of Holt, Fawcett and Riccio characterized the transcriptome of axons and growth cones derived from neurons cultured in multiple developmental stages and species [66, 67, 78]. The data extend those of Twiss and coworkers [69] in the sense that they identified a large variety of mRNAs transported into the axon. Moreover, mRNAs were differentially enriched in growth cones relative to axons, and specific mRNA abundance was developmentally regulated [67]. Embryonic axons were enriched in growth-related mRNAs, whereas adult axons were enriched in mRNAs encoding proteins with roles in nociception [66]. On the other hand, Riccio and collaborators identified, using SAGE of RNA from sympathetic axons, axonal mRNA encoding myo-inositol monophosphatase-1 (*Impa1*), a key enzyme that regulates the inositol cycle and the main target of lithium in neurons [78]. It is important to note that these data were obtained from RGC, sensory, and sympathetic axons cultured *in vitro*, which may not completely reflect the composition of the axonal transcriptome in myelinated axons *in vivo*. Furthermore, as technical resolution

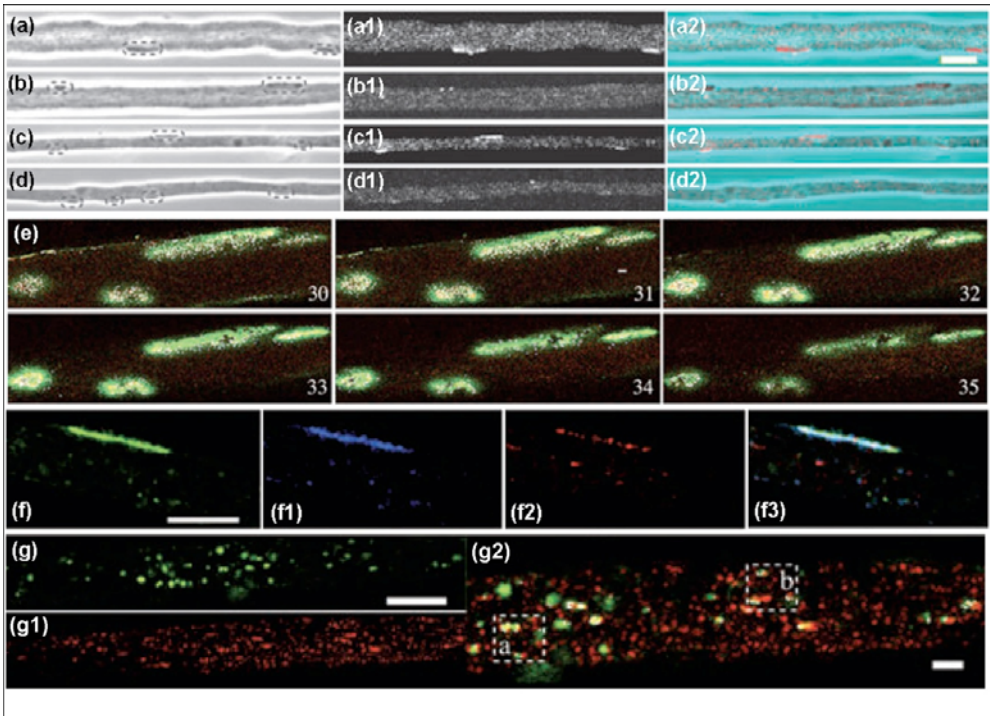

Fig. (2). Localization of ribosomes, β-actin mRNA, and its RNA binding protein ZBP1 in PARPs and axons. (a) Representative examples of *in situ* hybridization (ISH) detection of β-actin mRNA in axoplasmic whole-mounts isolated from (a-a2 and b-b2) rabbit, and (c-c2 and d-d2) rat nerve fibers. The β-actin mRNA anti-sense probe is localized in delimited domains in (a1) rabbit, and (c1) rat whole-mount ISH images. In contrast, the sense probe ISH yields diffuse background in (b1) rabbit, and (d1) rat whole-mounts. Merges of RGB-rendered phase images in (a–d) and corresponding (a1–d1) ISH images in (a2–b2), respectively, show that there is a close correspondence between PARP structural correlates (circled with dotted lines in left panel) and the localization and distribution density of anti-sense β-actin mRNA ISH signals. Grayscale images shown in (a–d) and (a1–d1) were assigned blue-green and red colors, respectively, from a lookup table to highlight correspondence (a2 and c2), or no correspondence (b2 and d2) in merged images. (e) Confocal microscopic evaluation of PARP-containing RNA and ZBP-1 in axoplasmic whole-mounts isolated from Mauthner fiber. NIH ImageJ software was used to analyze a series of six consecutively numbered slices (e30–35). Apparent co-localization is indicated by bright signals, in which the intensity ratio of YOYO-1 and anti-ZBP-1 fluorochromes is ≥80%, and the overlap ratio is ≥0.9. (f) Co-distribution of RNA (green), labeled by YOYO-1, (f1) ribosomes (blue), labeled with ribosome anti-P protein, and (f2) immunofluorescence of anti-ZBP-1 (red) in a surface PARP of an axoplasmic whole-mount from a rat ventral root fiber; (f3) a merged image of (f), (f1), and (f2). (g) Putative 'in-transit' RNA/ZBP-1-containing 'particles' within the axoplasmic core of a whole-mount from a rat ventral root fiber is suggested from inspection of (g) RNA (green) (g1) anti-ZBP-1immunofluorescence (red), and merge image (g2). Calibration bars: 10 μm. Modified from Sotelo-Silveira *et al* 2008 [28] (Color Figures will appear in the online version).

improves it is clear that not only axonal maintenance related messages localize in axons. Among others, mRNAs founded codes for receptors [67, 79], mRNAs involved in pathways like protein synthesis, oxidative phosphorylation, cancer, neurological disease, and signaling [67] plus mRNAs coding for specific functions of the neurons in study [66]. These findings lead us and others to hypothesize that axonal transcriptome composition and function is highly regulated and its functionality may be specific for different groups of neurons.

Analysis of micro RNA (miRNA) in the axonal compartment has been performed in sympathetic neuron cultures [80, 81]. More than 100 different miRNAs have been identified in these reports, and 5 of them were highly enriched in the axon relative to the cell body. Micro RNAs are a small class of RNAs that either repress the translation or elicit the degradation of specific subsets of mRNAs depending on the extent of miRNA-mRNA complementarity. *In silico* searches for putative targets of miRNAs found mRNAs coding for ribosomal proteins, cytoskeletal proteins, molecular motors, receptors, and ion channels as well as nuclear-encoded mitochondrial mRNAs [80], all of which have been identified in the axonal compartment [1, 2, 27, 66, 74, 78].

RNA TRANSPORT AND TRANSLATIONAL REGULATION IN THE AXONAL DOMAIN

The specific localization and local translation of mRNAs require sophisticated regulation by multiple mechanisms. In the mRNA sequence, there are *cis*-acting elements in the 5' or 3' UTRs that were called "zip codes" [34]. These sequences, different for each mRNA, interact with a variety of *trans*-acting factors (TAFs). These factors are classified according to their function either as *cis*-acting binding proteins, molecular motor proteins or scaffolding proteins [34]. The transport of RNA inside the cell is dependent on both microtubules and actin filaments, as well as molecular motors associated with each cytoskeletal component: kinesins and dyneins for microtubules, and myosins for actin filaments.

Long-range transport tends to involve microtubule-based mechanisms, while actin filaments tend to be involved in short-range transport and RNA anchoring [82].

One of the best-studied systems is the β-actin mRNA transport mechanism in developing neurons. After the discovery of the *cis*-acting signal (a 52-nucleotide sequence in the 3'-UTR mRNA) and the *trans*-acting factor (zipcode-binding protein 1 or ZBP1) involved in β-actin localization at the fibroblast's leading edge, several other proteins that also interact at the 3'-UTR of β-actin mRNA have been described. β-actin mRNA is assembled in an RNP complex that includes ZBP1, ZBP2, and hnRNP-R in neuronal cultures. This assembly is essential for axonal β-actin mRNA translocation [25, 70]. As first demonstrated in fibroblasts [83], ZBP1 binding to the 3'UTR of β-actin mRNA represses its translation in neurons [71]. Exposure of cultured cortical neurons to BDNF induces ZBP1 phosphorylation, activating its local synthesis in the axon, influencing growth cone turning [71]. While the precise role of hnRNP-R is still unknown, its direct binding of β-actin mRNA has already been demonstrated [70]. Importantly, hnRNP-R is a survival motor neuron (SMN) protein binding partner. The latter, involved in motor neuron death in spinal muscular atrophy (SMA), interacts with several RNA processing factors in axons. Deletion of the SMN gene causes β-actin mRNA level in cultured neuronal growth cones to decrease [84], and has been shown to associate with β-actin mRNA [85] suggesting an important functional role. Regarding β-actin mRNA trafficking, it has been reported that β-actin mRNA-ZBP1 complex assembly occurs in the nucleus, but initially requires binding of ZBP2 to the nascent RNA for cooperative association of ZBP1 [86]. Later, β-actin mRNA-containing-RNPs travel inside axons by fast bidirectional transport, suggesting a microtubule-dependent movement [25], probably involving kinesin and dynein [33]. The importance of *cis* signals within the 3´UTR was shown for Tau mRNA, for which axonal transport was dependent on a 240-bp sequence [87]. A similar mechanism was shown to operate in sympathetic axons for *Impa1* mRNA [78].

RNA is transported within the cell primarily as RNPs, which differ in their protein composition and function [88]. From the translational point of view, RNAs can be found in translationally active structures (translating polysomes), or in complexes in which the translational process is repressed. These complexes include processing bodies [89], stress granules [90], micro RNP complexes [91], and RNA granules [92]. Interestingly, all of these types of RNPs were found in neurons and seem to be very dynamic structures, exchanging their components and converting from one class to another [88, 93]. Below, we will highlight findings related to regulation by microRNA, RNA granules, and signalling cascades.

Micro RNAs (miRNAs) regulate mRNA expression at the level of translation and/or stability [91], in collaboration with a series of protein cofactors that are important at different levels of the miRNA pathway. Among the final steps of this pathway is the processing by a specific ribonuclease, called Dicer, and its incorporation into miRNPs complexes or RNA-induced silencing complex (RISC). Several key components of the miRNP complex, including argonaute-family members FMRP and Dicer, were found in axons and growth cones of peripheral nervous system developing axons *in vitro* [81, 94]. More importantly, these two papers showed that the axon has the ability to autonomously silence mRNA. Micro RNA 338 is the only miRNA whose functionality has been determined in axons. This miRNA regulates cytochrome c oxidase complex IV mRNA levels and therefore the oxidative phosphorylation level in the axon [81]. *In vivo*, β-tubulin RNAi treatment of sciatic nerves decreases β-tubulin mRNA and protein levels in axons throughout RISC formation [95].

RNA granules contain mRNAs, ribosomes, and multiple proteins [96]. In these granules, mRNA translation is repressed at the elongation step. Transport particles, in which translation is inhibited at the initiation step, do not include ribosomes [88]. Both types of particles have been proposed to mediate RNA trafficking, but RNA granules also appear to act as a storage compartment that can easily release mRNAs to the active translating pool [92]. In our model, RNPs travel through the axon until they reach locations (such as PARPs) where mRNA translation can occur. β-actin mRNA was found in PARPs where it partially co-localizes with its own TAF, ZBP-1, in mature axons [28] (Fig. **2**). Myosin Va and kinesin KIF3A also were enriched in PARPs. In addition, mRNA encoding myosin Va mRNA was found in PARPs, as well as in the cortical zone of rat sciatic nerve axons (Calliari *et al*, unpublished), consistent with our observations in axons of cultured neurons [66], in which a wide variety of axonal mRNAs may support diverse cellular functions. Neither kinesin KIF5A nor dynein were detected in PARPs [2]. The presence of translational machinery, TAFs, and PARPs suggest that these structures are specific target domains inside axons [17]. However, the actual translation in PARPs remains to be conclusively demonstrated.

Translational control in axons appears to be mediated by the mTOR pathway, demonstrated primarily *in vitro*. mTOR regulates ribosomal biogenesis and protein translation through the phosphorylation of multiple substrates [97, 98]. mTOR seems to be important in axonal regeneration after injury. Inhibition of mTOR by rapamycin results in both a decrease in incorporation of radiolabeled amino acids into axonal proteins and a reduction of growth cone formation in sensory and retinal cultured neurons after axotomy [99]. Moreover, deletion of PTEN, a negative regulator of mTOR, leads to increased axonal regeneration in adult retinal ganglion cells after optic nerve injury *in vivo* [100]. Although PTEN deletion in these experiments has a global effect, the local protein synthesis in the axon could also be affected, suggesting a role for the mTOR pathway in axonal translational control. *In vivo*, experiments using single axonal wholemounts implicated F-actin organization and cyclic AMP in the modulation of axonal protein synthesis [28]; in addition, other pathways already demonstrated to modulate axonal protein synthesis *in vitro* also could be involved.

ORIGIN OF AXONAL RNA: NEURONAL SOMA AND/OR SCHWANN CELL

At least some axonal RNAs are synthesized in soma. However, most of the experiments supporting RNA synthe-

sis in the soma were performed in dissociated cultured neurons in which axons are only about a hundred microns long, without associated glia. In the case of a human motor neuron axon, the RNA would have to travel roughly a meter to reach the synaptic terminal. At velocities reported for *in vitro* systems [96] that range between 0.2 and 1.5μm/sec, total time for transport for a 1-meter axon would be between 7 and 55 days. Even with mRNA stabilization through RNA binding proteins, these times seem not to be compatible with RNA integrity throughout its axonal journey. For example, mRNA half-life measured in embryonic stem cells averaged 7 h [101]. Moreover, in large motor neurons the axonal domain contains up to 100-fold the mass of the perikaryon [32], leaving the perikaryon with a large cytoplasmic mass to support. In this respect, the proposal that the Schwann cell could provide RNAs and ribosomes to the axon has been shown as an increasingly attractive mechanism [3, 4, 17]. In the light of the findings to be revised in the next paragraphs, the close functional relationship between myelin health and structure of axons, as noted by Brady and coworkers [102], could be also be seen and interpreted in the context of transfer of macro molecules between these two cells.

The first evidence of local synthesis and transfer of RNA was obtained in the squid giant axon using radiolabeled uridine [3, 103, 104]. In these early experiments, giant fibers were incubated with radiolabeled RNA precursors in the absence of cell bodies, yet radiolabeled RNA was recovered from axoplasm. RNAs found in the axon were further identified as rRNAs, tRNAs and mRNAs [105]. The cell-to-cell transfer of RNA in this model was shown to be modulated by neurotransmitters [16, 106].

In rats, local synthesis of RNA was demonstrated *in vivo* by quantitative autoradiography of injured sciatic nerves [62]. Later findings in our laboratory (Sotelo *et al*., unpublished observations), dealing with *in vitro* labeling of decentralized rat sciatic fibers with bromo-uridine (BrU), have conclusively shown that Schwann cells deliver RNA to the axon. Confocal analysis showed that newly synthesized RNA was present in both the Schwann cell cytoplasm and the axon. Nodes of Ranvier and Schmidt-Lanterman clefts contained newly synthesized RNA, suggesting that these structures are involved in the cell-to-cell RNA transfer. An mRNA candidate to be locally transferred could be neurofilament mRNA, since *in situ* hybridization analysis of NF-L [1] and NF-H (Kun *et al*., unpublished observations) mRNAs in rat sciatic nerve found them in Schwann cell cytoplasm. These experiments demonstrated that mRNAs coding for the three subunits of neurofilaments were present in normal nerves and increased their levels after nerve injury. Both mRNAs also were found in the inner Schwann-cell cytoplasm and axonal domain, consistent with mRNA transfer from glia to axon. The expression of neuronal mRNAs (NF-L, NF-M) has also been shown in Schwann cells of developing and injured rat nerves [107, 108]. It will be important to study how the transport into the axon is orchestrated during regeneration, because this will imply intercellular traffic in both directions due to Schwann cell recycling of degenerating axons.

Interestingly, other evidence suggests that ribosomes also are transferred from Schwann cells to the axons they ensheath in vertebrates. Evidence supporting this transfer has been obtained using multiple approaches, including EM [57, 58], immuno-EM (polyclonal antiribosome antibodies)[18] (Fig. **1**), and GFP-tagged ribosomal proteins in the distal stump of the slow Wallerian degeneration mutant mice, *Wld*^{s} [109, 110]. Taken together, these data support the hypothesis of glia-to-axon transfer of both proteins [111] and RNA [104]. While there were some indications by Edstrom and coworkers in the decade of 1960 that transfer of RNA from glia to axon at the CNS (Mauthner axons from goldfish) may be occurring, there is no extensive evidence about this type of exchange happening at the central nervous system yet. Since oligodendrocytes have similar mechanism of transporting RNA particles into the innermost tiers of myelin [112] it may be feasible to speculate that similar exchanges may occur in CNS, but this issue will need careful experimental analysis in the future.

The mechanism of the cell-to-cell transfer remains to be determined, but it is worth noting that examples of intercellular transport can be found throughout biology. For example, exosomes have been shown to be involved in intercellular macromolecular transfer of lipids, proteins, and genetic material by trans-endocytosis [113]. In the nervous system, glial and neuronal exosomes have been documented to contain mitochondrial DNA [114] and mRNA [115]. Another example involves the formation of 50- to 200-nm diameter membranous structures called nanotubes. Rich in F-actin and myosin Va, they have been proposed to mediate translocation of organelles and membrane proteins from one cell to another [116, 117]. Nanotubes and similar structures have been detected in a wide variety of cells *in vitro*, while tubules of a similar diameter have been observed by freeze-fracture EM on mammalian sciatic nerves at the adaxonal side of internodal myelin [118]. Moreover, glial finger-like structures containing ribosomes have been observed invading the axon in squid nerve fiber (Kun, unpublished) and vesicles containing ribosomes have been detected in rat sciatic nerve axons [18, 109] (Fig. **1c**), consistent with trans-endocytosis. Finally, the engulfment of glial structures (nuclei) by the axon has been observed in crayfish during regeneration [119].

CONCLUSIONS

As discussed above, local protein synthesis in axons has been demonstrated by a number of approaches and experimental models. The multiple systems used in these demonstrations (variety of species used, neurons studied, physiological conditions analyzed, axonal responses to different stimulus) imply a high degree of likelihood that this process is occurring in axons in general. *In vitro* experiments with dissociated neurons are unlikely to be good model systems for study given the lack of associated cells and the short length of their axons. There are multiple questions that remain to be addressed. Do short and long axons both have axonal protein synthesis? Are the regeneration and growth cone sprouting programs the same *in vivo* and *in vitro*? What are the differences between axonal transcriptomes from normal and pathological conditions for a particular type of neu-

ron? What is the role of axonal mRNAs in normal and pathological conditions? Is the full knowledge of the transcriptome an asset to establish new therapeutic approaches in different types of neuronal degeneration processes? The possibility of an integrated response between the glial cell and the axon that includes axonal protein synthesis is an important and evolving field that will impact the understanding of the cell biology of the axon in both normal and pathological conditions.

ACKNOWLEDGMENTS

This work has been funded in part by grants of CSIC, ANII, PEDECIBA, NIH (RO1 and RO3) and a PEW Latin American fellowship.

ABBREVIATIONS

DRG	=	Dorsal root ganglion
EM	=	Electron microscopy
ISH	=	*In situ* hybridization
mTOR	=	Mammalian target of Rapamycin
NF	=	Neurofilament
PARPs	=	Periaxoplasmic ribosomal plaques
RGC	=	Retinal ganglion cells
RN	=	Node of Ranvier
RNP	=	Ribonucleoprotein particle
SLC	=	Schmidt-Lanterman cleft
TAF	=	Trans-acting factors
UTR	=	Untranslated region
ZBP1	=	Zipcode binding protein-1

REFERENCES

[1] Sotelo-Silveira JR, Calliari A, Kun A, *et al*. Neurofilament mRNAs are present and translated in the normal and severed sciatic nerve. J Neurosci Res 2000; 62: 65-74.

[2] Sotelo-Silveira JR, Calliari A, Cardenas M, Koenig E, Sotelo JR. Myosin Va and kinesin II motor proteins are concentrated in ribosomal domains (periaxoplasmic ribosomal plaques) of myelinated axons. J Neurobiol 2004; 60: 187-96.

[3] Giuditta A, Chun JT, Eyman M, Cefaliello C, Bruno AP, Crispino M. Local gene expression in axons and nerve endings: the glia-neuron unit. Physiol Rev 2008; 88: 515-55.

[4] Twiss JL, Fainzilber M. Ribosomes in axons--scrounging from the neighbors? Trends Cell Biol 2009; 19: 236-43.

[5] Lasek RJ, Dabrowski C, Nordlander R. Analysis of axoplasmic RNA from invertebrate giant axons. Nat New Biol 1973; 244: 162-5.

[6] Black MM, Lasek RJ. The presence of transfer RNA in the axoplasm of the squid giant axon. J Neurobiol 1977; 8: 229-37.

[7] Ingoglia NA, Giuditta A, Zanakis MF, *et al*. Incorporation of 3H-amino acids into proteins in a partially purified fraction of axoplasm: evidence for transfer RNA-mediated, post-translational protein modification in squid giant axons. J Neurosci 1983; 3: 2463-73.

[8] Scheffer JW, Howe N, Gunning PW, Austin L. Axoplasmic transport of transfer RNA in the chick optic system. J Neurochem 1984; 42: 698-704.

[9] Soffer RL. Post-translational modification of proteins catalyzed by aminoacyl-tRNA-protein transferases. Mol Cell Biochem 1973; 2: 3-14.

[10] Edstrom JE, Eichner D, Edstrom A. The ribonucleic acid of axons and myelin sheaths from Mauthner neurons. Biochim Biophys Acta 1962; 61: 178-84.

[11] Koenig E. Ribosomal RNA in Mauthner axon: implications for a protein synthesizing machinery in the myelinated axon. Brain Res 1979; 174: 95-107.

[12] Giuditta A, Menichini E, Perrone CC, *et al*. Active polysomes in the axoplasm of the squid giant axon. J Neurosci Res 1991; 28: 18-28.

[13] Koenig E, Martin R. Cortical plaque-like structures identify ribosome-containing domains in the Mauthner cell axon. J Neurosci 1996; 16: 1400-11.

[14] Sotelo JR, Kun A, Benech JC, Giuditta A, Morillas J, Benech CR. Ribosomes and polyribosomes are present in the squid giant axon: an immunocytochemical study. Neuroscience 1999; 90: 705-15.

[15] Alvarez J, Giuditta A, Koenig E. Protein synthesis in axons and terminals: significance for maintenance, plasticity and regulation of phenotype. With a critique of slow transport theory. Prog Neurobiol 2000; 62: 1-62.

[16] Giuditta A, Eyman M, Kaplan BB. Gene expression in the squid giant axon: neurotransmitter modulation of RNA transfer from periaxonal glia to the axon. Biol Bull 2002; 203: 189-90.

[17] Sotelo-Silveira JR, Calliari A, Kun A, Koenig E, Sotelo JR. RNA trafficking in axons. Traffic 2006; 7: 508-15.

[18] Kun A, Otero L, Sotelo-Silveira JR, Sotelo JR. Ribosomal distributions in axons of mammalian myelinated fibers. J Neurosci Res 2007; 85: 2087-98.

[19] Mohr E, Fehr S, Richter D. Axonal transport of neuropeptide encoding mRNAs within the hypothalamo-hypophyseal tract of rats. Embo J 1991; 10: 2419-24.

[20] Mohr E, Richter D. Diversity of mRNAs in the Axonal Compartment of Peptidergic Neurons in the Rat. Eur J Neurosci 1992; 4: 870-6.

[21] Wensley CH, Stone DM, Baker H, Kauer JS, Margolis FL, Chikaraishi DM. Olfactory marker protein mRNA is found in axons of olfactory receptor neurons. J Neurosci 1995; 15: 4827-37.

[22] Weiner OD, Zorn AM, Krieg PA, Bittner GD. Medium weight neurofilament mRNA in goldfish Mauthner axoplasm. Neurosci Lett 1996; 213: 83-6.

[23] Bassell GJ, Zhang H, Byrd AL, *et al*. Sorting of beta-actin mRNA and protein to neurites and growth cones in culture. J Neurosci 1998; 18: 251-65.

[24] Aronov S, Aranda G, Behar L, Ginzburg I. Axonal tau mRNA localization coincides with tau protein in living neuronal cells and depends on axonal targeting signal. J Neurosci 2001; 21: 6577-87.

[25] Zhang HL, Eom T, Oleynikov Y, *et al*. Neurotrophin-induced transport of a beta-actin mRNP complex increases beta-actin levels and stimulates growth cone motility. Neuron 2001; 31: 261-75.

[26] Lee SK, Hollenbeck PJ. Organization and translation of mRNA in sympathetic axons. J Cell Sci 2003; 116: 4467-78.

[27] Willis DE, van Niekerk EA, Sasaki Y, *et al*. Extracellular stimuli specifically regulate localized levels of individual neuronal mRNAs. J Cell Biol 2007; 178: 965-80.

[28] Sotelo-Silveira J, Crispino M, Puppo A, Sotelo JR, Koenig E. Myelinated axons contain beta-actin mRNA and ZBP-1 in periaxoplasmic ribosomal plaques and depend on cyclic AMP and F-actin integrity for *in vitro* translation. J Neurochem 2008; 104: 545-57.

[29] Taylor AM, Berchtold NC, Perreau VM, Tu CH, Li Jeon N, Cotman CW. Axonal mRNA in uninjured and regenerating cortical mammalian axons. J Neurosci 2009; 29: 4697-707.

[30] Koenig E. Evaluation of local synthesis of axonal proteins in the goldfish Mauthner cell axon and axons of dorsal and ventral roots of the rat *in vitro*. Mol Cell Neurosci 1991; 2: 384-94.

[31] Giuditta A, Kaplan BB, van Minnen J, Alvarez J, Koenig E. Axonal and presynaptic protein synthesis: new insights into the biology of the neuron. Trends Neurosci 2002; 25: 400-4.

[32] Alvarez J, Benech CR. Axoplasmic incorporation of amino acids in a myelinated fiber exceeds that of its soma: a radioautographic study. Exp Neurol 1983; 82: 25-42.

[33] Shav-Tal Y, Singer RH. RNA localization. J Cell Sci 2005; 118: 4077-81.

[34] Bassell GJ, Oleynikov Y, Singer RH. The travels of mRNAs through all cells large and small. Faseb J 1999; 13: 447-54.

[35] Wang DO, Kim SM, Zhao Y, *et al*. Synapse- and stimulus-specific local translation during long-term neuronal plasticity. Science 2009; 324: 1536-40.
[36] Eyman M, Cefaliello C, Ferrara E, De Stefano R, Crispino M, Giuditta A. Synaptosomal protein synthesis is selectively modulated by learning. Brain Res 2007; 1132: 148-57.
[37] Martin KC. Local protein synthesis during axon guidance and synaptic plasticity. Curr Opin Neurobiol 2004; 14: 305-10.
[38] Yoon BC, Zivraj KH, Holt CE. Local translation and mRNA trafficking in axon pathfinding. Results Probl Cell Differ 2009; 48: 269-88.
[39] Yao J, Sasaki Y, Wen Z, Bassell GJ, Zheng JQ. An essential role for beta-actin mRNA localization and translation in Ca2+-dependent growth cone guidance. Nat Neurosci 2006; 9: 1265-73.
[40] Lin AC, Holt CE. Local translation and directional steering in axons. Embo J 2007; 26: 3729-36.
[41] Palay SL, Palade GE. The fine structure of neurons. J Biophys Biochem Cytol 1955; 1: 69-88.
[42] Lyser KM. Early Differentiation of Motor Neuroblasts in the Chick Embryo as Studied by Electron Microscopy. I. General Aspects. Dev Biol 1964; 10: 433-66.
[43] Lyser KM. Early differentiation of motor neuroblasts in the chick embryo as studied by electron microscopy. II. Microtubules and neurofilaments. Dev Biol 1968; 17: 117-42.
[44] Skoff RP, Hamburger V. Fine structure of dendritic and axonal growth cones in embryonic chick spinal cord. J Comp Neurol 1974; 153: 107-47.
[45] Tennyson VM. The fine structure of the axon and growth cone of the dorsal root neuroblast of the rabbit embryo. J Cell Biol 1970; 44: 62-79.
[46] Tennyson VM. Electron microscopic study of the developing neuroblast of the dorsal root ganglion of the rabbit embryo. J Comp Neurol 1965; 124: 267-317.
[47] Bunge MB. Fine structure of nerve fibers and growth cones of isolated sympathetic neurons in culture. J Cell Biol 1973; 56: 713-35.
[48] Caley DW, Maxwell DS. An electron microscopic study of the neuroglia during postnatal development of the rat cerebrum. J Comp Neurol 1968; 133: 45-70.
[49] Palay SL, Sotelo C, Peters A, Orkand PM. The axon hillock and the initial segment. J Cell Biol 1968; 38: 193-201.
[50] Spencer PS, Raine CS, Wisniewski H. Axon diameter and myelin thickness. Unusual relationships in dorsal root ganglia. Anat Rec 1973; 176: 225-43.
[51] Zenker W, Hogl E. The prebifurcation section of the axon of the rat spinal ganglion cell. Cell Tissue Res 1976; 165: 345-63.
[52] Dimova RN, Markov DV. Changes in the mitochondria in the initial part of the axon during regeneration. Acta Neuropathol 1976; 36: 235-42.
[53] Steward O, Ribak CE. Polyribosomes associated with synaptic specializations on axon initial segments: localization of protein-synthetic machinery at inhibitory synapses. J Neurosci 1986; 6: 3079-85.
[54] Zelena J. Ribosome-like particles in myelinated axons of the rat. Brain Res 1970; 24: 359-63.
[55] Zelena J. Ribosomes in the axoplasm of myelinated nerve fibres. Folia Morphol (Praha) 1972; 20: 91-3.
[56] Zelena J. Ribosomes in myelinated axons of dorsal root ganglia. Z Zellforsch Mikrosk Anat 1972; 124: 217-29.
[57] Li YC, Li YN, Cheng CX, *et al*. Subsurface cisterna-lined axonal invaginations and double-walled vesicles at the axonal-myelin sheath interface. Neurosci Res 2005; 53: 298-303.
[58] Li YC, Cheng CX, Li YN, Shimada O, Atsumi S. Beyond the initial axon segment of the spinal motor axon: fasciculated microtubules and polyribosomal clusters. J Anat 2005; 206: 535-42.
[59] Martin R, Fritz W, Giuditta A. Visualization of polyribosomes in the postsynaptic area of the squid giant synapse by electron spectroscopic imaging. J Neurocytol 1989; 18: 11-8.
[60] Martin R, Vaida B, Bleher R, Crispino M, Giuditta A. Protein synthesizing units in presynaptic and postsynaptic domains of squid neurons. J Cell Sci 1998; 111 (Pt 21): 3157-66.
[61] Koenig E, Martin R, Titmus M, Sotelo-Silveira JR. Cryptic peripheral ribosomal domains distributed intermittently along mammalian myelinated axons. J Neurosci 2000; 20: 8390-400.
[62] Benech C, Sotelo JR, Jr., Menendez J, Correa-Luna R. Autoradiographic study of RNA and protein synthesis in sectioned peripheral nerves. Exp Neurol 1982; 76: 72-82.
[63] Eng H, Lund K, Campenot RB. Synthesis of beta-tubulin, actin, and other proteins in axons of sympathetic neurons in compartmented cultures. J Neurosci 1999; 19: 1-9.
[64] Sotelo JR, Benech CR, Kun A. Local radiolabeling of the 68 kDa neurofilament protein in rat sciatic nerves. Neurosci Lett 1992; 144: 174-6.
[65] Lasek RJ, Garner JA, Brady ST. Axonal transport of the cytoplasmic matrix. J Cell Biol 1984; 99: 212s-21s.
[66] Gumy LF, Yeo GS, Tung YC, *et al*. Transcriptome analysis of embryonic and adult sensory axons reveals changes in mRNA repertoire localization. Rna 17: 85-98.
[67] Zivraj KH, Tung YC, Piper M, *et al*. Subcellular profiling reveals distinct and developmentally regulated repertoire of growth cone mRNAs. J Neurosci 30: 15464-78.
[68] Zhang HL, Singer RH, Bassell GJ. Neurotrophin regulation of beta-actin mRNA and protein localization within growth cones. J Cell Biol 1999; 147: 59-70.
[69] Willis D, Li KW, Zheng JQ, *et al*. Differential transport and local translation of cytoskeletal, injury-response, and neurodegeneration protein mRNAs in axons. J Neurosci 2005; 25: 778-91.
[70] Glinka M, Herrmann T, Funk N, *et al*. The heterogeneous nuclear ribonucleoprotein-R is necessary for axonal beta-actin mRNA translocation in spinal motor neurons. Hum Mol Genet 19: 1951-66.
[71] Sasaki Y, Welshhans K, Wen Z, *et al*. Phosphorylation of zipcode binding protein 1 is required for brain-derived neurotrophic factor signaling of local beta-actin synthesis and growth cone turning. J Neurosci 30: 9349-58.
[72] Yudin D, Hanz S, Yoo S, *et al*. Localized regulation of axonal RanGTPase controls retrograde injury signaling in peripheral nerve. Neuron 2008; 59: 241-52.
[73] Calliari A, Sotelo-Silveira J, Costa MC, *et al*. Myosin Va is locally synthesized following nerve injury. Cell Motil Cytoskeleton 2002; 51: 169-76.
[74] Kaplan BB, Gioio AE, Hillefors M, Aschrafi A. Axonal protein synthesis and the regulation of local mitochondrial function. Results Probl Cell Differ 2009; 48: 225-42.
[75] Hillefors M, Gioio AE, Mameza MG, Kaplan BB. Axon viability and mitochondrial function are dependent on local protein synthesis in sympathetic neurons. Cell Mol Neurobiol 2007; 27: 701-16.
[76] Aschrafi A, Natera-Naranjo O, Gioio AE, Kaplan BB. Regulation of axonal trafficking of cytochrome c oxidase IV mRNA. Mol Cell Neurosci 43: 422-30.
[77] Merianda TT, Lin AC, Lam JS, *et al*. A functional equivalent of endoplasmic reticulum and Golgi in axons for secretion of locally synthesized proteins. Mol Cell Neurosci 2009; 40: 128-42.
[78] Andreassi C, Zimmermann C, Mitter R, *et al*. An NGF-responsive element targets myo-inositol monophosphatase-1 mRNA to sympathetic neuron axons. Nat Neurosci 13: 291-301.
[79] Brittis PA, Lu Q, Flanagan JG. Axonal protein synthesis provides a mechanism for localized regulation at an intermediate target. Cell 2002; 110: 223-35.
[80] Natera-Naranjo O, Aschrafi A, Gioio AE, Kaplan BB. Identification and quantitative analyses of microRNAs located in the distal axons of sympathetic neurons. Rna 16: 1516-29.
[81] Aschrafi A, Schwechter AD, Mameza MG, Natera-Naranjo O, Gioio AE, Kaplan BB. MicroRNA-338 regulates local cytochrome c oxidase IV mRNA levels and oxidative phosphorylation in the axons of sympathetic neurons. J Neurosci 2008; 28: 12581-90.
[82] Holt CE, Bullock SL. Subcellular mRNA localization in animal cells and why it matters. Science 2009; 326: 1212-6.
[83] Huttelmaier S, Zenklusen D, Lederer M, *et al*. Spatial regulation of beta-actin translation by Src-dependent phosphorylation of ZBP1. Nature 2005; 438: 512-5.
[84] Rossoll W, Jablonka S, Andreassi C, *et al*. Smn, the spinal muscular atrophy-determining gene product, modulates axon growth and localization of beta-actin mRNA in growth cones of motoneurons. J Cell Biol 2003; 163: 801-12.
[85] Todd AG, Morse R, Shaw DJ, McGinley S, Stebbings H, Young PJ. SMN, Gemin2 and Gemin3 associate with beta-actin mRNA in the cytoplasm of neuronal cells *in vitro*. J Mol Biol 401: 681-9.

[86] Pan F, Huttelmaier S, Singer RH, Gu W. ZBP2 facilitates binding of ZBP1 to beta-actin mRNA during transcription. Mol Cell Biol 2007; 27: 8340-51.
[87] Aronov S, Aranda G, Behar L, Ginzburg I. Visualization of translated tau protein in the axons of neuronal P19 cells and characterization of tau RNP granules. J Cell Sci 2002; 115: 3817-27.
[88] Sossin WS, DesGroseillers L. Intracellular trafficking of RNA in neurons. Traffic 2006; 7: 1581-9.
[89] Kulkarni M, Ozgur S, Stoecklin G. On track with P-bodies. Biochem Soc Trans 38: 242-51.
[90] Buchan JR, Parker R. Eukaryotic stress granules: the ins and outs of translation. Mol Cell 2009; 36: 932-41.
[91] Fabian MR, Sonenberg N, Filipowicz W. Regulation of mRNA translation and stability by microRNAs. Annu Rev Biochem 79: 351-79.
[92] Krichevsky AM, Kosik KS. Neuronal RNA granules: a link between RNA localization and stimulation-dependent translation. Neuron 2001; 32: 683-96.
[93] Thomas MG, Loschi M, Desbats MA, Boccaccio GL. RNA granules: the good, the bad and the ugly. Cell Signal 23: 324-34.
[94] Hengst U, Cox LJ, Macosko EZ, Jaffrey SR. Functional and selective RNA interference in developing axons and growth cones. J Neurosci 2006; 26: 5727-32.
[95] Murashov AK, Chintalgattu V, Islamov RR, *et al*. RNAi pathway is functional in peripheral nerve axons. Faseb J 2007; 21: 656-70.
[96] Kiebler MA, Bassell GJ. Neuronal RNA granules: movers and makers. Neuron 2006; 51: 685-90.
[97] Ma XM, Blenis J. Molecular mechanisms of mTOR-mediated translational control. Nat Rev Mol Cell Biol 2009; 10: 307-18.
[98] Gingras AC, Raught B, Sonenberg N. mTOR signaling to translation. Curr Top Microbiol Immunol 2004; 279: 169-97.
[99] Verma P, Chierzi S, Codd AM, *et al*. Axonal protein synthesis and degradation are necessary for efficient growth cone regeneration. J Neurosci 2005; 25: 331-42.
[100] Park KK, Liu K, Hu Y, *et al*. Promoting axon regeneration in the adult CNS by modulation of the PTEN/mTOR pathway. Science 2008; 322: 963-6.
[101] Sharova LV, Sharov AA, Nedorezov T, Piao Y, Shaik N, Ko MS. Database for mRNA half-life of 19 977 genes obtained by DNA microarray analysis of pluripotent and differentiating mouse embryonic stem cells. DNA Res 2009; 16: 45-58.
[102] Witt A, Brady ST. Unwrapping new layers of complexity in axon/glial relationships. Glia 2000; 29: 112-7.
[103] Fischer S, Gariglio P, Tarifeno E. Incorporation of H3-uridine and the isolation and characterization of RNA from squid axon. J Cell Physiol 1969; 74: 155-62.
[104] Cutillo V, Montagnese P, Gremo F, Casola L, Giuditta A. Origin of axoplasmic RNA in the squid giant fiber. Neurochem Res 1983; 8: 1621-34.
[105] Rapallino MV, Cupello A, Giuditta A. Axoplasmic RNA species synthesized in the isolated squid giant axon. Neurochem Res 1988; 13: 625-31.
[106] Eyman M, Cefaliello C, Ferrara E, *et al*. Local synthesis of axonal and presynaptic RNA in squid model systems. Eur J Neurosci 2007; 25: 341-50.
[107] Roberson MD, Toews AD, Goodrum JF, Morell P. Neurofilament and tubulin mRNA expression in Schwann cells. J Neurosci Res 1992; 33: 156-62.
[108] Fabrizi C, Kelly BM, Gillespie CS, Schlaepfer WW, Scherer SS, Brophy PJ. Transient expression of the neurofilament proteins NF-L and NF-M by Schwann cells is regulated by axonal contact. J Neurosci Res 1997; 50: 291-9.
[109] Court FA, Hendriks WT, MacGillavry HD, Alvarez J, van Minnen J. Schwann cell to axon transfer of ribosomes: toward a novel understanding of the role of glia in the nervous system. J Neurosci 2008; 28: 11024-9.
[110] Alvarez J. The autonomous axon: a model based on local synthesis of proteins. Biol Res 2001; 34: 103-9.
[111] Lasek RJ, Gainer H, Barker JL. Cell-to-cell transfer of glial proteins to the squid giant axon. The glia-neuron protein trnasfer hypothesis. J Cell Biol 1977; 74: 501-23.
[112] Carson JH, Gao Y, Tatavarty V, *et al*. Multiplexed RNA trafficking in oligodendrocytes and neurons. Biochim Biophys Acta 2008; 1779: 453-8.
[113] Simons M, Raposo G. Exosomes--vesicular carriers for intercellular communication. Curr Opin Cell Biol 2009; 21: 575-81.
[114] Guescini M, Genedani S, Stocchi V, Agnati LF. Astrocytes and Glioblastoma cells release exosomes carrying mtDNA. J Neural Transm 117: 1-4.
[115] Smalheiser NR. Exosomal transfer of proteins and RNAs at synapses in the nervous system. Biol Direct 2007; 2: 35.
[116] Scherer SS, Wrabetz L. Molecular mechanisms of inherited demyelinating neuropathies. Glia 2008; 56: 1578-89.
[117] Rustom A, Saffrich R, Markovic I, Walther P, Gerdes HH. Nanotubular highways for intercellular organelle transport. Science 2004; 303: 1007-10.
[118] Kruger L, Stolinski C, Martin BG, Gross MB. Membrane specializations and cytoplasmic channels of Schwann cells in mammalian peripheral nerve as seen in freeze-fracture replicas. J Comp Neurol 1979; 186: 571-601.
[119] Pearce J, Lnenicka GA, Govind CK. Regenerating crayfish motor axons assimilate glial cells and sprout in cultured explants. J Comp Neurol 2003; 464: 449-62.

Received: January 25, 2011 Revised: March 07, 2011 Accepted: March 08, 2011

3. HIPOTESIS

Actualmente, es aceptado por la comunidad científica, que algunos ARNs presentes en el axón provienen del soma neuronal, como consecuencia de la transcripción del genoma de la neurona, y el posterior transporte de los ARNs desde el pericarion hacia el dominio axonal. Nuestra hipótesis de trabajo plantea que la célula de Schwann es una fuente local de ARN axonal (ribosomal y mensajero), alternativa y no excluyente de la somática, tanto en condiciones normales como de regeneración axonal luego de una lesión. En este contexto los ARNs con destino axonal son transcritos en el núcleo de la célula de Schwann, a partir de su genoma y posteriormente transferidos al axón con el cual establece contacto.

4. OBJETIVO GENERAL

Los objetivos generales de la presente tesis fueron demostrar la transferencia de ARNs desde la célula de Schwann al axón, determinar parte del mecanismo de transporte de estos ARNs y dilucidar la identidad de los ARNs transferidos.

5. OBJETIVOS ESPECIFICOS

1) Demostrar que la célula de Schwann es fuente de ARN con destino axonal en fibras mielínicas normales del SNP.

2) Demostrar que este proceso también tiene lugar durante la regeneración axonal de las fibras mielínicas del SNP.

3) Determinar si los microtúbulos están implicados en el transporte de los ARNs axonales transferidos de la célula de Schwann al axón de las fibras mielínicas del SNP.

4) Determinar si los filamentos de actina están implicados en el transporte y la transferencia de los ARNs axonales transferidos de la célula de Schwann al axón de las fibras mielínicas del SNP.

5) Identificar los motores moleculares implicados en el transporte y la transferencia de los ARNs desde la célula de Schwann al axón de las fibras mielínicas del SNP.

6) Determinar la identidad de los ARNs axonales provenientes de la célula de Schwann en fibras mielínicas del Sistema Nervioso Periférico.

6. MATERIALES Y METODOS

Para llevar a cabo los objetivos de la presente tesis de Doctorado se implementaron diferentes estrategias. Para demostrar la transferencia de ARNs desde la célula de Schwann al axón en fibras mielínicas del SNP, tanto normales como en regeneración, se realizó la incubación de los nervios descentralizados en medio de cultivo (*in vitro*) conteniendo bromouridina (BrU). Por otra parte, también se realizó el marcado de los ARN neosintetizados *in vivo*, con el fin de demostrar que lo observado en los experimentos *in vitro*, también ocurre *in vivo*. La BrU es un análogo de la uridina, que se incorpora a las moléculas de ARN neosintetizadas a medida que se transcriben. Los ARN así marcados pueden ser luego reconocidos mediante un anticuerpo generado contra bromo-deoxiuridina (BrdU), el cual también reconoce BrU. El marcado *in vitro* de los ARN neosintetizados con BrU fue la estrategia básica de toda la presente tesis. La localización de los ARN-BrU en el tejido se determinó mediante inmunocitoquímica y microscopía confocal de las fibras de nervio ciático. Mediante éstas dos últimas técnicas también se realizaron experimentos de co-localización de los ARN-BrU con diferentes estructuras celulares (ribosomas, mitocondrias, componentes del citoesqueleto). Para determinar los mecanismos de transporte, la estrategia principal utilizada constituyó la disrupción de los microtúbulos o los filamentos de actina, mediante el uso de drogas adecuadas, y la cuantificación de los ARN-BrU en diferentes dominios de las fibras mielínicas mediante inmunocitoquímica y microscopía confocal cuantitativa. En el caso del análisis de la identidad de los motores moleculares que podrían estar implicados en el transporte y la transferencia de los ARN-BrU la estrategia principal fue la determinación de la co-localización entre dichas moléculas (motor molecular - ARN-BrU) mediante microscopia FRET cuantitativa y confocal. Además, en el caso particular del motor miosina Va, se realizaron experimentos de marcación de los ARN con BrU en ratones mutantes nulos para dicha molécula. Por último, para identificar los ARN candidatos a ser transferidos desde la célula de Schwann al axón, se llevó a cabo, principalmente, la secuenciación masiva de los ARN-BrU purificados a partir de nervios ciáticos en regeneración.

6.1. Marcación con bromouridina de ARNs neosintetizados en las células de Schwann de nervios ciáticos

Para los experimentos realizados en el Departamento de Proteínas y Acidos Nucleicos, IIBCE, Montevideo, Uruguay, los protocolos de experimentación animal utilizados fueron aprobados por la Comisión de Ética en el Uso de Animales (CEUA) del Instituto de Investigaciones Biológicas Clemente Estable, Montevideo, Uruguay y están de acuerdo con las pautas de la Comisión Nacional de Experimentación Animal (CNEA) y las leyes Uruguayas. En el caso de los experimentos realizados en el *McLaughlin Research Institute* (MRI), Montana, USA, los protocolos de experimentación animal utilizados fueron aprobados por el *Institutional Animal Care and Use Committee* del MRI y están de acuerdo con la Guía para el Cuidado y Uso de Animales de Laboratorio del *National Institute of Health*, USA. Todos los procedimientos quirúrgicos fueron realizados bajo anestesia (ketamina/xilacina), y se suministró ibuprofeno en los casos necesarios, para minimizar el dolor de los animales.

En los experimentos presentados aquí se utilizaron ratas Sprague-Dawley de 3-4 meses de edad, ratones CD1 de 3-4 meses de edad y ratones C57BL/6J normales y mutantes nulos *Myo5a*$^{d\text{-}120J}$/*Myo5a*$^{d\text{-}120J}$ (*dilute lethal*) de 12-16 días de edad.

Para los experimentos realizados en nervios normales, las ratas fueron decapitadas y se extirparon segmentos de 2 cm de longitud de cada nervio ciático. Los segmentos fueron entonces incubados con 10 mg/mL de BrU (SIGMA) en medio Neurobasal (Invitrogen), durante 6 h a 37°C y 5% CO_2. En el caso de los experimentos realizados con nervios en regeneración, los animales fueron anestesiados con 5/10 mg/kg ketamina/xilacina por vía intraperitoneal para realizar una pequeña incisión (~1 cm) en la piel y separar la musculatura de las patas traseras. Con una aguja de crochet, se levantó el nervio ciático de cada pata a través de la pequeña incisura y se seccionó el mismo. La incisura fue cerrada mediante sutura y transcurridas 18 h post-lesión, los animales fueron sacrificados y se retiraron los cabos proximales de la lesión (~1 cm). Esos segmentos fueron incubados con 10 mg/mL de bromouridina (BrU, Sigma) en medio Neurobasal durante 6 h a 37°C y 5% CO_2,

o durante 1 hora (para los experimentos *pulse-chase*) a 37°C y 5% de CO_2. En los ensayos de *pulse-chase*, la incubación en medio con BrU fue seguida de lavados en medio Neurobasal sin BrU (4x5 min) y una incubación adicional en dicho medio durante 45 min, a 37°C, 5% CO_2. Por último, para los experimentos realizados *in vivo* en nervios ciáticos en regeneración utilizamos dos estrategias diferentes. Por un lado, se seccionaron los nervios ciáticos de ratas como fue descrito anteriormente. Luego de 18 h, las ratas fueron anestesiadas nuevamente, y la sutura re-abierta, dejando al aire el nervio ciático seccionado. Se construyó un contenedor con un tubo de plástico cortado al medio y sellado con vaselina en ambos extremos, alrededor del cabo proximal. El contenedor con el cabo proximal se llenó con una solución de 10 mg/mL BrU en medio neurobasal y se incubó de esta manera, durante 3 h. La segunda estrategia de marcado de ARNs *in vivo*, se realizó mediante inyección intraperitoneal de BrU (10 mg/g) en ratones a los que previamente se seccionaron los nervios ciáticos (18 h antes del momento de la inyección). Se permitió el marcado de los ARNs neosintetizados por espacio de 30 min, luego de los cuales los ratones fueron sacrificados mediante dislocación cervical y se extrajeron los cabos proximales.

Se realizaron experimentos utilizando diferentes drogas, que incluyeron: α-amanitina (10 µg/mL, Sigma), Latrunculina A (0,07, 0,2, 0.6 y 1,8 µg/mL, Sigma) y colchicina (50 µM, Sigma). En todos los casos, las drogas fueron agregadas al medio con BrU en el que se incubaron los segmentos de nervio ciático, durante todo el tiempo de incubación.

6.2. Tratamiento con ribonucleasa A

Luego de la incubación en medio conteniendo BrU, los segmentos de nervio fueron incubados con 5 o 10 mg/mL de ribonucleasa A en *buffer* PHEM (60 mM PIPES, 25 mM HEPES, 10 mM EGTA, 2 mM $MgCl_2$, pH7,4), durante 1 h a 37°C. A continuación se realizaron 10 lavados en *buffer* PHEM a temperatura ambiente (TA).

6.3. Permeabilización con tritón para remover la tubulina monomérica

Para los experimentos que involucraron la visualización de los microtúbulos, se realizó una permeabilización previa a la fijación de los segmentos de nervio ciático, utilizando un protocolo adaptado de Khawaja *et al.*, (1988). Para visualizar los microtúbulos se utilizan anticuerpos contra tubulina, que reconocen tanto la tubulina incorporada en el polímero (microtúbulos) como su forma monomérica. El protocolo que explicaremos a continuación permite la extracción del monómero, al mismo tiempo que estabiliza los microtúbulos. De esta forma, los microtúbulos se pueden visualizar mediante la marcación con un anticuerpo contra tubulina sin el enmascaramiento de su señal por el monómero tubulina.

Los segmentos de nervio ciático fueron incubados en *buffer* PEM (85 mM PIPES pH6,94, 10 mM EGTA, 1 mM $MgCl_2$) durante 10 min a 25°C y permeabilizados durante 1 h con 0,5% Tritón X-100 en *buffer* PEM. La permeabilización de los nervios tratados con colchicina fue realizada en presencia de dicha droga (50 µM), para impedir la repolimerización de los microtúbulos. Finalmente, los segmentos de nervio ciático fueron lavados una vez con *buffer* PEM, durante 5 min a 25°C.

6.4. Preparación de los segmentos de nervio ciático para inmunocitoquímica e hibridación *in situ*

Los segmentos de nervio ciático fueron fijados en paraformaldehido al 3% en *buffer* PHEM, (TA), durante 30 min en el caso de los nervios procesados para *teasing*, o durante 1 h en el caso de los nervios procesados para criosecciones. Posteriormente, los segmentos fueron lavados 4 veces en *buffer* PHEM, durante 5 min, a TA.

Los nervios procesados para *teasing* fueron tratados con 0,2 mg/mL de colagenasa (Sigma), 5 mM $CaCl_2$ en *buffer* PHM (60 mM PIPES, 25 mM HEPES, 2 mM $MgCl_2$) durante 1 h a 37°C. Se retiró el epineuro de los segmentos de nervio y se procedió a un paso de permeabilización con Tritón X-100 al 0,1% en *buffer* PHEM, durante 30 min (TA). Finalmente, los segmentos de nervio fueron lavados en *buffer* PHEM (3x5 min, TA).

Para la generación de criosecciones, los segmentos de nervio fueron crioprotegidos mediante inmersión en sacarosa al 15% durante toda la noche a 4°C y luego inmersión en sacarosa al 30% nuevamente toda la noche a 4°C. Finalmente los segmentos de nervio fueron incluidos en Cryo-Glue (SLEE Mainz) y cortados a 10-15 µm en criostato. Las secciones fueron utilizadas inmediatamente o mantenidas a -20°C hasta su uso.

6.5. Inmunocitoquímica

El protocolo de inmunocitoquímica fue el mismo para los nervios procesados para *teasing* y las criosecciones, salvo en los casos que se especifican. El *buffer* de incubación (BI) utilizado en todos los pasos fue 0,1% BSA, 2% glicina en *buffer* PHEM. Las muestras fueron incubadas en *buffer* de bloqueo (BB -suero de cabra al 10% en BI) durante 30 min (TA). A continuación se incubaron con los anticuerpos primarios apropiados, durante toda la noche a 4°C en el caso de los nervios procesados para *teasing* o 2 h (TA) en el caso de las criosecciones. Los anticuerpos primarios utilizados en el presente trabajo fueron: anti-bromodeoxiuridina (1/20, Roche), anti-bromodeoxiuridina (1/300, Sigma), anti-bromodeoxiuridina (1/200, ABBIOTEC), anti-ribosomas (1/1000, (Kun *et al.*, 2007)), anti-subunidad 1 del complejo IV mitocondrial (1/200, Abcam), anti-CASPR (1/300, Abcam), anti-miosina Va (1/100, generosamente cedido por Roy Larson), anti-β-tubulina (1/100, Abcam), anti-KIF5B (1/50, Sigma), anti-KIF1A (1/200, Abnova) y anti-KIF1B (1/200, Abnova). Luego de la incubación con los anticuerpos primarios, las muestras fueron lavadas con *buffer* de incubación (6x5 min, TA): La incubación con los anticuerpos secundarios se realizó (1 h, TA) incluyéndose las sondas fluorescentes si correspondía. Los anticuerpos secundarios utilizados fueron: anti-conejo hecho en cabra conjugado a Alexa 488, Alexa 555 y Alexa 633 (1/1000, Invitrogen) y anti-ratón hecho en cabra conjugado a Alexa 488, Alexa 555 y Alexa 633 (1/1000, Invitrogen). Las sondas fluorescentes mencionadas fueron: DAPI (0.3 nM, Invitrogen), faloidina conjugada a Alexa-543 (1/150, Invitrogen) y faloidina conjugada a Alexa-633 (1/150, Invitrogen). Se procedió, entonces, a lavar nuevamente las muestras (6x5 min, TA). Finalmente, las criosecciones fueron montadas utilizando Pro-Long Gold Antifade (Invitrogen). En el caso de los

nervios procesados para *teasing*, el montaje en Pro-Long Gold Antifade (Invitrogen) fue precedido por el peinado de las fibras utilizando una pinza de relojero #5.

6.6. Hibridación *in situ*

Para la generación de las sondas utilizadas en hibridación *in situ* se clonó un fragmento (nucleótidos 1858 a 1959, NM_010910) del gen que codifica para la subunidad liviana de los neurofilamentos (NF-L) en el plásmido pJET (Fermentas). Dicho plásmido fue utilizado como molde en reacciones de PCR para generar moléculas de ADN doble cadena que fueron subsecuentemente utilizadas como molde para la síntesis de sondas de ARN. Los oligonucleótidos utilizados en las reacciones de PCR contenían, además de los nucleótidos específicos necesarios para amplificar el fragmento de 101 nucleótidos del NF-L, las secuencias promotoras T7 (oligonucleótido líder) y SP6 (oligonucleótido reverso). De esta manera, los fragmentos de ADN doble cadena generados pudieron ser utilizados para la síntesis de sondas de ARN mediante transcripción *in vitro.* La transcripción se llevó a cabo utilizando el *DIG RNA Labeling Kit* (Roche), marcando las sondas co-transcripcionalmente con digoxigenina. Se sintetizaron las sondas antisentido y sentido cada una a partir de uno de los promotores disponibles. Las sondas fueron purificadas, cuantificadas y mantenidas a -80°C hasta su uso.

Para los experimentos de hibridación *in situ* se utilizaron criosecciones de 10 µm de espesor. Todas las incubaciones fueron realizadas a TA, a menos que se indique. Se bloqueó la peroxidasa endógena del tejido, mediante incubación (1 h) con 0,03% H_2O_2. Las criosecciones fueron luego lavadas con 4X SSC (3x5 min) e incubadas en *buffer* de hibridación (4X SSC, 50% formamida, 10% dextran sulfato, 0,1 mg/mL ARNt, 0,5 mg/mL ADN de esperma de salmón) por 2 h a 54°C. La etapa de hibridación con las sondas (NF-L antisentido y sentido) se realizó utilizando una concentración final de 0,5 ng/mL de las mismas en *buffer* de hibridación (4 h a 54°C). Se realizaron lavados (2x10 min) de rigurosidad creciente: 4X SSC + 50% formamida, 2X SSC, 1X SSC, 0,5X SSC y 0,25X SSC. Las criosecciones fueron tratadas con el protocolo de inmunocitoquímica ya descrito, para revelar la señal de las

sondas. Para ello se utilizó un anticuerpo anti-digoxigenina conjugado a peroxidasa (1/20, Roche) y el *TSA Amplification Kit* (Invitrogen), siguiendo las instrucciones del fabricante.

6.7. Microscopia confocal

Los experimentos de inmunocitoquímica e hibridación *in situ* fueron visualizados en un microscopio confocal Olympus FV300, equipado con un lente Plan Apo N 60x de inmersión en aceite y cuatro líneas láser (405, 488, 543 y 633 nm). Para todos los análisis cuantitativos se adquirieron al menos 10 campos. En todos los casos donde se comparó niveles de fluorescencia entre dos muestras, todos los parámetros (intensidad de los láseres, voltaje de los fotomultiplicadores, etc) durante la adquisición de las imágenes fueron mantenidos constantes. Las imágenes fueron procesadas con los programas Fluoview e ImageJ.

6.8. Microscopía FRET confocal

Para los análisis de microscopía FRET confocal se adquirieron imágenes utilizando muestras con marcación simple (sólo el donador y sólo el aceptor) y doble (donador y aceptor, ambos marcados en la misma muestra). Se colectaron cuatro imágenes de referencia del aceptor sólo (excitando con ambos láser y recogiendo en el canal del aceptor), cuatro del donador sólo (excitando con el láser del donador y recogiendo en ambos canales) y al menos seis imágenes del doble marcado (excitando con el láser del donador y recogiendo en ambos canales y excitando con el aceptor y recogiendo en el canal del aceptor). Para evaluar el nivel de *background* se incluyeron muestras tratadas para inmunocitoquímica en las que se excluyó la incubación con anticuerpos primarios. Las imágenes de dichas muestras fueron tomadas excitando con los láseres del aceptor y el donador en ambos canales. Todas las imágenes fueron adquiridas utilizando el mismo voltaje en los fotomultiplicadores y una baja intensidad de los láseres. El análisis de FRET cuantitativo se realizó utilizando el plug-in PFRET para ImageJ (Keck Center for Cellular Imaging, University of Virginia, Charlottesville, VA) (Elangovan *et al.*,

2003; Wallrabe *et al.*, 2003, 2006; Chen and Periasamy, 2006). Las imágenes control se utilizaron para calcular el valor de *background*, el cual se sustrajo de las imágenes analizadas. Se crearon regiones de interés (ROIs) automáticamente utilizando el programa PFRET. Para todos los análisis de FRET realizados se utilizaron restricciones idénticas. Los datos generados fueron procesados utilizando Excel.

6.9. Purificación de ARNs bromouridinados

Los ARNs bromouridinados fueron purificados mediante inmunoprecipitación. Para ello, los cabos proximales de nervios ciáticos en regeneración fueron incubados en medio conteniendo BrU como fue explicado anteriormente o en medio sin BrU siguiendo el mismo protocolo. Dado que la purificación de los ARNs bromouridinados se realizó mediante inmunoprecipitación, se incluyó un grupo control en el cual los ARNs no se marcaron con BrU. De esta manera fue posible valorar el grado de purificación inespecífica, es decir cuántos de los ARNs purificados se recogen debido a interacciones inespecíficas del anticuerpo utilizado durante la inmunoprecipitación.

Inmediatamente a la incubación en medio de cultivo, los nervios fueron homogenizados en Trizol (Sigma), con el que se procedió a la purificación del ARN total de la muestra. El ARN total purificado fue cuantificado y se utilizó en reacciones de inmunoprecipitación con el fin de purificar los ARN bromouridinados presentes en la muestra de ARN total. Las reacciones de inmunoprecipitación fueron llevadas a cabo utilizando bolillas magnéticas, (Dynabeads, Invitrogen) conjugadas a Proteína-G. Se mezclaron 40 µL de bolillas magnéticas con 10 µg de anti-bromodeoxiuridina (Abbiotec) en *buffer* RSB (Tris-Cl 10 mM, pH7,4, NaCl 100 mM, $MgCl_2$ 2,5 mM, Tritón X-100 0,4%). La mezcla se incubó con agitación (1 h, 4°C) para permitir la unión de los anticuerpos a la Proteína-G. Las bolillas fueron lavadas (3x) con *buffer* RSB y resuspendidas en 150 µL de *buffer* RSB conteniendo 80U de inhibidor de ribonucleasas (RNaseOUT, Life Technologies) y 2,5 µg de ARNt (Sigma). Las bolillas fueron entonces incubadas en presencia de 20 µg de ARN total purificado a partir de los nervios incubados con BrU o ARN total purificado a

partir de los nervios incubados en medio sin BrU (1 h, 4°C). Las bolillas fueron lavadas (3x) con *buffer* RSB. Finalmente, los ARNs unidos a los anticuerpos fueron eluidos en *buffer* de lisis del *kit* de purificación de ARN *RNAqueous-micro Total RNA Isolation Kit* (Life Technologies). Mediante este mismo *kit* se procedió a la purificación de los ARNs presentes en el inmunoprecipitado, siguiendo las instrucciones del fabricante e incluyendo un paso de digestión con ADNasa. Las muestras fueron cuantificadas utilizando el *Quant-It RNA Assay Kit* (Life Technologies) y mantenidas a -80°C hasta su uso. Dado las características de nuestro diseño experimental, a partir de este paso, para todos los ensayos que realizamos con los ARNs purificados, utilizamos volúmenes iguales de la muestra proveniente de los nervios incubados con BrU (en adelante "ARN-BrU") y de la muestra proveniente de los nervios incubados en medio sin BrU (de aquí en adelante "ARN control")

6.10. Experimentos de reacción en cadena de la polimerasa (PCR)

Las reacciones de PCR fueron realizadas utilizando el *MasterAmp RT-PCR kit*, siguiendo las instrucciones del fabricante. Para las reacciones de RT-PCR se utilizaron 5 ng de ARN control o ARN-BrU sin inmunoprecipitar. En el caso de las muestras luego de la inmunoprecipitación se colocaron 5 ng (contenidos en 1 µL) de ARN-BrU o igual volumen de ARN control, en cada reacción de RT-PCR. Los pares de oligonucleótidos utilizados fueron:

a) CCGGTTCTTCTCTCTAGGTCCC NF-L *forward*;
   GTAGGAGGTCGAAAAGTACGGC NF-L *reverse*.
b) AGTCGAGGCCCCCCAAGCTCA NF-M *forward*;
   CAGAGGCTGCCAATTCCTCTGC NF-M *reverse*.
c) AGCTGCGATGGCATCGACTCTCTC Ank-G *forward*;
   AGCGCTTTCTCCACCGTCGTGTCAG Ank-G *reverse*.

El protocolo de reacción incluyó los siguientes pasos: 1) una rampa inicial de aumento de temperatura desde 50 a 60°C, con un Δt = 1°C, 1 min/paso, 2) 20 min de incubación a 60°C, 3) 30 ciclos de 30 seg a 96°C de desnaturalización, 30 seg a 52°C de *annealing* y 1 min a 68 °C de extensión. Las reacciones de amplificación fueron visualizadas mediante electroforesis en gel de poliacrilamida y tinción con plata.

6.11. Generación de bibliotecas de ADNc y secuenciación masiva de los ARNs bromouridinados

La secuenciación masiva se realizó utilizando la tecnología Ion Torrent (Life Technologies). Dado que nuestro interés se centró en la identificación de los ARNm presentes en la muestra, procedimos en primer lugar a retirar los ARNr presentes en la misma, utilizando el *kit Low input RiboMinus eukaryote system v2* (Life Technologies) y siguiendo las instrucciones del fabricante. Para las reacciones de remoción de los ARNr, utilizamos 50 ng de ARN total procedente de la inmunoprecipitación de la muestra BrU, contenidos en 15 µL, e igual volumen de la muestra control (la cual contenía cantidades no cuantificables de ARN). Incluimos además, un conjunto de ARNs control externos (*ERCC ExFold RNA Spike-In mixes*, Ambion). Las bibliotecas fueron generadas utilizando el *Ion-Total RNA-Seq kit v2* (Life Technologies), a partir de 10 µL de las muestras control o BrU, producto de la remoción de los ARNr, siguiendo las instrucciones del fabricante. Las bibliotecas control y BrU fueron marcadas con un "código de barra" diferente para cada una utilizando el *Ion Xpress Barcode Adapters 1-16* (Life Technologies). Las bibliotecas fueron combinadas y se procedió a realizar la PCR en emulsión utilizando el *Ion PGM template OT2 200 Kit* (Life Technologies). La secuenciación se realizó en chips *Ion 318 chip* (Life Technologies) utilizando el *Ion PGM 200 Sequencing Kit v2* y siguiendo las instrucciones del fabricante.

Para evaluar los parámetros de calidad de las secuencias se utilizó el programa libre *fastqc* (http://www.bioinformatics.bbsrc.ac.uk/projects/fastqc). El "recorte" (*trimming*) por calidad (>20) y largo (>50) de las secuencias obtenidas se realizó mediante el programa libre *sickle*. Para el alineamiento de las lecturas contra los cromosomas nucleares (NC_005100 a NC_120 y NC_024475) y mitocondrial (KM_577634) de *Rattus norvegicus* utilizamos el programa *CLC Genomics Workbench 6.5* (CLC Bio). Realizamos un análisis de RNASeq, con los parámetros por defecto del programa. De esta manera se obtuvieron tablas con el número de lecturas que alinearon a cada gen. Se calculó así mismo el RPKM para cada uno. Los datos finales fueron analizados en EXCEL, conservando en la lista aquellos ARNm que presentaran más de 5 lecturas un valor de RPKM>1. El análisis ontológico se realizó utilizando el

programa *on line Database for Annotation, Visualization and Integrated Discovery (DAVID)* v6.7 (http://David.abcc.ncifcrf. gov/) (Huang *et al.*, 2009a; b). La lista de ARN-BrU obtenida se comparó con las siguientes listas: a) genes expresados en nervio ciático en regeneración (24 horas) determinados a partir de experimentos de microarreglos (Li *et al.*, 2013); b) ARNm presentes en axones motores maduros (Farías J., Tesis de Maestría "Análisis del transcriptoma de axones mielínicos mediante secuenciación masiva", PEDECIBA, Area Biología, Agosto 2014); c) ARNm que interactúan con miosina Va determinados mediante microarreglos (trabajo V de esta tesis). Los diagramas de Venn fueron generados utilizando la herramienta disponible *online* del Centre de Recherche Public Santé (http://www.bioinformatics.lu/venn.php).

7. RESULTADOS

La realización de esta tesis implicó la participación de dos grupos de trabajo del Instituto de Investigaciones Biológicas Clemente Estable (el Departamento de Proteínas y Ácidos Nucleicos y el Departamento de Genómica) así como numerosas colaboraciones a nivel internacional, que dieron lugar a varias publicaciones, algunas de las cuales serán presentadas en este apartado. En los siguientes párrafos quisiera dejar constancia de mi participación formal en cada una de ellas.

Trabajo II: Diseño de todos los experimentos en colaboración con el Dr. Sotelo y el Dr. Mercer. Realización de los experimentos que dieron lugar a las figuras 2, 3, 4, 5, 6, 7, 8, 9, S1, S2, S3 y S4. Colaboración con los Dres. Sotelo y Mercer en la redacción del manuscrito.

Trabajo III: Diseño de todos los experimentos en colaboración con Horst Wallrabe. Realización de todos los experimentos y análisis del artículo. Redacción del manuscrito.

Trabajo IV: Diseño y realización de todos los experimentos. Redacción del manuscrito.

Trabajo V: Colaboración con la Mag. Farías en la realización de los experimentos que dieron lugar a la figura 4.

7.1. Capítulo I.

Transferencia de ARN desde la célula de Schwann al axón.

7.1.1. RESUMEN

En el trabajo presentado en este capítulo, se aportaron las pruebas de la existencia de una transferencia de ARNs desde la célula de Schwann al axón en el SNP. Para demostrar este fenómeno, los nervios ciáticos (intactos o previamente seccionados), fueron extirpados e incubados en medio de cultivo conteniendo bromouridina (BrU). Así, el ARN neosintetizado en los nervios ciáticos normales y en regeneración se marcó co-transcripcionalmente. El ARN marcado (ARN-BrU) fue posteriormente identificado mediante un anticuerpo anti-BrdU en las fibras peinadas, mediante inmunomicroscopía confocal. El diseño experimental utilizado (figura 2A-D, trabajo II) impide que los ARNs neosintetizados en el núcleo neuronal sean marcados con BrU porque los cuerpos neuronales no están presentes durante la marcación. La señal de los ARN-BrU puede observarse en el citoplasma de la célula de Schwann, pero también en el axón (figura 2, trabajo II). Por esta razón, se postuló que estos ARN-BrU solo podían haber sido sintetizados en la célula de Schwann y llegar al axón por transferencia de célula a célula. La transferencia es un evento dinámico, pudiendo observarse que el aumento de la señal de los ARN-BrU en el axón es dependiente del tiempo de incubación del nervio en medio con BrU (figura S1, trabajo II). El tiempo de incubación del nervio en BrU también influye en la distancia alcanzada por los ARN-BrU dentro del axón (figura 2, trabajo III). Para comprobar que la presencia de ARN-BrU en el axón no se debe a artefactos producidos por el hecho de realizar el marcado en explantos de nervio ciático, se llevó también a cabo la marcación de los ARNs neosintetizados *in vivo*. La distribución de los ARN-BrU en las fibras de los experimentos *in vivo* es la misma que se observa en los experimentos *in vitro*, tanto en nervios en regeneración de rata (figura S2, trabajo II), como en nervios de ratón (figura S4, trabajo II). Se pudo observar que la transferencia glia-axón de ARNs tiene lugar durante la regeneración axonal, pero también en las fibras normales, sólo que en menor cantidad (figura 2G, trabajo II). Al parecer, la transferencia de ARN desde la célula de Schwann al axón es un evento normal pero juega un papel de mayor importancia durante la regeneración axonal en nervios lesionados.

Los ARN-BrU se concentran en los nodos de Ranvier (figuras 2E, S2 y S4, trabajo II) y las incisuras de Schmidt-Lantermann (figura 2H, trabajo II). Lo que llevó a postular que estos son los sitios por donde ocurre la transferencia. A una menor magnificación, la señal de BrU muestra una alta concentración en los extremos lesionados de los axones que decrece en dirección proximal (figuras 3, S2 S4, trabajo II). Los ARN neosintetizados co-localizan parcialmente con la señal de los ribosomas detectados mediante inmunohistoquímica (figura 3A, trabajo II). Por una parte, esto sugiere que los ARNs ribosomales pueden ser parte de la población de ARNs transferidos. Por otra, existen ARNs de otra naturaleza (quizá ARNm, lo que discutiremos más adelante) que también son transferidos, y por último, que los ARNm y los ribosomas pueden ser transferidos por separado.

En este trabajo, se realizaron también una serie de controles que permitieron inferir que la señal del anticuerpo que reconoce la BrU, se debe al reconocimiento de moléculas de ARN neosintetizado. Estos controles incluyeron la inmunomarcación de fibras que fueron incubadas en medio sin BrU (figura 4B y B', trabajo II), la inmunomarcación en ausencia de anticuerpo primario (figura 4C y C'), y el tratamiento de las fibras con ARNasa posteriormente a la incubación de las fibras en medio con BrU (figura 4D y D'). En ninguno de estos controles se observa marcación, lo que demuestra que la señal del anticuerpo anti-BrdU observada en las fibras del SNP se debe al reconocimiento de moléculas de ARN neosintetizado.

Se indagó si el ARN-BrU podía originarse por la síntesis mitocondrial de ARN y para ello se realizaron ensayos de inmunomarcación utilizando un anticuerpo que reconoce una proteína mitocondrial. La señal de este anticuerpo co-localiza con los ARN-BrU, aunque la mayor parte de la señal del anticuerpo contra ARN-BrU no lo hace (figura 5, trabajo II). Es decir, la transcripción de ARNs en la mitocondria da lugar a una pequeña porción de la señal de ARNs neosintetizados en el axón, pero no a la gran mayoría. Estos ARNs tienen que tener otro origen. Al realizar la marcación con BrU en presencia de alfa-amanitina (un inhibidor de la ARN polimerasa II), la señal de los ARNs neosintetizados en el dominio axonal disminuye cerca de dos veces (figura 7 A-E, trabajo II). Estos experimentos tienen dos connotaciones importantes. Por un lado, apoyan el postulado de que estos ARNs fueron sintetizados en el núcleo

de la célula de Schwann, dado que el núcleo neuronal no está presente en el momento de la marcación con BrU. Por otra parte, también demuestran que los ARNs mensajeros son parte de la población de ARNs neosintetizados y transferidos al axón. Para comprobar esto, al menos para un ARNm en particular, se realizaron experimentos de hibridación *in situ*, utilizando una sonda que reconoce el ARNm de la subunidad liviana de los neurofilamentos (NF-L). La señal de esta sonda co-localiza parcialmente con los ARNs neosintetizados transferidos al dominio axonal (figura 7F, G), lo que demuestra que el ARNm de NF-L puede ser parte de la población de ARNs sintetizados en la célula de Schwann y transferidos al axón.

En el trabajo II también se publicaron los resultados experientales que nos llevaron a responder parte del mecanismo de transporte de los ARNs transferidos desde la célula de Schwann al axón. Estos resultados serán presentados en el capítulo II de la presente tesis.

7.1.2. TRABAJO II.

Sotelo-Sosa J. R.; Canclini L.; Kun A.; Sotelo-Silveira, J.R.; Xu, L.; Wallrabe, H.; Calliari, A.; Rosso G.; Cal K.; Mercer, J.A. Myosin-Va-Dependent Cell-To-Cell Transfer of RNA from Schwann Cells to Axons. PLoS ONE, 8 (4), e61905, 2013

OPEN ACCESS Freely available online

PLOS ONE

Myosin-Va-Dependent Cell-To-Cell Transfer of RNA from Schwann Cells to Axons

José R. Sotelo[1]*, Lucía Canclini[1], Alejandra Kun[1,2], José R. Sotelo-Silveira[3,4], Lei Xu[5], Horst Wallrabe[6], Aldo Calliari[8], Gonzalo Rosso[1], Karina Cal[1], John A. Mercer[5,7]*

1 Department of Proteins and Nucleic Acids, Instituto de Investigaciones Biológicas Clemente Estable, Montevideo, Uruguay, **2** Biochemistry Section, Facultad de Ciencias, Universidad de la República, Montevideo, Uruguay, **3** Department of Genetics, Instituto de Investigaciones Biológicas Clemente Estable, Montevideo, Uruguay, **4** Cell Biology Department, Facultad de Ciencias, Universidad de la República, Montevideo, Uruguay, **5** McLaughlin Research Institute, Great Falls, Montana, United States of America, **6** Department of Biology, University of Virginia, Charlottesville, Virginia, United States of America, **7** Institute for Stem Cell Biology and Regenerative Medicine, National Centre for Biological Sciences, Bangalore, India, **8** Biophysics Area, Department of Biochemistry, Molecular and Cell Biology, Facultad de Veterinaria, Universidad de la República, Montevideo, Uruguay

Abstract

To better understand the role of protein synthesis in axons, we have identified the source of a portion of axonal RNA. We show that proximal segments of transected sciatic nerves accumulate newly-synthesized RNA in axons. This RNA is synthesized in Schwann cells because the RNA was labeled in the complete absence of neuronal cell bodies both *in vitro* and *in vivo*. We also demonstrate that the transfer is prevented by disruption of actin and that it fails to occur in the absence of myosin-Va. Our results demonstrate cell-to-cell transfer of RNA and identify part of the mechanism required for transfer. The induction of cell-to-cell RNA transfer by injury suggests that interventions following injury or degeneration, particularly gene therapy, may be accomplished by applying them to nearby glial cells (or implanted stem cells) at the site of injury to promote regeneration.

Citation: Sotelo JR, Canclini L, Kun A, Sotelo-Silveira JR, Xu L, et al. (2013) Myosin-Va-Dependent Cell-To-Cell Transfer of RNA from Schwann Cells to Axons. PLoS ONE 8(4): e61905. doi:10.1371/journal.pone.0061905

Editor: Simone Di Giovanni, Hertie Institute for Clinical Brain Research, University of Tuebingen, Germany

Received November 2, 2012; **Accepted** March 15, 2013; **Published** April 23, 2013

Funding: JAM and JRS were supported by National Institutes of Health grant R03 TW007220. JRS-S, AK, AC and LC were supported by Pedeciba, MEyC, and ANII. JRS and AK were supported by Consejo Superior de Investigaciones Científicas and Fcien-UdelaR. JAM was supported by inStem institutional funds from the Department of Biotechnology, Government of India. The funders had no role in study design, data collection and analysis, decision to publish, or preparation of the manuscript.

Competing Interests: The authors have declared that no competing interests exist.

* E-mail: sotelo@iibce.edu.uy (JRS); jam@mri.montana.edu (JAM)

Introduction

The existence and extent of axonal protein synthesis has been a contentious issue for decades, but evidence supporting it has steadily accumulated. In turn, this raises the question of whether the mRNAs translated in the axon are transcribed in the cell body, glia, or both [1–7]. In recent years, evidence from multiple sources supports the hypothesis that Schwann cells in the peripheral nervous system transfer messenger RNA and ribosomes to the axons that they ensheath. Early evidence suggested transfer of newly-synthesized RNA and/or protein from Schwann cells to axons [8–12]. Later studies showed the presence of neurofilament subunits and the mRNAs that encode them in Schwann cells [13–17], suggesting mRNA transfer to axons because these proteins are considered to be axonal-specific proteins. Morphological evidence also has suggested cell-to-cell transfer of ribosomes [18–20]. The most conclusive evidence for ribosomal transfer comes from expression of a tagged ribosomal protein in sciatic nerves of *Wld*^{s} mice following injury [21], and in regenerating nerves of normal mice [22].

The present study shows that axons proximal to transections of rat and mouse sciatic nerves accumulate newly-synthesized RNA that is labeled by bromouridine in the absence of the neuronal cell bodies. The shortest, quickest routes for such RNA to travel from the Schwann cell nucleus to the axon are via the nodes of Ranvier or Schmidt-Lanterman incisures (Fig. 1), also suggested by Twiss and Fainzilber [6]. This BrU-labeled RNA is tightly packaged and F-actin is required for its transfer to axons. We also show that myosin-Va function is required for transfer, as homozygous *Myo5a* null mutant mice fail to accumulate newly-synthesized RNA in axons. Our results conclusively demonstrate cell-to-cell transfer of RNA. They also suggest that the mechanism of transfer may be similar to the mechanism by which melanosomes are transferred from melanocytes to keratinocytes, which also is disrupted to produce the diluted coat color of myosin-Va-deficient mice.

Materials and Methods

Ethics Statement

All mouse work performed at the McLaughlin Research Institute (MRI) was carried out in strict accordance with the recommendations in the Guide for the Care and Use of Laboratory Animals of the National Institutes of Health. The protocol was approved by the Institutional Animal Care and Use Committee (Protocol JAM-32). All surgery was performed under isoflurane anesthesia and all efforts were made to minimize suffering. MRI is fully accredited by AAALAC. All rat and mouse work performed at the Instituto de Investigaciones Biológicas Clemente Estable (IIBCE) was carried out in strict accordance with that institution's Comité de Ética en el Uso de Animales

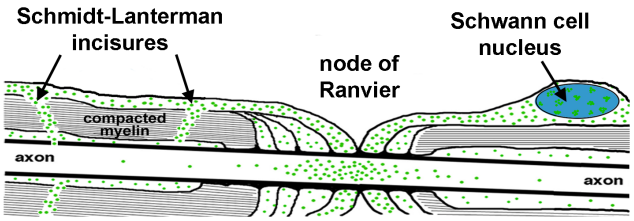

Figure 1. Possible routes for transfer of newly-synthesized RNA from Schwann cells to axons. Diagram of a peripheral fiber showing a longitudinal section of parts of two adjacent Schwann cells and the axon they ensheath. This schematic depicts hypothesized routes (nodes of Ranvier and Schmidt-Lanterman incisures) of transport of BrU-labeled RNA (green dots) between the Schwann cell nucleus and the axon.
doi:10.1371/journal.pone.0061905.g001

(CEUA-IIBCE) under law 18.611 of the República Oriental del Uruguay. The specific protocol was approved by the CEUA-IIBCE (Protocol Sotelo-013/09/2011). All surgery was performed under pentobarbital anesthesia and all efforts were made to minimize suffering.

Sciatic Nerve Transection

Adult Sprague-Dawley or Wistar rats were anesthetized with 50 mg/kg pentobarbital. An incision was made at mid-thigh and the sciatic nerve was transected (diagram, Fig. 2A). Incisions were closed with cyanoacrylate glue. After 18 h recovery, the rats were euthanized and a 2-cm sciatic nerve segment proximal to the transection was removed (Fig. 2B); equivalent contralateral uninjured segments were used as negative controls. The segments were incubated in Neurobasal medium (Invitrogen) containing 2.5 mM bromouridine (BrU, Sigma) for 1, 3 or 6 h at 37°C, 5% CO_2 (Fig. 2C). Representative nodes of Ranvier for all three time points are shown in Fig. S1 in File S1. Only 6-h incubations are shown in all other figures. A negative control in which transected nerve segments were incubated for 6 h in Neurobasal medium lacking BrU also was performed. As an *in situ* control for artifacts that might be caused by explanting the nerve segments for BrU labeling, transection of both sciatic nerves was followed by a proximal crush injury (achieving axonotmesis) after 18 h, instead of the second transection and explantation shown in Fig. 2. BrU was then applied in situ to the left sciatic nerve in the thigh for 3 h under anesthesia [10]. Meanwhile, the injured contralateral nerve was explanted and incubated in BrU for 3 h. In all experiments, segments were washed 10 times for 5 min each in ice-cold PHEM buffer (60 mM PIPES, 25 mM HEPES, 10 mM EGTA, 2 mM $MgCl_2$) to remove unincorporated BrU, then fixed for 30 min in 3% paraformaldehyde in PHEM at room temperature. Segments were treated for 1 h at 37°C with 0.2 mg/ml collagenase (Sigma) in PHEM with 5 mM $CaCl_2$ and without EGTA. The nerve fibers were released from epineurium with #5 forceps and teased at the injured end with 26-gauge needles (Fig. 2D). The segments were permeabilized with 0.1% triton X-100 in PHEM buffer for 30 min at room temperature.

Immunocytochemistry

The incubation buffer for all steps was 0.1% BSA and 50 mM glycine in PHEM buffer. Nerve segments were prepared for immunocytochemistry by blocking in 5% normal goat serum for 30 min at 37°C. Permeabilized fibers were incubated with anti-BrdU (Sigma, 1:300), anti-CASPR (Abcam, 1:300), anti-myosin Va (kindly supplied by Roy Larson, 1:100), or antiserum against purified ribosomes [20] (1:1000) for 1 h at 37°C. Fibers were washed 6 times 5 min each. Secondary antibodies (goat anti-mouse or goat anti-rabbit conjugated with Alexa 488, 546, or 633, all from Invitrogen, all 1:1000) were incubated for 45 min at 37°C. F-actin was detected using fluorescent phalloidin (Invitrogen) added together with secondary antibodies. Fibers were then washed 6 times 5 min each. Finally, individual fibers were teased and mounted in ProLong Antifade (Invitrogen).

α-Amanitin Treatment

RNA polymerase II was inhibited by adding 10 μg/ml α-amanitin (Sigma) during the BrU labeling step described above.

Ribonuclease Treatment

After the wash step to remove soluble BrU, sciatic nerve segments were incubated with RNAse in PHEM buffer at 5 or 10 mg/ml for 1 h, at 37°C. Segments were washed 10 times 5 min in PHEM at room temperature.

Latrunculin A Treatment

F-actin was depolymerized by the addition of 0.07, 0.2, 0.6, or 1.8 μg/ml Latrunculin A (Sigma) during the BrU labeling step.

In situ Hybridization

Incubations were performed at room temperature unless otherwise stated. Frozen 10-μm sections of uninjured mouse sciatic nerves were blocked with 0.03% H_2O_2 for 1 h, washed 3 times 5 min in 4X SSC, and prehybridized in 4X SSC, 50% formamide, 10% dextran sulfate, 0.1 mg/ml tRNA, and 0.5 mg/ml sheared salmon sperm DNA for 2 h at 54°C. Hybridization was carried out for four hours at 54°C in the same buffer plus 0.5 ng/ml of *in vitro* transcribed digoxigenin labeled probe complementary to the small subunit of neurofilament mRNA (nucleotides 1858 to 1959, NM_010910). Sections were washed twice for 10 min in 4X SSC plus 30% formamide at 54°C, then twice for 5 min each in 2X, 1X, 0.5X, and 0.25X SSC. Sections were postfixed in 3% paraformaldehyde in PHEM for 5 min and washed three times for 5 min in PHEM. Blocking was performed as described for immunocytochemistry above. Incubation with primary antibodies (mouse anti-BrdU, HRP-Sheep anti-digoxigenin) was performed overnight at 4°C. Sections were washed 3 times for 10 min in PHEM and then incubated in tyramide amplification reagent according to the instructions of the manufacturer (Invitrogen) for 10 min. Excess tyramide was removed by washing 3 times for 5 min with PHEM. Secondary antibody (Goat anti-mouse Alexa 546 and goat anti-rabbit Alexa 633, Invitrogen) incubations were performed for two hours. Three washes for 5 min with PHEM were performed before mounting in ProLong (Invitrogen).

Confocal Microscopy

Teased fibers were visualized with an Olympus FV-300 confocal microscope, equipped with a Plan Apo N 60X oil NA 1.42 lens and 488, 543 and 633 nm laser lines. Images were processed with Fluoview and ImageJ software. Nodes of Ranvier chosen for quantitative analysis were all within 100 μm of the injured end.

FRET Analysis

To estimate the distance between myosin-Va and newly-synthesized RNA, we performed quantitative fluorescence resonance energy transfer (FRET) between the secondary antibodies recognizing the primary antibodies described above. Images were collected for FRET analysis using single-labeled donor or acceptor samples and double-labeled samples: 4 single-label donor refer-

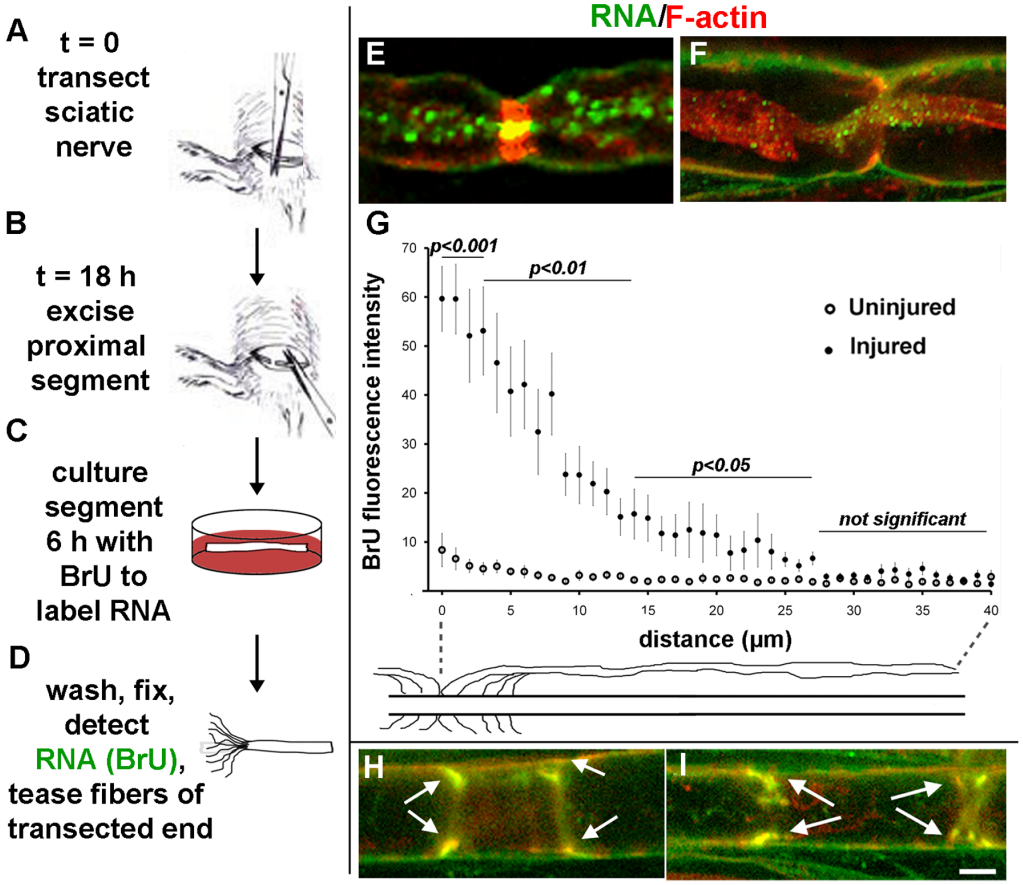

Figure 2. Newly-synthesized RNA is transferred from Schwann cells to axons after sciatic nerve transection. A–D, experimental procedure. **E–F**, single confocal planes of fibers at nodes of Ranvier showing BrU incorporation (green) and F-actin (red). **G**, Axonal BrU fluorescence intensity plotted as a function of distance from the node of Ranvier for uninjured control (open circles) and injured (closed circles) nerves. Statistical significance at each distance between injured and uninjured nerves was determined by Student's t-test. Error bars represent standard errors. **H–I**, single confocal planes showing BrU labeling (green) of F-actin-rich (red) Schmidt-Lanterman incisures (arrows). Bars = 5 μm.
doi:10.1371/journal.pone.0061905.g002

ence images (donor excitation in both donor and acceptor channels); 4 single-label acceptor reference images (donor and acceptor excitation, both in the acceptor channel); six double-label images (donor excitation in donor and acceptor channels, acceptor excitation in acceptor channel). FRET analysis was performed using the precision FRET (PFRET) algorithm plugin for ImageJ [23–25]. Additional images of nonlabeled samples were taken for background subtraction of autofluorescence. Twenty nodes of Ranvier were analyzed in two separate experiments. The selection of appropriate ROIs was made automatically by ImageJ software. Supporting data are shown in Fig. S3 in File S1.

Mouse Sciatic Nerve Transections

The mouse experiments were performed as described above for rats, with the following differences: Age-matched 12–16-day-old C57BL/6J control and *Myo5a*$^{d\text{-}120J}$/*Myo5a*$^{d\text{-}120J}$ *(dilute-lethal)* null mutant mice were anesthetized with isoflurane in oxygen before transection. After euthanasia on the following day, a ~3-mm proximal segment was removed and cultured in BrU. After immunocytochemistry, segments were frozen in OCT and 10-μm longitudinal sections were mounted on slides for confocal microscopy using an Olympus FV-1000. Intraperitoneal injection of the mice with BrU gave identical results to *in vitro* culture, controlling for artifacts that might be caused by the *in vitro* BrU labeling protocol. Intraperitoneal injection also was performed on older (2 mo) wild-type mice and teased fibers were examined as described for rats above.

Results

RNA Transfer from Schwann Cells to Axons

To assay for cell-to-cell transfer of RNA, newly-synthesized RNA was labeled with BrU in a rat sciatic nerve transection protocol (Figure 2A–D). This protocol separates the axons from their cell bodies, making it impossible for the neuronal nucleus to be the source of any newly-synthesized RNA imaged with BrU. Within the nerve segments, we observed two general classes of fibers: those that had little or no BrU signal, likely representing dead or dying fibers that did not survive the injury and explantation, while the other class had robust BrU signals (green).

The most prominent labeling observed was a punctate labeling of axons at nodes of Ranvier (Figure 2E and F). This label gradually decreased with distance from the node (Fig. 2G). The gradient of BrU signal from the nodes of Ranvier to 40 microns in each direction is plotted in Fig. 2G. Analyzing injured vs. uninjured axons at each distance by Student's t-test, the values were statistically different between 0–2 μm ($p<0.001$), 3–13 μm ($p<0.01$), and 14–27 μm ($p<0.05$). Another possible path for transport of material between Schwann cells and axons is through

Schmidt-Lanterman incisures [6]. We saw extensive BrU labeling of these as well (Fig. 2H and I, arrows).

At lower magnification, the heterogeneity of BrU labeling in individual fibers at the injured end of the nerve segment and the distal-proximal gradient of labeling from the transection site is shown in Fig. 3A (green). The concentration of ribosomes is greatly increased (red), but the ribosomal distribution is only partially coincident with the newly-synthesized RNA distribution. The BrU gradient over the 750 μm from the transection site is quantified in Fig. 3B. A distal-to-proximal series of a single representative labeled fiber is shown in Fig. 3C–H, counterstained with fluorescent phalloidin to label F-actin (red). In this single fiber, we observe BrU labeling prominent in axons at the injured tip (Fig. 3C), punctate labeling at nodes of Ranvier (Fig. 3E and G) and in the nuclei (Fig. 3D and F) and outer cytoplasmic wraps of the Schwann cells. The most proximal micrograph (Fig. 3H) shows that the nodal labeling tends to decrease as a function of distance from the injured end, as it lacks axonal RNA.

To ensure that the immunoreactivity we detected was actually due to the incorporation of BrU into RNA synthesized in Schwann cells, we performed a series of negative controls (Fig. 4) in addition to the uninjured negative control (Fig. 2G). The standard conditions are shown in Fig. 4A. The negative controls included performing the procedure in the absence of BrU (Fig. 4B), without primary anti-BrU antibody (Fig. 4C), and with 10 mg/ml ribonuclease A (RNase A) (Fig. 4D). All showed little or no BrU labeling of Schwann cells or axons. Consistent with packaging of the labeled RNA, 5 mg/ml RNase only reduced the BrU signal (data not shown), but 10 mg/ml eliminated it altogether. We also performed the procedure without allowing any time for incubation in BrU to control for nonspecific binding/aggregation of BrU (no labeled RNA was detected, data not shown). To eliminate the possibility that the axonal BrU labeling we observed originated in axonal mitochondria, we labeled mitochondria with antibody raised against complex IV subunit 1 (Fig. 5). There was little overlap between the mitochondrial marker and the BrU signal, indicating that the majority of RNA we observed was not of mitochondrial origin. More importantly, mitochondria appeared as "holes" in regions with high BrU signal (arrows in Fig. 5), suggesting no colocalization. Finally, to show that the observation of labeled axonal RNA was not an artifact of the explant protocol, we performed the labeling in the rat thigh after transection and a

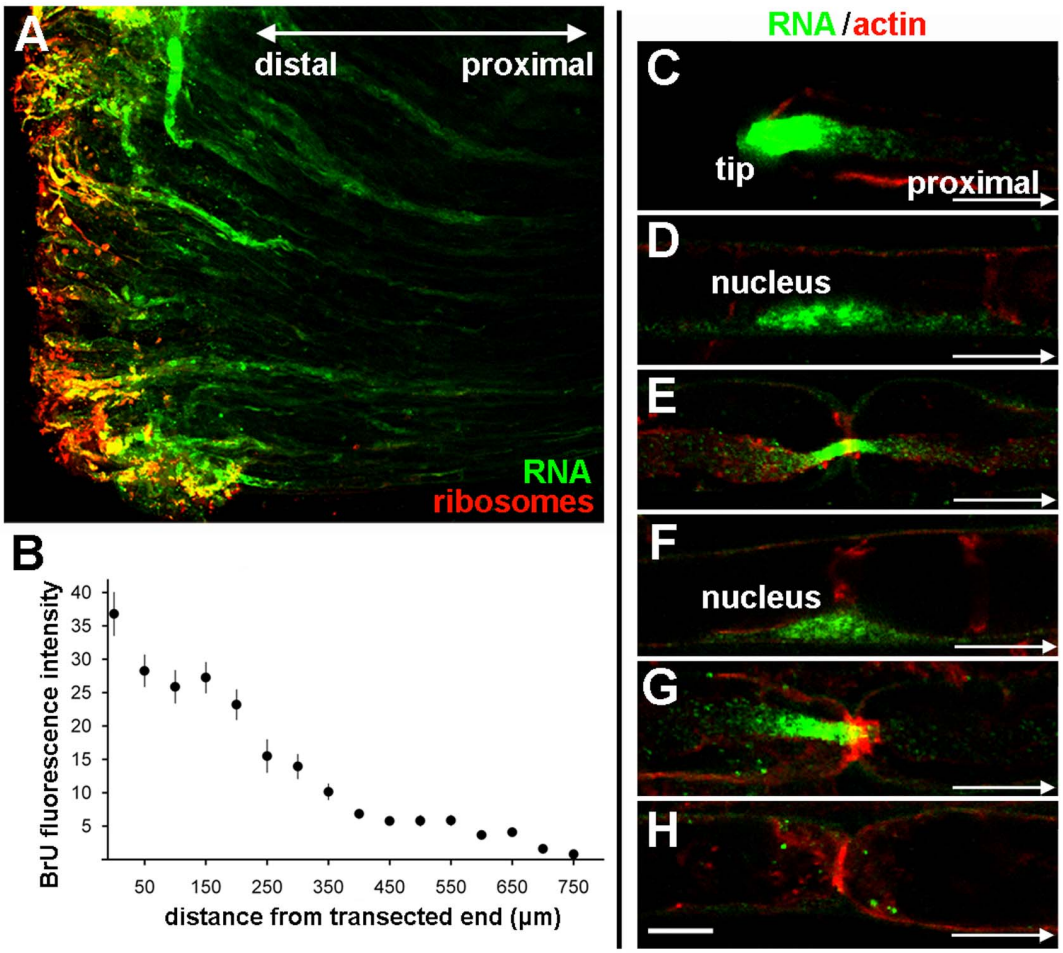

Figure 3. Levels of newly-synthesized RNA decline as a function of distance from nerve injury. A, low-magnification micrograph of transected end showing newly-synthesized RNA (green) and ribosomes detected by anti-P antibody (red). Bar = 100 μm. **B**, BrU-RNA signal plotted as a function of distance from the transection. Each point represents the mean of 10 nerve fragments with standard errors. **C–H**, series of images of a single fiber from the transected end, distal to proximal, showing newly-synthesized RNA labeled by BrU (green) and F-actin (red). **C**, transected end with a high concentration of newly-synthesized BrU-RNA. **D**, first proximal Schwann-cell nucleus from the tip. **E**, first node of Ranvier proximal from the tip. **F**, second Schwann cell nucleus. **G**, second node of Ranvier. **H**, third node of Ranvier. Bar = 10 μm.
doi:10.1371/journal.pone.0061905.g003

crush injury 18 h later, followed by 3 h labeling *in vivo* and in situ (Fig. S2 in File S1). The gradient of BrU labeling from the transection site and the distribution at the nodes of Ranvier were indistinguishable from those observed with *in vitro* labeling. Together, these controls conclusively demonstrate that we are observing transfer of newly-synthesized RNA from Schwann cells to axons.

To demonstrate spatially that the axons are labeled with BrU, we show Z-stacks of fibers in Fig. 6. A single central longitudinal optical section through the axon is shown in Fig. 6A, while the entire stack is shown in Fig. 6B. Cross-sections (boxes in Fig. 6B) are shown in Fig. 6C, D, and E, demonstrating that the axons are indeed labeled and separated from the labeled Schwann cells by unlabeled compact myelin. A significant fraction of BrU was detected on the surface of the fiber, suggesting that the bands of Cajal (spirally shaped outer Schwann cell cytoplasm) contain newly-synthesized RNA (arrows).

To better classify the nature of the transferred axonal RNA, we performed the BrU labeling in the presence of 10 μg/ml alpha-amanitin, which inhibits RNA Polymerase II [26]. The labeling of Schwann cell nuclei (Fig. 7A and B) was reduced. Moreover, in treated fibers nucleoli labeled much more intensely than the rest of the nucleus, consistent with inhibition of transcription by RNA polymerase II, but not rRNA transcription. Inhibition with alpha-amanitin reduced the axonal BrU signal significantly (Fig. 7C and D). Quantitatively, mean measurements with standard error were 55.1 ± 5.1 and 24.0 ± 5.8 for control and alpha-amanitin respectively; the difference was significant at $p = 0.0007$ by Student's t-test. Pooled data are graphed in Fig. 7E, showing that a statistically-significant reduction in BrU intensity occurred throughout the gradient from nodes of Ranvier. These results are consistent with RNA polymerase II as the origin of a significant fraction of transferred RNA.

To assay for steady-state mRNA encoding a known axonal marker, we performed fluorescent *in situ* hybridization with an antisense probe to neurofilament-L (NF-L) mRNA. Our results showed that NF-L mRNA colocalizes with BrU-RNA in both Schwann cells and axons (Fig. 7F and G). While this experiment does not demonstrate cell-to-cell transfer, it is highly suggestive of

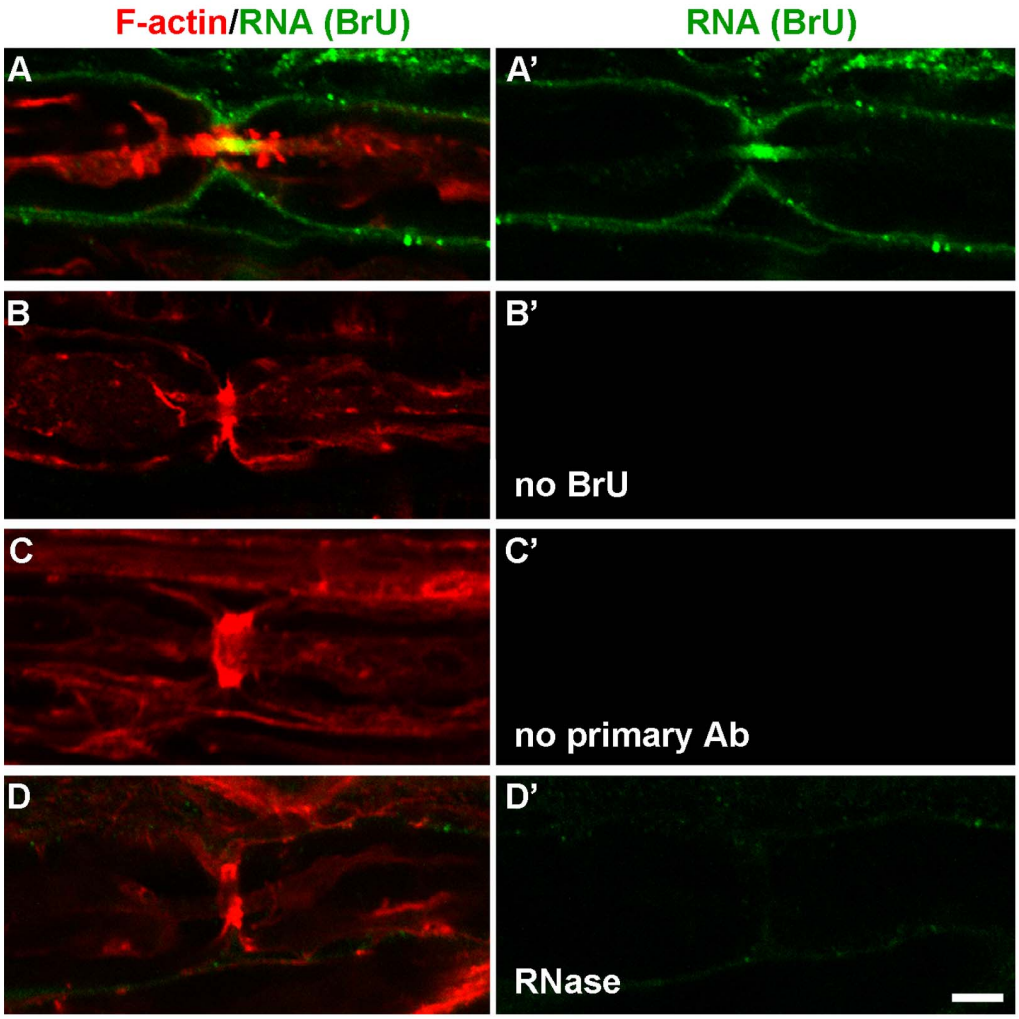

Figure 4. Negative controls for observation of axonal BrU labeling. In all panels, newly-synthesized RNA is shown in green, with F-actin counterstaining shown in red. **A and A'**, experimental condition; fibers were incubated with BrU. **B and B'**, negative control incubated with medium without BrU. **C and C'**, negative control incubated in BrU, but primary anti-BrdU antibody was omitted. **D and D'**, negative control incubated with 10 mg/ml RNAse. Both BrU and F-actin channels at a single confocal plane are shown in **A**–**D**, whereas the BrU channel alone is shown in **A'**–**D'**.
doi:10.1371/journal.pone.0061905.g004

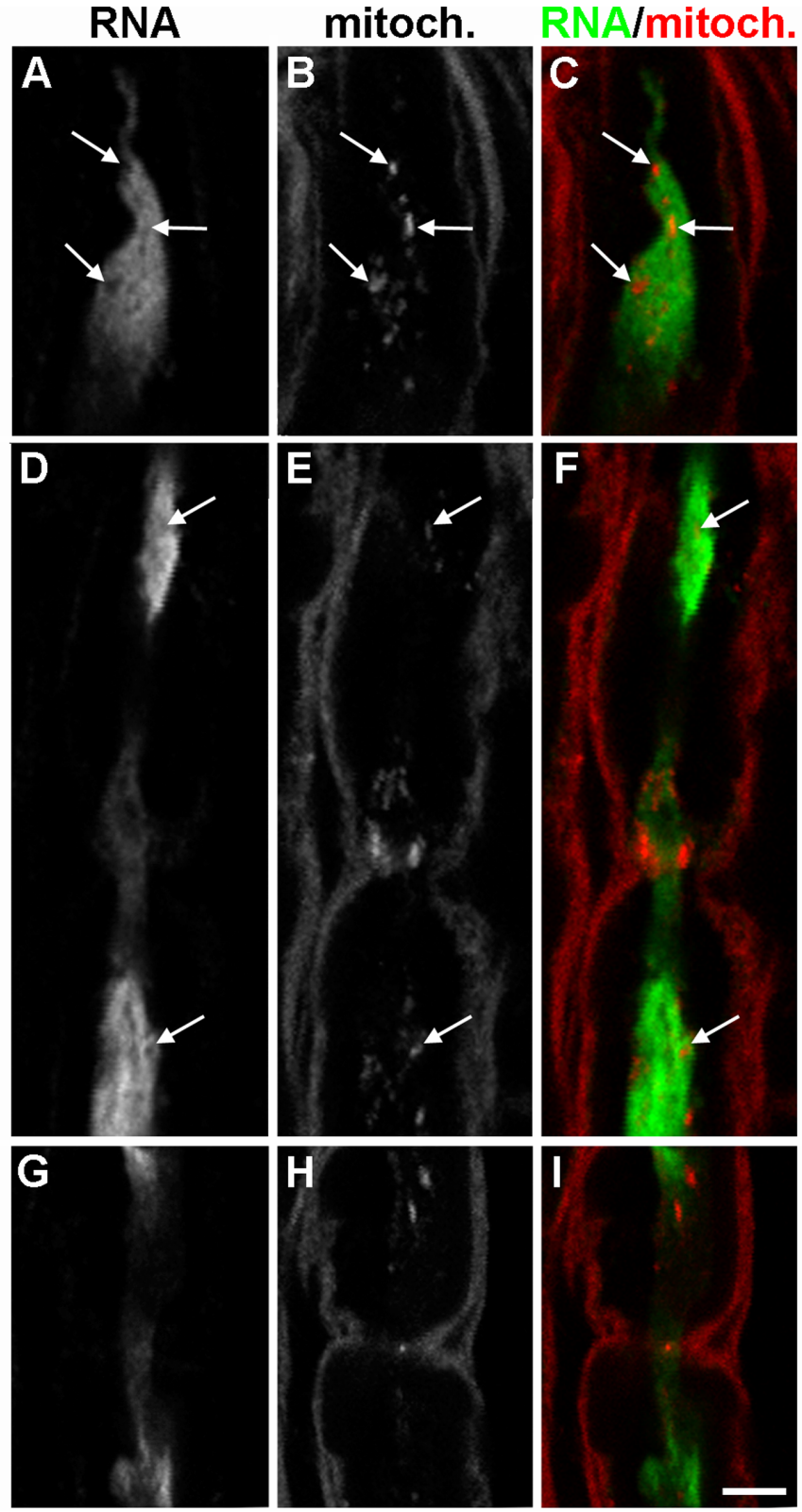

Figure 5. Most newly-synthesized axonal RNA is not mitochondrial. Cryosections of injured BrU-labeled (green) sciatic nerve fragments were stained for BrU **(A, D, G)** and a monoclonal antibody against the mitochondrial Complex IV Subunit I **(B, E, H)**. A paranodal axon is shown in **A–C** and nodes of Ranvier are shown in **D–I**. Mitochondria corresponding to empty spaces in A and D are designated by arrows. Bar = 5 μm.
doi:10.1371/journal.pone.0061905.g005

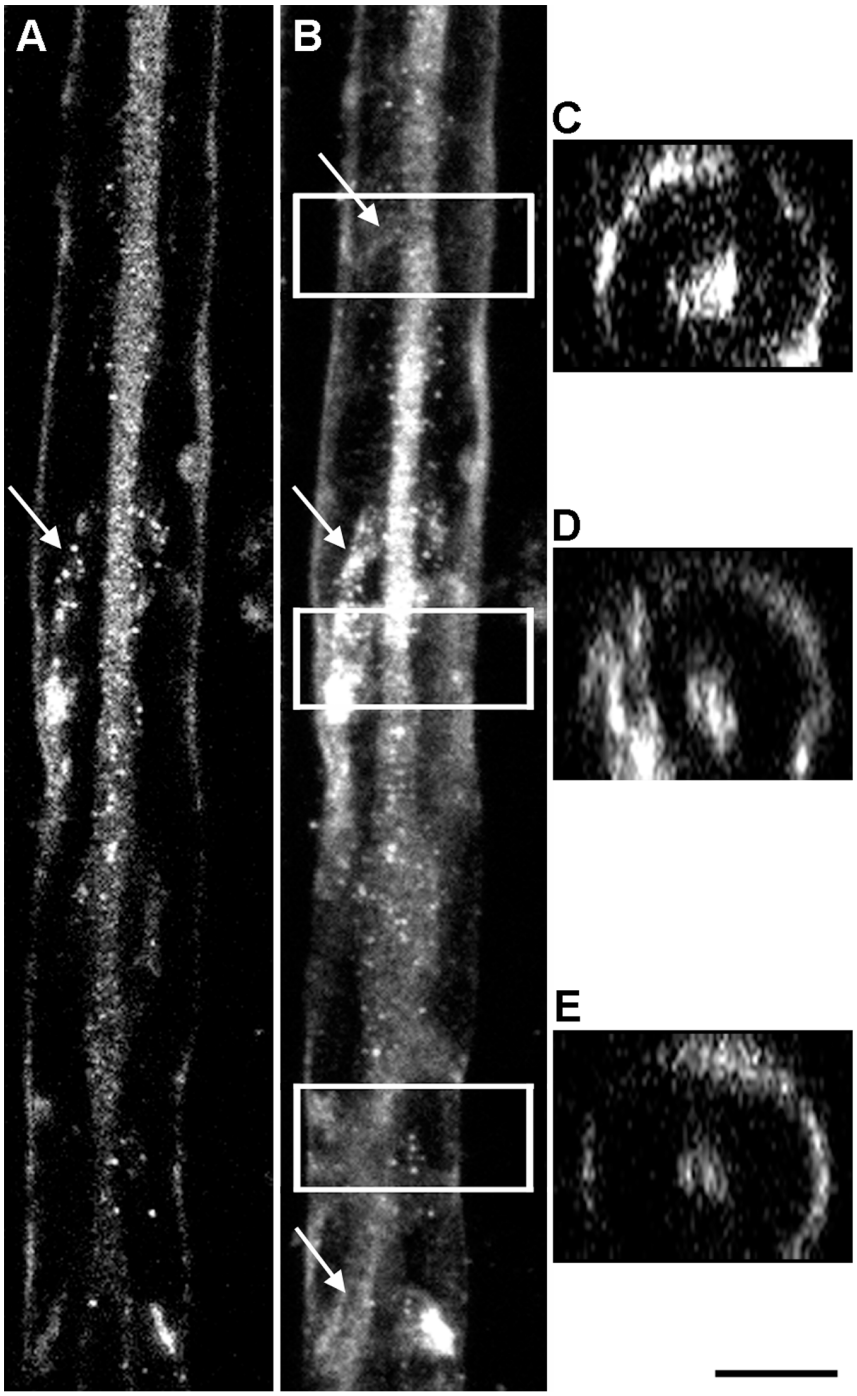

Figure 6. Newly synthesized RNA is present in axons and bands of Cajal. A, confocal plane including a BrU-labeled axon. The myelin is unlabeled. The external border of the myelin is the outer wrap of Schwann cell cytoplasm that includes bands of Cajal. **B**, stack of confocal planes with the plane shown in A as the midpoint, showing the spiraling bands of Cajal (arrows). **C, D, E**, projected cross-sections boxed in the stack shown in panel B showing the separation between newly-synthesized RNA in the axon and band of Cajal. Bar = 10 μm.
doi:10.1371/journal.pone.0061905.g006

transfer since NF-L protein was not detected in Schwann cells (data not shown).

RNA Transfer is F-actin Dependent

The high concentrations of newly-synthesized RNA in actin-rich regions suggested the involvement of actin in cell-to-cell transfer of RNA. To test this hypothesis, we depolymerized F-actin with 0.07–1.8 μg/ml latrunculin A. A representative labeled fiber at each concentration is shown in the left column of Fig. 8. Quantitation of axonal BrU labeling for each latrunculin A concentration is graphed in the right column of Fig. 8. While the graphs in the right column show normalized fluorescence intensities, the absolute intensities for control and 1.8 μg/ml latrunculin A samples are plotted in Fig. 8K. Student's t-test of

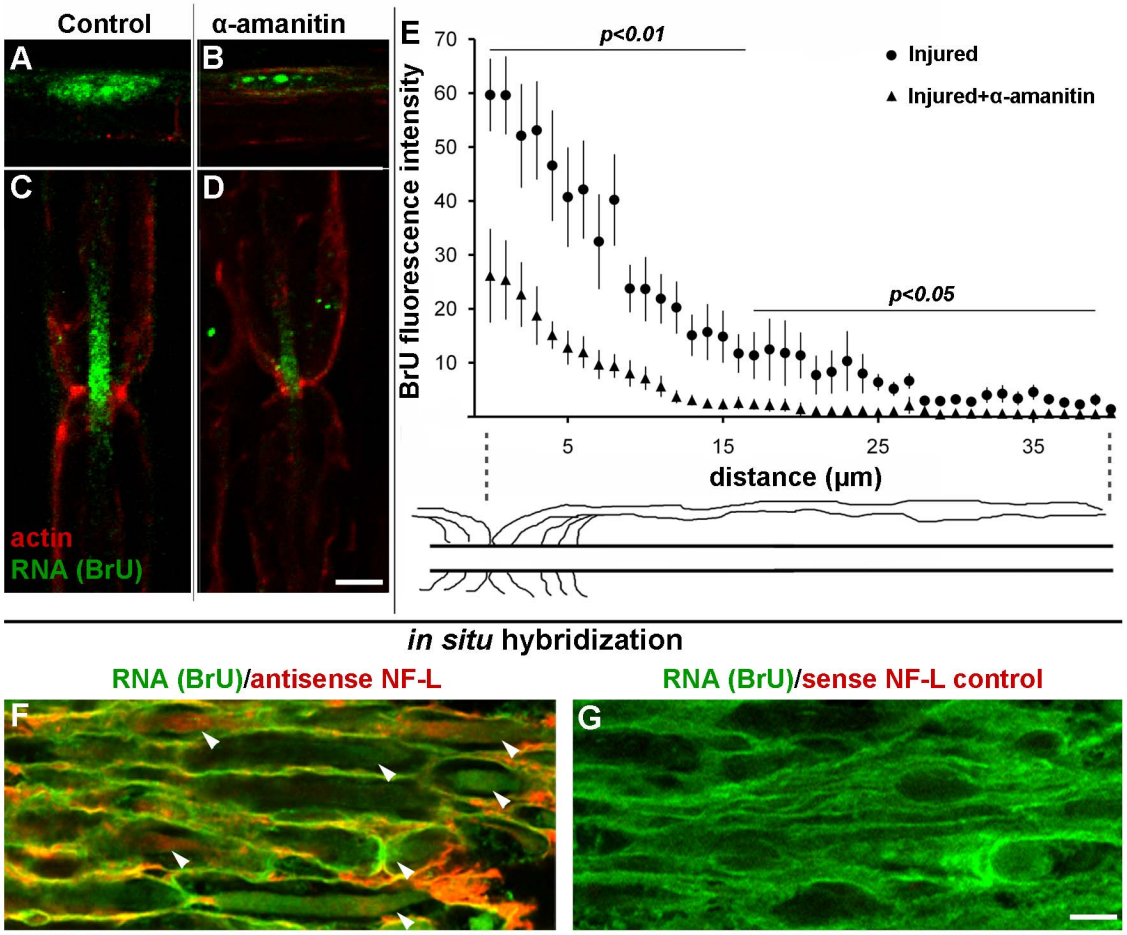

Figure 7. Most of the newly-synthesized RNA is produced by RNA Polymerase II. A–E, injured control nerves without α-amanitin (**A and C**), and injured nerves treated with α-amanitin during the BrU labeling period (**B and D**) were stained for BrU (green) and F-actin with phalloidin (red). **A and B**, Schwann cell nuclei; **C** and **D**, nodes of Ranvier. Bar = 10 μm. **E**, BrU-RNA fluorescence intensities plotted as a function of distance from the node of Ranvier for controls without α-amanitin (circles) and nerves treated with 10 μg/ml α-amanitin (triangles). Statistical significance at each distance was determined by Student's t-test. Error bars represent standard errors. **F**, Neurofilament L (NF-L) mRNA is found in both Schwann cells and axons by *in situ* hybridization (red) and BrU-RNA (green). Arrows are pointing to axons. **G**, negative control NF-L sense probe. Bar = 5 μm.
doi:10.1371/journal.pone.0061905.g007

control vs. experimental intensities in edges and axons were significant with $p = 0.02$ and $p < 0.0001$ respectively. In other words, the relative decrease of BrU signal in the axon was complemented by an increase of signal in the Schwann cells, consistent with inhibition of transport from the latter to the former.

RNA Transfer is Myosin-Va-dependent

The requirement for actin in turn suggested a role for myosin motors, so we performed immunofluorescent detection of myosin-Va after transection. We observed significant colocalization of myosin-Va with newly-synthesized RNA (Fig. 9A–C). To estimate the distance between myosin-Va and newly-synthesized RNA, we performed quantitative fluorescence resonance energy transfer (FRET) between the secondary antibodies detecting the anti-myosin-Va and anti-BrU primary antibodies. The spectral bleedthrough-corrected processed FRET (PFRET) signal [24] was observed in axons and Schwann cell cytoplasm at the nodes of Ranvier (Fig. 8D). Specific FRET signals, as demonstrated by E%, an expression of distances between fluorophores of 1–10 nm, were enriched in axons near the nodes of Ranvier (Fig. 8E, Fig. S3 in File S1). Thus, our data are consistent with a close association of myosin-Va with BrU-RNA in axons.

As a genetic test for a requirement for myosin-Va function in cell-to-cell transfer of RNA, we modified the sciatic nerve transection and BrU labeling procedure developed for adult rats for 12–17-day-old mice, allowing us to perform the experiment on *dilute-lethal* ($Myo5a^{d\text{-}l20J}/Myo5a^{d\text{-}l20J}$) null mutant pups. These mice lack myosin-Va, which causes them to die at 19–21 days of age [27]. To compensate for the smaller diameter of mouse fibers, instead of teasing whole-mount preparations, the segments proximal to the transection were frozen and longitudinally sectioned. The results (Fig. 10) were striking: while wild-type littermate controls (Fig. 10B) had fibers and axons filled with BrU, as well as prominent labeling of bands of Cajal (Fig. 10D, arrowheads), axons of mutant mice had no detectable BrU labeling (Fig. 10A and C). Nodes of Ranvier (arrows) were identified by immunofluorescent detection of the paranodal marker Caspr [28]. To quantify the difference between mutant and wild-type fibers, we measured fluorescence intensities using 20-pixel wide linescans across 50 fibers chosen blindly from 5 mice of each genotype. There were two criteria: the first was greater width, to ensure a bias toward measuring diameters that included

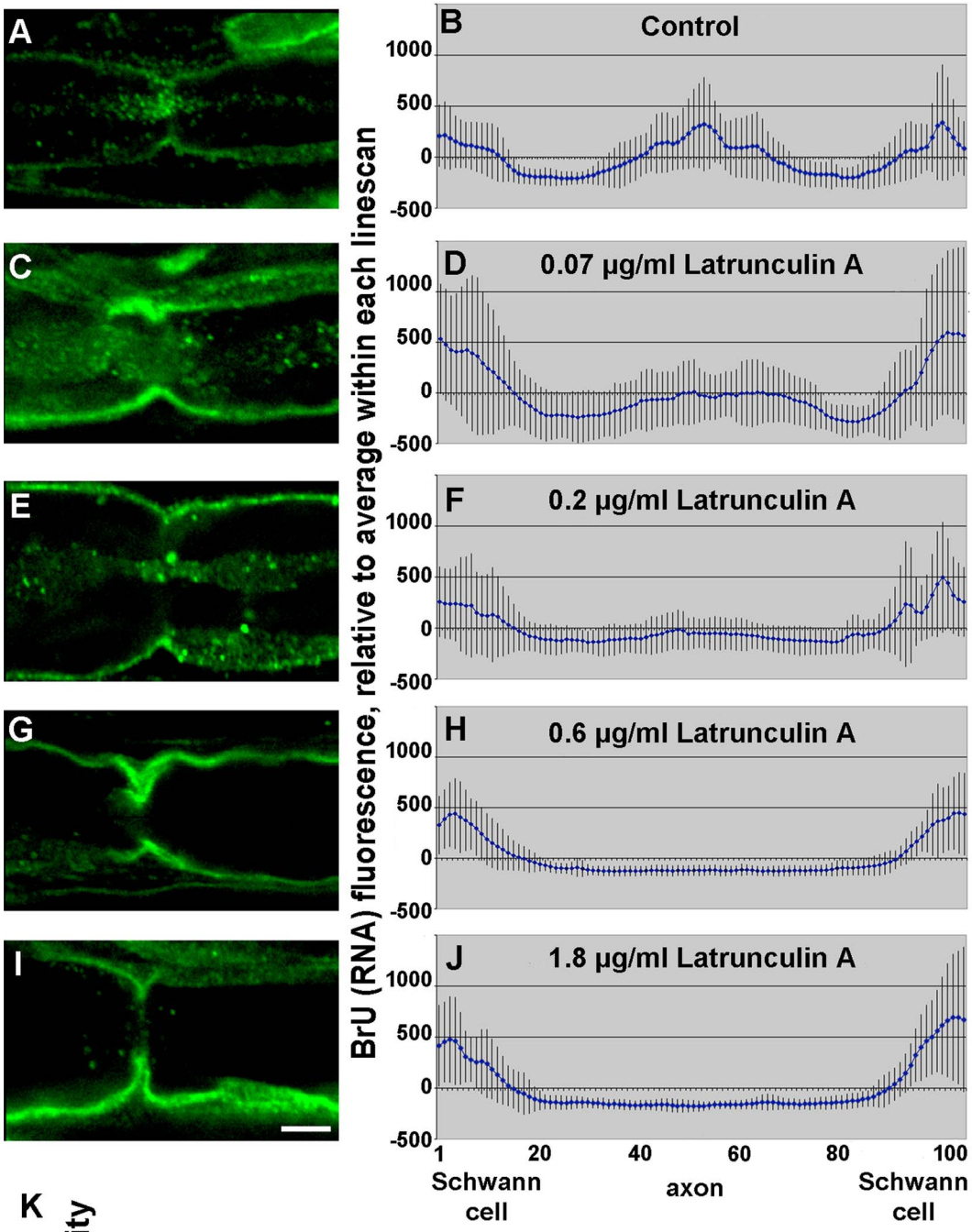
A
B
Control
C
D
0.07 µg/ml Latrunculin A
E
F
0.2 µg/ml Latrunculin A
G
H
0.6 µg/ml Latrunculin A
I
J
1.8 µg/ml Latrunculin A
BrU (RNA) fluorescence, relative to average within each linescan
1000
500
0
-500
1
20
40
60
80
100
Schwann cell
axon
Schwann cell

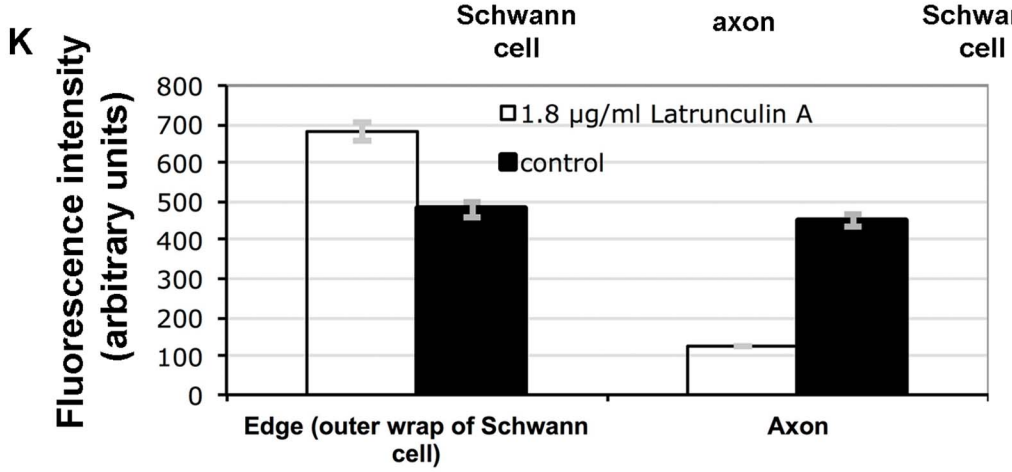
K
Fluorescence intensity (arbitrary units)
800
700
600
500
400
300
200
100
0
1.8 µg/ml Latrunculin A
control
Edge (outer wrap of Schwann cell)
Axon

Figure 8. Actin depolymerization in injured sciatic nerves prevents transfer of RNA into axons. A, C, E, G, I, representative confocal images of BrU labeling at nodes of Ranvier. Bar = 10 μm. **B, D, F, H, J**, quantification of BrU fluorescence from 10 or more line scans across perinodal regions normalized to the mean of each linescan. Error bars represent standard errors. **A and B**, control BrU labeling without Latrunculin A; **C and D**, 0.07 μg/ml Latrunculin A during BrU labeling; **E and F**, 0.2 μg/ml; **G and H**, 0.6 μg/ml; **I and J**, 1.8 μg/ml. **K**, absolute BrU fluorescence intensities for the 8 bins at each edge combined (n = 304), representing RNA in the outer Schwann cell wrap, and the 20 bins in the center of each linescan (n = 380), representing RNA in the axon, for the control untreated and highest latrunculin A concentration (1.8 μg/ml) nerves. Error bars represent standard errors.
doi:10.1371/journal.pone.0061905.g008

axons, and the second was doing linescans more than 100 μm from nodes of Ranvier, since the gradient observed in rat axons was not observed in mice. We normalized and binned the values, then graphed intensity by position along the lines (Fig. 10E), quantitatively demonstrating the lack of axonal labeling. While the values plotted in Fig. 10E were normalized to the mean of each linescan, differences in absolute intensities were apparent as well (Fig. 10F). Student's t-tests of mutant vs. wild-type edges and axons both showed significant differences ($p<0.0001$). Thus, as with the latrunculin A inhibition experiment, the decrease in axonal signal is accompanied by an increase in Schwann cell signal, consistent with inhibition of transport, not synthesis.

Finally, we performed two controls to demonstrate that these observations was not an artifact of labeling an explanted nerve fragment. First, we performed the mice experiment described above using intraperitoneal injection of BrU with identical results (data not shown). Second, we performed the same experiment with intraperitoneal injection on 2-month-old wild-type mice (Fig. S4 in File S1), obtaining results similar to the results of the rat experiments, with gradients extending from nodes of Ranvier.

Discussion

Evidence supporting the transfer of RNA and proteins from glia to axons, providing an additional source of macromolecules to the axon, has been previously reported but is not universally accepted. Pioneering work in the Mauthner axon of goldfish [9] suggested transfer of RNA. In mammals, autoradiography in rat sciatic nerve axons first suggested cell-to-cell transfer [10]. Biochemical assays following disruption of interactions between glia and squid giant axons [1,11] further supported the transfer hypothesis in invertebrates. Ultrastructural studies of first internodal regions of motor axons [19] suggested cell-to-cell transfer of ribosomes, as they showed double-walled vesicles filled with what appear to be ribosomes at the glia-axon interface. This was supported by similar observations during the immunolocalization of ribosomes in sciatic nerve axons [20]. Van Minnen and coworkers used GFP tagging of a ribosomal protein expressed in a lentivirus to show that ribosomes assembled in Schwann cells were likely transferred to the axon [21,22].

Here, by labeling newly-synthesized RNA at the site of axon injury in the complete absence of neuronal cell bodies, we have clearly shown that RNA is concentrated in the likely pathways for cell-to-cell transfer [6] at the nodes of Ranvier and Schmidt-Lanterman incisures (Figs. 2 and 3), that particles have been transferred into the axon, and that the cell-to-cell transfer is actin- and myosin-Va dependent. Our data complement the demonstration of tagged ribosomes in axons [21,22], but there is an important difference: their experiments suggesting cell-to-cell ribosome transfer was done in axons distal to the injury site while our demonstration of cell-to-cell RNA transfer was documented directly at the regenerating end of axons proximal to the injury using a pulse-chase protocol in the complete absence of neuronal cell bodies. The labeling we observed is not an artifact of culturing the nerve fragments *in vitro* for three reasons: first, labeling *in situ* by leaving the injured nerve inside the rat thigh gave indistinguishable results (Fig. S2 in File S1); second, intraperitoneal injection of BrU in the mouse experiment gave the same results as explant culture of the nerve segment; and third, *in vivo* labeling with tritiated uridine gave similar results, but with far lower accuracy in location [10].

We do not yet know whether ribosomes and RNA are transferred separately or together, but our imaging of both (Fig. 3A) does not indicate complete coincidence. Moreover, our other experiments indicate that a large proportion of transferred

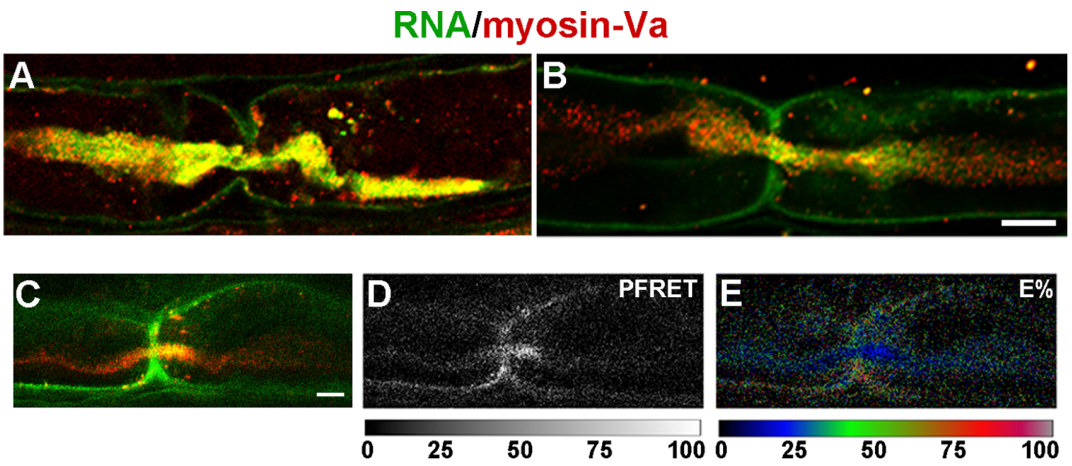

Figure 9. Colocalization of myosin-Va and newly-synthesized RNA in fibers of injured sciatic nerve axons. A, B, and C, confocal micrographs of nodes of Ranvier showing newly-synthesized RNA detected by BrU incorporation (green) and myosin-Va detected by immunofluorescence (red); **D**, processed FRET (PFRET) image for the node shown in panel C. **E**, FRET efficiency (E%) image for the node shown in panels C and D. Scales below panels D and E show lookup tables. Bars = 5 μm.
doi:10.1371/journal.pone.0061905.g009

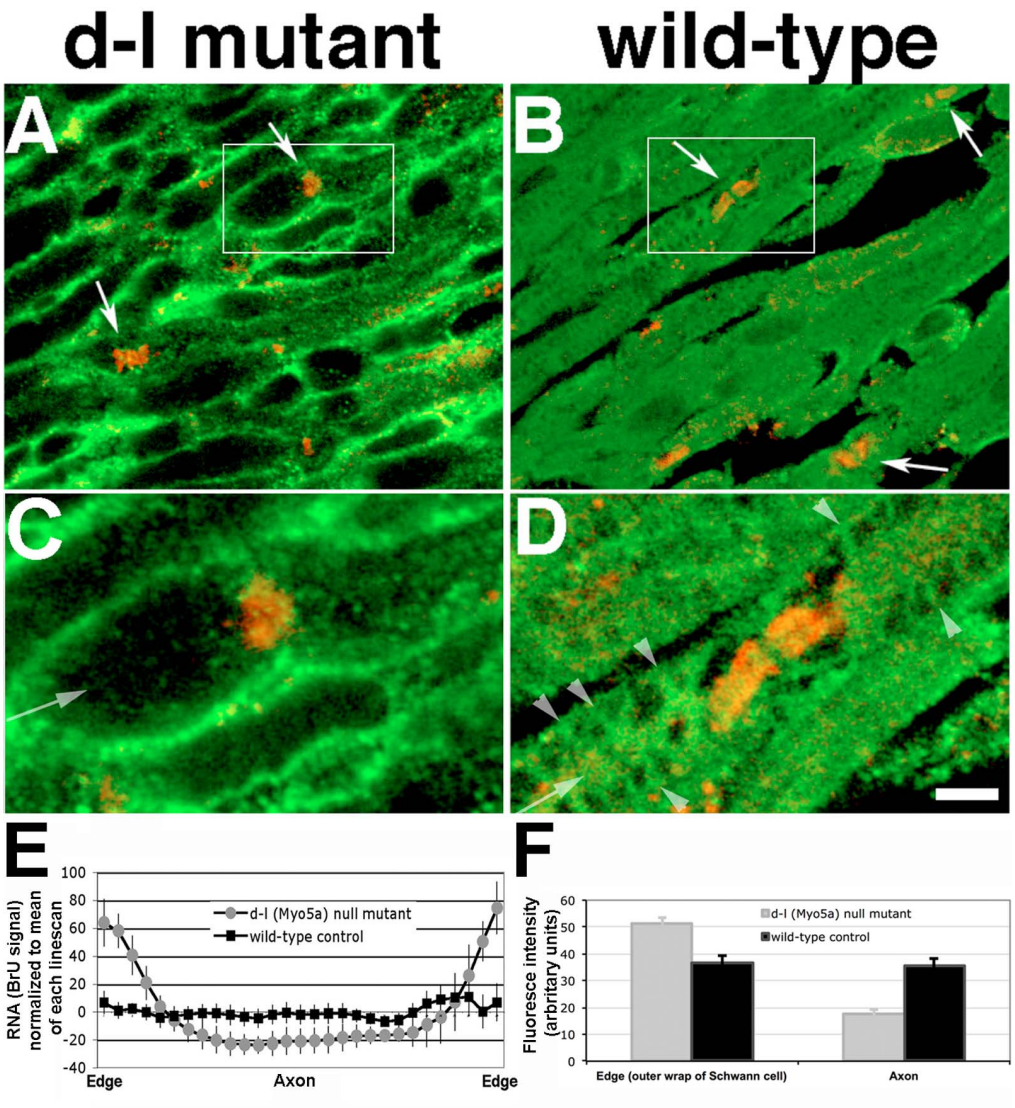

Figure 10. Myosin-Va function is required for transfer of RNA from Schwann cells to axons. Longitudinal 10-μm sections of transected sciatic nerves from null (d-l) *Myo5a* mutant mice have reduced axoplasmic levels of newly synthesized RNA. **A and C**, null mutant; **B and D**, wild-type control. RNA labeled by BrU is shown in green, the paranodal marker Caspr in red. Panels C and D show higher magnification views of boxed regions in panels A and B respectively. Arrows, nodes of Ranvier; arrowheads, bands of Cajal (compare to arrows in Fig. 6). Micrographs are single optical sections from Z-stacks imaged with a laser scanning confocal microscope. Bar = 5 μm. **E**, linescan quantitation of abundance of BrU-labeled RNA across fibers from d-l mutant and wild-type control mice. Edges are the outer wraps of Schwann cells; center approximates the location of the axon. Intensity measurements were normalized to the mean of each linescan. Bars represent standard deviations. **F**, Absolute BrU fluorescence intensities in edges (as shown in **E**, 4 bins at each end combined; n = 160) and centers (10 central bins combined; n = 200). Error bars represent standard errors.
doi:10.1371/journal.pone.0061905.g010

RNA is likely to be mRNA, since most of the axonal RNA was absent in fibers treated with the RNA polymerase II inhibitor alpha-amanitin (Fig.7A–D). Both of these results indicate that our initial BrU experiments were not merely detecting ribosomal RNA. Moreover, we observed only very slight colocalization of BrU with mitochondrial markers, suggesting that very little or none of the newly-synthesized axonal RNA is of mitochondrial origin; nor is it taken up by mitochondria. More importantly, the BrU signal was lower in mitochondria. The BrU labeling was highly punctate and RNase-resistant, suggesting that ribonucleoprotein particles are transferred, similar to previous reports on cytoplasmic RNA transport within neuronal and non-neuronal cells [4,29–31]. We also show that transcripts encoding a well-known neuronal marker protein, NF-L, are present at high levels in uninjured mouse sciatic nerve Schwann cells. While this experiment does not demonstrate cell-to-cell transfer, it is consistent with our model.

Our data begin to delineate the mechanism of cell-to-cell transfer of RNA from Schwann cells to axons, as we have clearly demonstrated that myosin-Va function is required for transfer (Fig. 10). There is an interesting parallel between this requirement and the requirement for myosin-Va function in another neural crest-derived system: the cell-to-cell transfer of melanosomes from melanocytes into hair bulbs and keratinocytes. It is important to note that while the absence of myosin-Va drastically alters melanosome transfer [32], there is no evidence directly implicating myosin-Va in the cell-to-cell transfer itself; more likely, its role may be limited to retaining melanosomes in the periphery of the

melanocyte. We propose a similar mechanism in this case, with myosin-Va helping to retain RNA in the regions of the Schwann cell cytoplasm from which the transferred RNA is taken or donated. Whether the Schwann cell, axon, or both play the active role of cell-to-cell transfer remains an entirely open question.

There are three primary differences between the mouse data and the rat data. The first is the lack of any gradient of BrU immunoreactivity spreading out from the nodes of Ranvier. This is likely caused by a higher metabolic rate in the very young mice relative to that of the adult rats; shortening of the BrU labeling period to as little as 20 min did not produce a gradient (data not shown). Consistent with this hypothesis, labeling the injured sciatic nerves of 2-month-old, wild-type mice yielded similar results to the rat experiments (Fig. S4 in File S1). The second is the difficulty in distinguishing axons in the wild-type fibers, again due to the young age of the mice. The third difference is the thickness and raggedness of the Schwann-cell labeling in the mutant mice, likely because myelination is in progress at this age.

While the data presented here are from injured nerves (with the exception of the comparison of BrU gradients in Injured to Uninjured (Fig. 2) and *in situ* hybridization data in Fig. 7), they are provocative when combined with previous observations in uninjured axons: depolymerization of F-actin by cytochalasin B inhibits axonal protein synthesis [33], and that myosin-Va and the mRNA encoding it are present in periaxoplasmic ribosomal plaques in uninjured axons [34]. This raises interesting questions: first, is myosin-Va function required for axonal protein synthesis from mRNAs that originate in the neuronal soma; and second, does cell-to-cell transfer of RNA occur developmentally? We are addressing both questions using transgenic and knock-in mice with tissue-specific expression of tagged mRNAs and proteins.

In summary, these data confirm and extend our understanding of the complex relationship between glia and the axons they ensheath. This relationship is crucial in understanding mechanisms underlying responses to injury and neurodegeneration, as well as in designing therapeutic strategies that exploit intercellular transport for both retrograde signaling to the cell body [35] and controlling regeneration. The close associations and complex topologies of Schwann cell and axonal plasma membranes make assessment of intercellular transfer mechanisms difficult; however, our data suggest essential roles for both F-actin and myosin-Va in this mechanism.

Supporting Information

File S1 Contains Figures S1, S2, S3, and S4 with legends.
(DOCX)

Acknowledgments

We thank Mike Kavanaugh and Dave Bonislawski for assistance with confocal microscopy, supported by National Institutes of Health grant P20 RR015583. We thank Tejas Gupte, Farah Haque, John Bermingham, and members of Jim Spudich's laboratory (Stanford) for critiquing the manuscript.

Author Contributions

Conceived and designed the experiments: JRS LC AK JRS-S HW JAM. Performed the experiments: JRS LC AK LX HW GR KC AC. Analyzed the data: JRS LC AK LX JRS-S HW. Contributed reagents/materials/analysis tools: HW. Wrote the paper: JRS LC AK JRS-S JAM.

References

1. Lasek RJ, Gainer H, Barker JL (1977) Cell-to-cell transfer of glial proteins to the squid giant axon. The glia-neuron protein transfer hypothesis. J Cell Biol 74: 501–523.
2. Alvarez J (2001) The autonomous axon: a model based on local synthesis of proteins. Biol Res 34: 103–109.
3. Brittis PA, Lu Q, Flanagan JG (2002) Axonal protein synthesis provides a mechanism for localized regulation at an intermediate target. Cell 110: 223–235.
4. Sotelo-Silveira JR, Calliari A, Kun A, Koenig E, Sotelo JR (2006) RNA trafficking in axons. Traffic 7: 508–515.
5. Van Horck FP, Holt CE (2008) A cytoskeletal platform for local translation in axons. Sci Signal 1: pe11.
6. Twiss JL, Fainzilber M (2009) Ribosomes in axons–scrounging from the neighbors? Trends Cell Biol 19: 236–243.
7. Crispino M, Cefaliello C, Kaplan B, Giuditta A (2009) Protein synthesis in nerve terminals and the glia-neuron unit. Results Probl Cell Differ 48: 243–267.
8. Edstrom JE, Eichner D, Edstrom A (1962) The ribonucleic acid of axons and myelin sheaths from Mauthner neurons. Biochim Biophys Acta 61: 178–184.
9. Jakoubek B, Edstrom JE (1965) RNA changes in the Mauthner axon and myelin sheath after increased functional activity. J Neurochem 12: 845–849.
10. Benech C, Sotelo JR, Menendez J, Correa-Luna R (1982) Autoradiographic study of RNA and protein synthesis in sectioned peripheral nerves. Exp Neurol 76: 72–82.
11. Cutillo V, Montagnese P, Gremo F, Casola L, Giuditta A (1983) Origin of axoplasmic RNA in the squid giant fiber. Neurochem Res 8: 1621–1634.
12. Eyman M, Cefaliello C, Ferrara E, De Stefano R, Lavina ZS, et al. (2007) Local synthesis of axonal and presynaptic RNA in squid model systems. Eur J Neurosci 25: 341–350.
13. Sotelo JR, Benech CR, Kun A (1992) Local radiolabeling of the 68 kDa neurofilament protein in rat sciatic nerves. Neurosci Lett 144: 174–176.
14. Roberson MD, Toews AD, Goodrum JF, Morell P (1992) Neurofilament and tubulin mRNA expression in Schwann cells. J Neurosci Res 33: 156–162.
15. Kelly BM, Gillespie CS, Sherman DL, Brophy PJ (1992) Schwann cells of the myelin-forming phenotype express neurofilament protein NF-M. J Cell Biol 118: 397–410.
16. Fabrizi C, Kelly BM, Gillespie CS, Schlaepfer WW, Scherer SS, et al. (1997) Transient expression of the neurofilament proteins NF-L and NF-M by Schwann cells is regulated by axonal contact. J Neurosci Res 50: 291–299.
17. Sotelo-Silveira JR, Calliari A, Kun A, Benech JC, Sanguinetti C, et al. (2000) Neurofilament mRNAs are present and translated in the normal and severed sciatic nerve. J Neurosci Res 62: 65–74.
18. Pearce J, Lnenicka GA, Govind CK (2003) Regenerating crayfish motor axons assimilate glial cells and sprout in cultured explants. J Comp Neurol 464: 449–462.
19. Li YC, Li YN, Cheng CX, Sakamoto H, Kawate T, et al. (2005) Subsurface cisterna-lined axonal invaginations and double-walled vesicles at the axonal-myelin sheath interface. Neuroscience research 53: 298–303.
20. Kun A, Otero L, Sotelo-Silveira JR, Sotelo JR (2007) Ribosomal distributions in axons of mammalian myelinated fibers. J Neurosci Res 85: 2087–2098.
21. Court FA, Hendriks WT, Macgillavry HD, Alvarez J, van Minnen J, et al. (2008) Schwann cell to axon transfer of ribosomes: toward a novel understanding of the role of glia in the nervous system. J Neurosci 28: 11024–11029.
22. Court FA, Midha R, Cisterna BA, Grochmal J, Shakhbazau A, et al. (2011) Morphological evidence for a transport of ribosomes from Schwann cells to regenerating axons. Glia 59: 1529–1539.
23. Wallrabe H, Chen Y, Periasamy A, Barroso M (2006) Issues in confocal microscopy for quantitative FRET analysis. Microsc Res Tech 69: 196–206.
24. Chen Y, Periasamy A (2006) Intensity range based quantitative FRET data analysis to localize protein molecules in live cell nuclei. Journal of Fluorescence 16: 95–104.
25. Elangovan M, Wallrabe H, Chen Y, Day RN, Barroso M, et al. (2003) Characterization of one- and two-photon excitation fluorescence resonance energy transfer microscopy. Methods 29: 58–73.
26. Bensaude O (2011) Inhibiting eukaryotic transcription: Which compound to choose? How to evaluate its activity? Transcription 2: 103–108.
27. Searle AG (1952) A lethal allele of dilute in the house mouse. Heredity 6: 395–401.
28. Einheber S, Zanazzi G, Ching W, Scherer S, Milner TA, et al. (1997) The axonal membrane protein Caspr, a homologue of neurexin IV, is a component of the septate-like paranodal junctions that assemble during myelination. J Cell Biol 139: 1495–1506.
29. Sossin WS, DesGroseillers L (2006) Intracellular trafficking of RNA in neurons. Traffic 7: 1581–1589.
30. Bassell GJ, Oleynikov Y, Singer RH (1999) The travels of mRNAs through all cells large and small. Faseb J 13: 447–454.
31. Kosik KS, Krichevsky AM (2005) The elegance of the microRNAs: a neuronal perspective. Neuron 47: 779–782.
32. Silvers WK (1979) The coat colors of mice. New York: Springer-Verlag. 379 p.
33. Sotelo-Silveira J, Crispino M, Puppo A, Sotelo JR, Koenig E (2008) Myelinated axons contain beta-actin mRNA and ZBP-1 in periaxoplasmic ribosomal

plaques and depend on cyclic AMP and F-actin integrity for in vitro translation. J Neurochem 104: 545–547.
34. Sotelo-Silveira JR, Calliari A, Cárdenas M, Koenig E, Sotelo JR (2004) Myosin Va and kinesin II motor proteins are concentrated in ribosomal domains (periaxoplasmic ribosomal plaques) of myelinated axons. J Neurobiol 60: 187–196.
35. Rishal I, Fainzilber M (2010) Retrograde signaling in axonal regeneration. Exp Neurol 223: 5–10.

Supporting Information File S1, Sotelo et al.

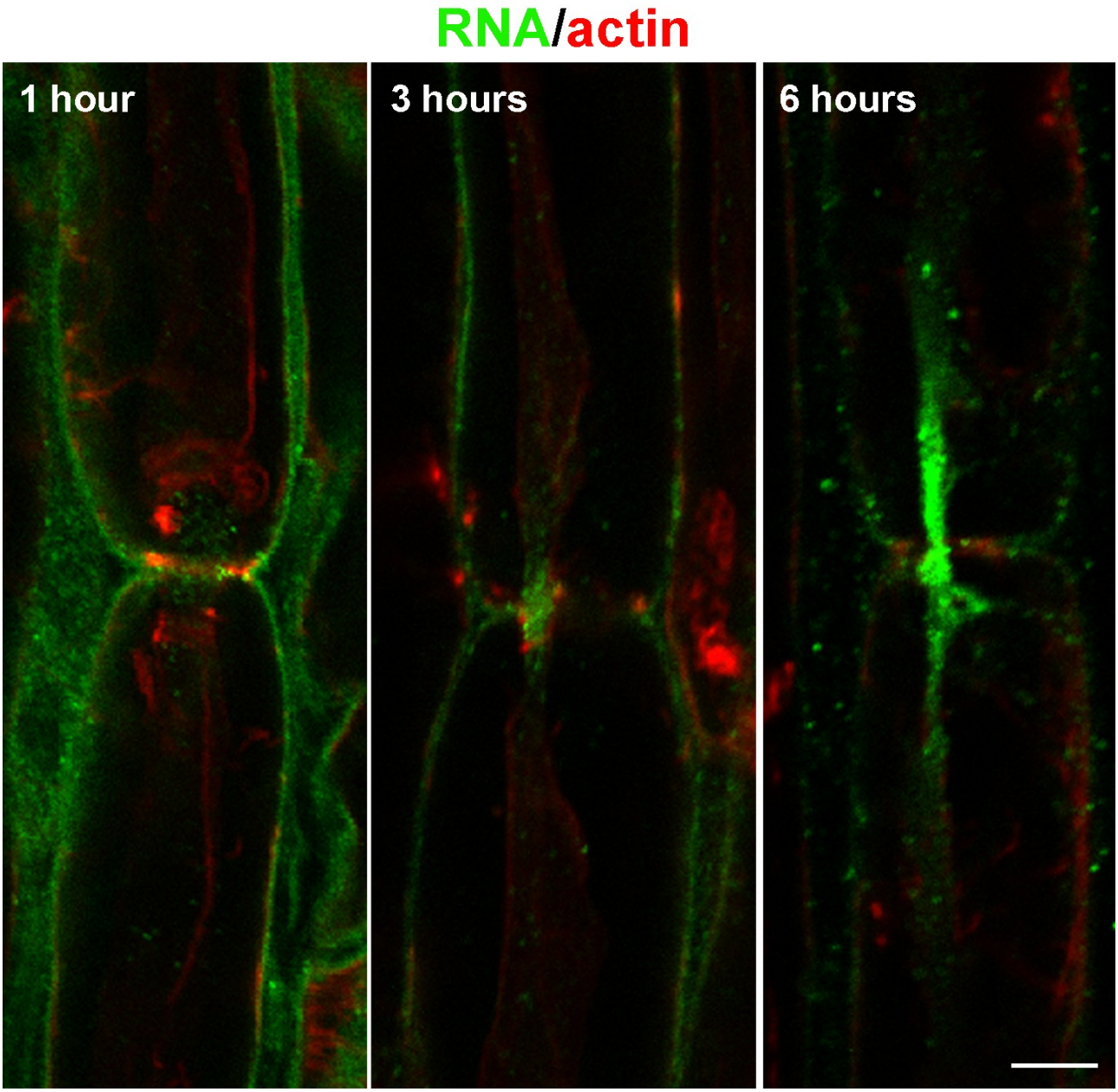

Figure S1
Time course of bromouridine (BrU) labeling of newly-synthesized RNA. Transected sciatic nerve fragments were obtained as shown in Fig. 2A-D except that they were incubated for 1 (left), 3 (middle), or 6 h (right) in BrU. Single confocal planes of single fibers at nodes of Ranvier show BrU incorporation (green) and F-actin (red).

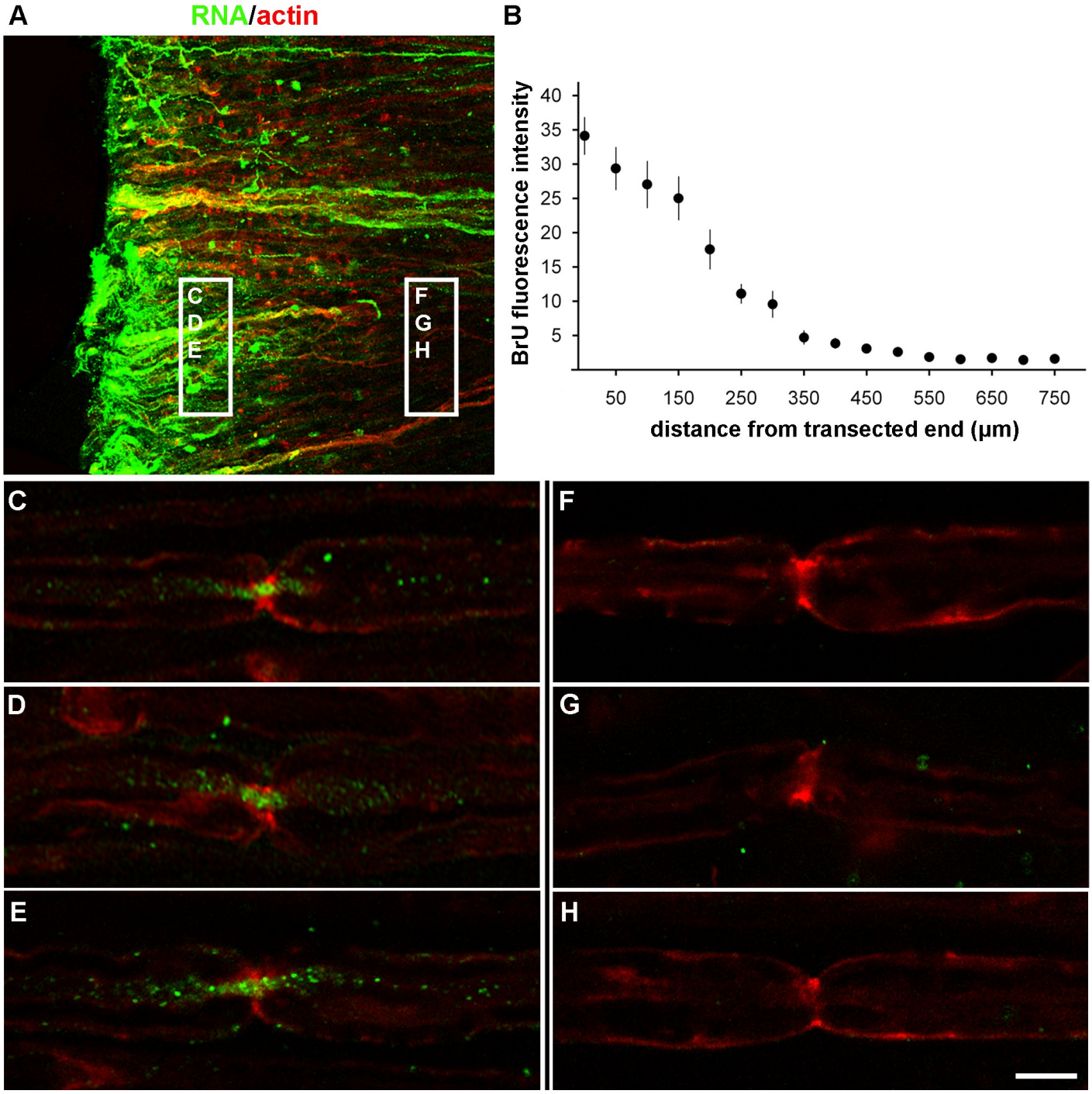

Figure S2
Control *in vivo* labeling with BrU. A, Low-magnification micrograph of transected end showing newly-synthesized RNA labeled by BrU incorporation (green) and actin labeled with phalloidin (red). Bar = 100 μm**. B,**BrU-RNA signal plotted as a function of distance from the transection. Each point represents the mean of 10 nerve fragments with standard errors. **C-H**, series of higher-magnification images offibers at nodes of Ranvier from the framed regions in panel. Bar = 10 μm**.**

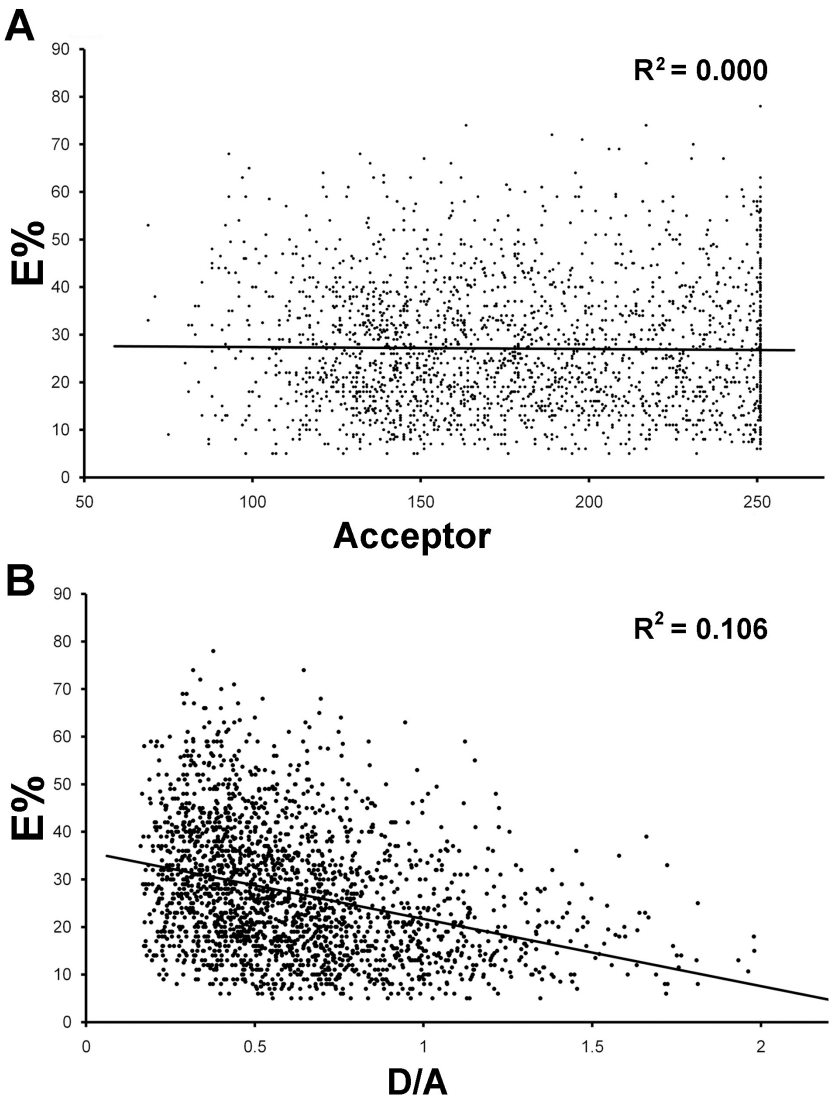

Figure S3

Analysis of FRET parameters in axons at nodes of Ranvier. A large database of regions of interest (ROIs -more than 2000), exclusively selected in axons at nodes of Ranvier, were assayed for E% and acceptor correlation (**A**) and E% and donor/acceptor ratio (D/A) correlation (**B**). **A.** R^2 value = 0.000; statistically not significant, no correlation. **B.** R^2 = 0.106; p< 0.000001.Trendlines and R^2 were calculated in Excel software.

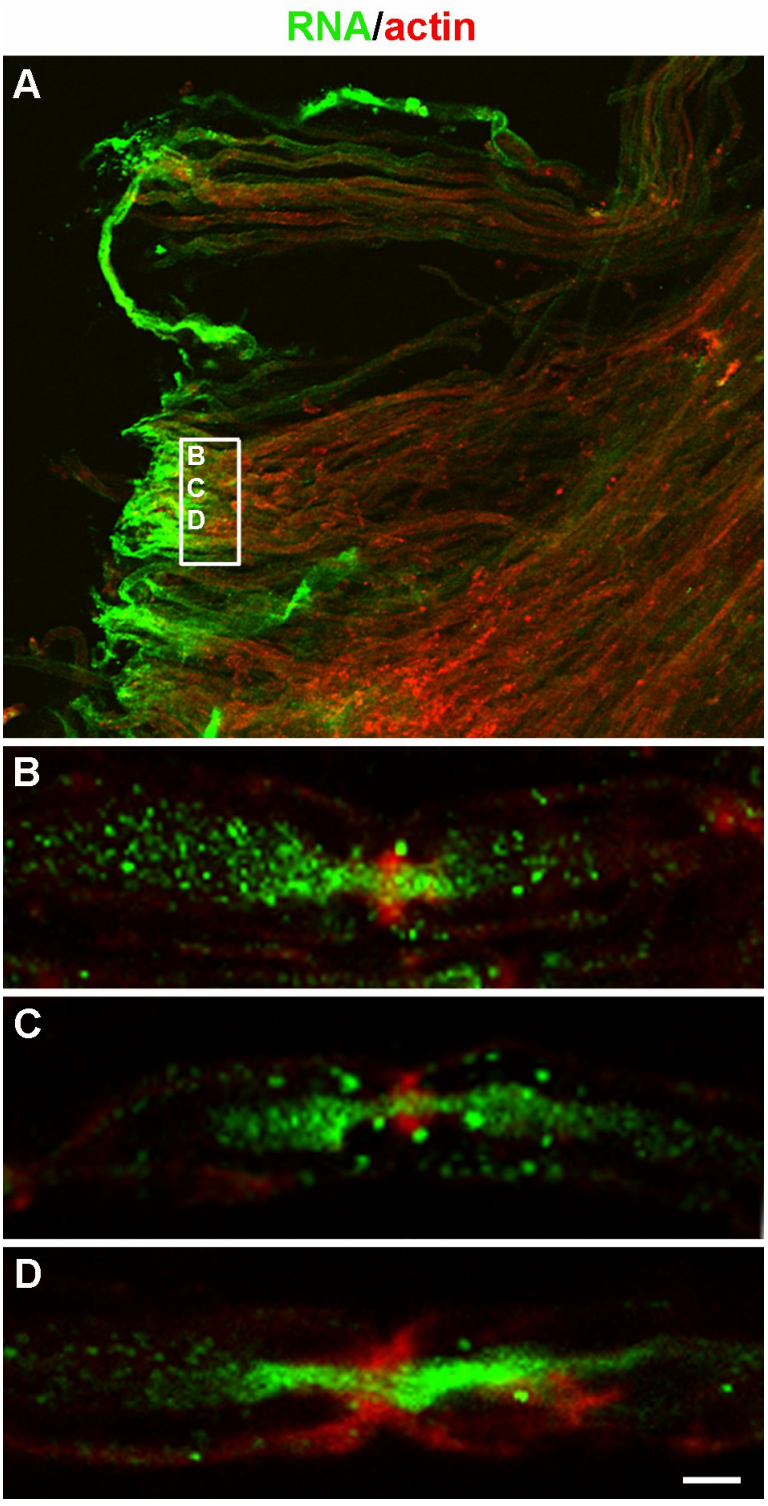

Figure S4
***In vivo*BrU labeling in adult mice. A,** Low-magnification micrograph of transected end showing newly-synthesized RNA labeled by BrU incorporation (green) and actin labeled with phalloidin (red). **B-D**, higher-magnification images ofnodes of Ranvier from the framed region in panel A. Bar = 5 µm**.**

7.2. Capítulo II.

Mecanismos de transporte y transferencia de ARN desde la célula de Schwann al axón.

7.2.1. RESUMEN

En la mayoría de los ensayos de inmunocitoquímica descritos en el capítulo I (trabajo II) se empleó faloidina para evidenciar el citoesqueleto de actina. La marcación de la actina filamentosa es muy útil para discriminar las distintas regiones de las fibras cuando se analizan en el microscopio confocal. Al desarrollar estos experimentos notamos el grado de co-localización entre los ARN-BrU y la actina filamentosa en estas regiones. Surgió entonces la siguiente interrogante, ¿el citoesqueleto de actina (conocido como mediador del transporte intracelular (Bassell *et al.*, 1999; Kiebler and Bassell, 2006; Sotelo-Silveira *et al.*, 2006; Gumy *et al.*, 2014)) podrá estar implicado en la transferencia de los ARNs desde la célula de Schwann al axón? La depolimerización del citoesqueleto de actina mediante latrunculina A disminuye la señal de ARN-BrU en el axón de una manera dependiente de la concentración de latrunculina A utilizada (figura 8, trabajo II), hasta abolirla por completo a una concentración de latrunculina A de 1.8 µg/mL (figura 8I, J y K, trabajo II). Concomitantemente, se observa una acumulación de los ARN-BrU en los bordes de la célula de Schwann en el nodo de Ranvier (figura 8K, trabajo II). Estos resultados demuestran que la transferencia de ARN desde la célula de Schwann al axón es dependiente de la funcionalidad del citoesqueleto de actina y refuerzan la propuesta de que el nodo de Ranvier es el sitio por el cual sucede dicha transferencia.

Que la transferencia de ARNs desde la célula de Schwann al axón sea dependiente del citoesqueleto de actina implica que debe ser dependiente también de alguno de los motores moleculares asociados al mismo. Se investigó, entonces, si la miosina Va podía estar implicada. Se realizaron experimentos de inmunomarcación de miosina Va y ARN-BrU en los que se observó la co-localización entre las señales de ambos (figura 9A, B, trabajo II, figura 3, trabajo III). En el trabajo II, también se realizó inmunomicroscopía FRET confocal (figuras 9C-E y S3, trabajo II) y se determinó que existe una asociación a nivel molecular entre los ARN-BrU y la miosina Va en la regiones axonal y de la célula de Schwann del nodo de Ranvier. La participación de la miosina Va en la transferencia glia-axón de ARNs se demostró a partir de experimentos con nervios ciáticos obtenidos de ratones nulos para el gen que

codifica la miosina Va (*dilute lethal*, *Myo5a*$^{d\text{-}120J}$/ *Myo5a*$^{d\text{-}120J}$). En las fibras de estos ratones, comparándolas con las de ratones normales, se constata la ausencia de señal de ARN-BrU en el axón, mientras que se observa un aumento de la misma en el citoplasma de la célula de Schwann en el nodo de Ranvier (figura 10, trabajo II). Al igual que en los experimentos empleando latrunculina A, la ausencia de ARN-BrU en el axón tiene lugar con la acumulación concomitante de los mismos en la célula de Schwann, lo que indica que la transferencia de ARNs sintetizados en la célula de Schwann hacia el axón es dependiente de miosina Va.

Posteriormente a la publicación del trabajo II, se continuó el análisis de FRET entre la miosina Va y los ARN-BrU (trabajo III), realizándolo en mayor profundidad. Este análisis permitió determinar que existen diferentes comportamientos en la interacción entre miosina Va y los ARN-BrU, que dependen del dominio celular analizado (figuras 5 y 6 trabajo III). La eficiencia en la transferencia de energía entre la miosina Va y los ARN-BrU es mayor, y por la tanto la distancia es menor, en el citoplasma de la célula de Schwann que en el axón (figura 7, trabajo III). Existen incluso diferencias en la interacción entre la miosina Va y los ARN-BrU en el propio citoplasma de la célula de Schwann. En la región del nodo de Ranvier la interacción es específica, mientras que en otras regiones del citoplasma de la célula de Schwann se observa un cierto grado de aleatoriedad en la interacción (figura 8, trabajo III). Aunque los experimentos genéticos fueron la prueba de que la miosina Va es necesaria para la transferencia glia-axón de ARNs, los experimentos de FRET permitieron discriminar la interacción entre estas moléculas. En resumen, la asociación entre ambas es más importante en el citoplasma de la célula de Schwann en el límite entre ésta y el axón, que en el propio axoplasma. En el resto del citoplasma de la célula de Schwann, los resultados del análisis de FRET indican que existe cierto grado de azar en dicha asociación (figura 8D-F, trabajo III), que sugiere que esta región puede ser donde los ARN-BrU se "cargan" a la miosina Va, o bien puede indicar la competencia por los ARN-BrU de la miosina Va con otros motores moleculares.

A partir de los resultados presentados hasta aquí en este capítulo se determinó que la transferencia glio-axonal de ARNs en el límite entre ambas células es dependiente del citoesqueleto de actina. Sin embargo, todavía

quedaban preguntas sin responder. ¿Cómo llegan los ARNs desde el núcleo de la célula de Schwann hasta el límite entre esta y el axón? Y una vez dentro del axón, ¿cómo se transportan los ARNs transferidos? ¿Están los microtúbulos involucrados en alguna de estas etapas del transporte del ARNs transferidos desde la célula de Schwann al axón? Por último, aunque no será motivo de esta tesis, ¿cuáles son los mecanismos de transferencia, de lo que únicamente sabemos que tienen que involucrar un sistema de transporte a través de las membranas citoplasmáticas de ambas células? En este capítulo también se presenta el trabajo realizado para intentar contestar las tres primeras preguntas.

Para ello, se comenzó por estudiar si los ARNs neosintetizados co-localizan con los microtúbulos. Se realizaron experimentos de inmunomarcación de los ARN-BrU y los microtúbulos, donde se observa la co-localización entre ambos (figura 1, trabajo IV) tanto en el citoplasma de la célula de Schwann como en el axón. La co-localización observada condujo a realizar experimentos en los cuales se desestabilizaron los microtúbulos mediante la incubación de los nervios en colchicina. La disrupción de los microtúbulos impide el transporte de los ARN-BrU desde el núcleo de la célula de Schwann hacia el nodo de Ranvier (figura 2, trabajo IV). En el axoplasma de las fibras incubadas con colchicina no se observa la presencia de ARN-BrU (comparar la figura 2A y B, trabajo IV) y la cuantificación de la señal del anticuerpo que reconoce BrU da niveles comparables al *background* (figura 2C, trabajo IV). Lo mismo sucede cuando se cuantifica el nivel de los ARN-BrU en el citoplasma de la célula de Schwann a nivel del nodo de Ranvier (figura 2D, trabajo IV). En estas mismas fibras se detecta una acumulación de los ARNs neosintetizados en el citoplasma adyacente al núcleo de la célula de Schwann cuando se incuba con colchicina y BrU durante 6 horas (figura 2E, trabajo IV). La acumulación de los ARNs neosintetizados en la proximidad del núcleo de la célula de Schwann causada por la colchicina, se hace más evidente en los experimentos de *pulse-chase* (figura 2F, trabajo IV). En resumen, la disrupción de los microtúbulos impide el transporte de los ARN-BrU en el citoplasma de la célula de Schwann una vez que los mismos abandonan el núcleo. Estos experimentos fueron una prueba más de que los ARN-BrU que se observan en el axón, provienen de la célula de Schwann. Pero además demuestran que los

microtúbulos están implicados en el transporte de los mismos hacia los puntos de transferencia (nodos de Ranvier e incisuras de Schmidt-Lantermann).

El transporte dependiente de microtúbulos está mediado por las kinesinas, hacia la periferia celular principalmente, y por las dineínas, en el sentido contrario (Holt and Bullock, 2009; Martin and Ephrussi, 2009; Jansen and Niessing, 2012). Dado la dirección del movimiento de los ARNs transferidos desde la célula de Schwann al axón, se investigó si las kinesinas podrían estar implicadas en el transporte de los ARN-BrU. Los experimentos fueron realizados para tres kinesinas que se expresan en el sistema nervioso: a) KIF5B, que además ha sido descrita como mediador del transporte de ribonucleopartículas en axones (Ohashi *et al.*, 2002; Kanai *et al.*, 2004; Dictenberg *et al.*, 2008), b) KIF1A, de expresión únicamente neuronal (Hirokawa *et al.*, 2010), y c) KIF1B, que además fue descrita como transportador de ARNm en glías (Carson *et al.*, 1997; Lyons *et al.*, 2009). Mediante microscopía FRET confocal, se determinó que los ARN-BrU interactúan a nivel molecular con KIF5B sólo en el dominio axonal (figura 3, trabajo IV). Por el contrario, KIF1A no interactúa en absoluto con los ARN-BrU pese a que co-localiza (figura 4, trabajo IV), dado que los experimentos de FRET dieron resultados negativos. Por último, en los experimentos realizados para conocer si KIF1B podía estar involucrada en el transporte de los ARN transferidos glia-axón, se puede observar la ausencia de co-localización entre KIF1B con los ARN-BrU tanto en el axón como en el citoplasma de la célula de Schwann del nodo de Ranvier (figura 5, trabajo IV). Se pueden observar algunas señales de co-localización entre ambas moléculas en las proximidades del núcleo de la célula de Schwann (figura 5, trabajo IV), que posiblemente correspondan a ARNs que permanecerán dentro de la célula de Schwann. En resumen, los resultados permiten proponer a KIF5B como una de las kinesinas responsable del transporte de los ARN-BrU dentro del dominio axonal. Por otra parte, permiten descartar que KIF1A y KIF1B estén implicadas en el transporte de los ARN transferidos desde la célula de Schwann al axón.

7.2.2. TRABAJO III.

Canclini L.; Wallrabe, H.; Di Paolo, P.; Kun A.; Calliari, A.; Sotelo-Silveira, J.R; Sotelo J. R. Association of Myosin Va and Schwann Cells-derived RNA in mammal myelinated axons, analyzed by immunocytochemistry and confocal FRET microscopy. Methods, 66, 153-161, 2014.

Methods 66 (2014) 153–161

Contents lists available at SciVerse ScienceDirect

Methods

journal homepage: www.elsevier.com/locate/ymeth

Association of Myosin Va and Schwann cells-derived RNA in mammal myelinated axons, analyzed by immunocytochemistry and confocal FRET microscopy

Lucía Canclini [a], Horst Wallrabe [b], Andrés Di Paolo [a], Alejandra Kun [b,c], Aldo Calliari [a,d], José Roberto Sotelo-Silveira [e,f], José Roberto Sotelo [a,*]

[a] Departamento de Proteínas y Acidos Nucleicos, Instituto de Investigaciones Biológicas Clemente Estable, Av. Italia 3318, Montevideo, CP 11600, Uruguay
[b] Department of Biology, University of Virginia, P.O. Box 400328, Charlottesville, VA 22904-4328, USA
[c] Sección Bioquímica, Facultad de Ciencias, Universidad de la República, Iguá 4225, Montevideo, CP 11400, Uruguay
[d] Area Biofísica, Departamento de Bioquímica, Biología Celular y Molecular, Facultad de Veterinaria, Alberto Lasplaces 1550, Montevideo, CP 11600, Uruguay
[e] Departamento de Genética, Instituto de Investigaciones Biológicas Clemente Estable, Av Italia 3318, Montevideo, CP 11600, Uruguay
[f] Departamento de Biología Celular, Facultad de Ciencias, Universidad de la República, Iguá 4225, Montevideo, CP 11400, Uruguay

ARTICLE INFO

Article history:
Available online 19 June 2013

Keywords:
Axon
Schwann cell
RNA cell-to-cell transfer
RNA transport
Myosin Va
Quantitative FRET microscopy

ABSTRACT

Evidence from multiple sources supports the hypothesis that Schwann cells in the peripheral nervous system transfer messenger RNA and ribosomes to the axons they ensheath. Several technical and methodological difficulties exist for investigators to unravel this process in myelinated axons – a complex two-cell unit. We present an experimental design to demonstrate that newly synthesized RNA is transferred from Schwann cells to axons in association with Myosin Va. The use of quantitative confocal FRET microscopy to track newly-synthesized RNA and determine the molecular association with Myosin Va, is described in detail.

1. Introduction

The functional unit in the Peripheral Nervous System (PNS) requires the intimate association of two different cell types: Schwann cells (SCs) with the neuronal axons. A central issue in the biology of peripheral myelinated axons is the source of macromolecules (proteins and RNA) present in the axoplasmic compartment: do all of them originate in the cell body, are some axonal proteins translated in the axon, or might a fraction of axonal protein or RNA originate in associated cells? Several reports have demonstrated axonal RNA having been synthesized in the neuronal soma [1–22]. Axonal RNAs are involved in local protein synthesis [1,5,7,8,13,15,19,22–30], but the question still remains where these RNAs came from: exclusively from the neuronal soma or SC nuclei? Most of the data showing RNA inside axons were obtained from experiments performed in dissociated cultured neurons in which axons are less than one hundred μm in length and lacking associated glia.

By using a physiologically more appropriate approach we have demonstrated that SCs are able to transcribe RNAs and transfer them to axons following sciatic nerve injury, providing an additional source of RNA to the axon [23,31]. In the same article [31] we show that the RNA transfer from SCs to axons is dependent on the actin cytoskeleton machinery and does not occur in *MyoVa* null-mutant (*dilute-lethal*) mice.

Several technical and methodological difficulties interfere with the unraveling of these functions of myelinated axons, particularly, RNA tracking and RNA–protein interaction identification. In this article we will focus on the description of experimental approaches that allowed us to overcome these difficulties. We used fluorescent confocal microscopy for tracking and identification of newly synthesized RNA in myelinated axons and quantitative intensity-based FRET microscopy to evidence RNA and motor protein association.

2. Materials and methods

2.1. Materials

(1) Bromouridine (BrU) solution: 10 mg /ml 5-BrU (Cat. No. 850187, Sigma) in Neurobasal medium (Invitrogen).

* Corresponding author. Address: Av Italia 3318, CP 11600 Montevideo, Uruguay.
E-mail addresses: lcanclini@fcien.edu.uy (L. Canclini), hw5m@virginia.edu (H. Wallrabe), apdipaolo@gmail.com (A. Di Paolo), kun@iibce.edu.uy (A. Kun), aldo@iibce.edu.uy (A. Calliari), coya@iibce.edu.uy (J.R. Sotelo-Silveira), sotelotalibo@gmail.com, sotelo@iibce.edu.uy (J.R. Sotel.

1046-2023/$ - see front matter © 2013 Elsevier Inc. All rights reserved.
http://dx.doi.org/10.1016/j.ymeth.2013.06.007

(2) PHEM buffer: 60 mM PIPES, 25 mM HEPES, 10 mM EGTA, 2 mM $MgCl_2$ at pH 7.2, stored at 4 °C.
(3) PHM buffer: 60 mM PIPES, 25 mM HEPES, 2 mM $MgCl_2$ at pH 7.2, stored at 4 °C.
(4) 3% Paraformaldehyde in PHEM, prepared shortly before use.
(5) Colagenase solution: 0.3 mg/ml colagenase, 5 mM $CaCl_2$ in PHM buffer, prepared before use.
(6) 0.1% Triton X-100 in PHEM buffer.
(7) Blocking buffer: 0.1% BSA, 2% glycine, 5% Normal Goat Serum (Invitrogen), in PHEM buffer, stored at 4 °C.
(8) Specific antibodies: Mouse monoclonal anti-bromodeoxyuridine antibody (working dilution 1/300, clone BU-33, Cat. No. B8434, Sigma). Rabbit polyclonal anti-myosin Va (working dilution 1/100, kindly supplied by Roy Larson).
(9) Secondary antibodies: Alexa Fluor 488 Goat anti-Rabbit antibody (Cat. No. A11034, Invitrogen) and Alexa Fluor 546 Goat anti-Mouse (Cat. No. A11030, Invitrogen).
(10) Alexa Fluor 546 phalloidin (Invitrogen).
(11) Prolong Gold Antifade mounting medium (Invitrogen).
(12) #5 Forceps.
(13) Slides and coverslips.
(14) Stereoscopic microscope equipped with optical fiber illumination.
(15) Olympus Bx61 FV300 confocal microscope equipped with Kr–Ar (488 nm) and He–Ne (543 nm) laser lines, DM570 dichroic filter, BA510IF, BA530RIF and BA560–600 emission filters and Plan Apo N 60X oil NA 1.42 lens.

2.2. Methods

2.2.1. Rat surgery and sciatic nerve BrU-labeling

(1) Adult rats are anesthetized with 5/10 mg/kg ketamine-xylacine.
(2) Sciatic nerves are exposed by a mid-thigh incision. Sciatic nerves are transected and the incision closed thereafter.
(3) Eighteen hours later rats are anesthetized again and 2 cm of sciatic nerve proximal to the transection is removed.
(4) Epineurium from the excised segments is removed by peeling with #5 forceps.
(5) Excised segments are incubated in BrU solution for 6 h at 37 °C and 5% CO_2.
(6) BrU-incubated segments are washed 10 times, 5 min each, in 1 ml of ice-cold PHEM buffer.

2.2.2. Immunocytochemistry

The following procedures are performed for immunocytochemistry:

(1) Fixation in 3% paraformaldehyde, 30 min at room temperature (RT).
(2) Washing four times, 5 min each, with PHEM buffer at RT at gentle stirring.
(3) Collagenase solution incubation for 1 h, at 37 °C.
(4) Incubation in 0.1% Triton X-100 for 30 min, at RT at gentle stirring.
(5) Washing three times, 5 min each, at RT at gentle stirring.
(6) 30 min in blocking buffer, at 37 °C or 1 h at RT at gentle stirring.
(7) Specific primary antibodies (in blocking buffer appropriate dilution) incubation, 1 h at 37 °C, 2 h at RT or over night at 4 °C.
(8) Washing six times, 5 min, each with PHEM buffer at RT at gentle stirring.
(9) Secondary antibodies (in blocking buffer appropriate dilution) incubation, 1 h at 37 °C or 2 h at RT.
(10) Washing six times, 5 min each, with PHEM buffer at RT at gentle stirring.
(11) Nerve fibers immersed in a drop of ProLong Gold antifade are teased apart with #5 forceps (on a glass slide) under a stereoscopic microscope.

Note: Specimens for FRET include (a) a double-label sample, i.e., fibers incubated with donor and acceptor antibodies; (b) a single-label donor sample; (c) a single-label acceptor sample; (d) an unlabeled sample, as control tissue to measure potential autofluorescence levels; and (e) other fibers are incubated without primary antibodies to establish potential secondary antibody background.

2.2.3. Confocal image acquisition

Images of myelinated fibers are acquired on a confocal microscope equipped with 488 and 543 nm laser lines and a 60X NA 1.42 lens.

Imaging conditions are optimized before data collection using double labeled and single labeled samples to maximize FRET signals, minimize spectral bleedthrough (SBT), avoid widespread saturation, avoid unintended photobleaching, and minimize background noise [32]. Through careful adjustments, optimal laser power levels (11% for Kr–Ar 488 nm laser and 55% for He–Ne 543 nm laser) are achieved, as well as PMT settings to meet these goals. The same PMT (500v) settings in donor and acceptor channels and low laser power is recommended, conducive to generate a robust uncorrected FRET (uFRET) signal at donor excitation in the acceptor channel, without at the same time saturating the donor emission signal in the donor channel.

Images are collected using single-label donor and acceptor samples and double-label samples: four single-label donor reference images (donor excitation in both donor and acceptor channels); four single-label acceptor reference images (donor and acceptor excitation, both in the acceptor channel); six (or more) double-label images (donor excitation in donor and acceptor channels, acceptor excitation in acceptor channel) [32,33]. Images of control samples are collected with donor and acceptor excitation lasers in both channels, including images in the donor channel at acceptor excitation to check for back-bleedthrough. All images are acquired at identical, previously optimized settings.

2.2.4. FRET analysis

A plug-in for ImageJ (Keck Center for Cellular Imaging, University of Virginia, Charlottesville, VA 22903) [33–36] is used for the quantitative FRET analysis (processed FRET - PFRET).

(1) The level of background noise is established manually in the acceptor and donor channels using the unlabeled or secondary antibodies control samples. The background noise was homogeneously low and is then subtracted by the PFRET software from all images used for the analysis.
(2) Regions of interest (ROIs) are created (automatically by the PFRET software or manually in ImageJ with the ROI manager function) in the background subtracted uFRET images.
(3) Image depth (8-bit/12bit), Förster distance R_0 value (64, for Alexa-fluor 488 and Alexa-fluor 546 FRET pair), quantum yields of donor (Qd: 0.92 for Alexa-fluor 488) and acceptor (Qa: 0.79 for Alexa-fluor 546), PMT gains (Pd and Pa: the same in both channels) and spectral sensitivity (Sd and Sa: according to information provided by Olympus, both photomultiplier tubes have the same sensitivity) are inserted in the software to obtain processed FRET (PFRET) by removing SBT. Energy transfer efficiency (E%) and distance (r) images are also generated. The PFRET software calculates the various parameters using the following formulas:

- Coef = [Pd/Pa] × [Sd/Sa] × [Qd/Qa]
- Quenched Donor (qD) = unquenched Donor (uD) + [DSBT]
- uD = qD + [Coef × PFRET (p)]
- uD/A = uD/Acceptor (A)
- SBT% (DSBT + ASBT) = 100 × [1−pFRET/uFRET]
- $E\%$ = 100 × [1−qD/uD]
- $r = R_0 \times [1/E\% - 1]^{1/6}$

where the coefficient (Coef) is designed to incorporate differences (if any) in PMT settings, detector spectral sensitivities and quantum yields; (qD) is the quenched donor; (DSBT) is the donor spectral bleedthrough; (ASBT) is the acceptor spectral bleedthrough; (uD) is the unquenched donor, (pFRET = p) is processed FRET; uD/A is the unquenched donor: acceptor ratio; $E\%$ is the energy transfer efficiency and r is the molecular distance.

3. Theory

In vivo RNA tracking has been largely limited to yeast until recently [37–42]. However, it is possible to pulse-chase label RNA using modified nucleosides to localize and measure RNA synthesis in cells. Three kinds of modified nucleosides have been used: radioactive, 5-ethynyluridine (EU) and 5-BrU. Labeling RNA with radioactive nucleosides is followed by tissue autoradiography [43], a slow and cumbersome method which does not allow the co-localization of RNA with other molecules. Incorporation of BrU or EU, on the other hand, can be detected by immunostaining [44] or cycloaddition reaction with azides [45,46] respectively. In both cases, the use of fluorescently-tagged antibodies or azide enables confocal co-localization experiments.

To evaluate local synthesis of axonal RNA in the PNS it is necessary to disconnect axons from their own neuronal soma, which is a known and well described source of axonal RNA [4–7,12,16–21,28–30,47]. We therefore developed a BrU RNA-labeling protocol that makes it impossible for the neuronal nucleus to be the source of any newly-synthesized axonal RNA, having transected the axon from the neuronal soma (see methods and Fig. 1). Furthermore, it is important to maximize local RNA synthesis to visualize the cell-to-cell RNA transfer process. Two strategies were used. First, our BrU RNA-labeling protocol was developed in transected and regenerating nerves, in which RNA synthesis is enhanced [1]. Second, instead of performing a pulse-chase protocol, we incubate the nerve segments 6 h in BrU and immediately fix the tissue to accumulate the signal of transferred BrU-RNA [3]).

Förster resonance energy transfer (FRET) relies on the energy transfer between two fluorophores, a donor (D) and an acceptor (A). An excited donor molecule will transfer energy to the acceptor only whether there is a sufficient overlap between the D emission and A absorption spectra, a favorable dipole–dipole orientation and most importantly when they are in close proximity (1–10 nm). One consequence of the energy transfer is the emission of fluorescence by the acceptor (without the direct excitation of the acceptor). In FRET microscopy the acceptor emission at donor excitation – having removed background noise and SBT – allows the estimation of $E\%$ (energy transfer efficiency percent), which provides an estimation of the donor–acceptor spatial proximity [32,48,49]. Since the qualitative occurrence of FRET between acceptor- and donor-labeled molecules does not discriminate between random and controlled/clustered associations, further quantitative analyses are necessary to establish that close proximity is not simply due to random associations. In a random distribution, increasing A concentration will increase $E\%$, because the chances of D to meet A increases (i.e., $E\%$ is dependent on A fluorescence intensity). In clustered interactions, increasing the amount of A-labeled molecules does not increase $E\%$, because a D molecule can only transfer energy to one A molecule at a time (i.e., $E\%$ is independent of A fluorescence intensity). Another indicator is that $E\%$ decreases when D levels and D:A ratios increase, a phenomenon called "donor geometric exclusion" [36]. This means that increasing levels of D molecule concentrations with respect to available acceptors prevent other D molecules to interact with a potential A molecule. Such phenomenon is only possible in a clustered distribution of D and A [33]. The application of FRET microscopy therefore allows a direct determination of the interaction of molecular partners in their natural environment at the same focal plane.

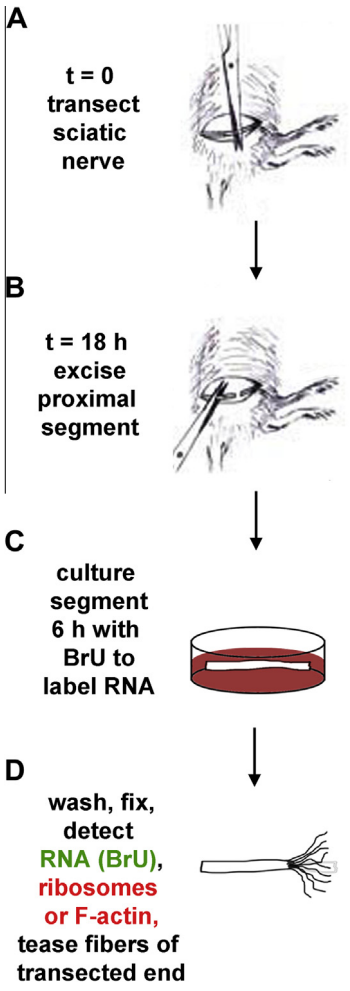

Fig. 1. Experimental procedure. (A) Sciatic nerve transection at time = 0. (B) Excision of proximal nerve segment 18 h later. (C) Segment incubation in BrU solution. (D) Immunocytochesmistry processing and teasing apart of individual fibers. This figure was adapted from Sotelo et al., 2013, doi: 10.1371/journal.pone.0061905.g002.

4. Results and discussion

4.1. Newly-synthesized RNA labeling in peripheral nerve fibers

To track newly-synthesized RNA in peripheral fibers we performed a modified pulse-chase protocol with BrU, in which the only possible RNA source is the SC nucleus (Fig. 1) [31]. Newly-synthesized BrU-labeled RNA is observed both, in the SC cytoplasm and axons. In axons, the BrU signal is higher in the vicinity of nodes of Ranvier. We hypothesize that punctate BrU-labeling corresponds to newly-synthesized RNA packaged in ribonucleoprotein particles (RNPs). Fibers were incubated in BrU 1 h (Fig. 2A and B),

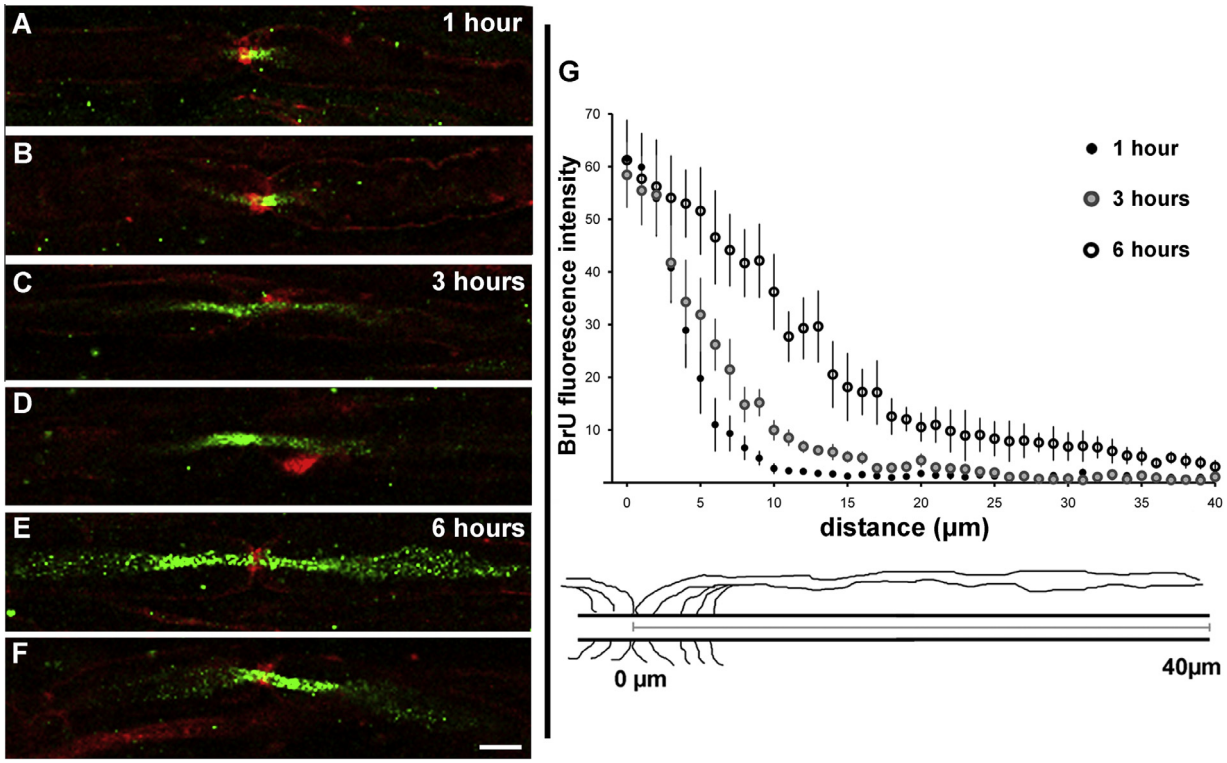

Fig. 2. Newly-synthesized BrU-labeled RNA tracking in peripheral nerve fibers. (A–F) Single confocal planes of fibers at nodes of Ranvier showing BrU incorporation (green) and F-actin (red). Fibers were incubated in BrU 1 h (A and B), 3 h (C and D) or 6 h (E and F). Size bar = 10 μm. (G) axonal BrU fluorescence intensity plotted as a function of distance from the node of Ranvier of nerves incubated in BrU for 1 h (black circles), 3 h (gray circles) or 6 h (open circles). Error bars represent standard errors. The schematic shows the node of Ranvier, axoplasm and myelin. The line inside the axoplasm represents the distance (40 μm) from the center of node of Ranvier toward internode, with the fluorescence intensity measured every 5 μm.

3 h (Fig. 2C and D) or 6 h (Fig. 2E and F) and counterstained with fluorescent phalloidin to visualize F-actin in SC and axons. Quantification of axonal BrU fluorescence intensity as a function of distance along axons from the node of Ranvier was plotted in Fig. 2G. This protocol allows newly-synthesized RNA tracking; shorter BrU incubation time yields lower levels of BrU-RNA, as well as shorter traveled distances in axons (Fig. 2A–G). We are suggesting that the ratio between the maximum distance attained by the BrU-signal and pulse duration is an expression of the velocity of newly-synthesized RNA transport in peripheral nerve fibers. Newly-synthesized RNA reaches the SC-axon boundary at the node of Ranvier in less than 1 h. With a mean distance of 200 μm from the SC nucleus to the nodes of Ranvier, the transport velocity of newly-synthesized BrU-labeled RNA (at least 200 μm/h) is in accordance with the microtubule-based transport speed in the SC cytoplasm (300–500 μm/h) [47]. However, in the axoplasm at nodes of Ranvier, newly-synthesized BrU-labeled RNA moves at a slower speed (6 μm/h, Fig. 2G). This speed is close to that of the slow axonal transport component A (4–40 μm/h) [50,51]. The underlying mechanism of this transport could potentially be

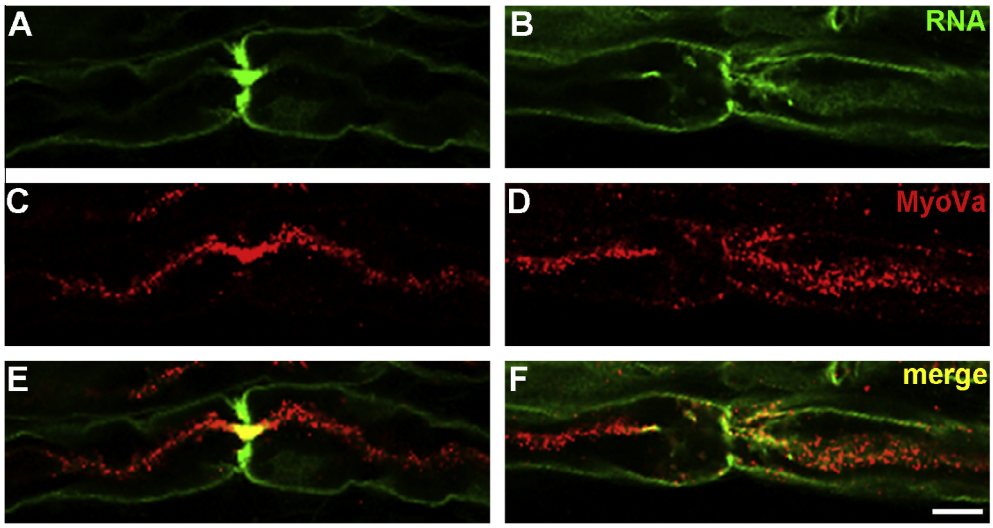

Fig. 3. Newly-synthesized BrU-labeled RNA and myosin Va co-localization in peripheral nerve fibers. Single confocal plane of a fiber at node of Ranvier showing BrU incorporation (green, A and B) and myosin Va (red, C and D) distribution. Co-localization of BrU and myosin Va signals is shown in E and F. Size bar = 10 μm.

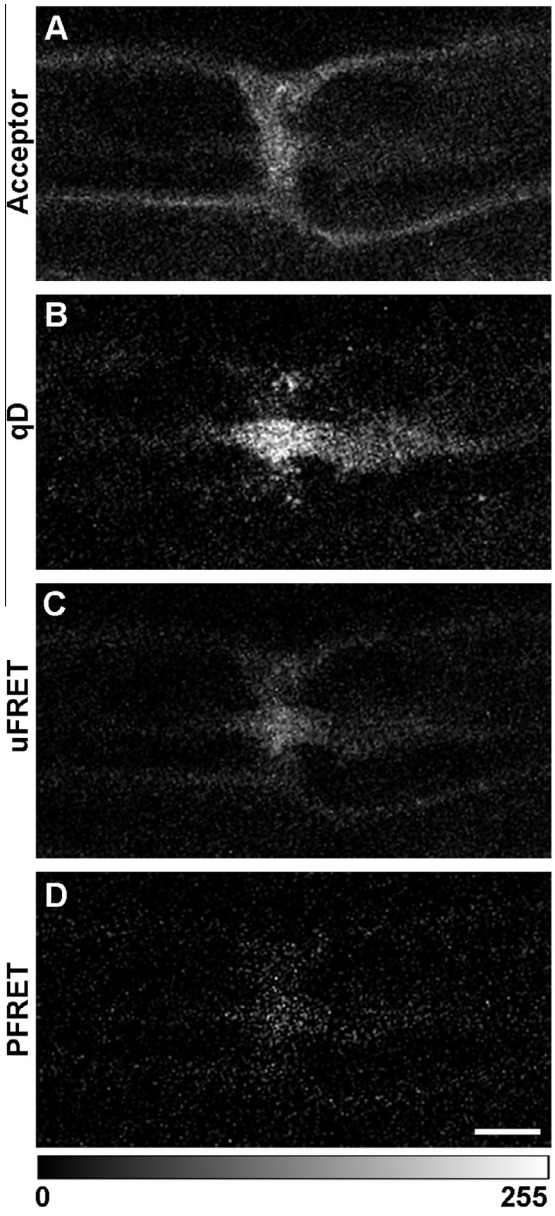

Fig. 4. Acceptor, qD, uFRET and PFRET distribution in peripheral nerve fibers. (A) Acceptor excitation/acceptor channel shows acceptor fluorescence intensity. (B) Donor excitation/donor channel shows the quenched donor (qD) fluorescence intensity. (C) Donor excitation/acceptor channel shows the uncorrected FRET (uFRET) intensity, which includes energy transfer level, donor cross-talk and acceptor bleedthrougth. (D) Corrected FRET image, where donor cross-talk and acceptor bleedthrougth were removed from uFRET. The resulting image represents the energy transfer level (PFRET). All images are single confocal plane of a fiber at the node of Ranvier. Size bar = 5 μm. Calibration bar = 0–255 gray-scale values.

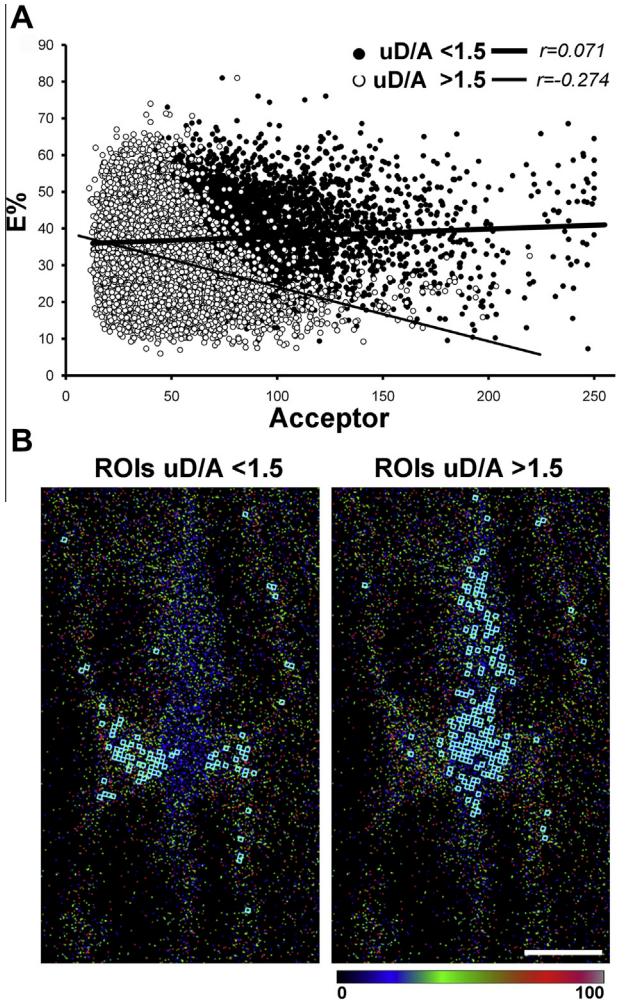

Fig. 5. Analysis of ROIs in the whole peripheral fiber. A large database of ROIs was generated of complete fiber images and assayed for *E*% and acceptor levels at specific uD/A ranges. (A) *E*% vs. acceptor levels chart at <1.5 (black circles) and >1.5 (white circles) uD/A ranges. Trend lines shown as visual helpers. Correlation coefficients are indicated. (B) *E*% pseudocolor image of a representative fiber at the node of Ranvier (single confocal plane) showing the localization of ROIs below and above 1.5 uD/A value. Size bar = 5 μm. Calibration bar = 0–100 gray-scale values.

unraveled if the molecular motors involved in this process would be better known. The precise characters of the transported RNAs in the axon, as well as their precise functions are unknown.

4.2. Immunofluorescent detection of co-localization between newly-synthesized RNA and myosin Va

Different patterns of myosin Va expression can be observed in peripheral fibers. Fig. 3 shows two representative examples of myosin Va signals. In most fibers, myosin Va is highly expressed in axons (Fig. 3C), while in other fibers, its expression is comparable to the SC cytoplasm and axons (Fig. 3D). Newly-synthesized RNA is abundant in SC and in axons at the node of Ranvier. In axons BrU signals show a decreased gradient from the nodal central point towards internodes (Fig. 3A and B). Co-localization between newly-synthesized RNA and myosin Va can be observed both in SC and axons, in spite of expression differences (Fig. 3E and F).

4.3. FRET analysis

To assess whether confocal co-localization between newly-synthesized BrU-labeled RNA and myosin Va is due to a real molecular association, an antibody-based FRET analysis was performed using the fluorescent secondary antibody (Alexa 546) recognizing anti-BrU (anti-BrdU) as acceptor and the fluorescent secondary antibody (Alexa 488) recognizing anti-myosin Va as donor. The differences of myosin Va expression inthe SC cytoplasm and axoplasm, described in Section 4.2, led us to perform two independent FRET assays to overcome the challenge that at optimized laser power levels for SC fluorescence, parts of axonal fluorescence is saturated or the opposite: at optimized axonal power levels, SC fluorescence is too weak. To be consistent, we chose specimen areas where fibers exhibited comparable levels of myosin Va in SC cytoplasm and axon. Background-subtracted double-label and single label

images were used to generate PFRET images (Fig. 4). Removal of the SBT contamination by the correction algorithm can be clearly observed comparing uFRET (Fig. 4C) and PFRET (Fig. 4D) images. Acceptor (Fig. 4A), qD (Fig. 4B) and PFRET (Fig. 4D) images were then used to calculate the three analysis parameters: acceptor, unquenched donor (uD) and *E*% values. Different bound constraints were applied to the data to eliminate outliers based on low A and D fluorescence, borderline *E*% values/SBT% correction thresholds, where the occurrence of FRET was doubtful. Therefore, acceptor, donor and uFRET bounds (10–254 gray-scale values) were established discarding ranges where SBT correction was >75%. PFRET and *E*% bounds (5–100) were applied, all based on ROIs mean values. The applied bounds produced a data set with a mean 58% SBT% correction and wide range of data points for different parameters to confidently interpret our experimental results. Displaying *E*% vs. acceptor and uD/A ratios reflected the typical behavior of clustered FRET partners, i.e., *E*% being independent of acceptor levels ($r = 0.045$) and negative dependent on uD/A ratios ($r = -0.308$). However, when the data is split at different uD/A ratios, two different populations of ROIs become visible (Fig. 5A). In the uD/A range below 1.5, *E*% is independent of acceptor values ($r = 0.071$), while in the uD/A range above 1.5, *E*% shows a weak negative dependence on acceptor level ($r = -0.274$); both conform to non-random association criteria, yet present an intriguing difference. Displaying these ROIs population on the images, they appeared at distinct locations on the fibers: ROIs of the uD/A ranges below 1.5 are mostly located in the SC cytoplasm (Fig. 5B), while ROIs in the higher uD/A ranges are mostly located in axons (Fig. 5B). The observed apparently different populations have interesting implications considering genetic experiments. In *MyoVa* null-mutant mice only axons are devoid of newly synthesized BrU-labeled RNA [31]. Is myosin Va associated with RNPs and/or are they being transported in axons, while in SC cytoplasm RNP are transported by other motors? We sought an opportunity to refine the data to eliminate the potential impact of factors inherent in FRET microscopy analysis, discussed in the next section.

4.4. Further refining FRET analysis

As discussed in Section 3, the impact of the uD/A ratio or its inverse A/uD ratio on *E*% levels may influence the results. While the negative dependence of *E*% on uD/A is a useful parameter to confirm a clustered assembly, rising uD/A is also an indicator of likely increases in non-FRET donors. One way to test the data set for linearity in the regression is to compare linear with polynomial regression to analyze just ranges within conforming linearity based on *E*% vs. A/uD. Looking at SC cytoplasm ROIs, *E*% vs. A/uD ratio polynomial trend line indicates an end of linearity at A/uD 2.5 va-

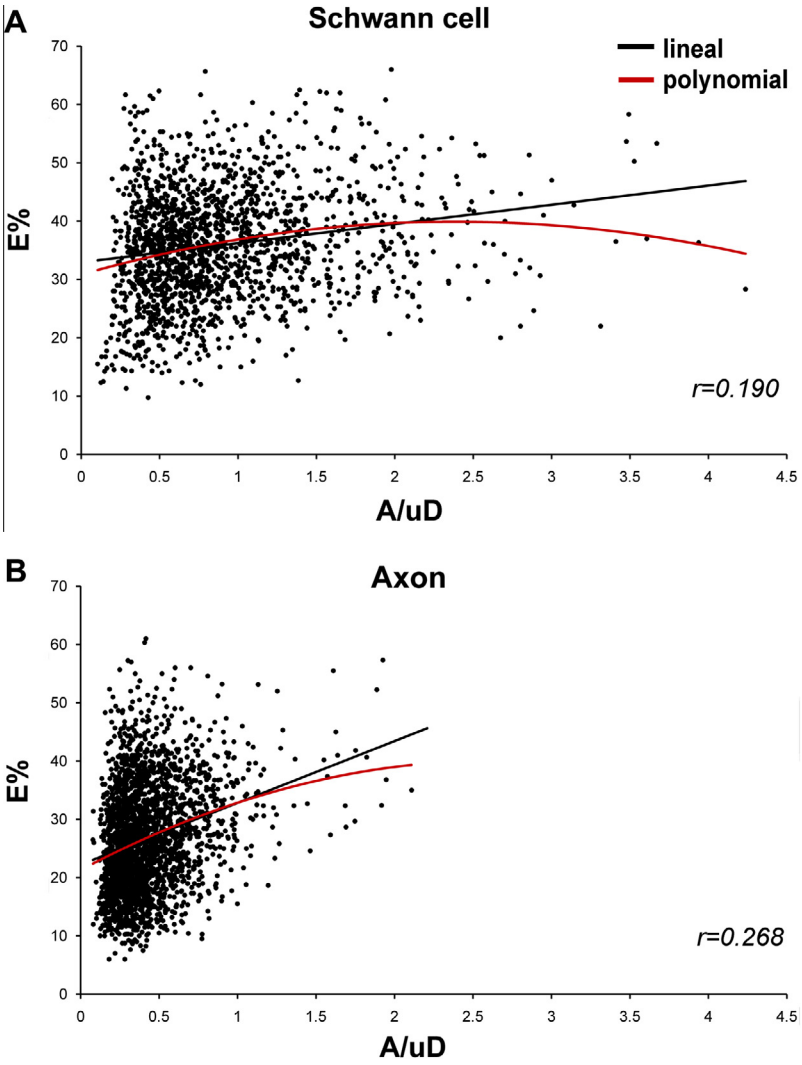

Fig. 6. *E*% vs. A/uD ratio for linearity analysis. SC cytoplasm (A) and axoplasm (B) ROIs were assayed for *E*% and A/uD ratio. Lineal (black) and polynomial (red) trend lines are shown. Correlation coefficients for lineal relationship are indicated.

lue (Fig. 6A). ROIs below A/uD 0.16 value are also contributing to loss of linearity. The polynomial trend line indicates an end of linearity at lower A/uD value in axoplasm at 1.25 (Fig. 6B). Data points beyond the plateau are most likely based on random interactions; we thus eliminated from both data sets ROIs showing lack of polynomial linearity based in SC cytoplasm values to compare the analysis in each cellular area, even though relatively few data points were beyond these thresholds. Eliminating these ROIs did not alter the fact that we are dealing with two distinct populations with an *E*% *p*-value of 8.22×10^{-148}. To further investigate the behavior of the two populations we plotted the *E*% frequency distribution in a histogram of ROIs located in axons and SC cytoplasm, highlighting the basis of their statistically significant difference (Fig. 7A). Furthermore, *E*% is independent of acceptor levels ($r = -0.032$) with a weak negative dependence on uD/A ratios ($r = -0.281$) in axoplasm (Fig. 7D and E). On the other hand, in SC cytoplasm, *E*% shows an independence of both acceptor ($r = -0.032$), but a very weak negative dependence on uD/A ratios ($r = -0.158$) (Fig. 7B and C). This behavior indicates that some degree of random interactions between newly-synthesized BrU-labeled RNA and myosin Va is present in the SC cytoplasm.

To further refine our FRET analysis in the SC cytoplasm, we only selected ROIs at the node of Ranvier level (Fig. 8A–C). Here, the analysis shows a significant clustered distribution between BrU-labeled RNA and myosin Va, based on *E*%'s independence on acceptor levels ($r = -0.084$ – Fig. 8A) and negative dependence on uD/A ratios ($r = -0.422$ – Fig. 8B), i.e., both clustering assay criteria are in agreement. In the rest of SC cytoplasm (Fig. 8D–F), chart analysis still shows some degree of randomness, while *E*% is independent of acceptor ($r = 0.085$ – Fig. 8D) there is only very weakly negative dependence on the uD/A ratio ($r = -0.130$ – Fig. 8E). *T*-test *p*-values of *E*% populations at the node of Ranvier level are statistically different (at $p = 2.5 \times 10^{-45}$) from *E*% population in the other regions of SC cytoplasm, and they are statistically different (at $p = 0.02$) to those in the axoplasm. These significant differences suggest that myosin Va may be associating with RNPs for transport/tethering

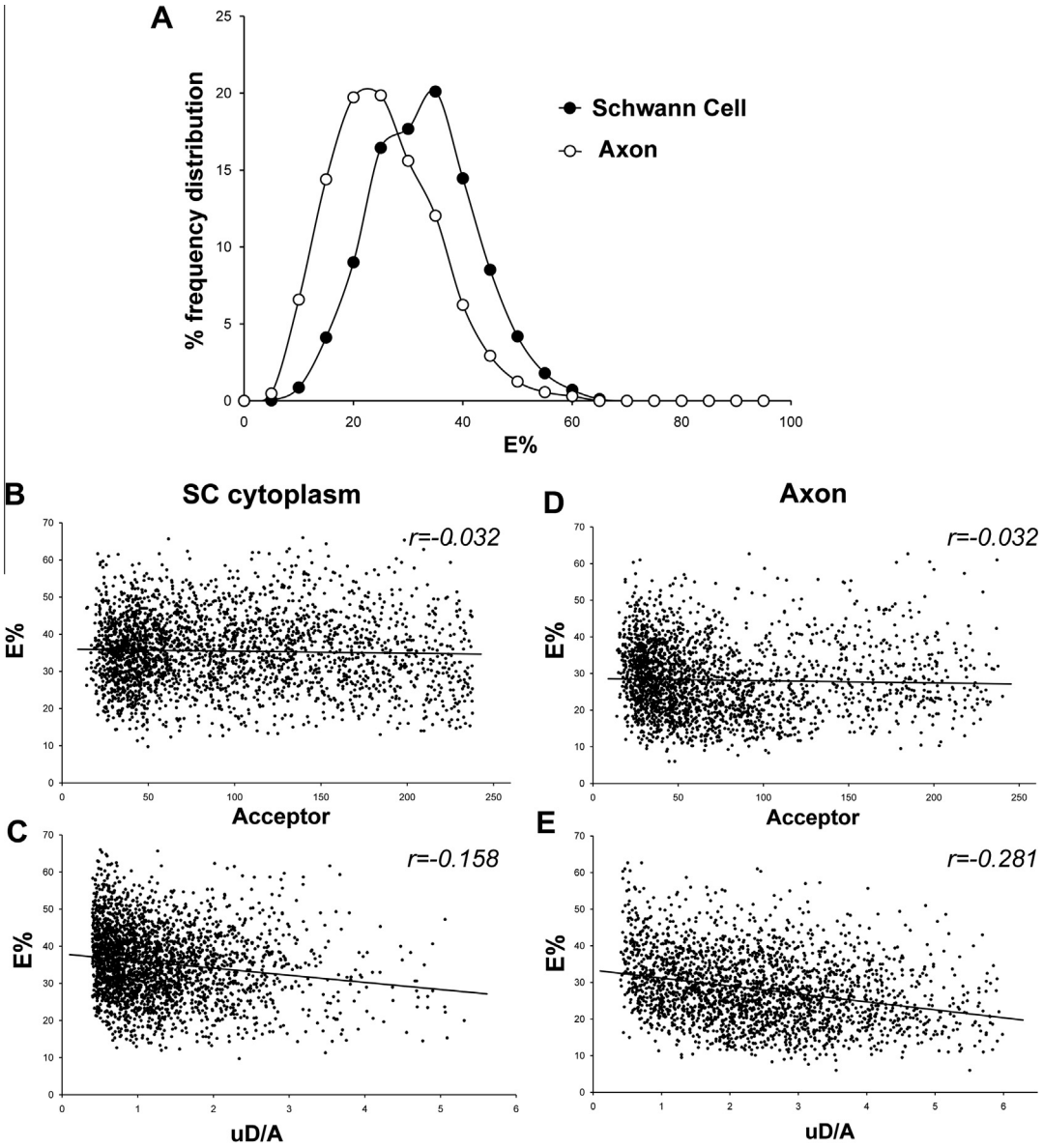

Fig. 7. *E*% analysis in SC cytoplasm and axoplasm. (A) *E*% frequency distribution histogram of ROIs located in axons (white circles) and SC cytoplasm (black circles) with a *p*-value of 8.22×10^{-148} between the two *E*% populations. (B) *E*% vs. acceptor levels of ROIs located in SC cytoplasm. (C) *E*% vs. uD/A ratio of ROIs located in SC cytoplasm. (D) *E*% vs. acceptor levels of ROIs located in axons. (E) *E*% vs. uD/A ratio of ROIs located in axons. Trend lines are shown as visual helpers. Correlation coefficients for each relationship are indicated.

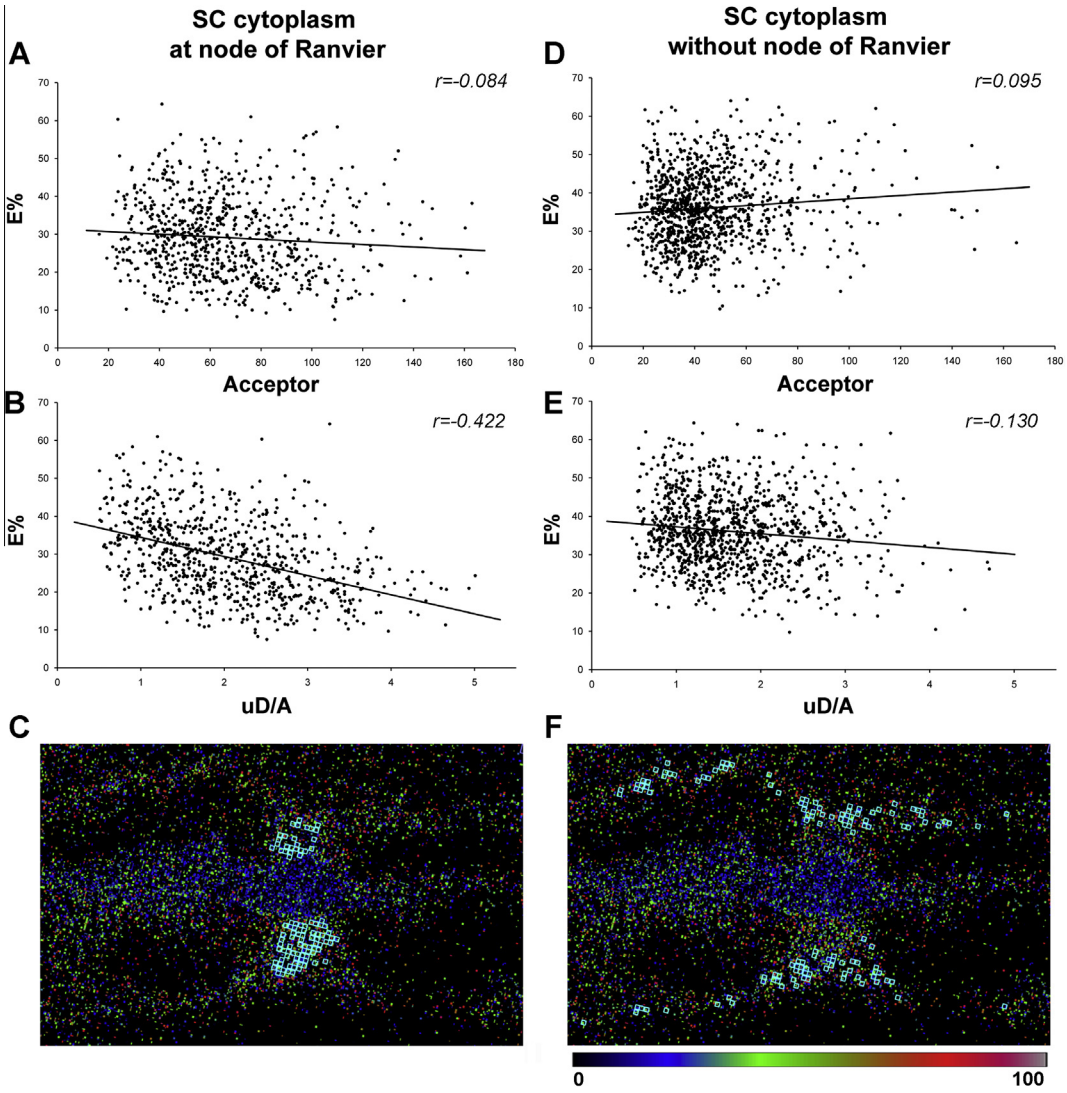

Fig. 8. FRET analysis refinement in SC cytoplasm. Two new ROIs sets were selected in the SC cytoplasm, separating the region at nodes of Ranvier (A–C) and the other SC cytoplasm regions (D–F). (A and D) *E%* vs. acceptor level charts. (B and E) *E%* vs. uD/A ranges charts. Trend lines are shown as visual helpers. Correlation coefficients are indicated. (C and F) *E%* pseudo-color image of a representative fiber (single confocal plane) showing the localization of ROIs in SC cytoplasm. Size bar = 5 μm. Calibration bar = 0–100 gray-scale values.

in SC cytoplasm at the node of Ranvier and with a lower degree in axons. The observed FRET in the rest of SC cytoplasm could be attributed to the fact that RNPs are being loaded on myosin Va. This also could mean that there are two different motors (like myosin Va and Kinesin) competing for loading RNPs.

5. Conclusions

An experimental design was developed that allows the tracking of Schwann cell-derived newly-synthesized RNA into axons of peripheral nerves fibers. The protocol is quite straightforward, and makes it possible to perform RNA labeling using BrU under normal conditions, or under different experimental situations including interventions by drugs, such as cytoskeleton disruptors and RNA transcription inhibitors, to explore the transfer mechanism, as well as, which kind of RNA is transferred to the axon. In addition, BrU-detection by immunocytochemistry is compatible with other immunocytochemical molecule detection methods allowing to track the co-localization of BrU-labeled RNA with other molecules, and the opportunity to perform quantitative FRET analyses between them. FRET is often used to establish co-localization or measure distance between molecules, but a more extensive data quantitative analysis is recommended to take advantage of this powerful technique. A rigorous deep analysis of FRET derived-data led us to establish that myosin Va interaction with BrU-labeled RNA depends on what cellular location we are analyzing. This suggests that both molecules have different functional relationships depending on which cell location we are studying. Our quantitative FRET analysis is completely in accordance with our genetic experimental results; *MyoVa* null-mutant mice cannot transfer RNA inside axons. Further FRET analysis of newly-synthesized RNA interaction with other molecular motors will lead us to better understand the mechanism of cell-to-cell RNA transfer in the Peripheral Nervous System.

6. Appendixes

6.1. Hints and notes

(1) 5-Bromouridine must be aliquoted and stored at −20 °C in dried conditions for up to 6 months. 5-Bromouridine solution must be prepared immediately before use. These conditions will ensure adequate BrU-labeling of newly-synthesized RNA.

(2) Secondary antibodies must be highly cross-absorbed to avoid background signals.
(3) All chemicals must be molecular biology grade to avoid cell molecular damage.
(4) Teasing fibers apart must be performed carefully to avoid fiber elongation, which produces aberrant morphologies. We recommend separating fibers in the transversal direction. Experience will help determining an optimal rate of force to be applied.
(5) Include BrU-labeling controls, such as incubation in medium without BrU, to check for unspecific immunocytochemistry labeling. BrU-labeled tissue treatment with RNAse is also recommended. Include secondary antibody controls and autofluorescence controls every time an experiment is performed.
(6) Take time to optimize imaging acquisition conditions, this is the most important step in quantitative FRET experiments. Ensure that your conditions will produce images without saturation. The PFRET plug-in will discard any saturated pixel from the analysis.

6.2. Equipment and supply list

6.2.1. Equipment

(1) Laminar flow hood (Clean Bench Hitachi).
(2) Culture Chamber (Sanyo CO_2 Incubator).
(3) Stemi SV6 stereoscopic microscope (Zeiss).
(4) Standard Dry Block Heater (Cat. No. 949511, TalBoys).
(5) Thermomixer (Cat. No. 535022069, Eppendorf).
(6) Spectrafuge Mini Centrifuge (Cat. No. C1301B, Labnet International).
(7) FV300 Confocal Microscope, equipped with a Plan Apo N 60X oil NA 1.42 lens; 405, 488, 543 and 633 nm laser lines (Olympus).

6.2.2. Supply list

SIGMA: 5-bromouridine 98% (Cat. No. 850187); PIPES (Cat. No. P6757); HEPES (Cat. No. H3375); EDTA (Cat. No. 03609); Magnesium Chloride (Cat. No. M8266); Potassium hydroxide (Cat. No. 221473); Paraformaldehyde (Cat. No. 16005); Collagenase from Clostridium histolyticum (Cat. No. C9407); Triton X-100 (Cat. No. 9002–93-1); Albumin from bovine serum (Cat. No. A7906); Glycine (Cat. No. G8898); Mouse monoclonal anti-bromodeoxyuridine antibody (Cat. No. B8434).

Invitrogen: Neurobasal Media (Cat. No. 21103); Normal Goat Serum (Cat. No. PCN5000); Alexa Fluor 488 Goat anti-Rabbit antibody (Cat. No. A11034); Alexa Fluor 546 Goat anti-Mouse (Cat. No. A11030); Alexa Fluor 546 Phalloidin (Cat. No. A22283); ProLong Gold Antifade Reagent (Cat. No. P36930).

Acknowledgements

We specially thank Dr. George Bloom (Department of Biology, University of Virginia, Charlottesville, USA) for his kind support and help for using his microscope and to the Keck Center for Cellular Imaging (University of Virginia, Charlottesville, USA) for the permission to use their image equipment, particularly the Biorad and Zeiss confocal microscopes.

References

[1] J.R. Sotelo-Silveira, A. Calliari, A. Kun, J.C. Benech, C. Sanguinetti, C. Chalar, J.R. Sotelo, J. Neurosci. Res. 62 (2000) 65–74.
[2] J.R. Sotelo-Silveira, A. Calliari, M. Cardenas, E. Koenig, J.R. Sotelo, J. Neurobiol. 60 (2004) 187–196.
[3] A. Aschrafi, A.D. Schwechter, M.G. Mameza, O. Natera-Naranjo, A.E. Gioio, B.B. Kaplan, J. Neurosci. 28 (2008) 12581–12590.
[4] G.J. Bassell, H. Zhang, A.L. Byrd, A.M. Femino, R.H. Singer, K.L. Taneja, L.M. Lifshitz, I.M. Herman, K.S. Kosik, J. Neurosci. 18 (1998) 251–265.
[5] H. Eng, K. Lund, R.B. Campenot, J. Neurosci. 19 (1999) 1–9.
[6] L.F. Gumy, G.S. Yeo, Y.C. Tung, K.H. Zivraj, D. Willis, G. Coppola, B.Y. Lam, J.L. Twiss, C.E. Holt, J.W. Fawcett, Rna 17 (2010) 85–98.
[7] B.B. Kaplan, A.E. Gioio, M. Hillefors, A. Aschrafi, Results Prob. Cell Differ. 48 (2009) 225–242.
[8] E. Koenig, Mol. Cell Neurosci. 2 (1991) 384–394.
[9] E. Koenig, R. Martin, J. Neurosci. 16 (1996) 1400–1411.
[10] E. Koenig, R. Martin, M. Titmus, J.R. Sotelo-Silveira, J. Neurosci. 20 (2000) 8390–8400.
[11] A. Kun, L. Otero, J.R. Sotelo-Silveira, J.R. Sotelo, J. Neurosci. Res. 85 (2007) 2087–2098.
[12] O. Natera-Naranjo, A. Aschrafi, A.E. Gioio, B.B. Kaplan, Rna 16 (2010) 1516–1529.
[13] J.R. Sotelo, C.R. Benech, A. Kun, Neurosci. Lett. 144 (1992) 174–176.
[14] J. Sotelo-Silveira, M. Crispino, A. Puppo, J.R. Sotelo, E. Koenig, J. Neurochem. 104 (2008) 545–557.
[15] O. Steward, C.E. Ribak, J. Neurosci. 6 (1986) 3079–3085.
[16] A.M. Taylor, N.C. Berchtold, V.M. Perreau, C.H. Tu, N. Li Jeon, C.W. Cotman, J. Neurosci. 29 (2009) 4697–4707.
[17] D. Willis, K.W. Li, J.Q. Zheng, J.H. Chang, A. Smit, T. Kelly, T.T. Merianda, J. Sylvester, J. van Minnen, J.L. Twiss, J. Neurosci. 25 (2005) 778–791.
[18] D.E. Willis, E.A. van Niekerk, Y. Sasaki, M. Mesngon, T.T. Merianda, G.G. Williams, M. Kendall, D.S. Smith, G.J. Bassell, J.L. Twiss, J. Cell Biol. 178 (2007) 965–980.
[19] H.L. Zhang, T. Eom, Y. Oleynikov, S.M. Shenoy, D.A. Liebelt, J.B. Dictenberg, R.H. Singer, G.J. Bassell, Neuron 31 (2001) 261–275.
[20] H.L. Zhang, R.H. Singer, G.J. Bassell, J. Cell Biol. 147 (1999) 59–70.
[21] K.H. Zivraj, Y.C. Tung, M. Piper, L. Gumy, J.W. Fawcett, G.S. Yeo, C.E. Holt, J. Neurosci. 30 (2010) 15464–15478.
[22] J.R. Sotelo-Silveira, A. Calliari, A. Kun, E. Koenig, J.R. Sotelo, Traffic 7 (2006) 508–515.
[23] C. Benech, J.R. Sotelo Jr., J. Menendez, R. Correa-Luna, Exp. Neurol. 76 (1982) 72–82.
[24] A. Giuditta, J.T. Chun, M. Eyman, C. Cefaliello, A.P. Bruno, M. Crispino, Physiol. Rev. 88 (2008) 515–555.
[25] J. Alvarez, A. Giuditta, E. Koenig, Prog. Neurobiol. 62 (2000) 1–62.
[26] A. Giuditta, B.B. Kaplan, J. van Minnen, J. Alvarez, E. Koenig, Trends Neurosci. 25 (2002) 400–404.
[27] J.L. Twiss, M. Fainzilber, Trends Cell Biol. 19 (2009) 236–243.
[28] B.C. Yoon, K.H. Zivraj, C.E. Holt, Results Prob. Cell Differ. 48 (2009) 269–288.
[29] J. Yao, Y. Sasaki, Z. Wen, G.J. Bassell, J.Q. Zheng, Nat. Neurosci. 9 (2006) 1265–1273.
[30] A.C. Lin, C.E. Holt, Embo J. 26 (2007) 3729–3736.
[31] L.C. José R. Sotelo1, Alejandra Kun, José R. Sotelo-Silveira, Lei Xu, Horst Wallrabe, Aldo Calliari, Gonzalo Rosso, Karina Cal, A. John Mercer, PLoS One 8 (2013).
[32] A. Periasamy, R.N. Day, American Physiological Society: Molecular Imaging FRET Microscopy and Spectroscopy Published for the American Physiological Society, Oxford University Press, Oxford, New York, 1887.
[33] H. Wallrabe, Y. Chen, A. Periasamy, M. Barroso, Microsc. Res. Tech. 69 (2006) 196–206.
[34] M. Elangovan, H. Wallrabe, Y. Chen, R.N. Day, M. Barroso, A. Periasamy, Methods 29 (2003) 58–73.
[35] Y. Chen, A. Periasamy, J. Fluoresc. 16 (2006) 95–104.
[36] H. Wallrabe, M. Elangovan, A. Burchard, A. Periasamy, M. Barroso, Biophys. J. 85 (2003) 559–571.
[37] L. Haim-Vilmovsky, N. Gadir, R.H. Herbst, J.E. Gerst, Rna 17 (2011) 2249–2255.
[38] N. Gadir, L. Haim-Vilmovsky, J. Kraut-Cohen, J.E. Gerst, Rna 17, 1551–1565.
[39] L. Haim-Vilmovsky, J.E. Gerst, Mol. Biol. 714, (2011) 237–247.
[40] G. Zipor, L. Haim-Vilmovsky, R. Gelin-Licht, N. Gadir, C. Brocard, J.E. Gerst, Proc. Nat. Acad. Sci. USA 106 (2009) 19848–19853.
[41] L. Haim-Vilmovsky, J.E. Gerst, Nat. Protoc. 4 (2009) 1274–1284.
[42] L. Haim, G. Zipor, S. Aronov, J.E. Gerst, Nat. Methods 4 (2007) 409–412.
[43] M. Uddin, G.G. Altmann, C.P. Leblond, J. Cell Biol. 98 (1984) 1619–1629.
[44] D.G. Wansink, W. Schul, I. van der Kraan, B. van Steensel, R. van Driel, L. de Jong, J. Cell Biol. 122 (1993) 283–293.
[45] C.W. Tornoe, C. Christensen, M. Meldal, J. Org. Chem. 67 (2002) 3057–3064.
[46] V.V. Rostovtsev, L.G. Green, V.V. Fokin, K.B. Sharpless, Angew Chem. Int. Ed. Engl. 41 (2002) 2596–2599.
[47] M.A. Kiebler, G.J. Bassell, Neuron 51 (2006) 685–690.
[48] Y. Sun, H. Wallrabe, S.A. Seo, A. Periasamy, Chemphyschem 12 (2011) 462–474.
[49] A. Periasamy, H. Wallrabe, Y. Chen, M. Barroso, Methods Cell Biol. 89 (2008) 569–598.
[50] D. Ma, B.T. Himes, T.B. Shea, I. Fischer, J. Neurosci. 20 (2000) 2112–2120.
[51] A. Brown, J. Cell Biol. 160 (2003) 817–821.

7.2.3. TRABAJO IV.

Canclini, L., Di Paolo, A., Farias J., Wallrabe, H., Kun, A., Sotelo-Silveira, J. R., Sotelo, J. R. Microtubule-based transport of Schwann cell-derived axonal RNAs. Manuscrito enviado para su publicación.

Cytoskeleton

Microtubule-based transport of Schwann cell-derived axonal RNAs

Journal:	*Cytoskeleton*
Manuscript ID:	Draft
Wiley - Manuscript type:	Research Article
Date Submitted by the Author:	n/a
Complete List of Authors:	Canclini, Lucía; Instituto de Investigaciones Biológicas Clemente Estable, Departamento de Genética; Instituto de Investigaciones Biológicas Clemente Estable, Departamento de Proteínas y Acidos Nucleicos Di Paolo, Andrés; Instituto de Investigaciones Biológicas Clemente Estable, Departamento de Proteínas y Acidos Nucleicos Farias, Joaquina; Instituto de Investigaciones Biológicas Clemente Estable, Departamento de Proteínas y Acidos Nucleicos; Instituto de Investigaciones Biológicas Clemente Estable, Departamento de Genómica Wallrabe, Horst; University of Virginia, Department of Biology Kun, Alejandra; Instituto de Investigaciones Biológicas Clemente Estable, Departamento de Proteínas y Acidos Nucleicos Sotelo Silveira, José; Instituto de Investigaciones Biológicas Clemente Estable (IIBCE), Departamento de Genómica Sotelo, José; Instituto de Investigaciones Biológicas Clemente Estable, Departamento de Proteínas y Acidos Nucleicos
Keywords:	cell-to-cell RNA transfer, RNA transport, colchicine, kinesin, FRET microscopy

Microtubule-based transport of Schwann cell-derived axonal RNAs.

Lucía Canclini[1,2], Andrés Di Paolo[1], Joaquina Farias[1,3], Horst Wallrabe[4], Alejandra Kun[1,5], José R. Sotelo-Silveira[3], José R. Sotelo[1].

1. Departamento de Proteínas y Acidos Nucleicos, Instituto de Investigaciones Biológicas Clemente Estable, Montevideo, Uruguay.
2. Departamento de Genética, Instituto de Investigaciones Biológicas Clemente Estable, Montevideo, Uruguay.
3. Departamento de Genómica, Instituto de Investigaciones Biológicas Clemente Estable, Montevideo, Uruguay.
4. Department of Biology, University of Virginia, Charlottesville, VA, USA.
5. Unidad asociada a Sección Bioquímica, Facultad de Ciencias, UdelaR, Montevideo, Uruguay

Running title: Microtubules in glia-to-axon RNA transfer

Corresponding author:

Name: José Roberto Sotelo
Address: Av. Italia 3318
Phone number: +59824871616
Fax: +59824875548
e-mail: sotelotalibo@gmail.com; jsotelo@iibce.edu.uy

Co-corresponding author:

Name: Lucía Canclini
Address: Av. Italia 3318
Phone number: +59824871616
Fax: +59824875548
e-mail: lcanclini@gmail.com; lcanclini@iibce.edu.uy

Keywords: cell-to-cell RNA transfer; RNA transport; colchicine; kinesin; FRET microscopy.

ABSTRACT

Cytoplasmic RNA transport occurs throughout microtubule and actin cytoskeleton networks and depends on molecular motors such as kinesins and dyneins (microtubules) and myosins (F-actin). Schwann cell-to-axon RNA transfer was demonstrated in normal peripheral fibers and increasingly so after nerve injury. This transfer is dependent on the F-actin cytoskeleton and myosin Va molecular motors. Here, we demonstrate that Schwann cell-to-axon RNA transfer is not only dependent on F-actin and myosin Va, but also on the microtubule cytoskeleton. Colchine-mediated disruption of microtubules completely interrupts Schwann cell-to-axon RNA transfer. In addition, we propose that KIF5B (kinesin-1) is involved in Schwann cell-derived RNA transport inside axons. We show that FRET interaction occurs between KIF5B and newly synthesized Schwann cell-derived RNA in axoplasm at node of Ranvier level. Kinesin-3 shows no such interaction.

INTRODUCTION

RNA transfer from Schwann cell to axon in normal and regenerating fibers in the Peripheral Nervous System was recently reported [Canclini et al., 2014; Sotelo et al., 2013]. In addition, ribosome transfer was also shown in distal segments of transected *Wld*^{S} [Court et al., 2008] and normal [Court et al., 2011] nerves. The transfer of ribosomes and mRNA from Schwann cell to axon involves the transcription of RNAs in the Schwann cell nucleus and its subsequent transport to the boundary between both cells. The process of RNA transport to distant subcellular sites, known as RNA localization, occurs along microtubules or actin filaments, and involves kinesins, dyneins, as well as myosins (for reviews see [Holt and Bullock, 2009; Jansen and Niessing, 2012; Martin and Ephrussi, 2009]). For instance, in the yeast *Saccharomyses cerevisiae*, specific mRNAs are transported to the bud tip by an actin-based myosin family member [Müller et al., 2007]. In *Drosophila* and *Xenopus* embryos, dynein and kinesin family members are directly responsible for the asymmetric localization of several mRNAs [Brendza et al., 2000; MacDougall et al., 2003; Messitt et al., 2008; Wilkie and Davis, 2001; Zimyanin et al., 2008]. In vertebrate neurons, kinesins play significant roles in mRNA targeting to dendrites [Hirokawa, 2006]. We previously showed that Schwann cell-to-axon RNA transfer is dependent on the actin cytoskeleton, because Latrunculin A-dependent disruption of F-actin decreased the amount of Schwann cell-newly synthesized RNA in axoplasm, while accumulating at the Schwann cell cytoplasm nodal *microvilli* [Sotelo et al., 2013]. Furthermore, we also reported a tight molecular association (FRET analysis) between Schwann cell-newly synthesized RNA and the actin-based molecular motor myosin Va [Canclini et al., 2014]. On the other hand, *Myo5* null mutant *dilute-lethal* mice have detectable newly synthesized RNA in Schwann cell but not in axons [Sotelo et al., 2013]. RNA transfer from Schwann cell to axon includes mRNA, because α-amanitin treated fibers decreased newly synthesized RNA in axoplasm and neurofilament light chain mRNA co-localized with Schwann cell derived RNAs in axons [Sotelo et al., 2013].

The main goal in this article is to elucidate the contribution of microtubule-based transport to the Schwann cell-to-axon RNA transfer in regenerating peripheral fibers as well as to determine whether kinesins are involved in this process.

RESULTS

BrU-RNA is transported throughout microtubules.

We performed confocal immunomicroscopy to assess the localization of BrU-labeled RNA in relation with microtubules (figure 1). Microtubule signal was found in Schwann cell cytoplasm, including outer cytoplasm in Cajal bands (figure 1A, red channel, arrowheads), Schmidt-Lantermann incisures (figure 1B, red channel, arrows) and node of Ranvier cytoplasm (figure 1C, red channel) and also in axoplasm (figure 1B and C, red channel). BrU-labeled RNA found in outer Schwann cell cytoplasm (figure 1A, green channel) co-localizes with microtubule signal (figure 1A, merged channels). At the Schmidt-Lantermann incisures level, BrU-labeled RNA found in Schwann cell cytoplasm and axoplasm (figure 1B, green channel) co-localizes with microtubule signal (figure 1B, merge channel). In addition, at the node of Ranvier, BrU signal (figure 1C, green channel) also co-localize with microtubule signal (figure 1C, merge channel). In summary, all cellular domains observed from regenerating sciatic nerve fibers showed co-localization between Schwann cell newly-synthesized RNAs and microtubules.

To determine if the Schwann cell-to-axon RNA transfer is dependent on microtubules, the microtubule network was disrupted by colchicine (figure 2). Colchicine treatment of fibers during the 6 hours of BrU-RNA labeling almost completely disrupts microtubule network (see red signal in figure 2A and B). In colchicine treated fibers, BrU-RNA signal is absent in axoplasm and Schwann cell cytoplasm at nodes of Ranvier (see green signal in figure 2A and B). Quantification of BrU-RNA signal in axoplasm at nodes of Ranvier of control fibers (figure 2C, black circles) showed the typical gradient distribution of fluorescence intensity, with a maximal signal in the nodal region that decreases towards both internodes. In contrast, axoplasm of colchicine treated fibers showed a background level of fluorescence intensity for BrU-RNA signal (figure 2C, open circles, $p<0.005$ in the 45 µm measured axoplasm). The same pattern was observed in the Schwann cell cytoplasm at the node of Ranvier, where colchicine treated fibers had a

background BrU-RNA fluorescence intensity level (211±14, figure 2D, white column) in contrast with the BrU-RNA intensity level of control ones (1223±58, figure 2D, black column, $p=5x10^{-9}$). Quantification of BrU-RNA fluorescence intensity in the first 30 µm from nucleus of Schwann cell outer cytoplasm, showed an apparent accumulation of BrU signal in the 5 microns near the nucleus comparing colchine-treated fibers with control ones (figure 2E), being statistically significant only over the first micron distance (456±72 in control vs 908±158 in colchicine treated fibers, p=0.01). To further confirm the BrU-RNA accumulation at the Schwann cell outer cytoplasm in colchicine-treated fibers, we performed BrU-RNA pulse-chase experiments. Fibers were incubated in BrU containing medium for 1 hour followed by washing and incubation in BrU-free medium for one further hour. Colchicine dependent accumulation of BrU-RNA at the Schwann cell outer cytoplasm near nuclei was confirmed. BrU-RNA signal fluorescence intensity in colchicine treated fibers (figure 2F, open circles) is higher than in control ones (figure 2F, black circles) in all 30 microns measured ($p<0.05$).

BrU-RNA is transported by kinesin-1 in axons but not by kinesin-3.

Microtubules-based RNA transport towards the cell periphery involves kinesin-mediated movement. KIF5s has been mentioned as RNA transport motors in neuronal processes [Dictenberg et al., 2008; Kanai et al., 2004; Ohashi et al., 2002]. Co-localization between BrU-RNA (figure 3A, Alexa 488-Ab - green) and KIF5B (figure 3A, Alexa 555-Ab - red, merge image, yellow) signals were observed in the axoplasm and Schwann cell cytoplasm at nodes of Ranvier. Confocal FRET analyses (figure 3B) were made between Alexa 488 Ab-KIF5B (as donor, figure 3C) and Alexa 555 Ab-BrU-RNA (as acceptor, figure 3D) to determine whether these molecules are in close association. BrU-RNA and KIF5B partners had a spectral bleedthrough (SBT)-uncorrected FRET (uFRET) observed in figure 3E. Processed FRET (pFRET) is displayed in figure 3F (after applying SBT corrections). E% distribution is shown in figure 3G. FRET interactions in crowded cellular environments occur either randomly and or in a controlled, specific manner,

such as clustering or complex formations; a mix of random and specific interaction events are also possible. To separate these two distribution types, an assay was developed [Kenworthy et al., 2000; H Wallrabe et al., 2007; Horst Wallrabe et al., 2003] which holds that in a controlled cellular event E% is independent on rising acceptor fluorescence and negative dependent on uD/A ratio. Applying this assay to the FRET data for the Alexa 488- Ab-BrU-RNA (donor) and Alexa 555-Ab-KIF5B (acceptor) or Alexa 488-Ab-KIF5B (donor) and Alexa 555-Ab-BrU-RNA (acceptor) combinations, it was shown that FRET interactions in the cytoplasm of Schwann cells were random encounters (E% showing independence on uD/A, r = 0.077, data not shown), whereas the opposite is true for the axoplasm (figure 3H, yellow ROIs). Figure 3I and J show the independence of E% in function of acceptor (A, r = 0) and the E% negative dependence on uD/A ratio (r = -0.179) of ROIs located at axoplasm, confirming the clustered FRET behavior of these ROIs. These results were obtained in three independent FRET experiments using Alexa 488-Ab-KIF5B as donor and Alexa 555-Ab-BrU-RNA as acceptor (configuration 1), and confirmed in experiments using Alexa 488-Ab-BrU-RNA as donor and Alexa 555-Ab-KIF5B as acceptor (configuration 2). As can be seen in figure 3K, E% frequency histogram of ROIs for configuration 1 experiments (black circles) is statistically equal (p=0.403) to ROIs of configuration 2 experiments (open circles). In summary, based on our findings KIF5B is implicated in the transport of Schwann cell-derived RNAs in axons but not in Schwann cell cytoplasm.

To determine the specificity of FRET analysis in our system, we performed confocal immunomicroscopy and confocal FRET microscopy with KIF1A, a neuronal specific kinesin family member which has not been reported to transport RNAs [Hirokawa et al., 2010]. KIF1A signal was observed specifically at the axoplasm in sciatic nerve fibers (figure 4A), where it partially co-localizes with BrU-labeled RNA signal (figure 4C, arrows). In spite of the apparent co-localization, FRET analysis gave negative results (i.e. KIF1A and BrU-RNA are not associated at the molecular level) since less than 0.3% of ROIs (9 in a total of 3130) remains after applying SBT corrections and the same constraints used in all FRET analyses (10-254 acceptor, donor and uFRET bounds, 5-254 E% and PFRET bounds, 1.25-

6 uD/A bounds). It seems that KIF1A is not the motor protein transporting Schwann cell-newly synthesized BrU-RNAs along axons.

Finally, whether KIF1B, reported as a molecular motor for mRNAs in oligodendrocytes [Carson et al., 1997; Lyons et al., 2009], could be responsible for BrU-RNA transport in Schwann cell and axons was tested. KIF1B was detected in Schwann cell outer cytoplasm (figure 5A, red) and in Schwann cell cytoplasm at the Node of Ranvier as well as axoplasm at the same place (figure 5B, red). In Schwann cell outer cytoplasm near the nucleus (figure 5A) BrU-RNA signal (green channel) show a punctate distribution that resembles ribonucleoparticles rows (see arrows as an example). KIF1B co-localizes with some BrU-RNA signals while they do not co-localizes with others (figure 5A, see arrows) Schwann cell cytoplasm near nucleus. Moreover, at nodes of Ranvier (figure 5B), neither co-localization was observed between KIF1B and BrU-RNA in Schwann cell cytoplasm nor in the axoplasm. These results suggest that BrU-RNA that co-localizes with KIF1B remains inside Schwann cells.

DISCUSSION

Specific RNAs can be localized to specific discrete regions of cell cytoplasm transported for long distances via microtubules [Sotelo-Silveira et al., 2006]. The results described here indicate that Schwann cell-derived RNAs found in axons are transported by the microtubule network. Colchicine completely interrupts the transfer of BrU-RNA to axons, as well as the transport from Schwann cell nucleus to Schwann cell cytoplasm at nodes of Ranvier. Moreover, BrU-RNA accumulates at the Schwann cell cytoplasm surrounding nucleus when microtubules are disrupted. We suggest that effect of colchicine on BrU-RNA distribution reflects the inhibition of RNA transport from the Schwann cell outer cytoplasm to the Schwann cell-axon boundary. We propose a model (figure 6) in which RNAs are transcribed in the Schwann cell nucleus, exported to the cytoplasm and transported to nodes of Ranvier by microtubules. At this point, Schwann cell newly-synthesized RNA probably translocates from the microtubule network to microfilaments. Our previous work [Sotelo et al., 2013] has demonstrated that the actin cytoskeleton and its associated molecular motor myosin Va, is necessary to cross the double membrane boundary between Schwann cell and axons at the nodes of Ranvier. It remains to be elucidated whether microtubules are the means by which Schwann cell-derived RNAs travel inside axons. In this regard, we determined that KIF5B (a Kinesin-1 family member) co-localizes with BrU-RNA. A deep analysis of FRET derived-data led us to determine that KIF5B interaction with BrU-RNA occurs in the axoplasm, leading to the proposition that Schwann cell-derived RNAs are transported inside axons by KIF5B. In addition to transport RNA containing granules in neuronal processes [Dictenberg et al., 2008; Kanai et al., 2004; Ohashi et al., 2002], KIF5 proteins have been implicated in mitochondrial transport in axons [Hirokawa et al., 2010]. BrU-RNA and KIF5B FRET results presented here cannot be due to interaction of KIF5B with mitochondria since we already demonstrated that mitochondria do not co-localizes with punctuate BrU-RNA signals in axons [Sotelo et al., 2013]. It was surprising to find FRET positive signals towards both internodes from nodes of Ranvier, since it is currently accepted that

microtubules have “plus-end out” orientation in axons [Baas et al., 1988] and KIF5 are plus-end directed motor proteins [Hirokawa and Noda, 2008]. However, not all microtubules have the canonical orientation in axons and 5% of them are “minus-end out” orientated in normal and regenerating sciatic nerve fibers *in vivo* [Kleele et al., 2014], which may explain our unexpected result. Alternatively, BrU-RNA could be transported by a different molecular motor integrating ribonucleoparticles that may also contain KIF5B. In this regard, proteomic analyses of BrU-RNA containing particles are needed. For instance, we have demonstrated that KIF1A and KIF1B, two Kinesin-3 family members, do not co-localize with BrU-RNA in axoplasm, leading to the proposal that these molecular motor are not component of Schwann cell-derived ribonucleoparticles found in axons. On the other hand, KIF1B motor protein could be transporting Schwann cell-resident RNAs because we just found very few co-localizations around Schwann cell nucleus.

In conclusion, we demonstrate that the delivery into axons of BrU-RNAs synthesized in Schwann cell nuclei is dependent on microtubules and is a complex, controlled and directed process that might be codified in the genome [Sotelo-Silveira et al., 2006].

MATERIALS & METHODS

Sciatic nerve transection and BrU incubation

Animal protocols were approved by the Comisión de Etica en el Uso de Animales (Animal Uses Ethics Commission -CEUA) at Instituto de Investigaciones Biológicas Clemente Estable, Montevideo, Uruguay and conform to Comisión Nacional de Experimentación Animal (Animal Experimentation National Commission - CNEA) guidelines and public law of Uruguay. Adult Sprague-Dawley rats were anesthetized with 5/10mg/kg ketamine/xylazine. A short incision was made at mid-thigh and the sciatic nerve was severed. After 18 h recovery, the rats were euthanized and a ~2 cm sciatic nerve segment proximal to the injury (proximal stump) was removed. Segments were incubated (37°C, 5% CO_2) in Neurobasal medium (Invitrogen) containing 10mg/ml bromouridine (BrU, Sigma) for 6 hours, or 1 hour (pulse chase experiments). Pulse-chase experiments were followed by four washes, 5 min each, in Neurobasal medium (Invitrogen) and a last incubation in Neurobasal medium (Invitrogen) for 40 min. In microtubules disruption experiments, 50μM colchicine (Sigma) was added to the culture media all the time.

Immunohistochemistry

Sciatic nerve segments were permeabilized before fixation according to Kahawaja *et al* [Khawaja et al., 1988] with a few modifications (see below) to remove monomeric tubulin for microtubule staining. Sciatic nerve segments were incubated 10 min in PEM buffer (85mM Pipes pH6.94, 10mM EGTA, 1mM $MgCl_2$) at 25°C, and then extracted for 1 hour with 0.5% triton X-100 in PEM buffer at 25°C. The extraction of colchicine-treated nerve segments was performed in buffer supplemented with colchicine (same concentration) to prevent repolymerization of microtubules during extraction. After tubulin extraction, sciatic nerve segments were rinsed once for 5 min in PEM buffer and fixed for 30 min in 3% paraformaldehyde in PEM buffer at 25°C. Segments were treated for 1 h at 37°C with 0.225 mg/ml collagenase (Sigma) in PHEM (60mM PIPES, 25mM HEPES,

10mM EGTA, 2mM $MgCl_2$) lacking EGTA and 5mM $CaCl_2$. The nerve fibers were released from epineurium with #5 forceps.

The incubation buffer for all immunocitochemistry steps was 0.1% BSA and 2% glycine in PHEM buffer. Nerve segments were prepared for immunocytochemistry by blocking in 10% normal goat serum for 30 min at 37°C. Permeabilized fibers were incubated with anti-BrdU (Roche, 1:20), anti-β-tubulin (Abcam, 1:100), anti-KIF5B (Sigma, 1:50), anti-KIF1A (Abnova, 1:200) and anti-KIF1B (Abnova, 1:200) over night at 4°C. Fibers were washed 3 times 10 min each. Secondary antibodies (goat anti-mouse and goat anti-rabbit conjugated with Alexa 488, 555, all from Invitrogen, all 1:1000) were incubated for 2 hours at Room Temperature (RT). F-actin was detected using Alexa 633-phalloidin (Invitrogen, 1:150) added together with secondary antibodies and nuclei were detected using DAPI (Invitrogen, 0.3nM). Fibers were then washed 3 times, 10 min each. Finally, individual fibers were teased and mounted in ProLong Antifade (Invitrogen). BrU-RNA was recognized with Alexa 488 antibody (Ab). Microtubules and KIFs proteins were recognized with Alexa 555 antibody.

Confocal Microscopy

Teased fibers were visualized on an Olympus FV-300 confocal microscope, equipped with a Plan Apo N 60X oil NA 1.42 lens and 405, 488, 543 and 633 nm laser excitation. For all quantitative analyses 10 or more fiber images were taken. Images were processed with Fluoview and ImageJ software. BrU-RNA antibody signal fluorescence intensity was measured along a line drawn on axoplasm, or Schwann cell cytoplasm. Fluorescence intensities were averaged between the 10 fibers every 2.5 µm along the axoplasm or Schwann cell cytoplasm (see figure 2, schematic C, E and F).

FRET analysis

Images were collected for FRET analysis using single-labeled donor and acceptor samples and double-labeled samples: four single-label donor reference images (donor excitation in both donor and acceptor emission channels); four single-label

acceptor reference images (donor and acceptor excitation, both in the acceptor emission channel); six to ten double-label images (donor excitation in donor and acceptor emission channels, acceptor excitation in acceptor emission channel). Control samples incubated without antibodies and incubated only with secondary antibodies were also included. Images of control samples were collected with donor and acceptor excitation lasers in both channels, including images in the donor channel at acceptor excitation to check for back-bleedthrough. All images were acquired at identical, previously optimized settings, using the same PMT in donor and acceptor channels and low laser power. Quantitative FRET analysis was performed using the PFRET plug-in for ImageJ (Keck Center for Cellular Imaging, University of Virginia, Charlottesville, VA22903) [Chen and Periasamy, 2006; Elangovan et al., 2003; Horst Wallrabe et al., 2006, 2003]. Background noise was subtracted using control images to calculate the gray-level value of background. Regions of interest (ROIs) were created automatically by the PFRET software. Data generated were processed using EXCEL. To eliminate outliers (data due to random interactions), the same restrictions were used in all FRET experiments performed with the different pair partners: acceptor, donor and uFRET bounds between 10 and 254 gray-scale values; PFRET and E% bounds between 5 and 254 gray-scale value; and lineal E% correlation with uD/A values between 1.25 and 6. FRET pairs were: a) Alexa 488 Ab-BrU-ARN as donor and Alexa 555 Ab-KIF5B as acceptor; b) Alexa 488 Ab-KIF5B as donor and Alexa 555 Ab-BrU-ARN as acceptor; c) Alexa 488 Ab-BrU-ARN as donor and Alexa 555 Ab-KIF1A as acceptor; d) Alexa 488 Ab-KIF1A as donor and Alexa 555 Ab-BrU-RNA as acceptor.

Acknowledgments

J.R.S., J.R.S.-S., A.K., and L.C. were supported by Pedeciba, MEyC, and ANII. J.R.S. and A.K. were supported by CSIC and Fcien-UdelaR. Authors have not conflict of interest.

REFERENCES

Baas PW, Deitch JS, Black MM, and Banker GA. 1988. Polarity orientation of microtubules in hippocampal neurons: uniformity in the axon and nonuniformity in the dendrite. Proceedings of the National Academy of Sciences of the United States of America 85:8335–9.

Brendza RP, Serbus LR, Duffy JB, and Saxton WM. 2000. A function for kinesin I in the posterior transport of oskar mRNA and Staufen protein. Science (New York, N.Y.) 289:2120–2.

Canclini L, Wallrabe H, Di Paolo A, Kun A, Calliari A, Sotelo-Silveira JR, and Sotelo JR. 2014. Association of Myosin Va and Schwann cells-derived RNA in mammal myelinated axons, analyzed by immunocytochemistry and confocal FRET microscopy. Methods (San Diego, Calif.) 66:153–61.

Carson JH, Worboys K, Ainger K, and Barbarese E. 1997. Translocation of myelin basic protein mRNA in oligodendrocytes requires microtubules and kinesin. Cell Motility and the Cytoskeleton 38:318–28.

Chen Y, and Periasamy A. 2006. Intensity range based quantitative FRET data analysis to localize protein molecules in live cell nuclei. Journal of Fluorescence 16:95–104.

Court FA, Hendriks WTJ, MacGillavry HD, Alvarez J, and van Minnen J. 2008. Schwann cell to axon transfer of ribosomes: toward a novel understanding of the role of glia in the nervous system. The Journal of Neuroscience : The Official Journal of the Society for Neuroscience 28:11024–9.

Court FA, Midha R, Cisterna BA, Grochmal J, Shakhbazau A, Hendriks WT, and Van Minnen J. 2011. Morphological evidence for a transport of ribosomes from Schwann cells to regenerating axons. Glia 59:1529–39.

Dictenberg JB, Swanger SA, Antar LN, Singer RH, and Bassell GJ. 2008. A direct role for FMRP in activity-dependent dendritic mRNA transport links filopodial-spine morphogenesis to fragile X syndrome. Developmental Cell 14:926–39.

Elangovan M, Wallrabe H, Chen Y, Day RN, Barroso M, and Periasamy A. 2003. Characterization of one- and two-photon excitation fluorescence resonance energy transfer microscopy. Methods (San Diego, Calif.) 29:58–73.

Hirokawa N. 2006. mRNA transport in dendrites: RNA granules, motors, and tracks. The Journal of Neuroscience : The Official Journal of the Society for Neuroscience 26:7139–42.

Hirokawa N, Niwa S, and Tanaka Y. 2010. Molecular motors in neurons: transport mechanisms and roles in brain function, development, and disease. Neuron 68:610–38.

Hirokawa N, and Noda Y. 2008. Intracellular transport and kinesin superfamily proteins, KIFs: structure, function, and dynamics. Physiological Reviews 88:1089–118.

Holt CE, and Bullock SL. 2009. Subcellular mRNA localization in animal cells and why it matters. Science (New York, N.Y.) 326:1212–6.

Jansen R-P, and Niessing D. 2012. Assembly of mRNA-protein complexes for directional mRNA transport in eukaryotes--an overview. Current Protein & Peptide Science 13:284–93.

Kanai Y, Dohmae N, and Hirokawa N. 2004. Kinesin transports RNA: isolation and characterization of an RNA-transporting granule. Neuron 43:513–25.

Kenworthy AK, Petranova N, and Edidin M. 2000. High-resolution FRET microscopy of cholera toxin B-subunit and GPI-anchored proteins in cell plasma membranes. Molecular Biology of the Cell 11:1645–55.

Khawaja S, Gundersen GG, and Bulinski JC. 1988. Enhanced stability of microtubules enriched in detyrosinated tubulin is not a direct function of detyrosination level. The Journal of Cell Biology 106:141–9.

Kleele T, Marinković P, Williams PR, Stern S, Weigand EE, Engerer P, Naumann R, Hartmann J, Karl RM, Bradke F, Bishop D, Herms J, Konnerth A, Kerschensteiner M, Godinho L, and Misgeld T. 2014. An assay to image neuronal microtubule dynamics in mice. Nature Communications 5:4827.

Lyons DA, Naylor SG, Scholze A, and Talbot WS. 2009. Kif1b is essential for mRNA localization in oligodendrocytes and development of myelinated axons. Nature Genetics 41:854–8.

MacDougall N, Clark A, MacDougall E, and Davis I. 2003. Drosophila gurken (TGFalpha) mRNA localizes as particles that move within the oocyte in two dynein-dependent steps. Developmental Cell 4:307–19.

Martin KC, and Ephrussi A. 2009. mRNA localization: gene expression in the spatial dimension. Cell 136:719–30.

Messitt TJ, Gagnon JA, Kreiling JA, Pratt CA, Yoon YJ, and Mowry KL. 2008. Multiple kinesin motors coordinate cytoplasmic RNA transport on a subpopulation of microtubules in Xenopus oocytes. Developmental Cell 15:426–36.

Müller M, Heuck A, and Niessing D. 2007. Directional mRNA transport in eukaryotes: lessons from yeast. Cellular and Molecular Life Sciences : CMLS 64:171–80.

Ohashi S, Koike K, Omori A, Ichinose S, Ohara S, Kobayashi S, Sato T-A, and Anzai K. 2002. Identification of mRNA/protein (mRNP) complexes containing Puralpha, mStaufen, fragile X protein, and myosin Va and their association with rough endoplasmic reticulum equipped with a kinesin motor. The Journal of Biological Chemistry 277:37804–10.

Sotelo JR, Canclini L, Kun A, Sotelo-Silveira JR, Xu L, Wallrabe H, Calliari A, Rosso G, Cal K, and Mercer JA. 2013. Myosin-Va-dependent cell-to-cell transfer of RNA from Schwann cells to axons. PloS One 8:e61905.

Sotelo-Silveira JR, Calliari A, Kun A, Koenig E, and Sotelo JR. 2006. RNA trafficking in axons. Traffic (Copenhagen, Denmark) 7:508–15.

Wallrabe H, Bonamy G, Periasamy A, and Barroso M. 2007. Receptor complexes cotransported via polarized endocytic pathways form clusters with distinct organizations. Molecular Biology of the Cell 18:2226–43.

Wallrabe H, Chen Y, Periasamy A, and Barroso M. 2006. Issues in confocal microscopy for quantitative FRET analysis. Microscopy Research and Technique 69:196–206.

Wallrabe H, Elangovan M, Burchard A, Periasamy A, and Barroso M. 2003. Confocal FRET microscopy to measure clustering of ligand-receptor complexes in endocytic membranes. Biophysical Journal 85:559–71.

Wilkie GS, and Davis I. 2001. Drosophila wingless and pair-rule transcripts localize apically by dynein-mediated transport of RNA particles. Cell 105:209–19.

Zimyanin VL, Belaya K, Pecreaux J, Gilchrist MJ, Clark A, Davis I, and St Johnston D. 2008. In vivo imaging of oskar mRNA transport reveals the mechanism of posterior localization. Cell 134:843–53.

Legends to figures

Figure 1. Newly-synthesized BrU-RNA co-localization with microtubules.
Regenerating sciatic nerves were incubated in BrU-containing medium and immunostained to visualize BrU-RNA (Alexa 488 antibody (Ab) - green) and microtubules (Alexa 555 Ab - red). **A,** Single confocal plane of Schwann cell outer cytoplasm. BrU-RNA and microtubules co-localization (merge signal, yellow) is observed at bands of Cajal (arrowheads). **B,** Single confocal planes at the axonal level of two Schmidt-Lanterman Incisures (arrows). Co-localization of BrU-RNA and microtubules is observed both in the Schwann cell cytoplasm and axoplasm (merge signal, yellow). **C,** Single confocal plane at the axonal level showing three examples of different nodes of Ranvier (NR). Co-localization of BrU-RNA and microtubules is observed both in the Schwann cell cytoplasm and axoplasm (merge signal, yellow). Bar: 5 µm.

Figure 2. Newly-synthesized BrU-RNA transport in the presence of colchicine.
Regenerating sciatic nerves were incubated in BrU-containing medium (A) or BrU-containing medium plus 50µM colchicine (B) and therefore immunostained. **A,** Single confocal plane from a node of Ranvier at the axonal level of fibers incubated with BrU, showing newly-synthesized BrU-RNA (Alexa 488 Ab - green), microtubules (Alexa 555 Ab - red) and actin (Alexa 633-phalloidin - gray). **B,** Single confocal plane from a node of Ranvier at the axonal level of fibers incubated with BrU plus 50µM colchicine, showing newly-synthesized BrU-RNA (Alexa 488 Ab - green), microtubules (Alexa 555 Ab - red) and actin (Alexa 633-phalloidin - gray). Bar: 10 µm. **C,** Quantification of newly-synthesized BrU-RNA signal (Alexa 488 Ab-BrU-RNA fluorescence intensity) along 45 µm from node of Ranvier towards internode of sciatic nerves axoplasm (incubated for 6 hours in BrU -black circles- or BrU plus 50µM colchicine -open circles). **D,** Quantification of newly-synthesized BrU-RNA signal (Alexa 488 Ab-BrU-RNA fluorescence intensity) in Schwann cell cytoplasm at node of Ranvier of sciatic nerves incubated for 6 hours in BrU (black

column) or BrU plus 50μM colchicine (white column). **E,** Quantification of newly-synthesized BrU-RNA signal (Alexa 488 Ab-BrU-RNA fluorescence intensity) in Schwann cell outer cytoplasm along 30 μm from nucleus of Schwann cells incubated for 6 hours in BrU (black circles) or BrU plus 50μM colchicine (open circles). **F,** Quantification of newly-synthesized BrU-RNA signal (Alexa 488 Ab-BrU-RNA fluorescence intensity) in Schwann cell outer cytoplasm along 30 μm from nucleus of Schwann cells incubated for 1 hour in BrU followed by 1 hour in BrU-free medium (black circles) or incubated 1 hour in BrU plus 50μM colchicine followed by 1 hour in BrU-free medium plus 50μM colchicine (open circles). Alexa 488-Ab BrU-RNA fluorescence intensity was measured along a line drawn on axoplasm, or Schwann cell cytoplasm. Fluorescence intensities were averaged between the 10 fibers every 2.5 μm along the axoplasm or Schwann cell cytoplasm. Data presented in all graphics are mean ± standard error. Statistical significance was determined by Student's t-test and is indicated when corresponds.

Figure 3. Newly-synthesized BrU-RNA co-localization and FRET analysis with KIF5B.

Regenerating sciatic nerves were incubated in BrU-containing medium and immunostained to visualize newly-synthesized BrU-RNA as well as KIF5B. **A,** Single confocal plane at the axonal level of node of Ranvier showing Alexa 488 Ab-BrU-RNA signal (green) and Alexa 555 Ab-KIF5B signal (red). Bar: 10μm. **B, FRET analysis.** All images are single confocal planes of the same node of Ranvier at the axonal level. Bar: 10μm. **C,** donor excitation/donor channel shows the quenched donor (Alexa 488 Ab-KIF5) fluorescence intensity. **D,** acceptor excitation/acceptor channel shows acceptor fluorescence intensity (Alexa 555 Ab-BrU-RNA). **E,** donor excitation/acceptor channel shows the uncorrected FRET (uFRET) intensity, which includes energy transfer level, donor cross-talk and acceptor bleedthrough. **F,** corrected FRET image, where donor cross-talk and acceptor bleedthrough were removed from uFRET. The resulting image represents the energy transfer level (PFRET). **G,** E% pseudocolor image. Calibration bar = 0-100 grayscale. **H,** the same focal plane showing the localization of ROIs (plotted in I and J). **I, J,** ROIs

located in axoplasm assayed for E% and acceptor levels (I) and E% and uD/A ratio (J) showing specific/clustered FRET behavior. Trend lines are shown as visual helpers. Correlation coefficients are indicated (r). **K,** E% frequency histogram from Alexa 488 Ab-KIF5B as donor and Alexa 555 Ab-BrU-RNA as acceptor FRET analysis (filled circles) and Alexa 488 Ab-BrU-RNA as donor and Alexa 555 Ab-KIF5B as acceptor FRET analysis (open circles). Statistical significance between the two FRET analyses was determined by Student's t-test (p=0.403).

Figure 4. Newly-synthesized BrU-RNA co-localization analysis with KIF1A. Regenerating sciatic nerves were incubated in BrU-containing medium and immunostained to visualize newly-synthesized BrU-RNA and KIF1A. **A,** Single confocal plane at the axonal level of node of Ranvier showing KIF1A signal (Alexa 555-Ab - red) and F-actin signal (Alexa 633-phalloidin - gray). **B,** Single confocal plane at the axonal level of the same node of Ranvier showing BrU signal (Alexa 488-Ab - green) and F-actin signal (Alexa 633-phalloidin - gray). **C,** Single confocal plane at the axonal level of node of Ranvier showing BrU-RNA signal (Alexa 488-Ab - green), KIF1A signal (Alexa 555-Ab - red) and F-actin signal (Alexa 633-phaloidin - gray). Arrows indicate co-localization signals between BrU-labeled RNA and KIF1A. Bar: 10μm.

Figure 5. Newly-synthesized BrU-RNA co-localization analysis with KIF1B. Regenerating sciatic nerves were incubated in BrU-containing medium and immunostained to visualize newly-synthesized BrU-RNA and KIF1B. **A,** Single confocal plane at Schwann cell outer cytoplasm next to the nucleus showing the KIF1B signal (Alexa 555-Ab - red) and BrU-RNA signal (Alexa 488-Ab - green). Arrows indicate ribonucleoparticles-like signals recognized by the anti-BrU antibody. **B,** Single confocal plane at the axonal level of node of Ranvier showing BrU-RNA signal (Alexa 488-Ab - green), KIF1B signal (Alexa 555-Ab - red) and F-actin signal (Alexa 633-phalloidin - gray). Bar: 10μm.

Figure 6. Model for RNA transfer from Schwann cell to axons.

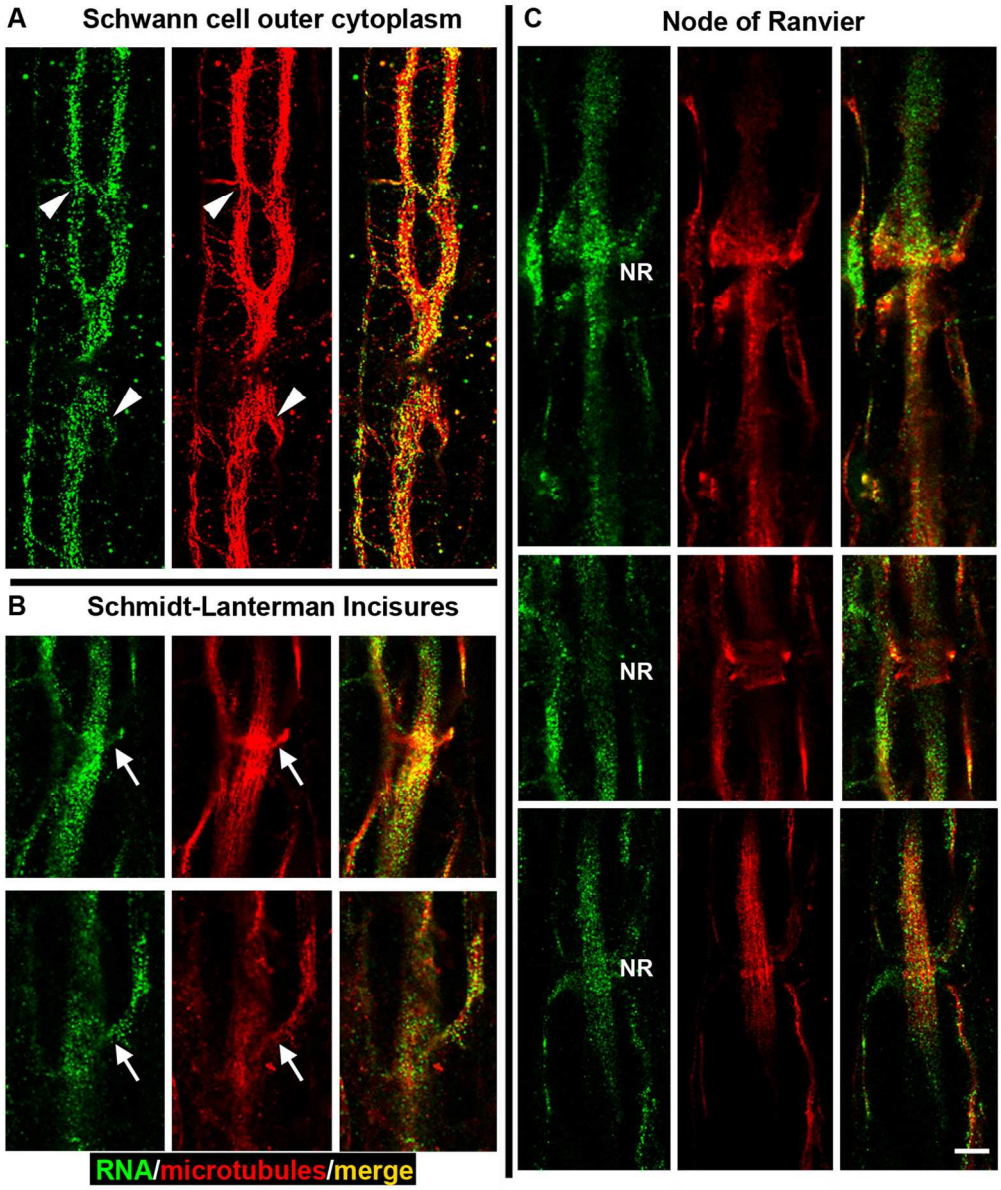

Figure 1. Newly-synthesized BrU-RNA co-localization with microtubules.
Regenerating sciatic nerves were incubated in BrU-containing medium and immunostained to visualize BrU-RNA (Alexa 488 antibody (Ab) - green) and microtubules (Alexa 555 Ab - red). A, Single confocal plane of Schwann cell outer cytoplasm. BrU-RNA and microtubules co-localization (merge signal, yellow) is observed at bands of Cajal (arrowheads). B, Single confocal planes at the axonal level of two Schmidt-Lanterman Incisures (arrows). Co-localization of BrU-RNA and microtubules is observed both in the Schwann cell cytoplasm and axoplasm (merge signal, yellow). C, Single confocal plane at the axonal level showing three examples of different nodes of Ranvier (NR). Co-localization of BrU-RNA and microtubules is observed both in the Schwann cell cytoplasm and axoplasm (merge signal, yellow). Bar: 5 μm.

129x155mm (300 x 300 DPI)

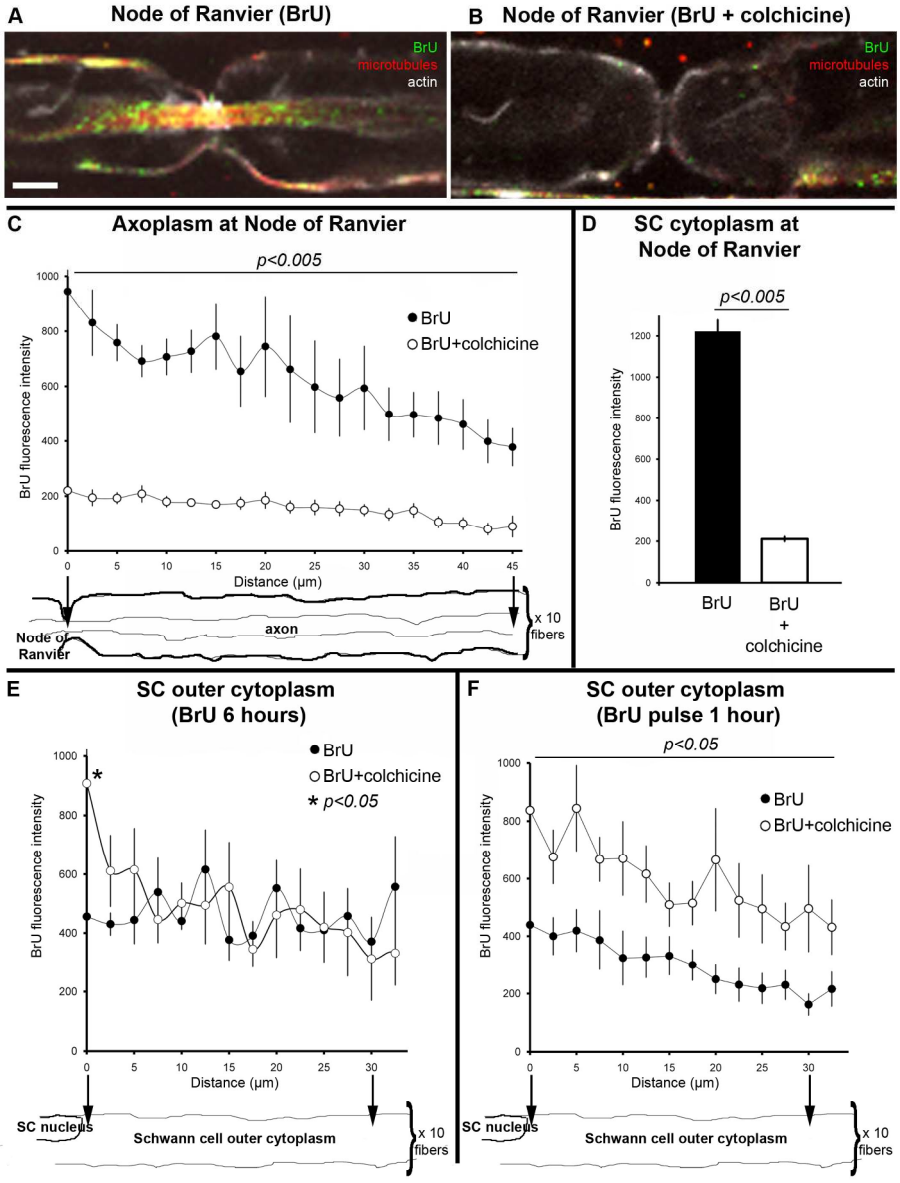

Figure 2. Newly-synthesized BrU-RNA transport in the presence of colchicine. Regenerating sciatic nerves were incubated in BrU-containing medium (A) or BrU-containing medium plus 50μM colchicine (B) and therefore immunostained. A, Single confocal plane from a node of Ranvier at the axonal level of fibers incubated with BrU, showing newly-synthesized BrU-RNA (Alexa 488 Ab - green), microtubules (Alexa 555 Ab - red) and actin (Alexa 633-phalloidin - gray). B, Single confocal plane from a node of Ranvier at the axonal level of fibers incubated with BrU plus 50μM colchicine, showing newly-synthesized BrU-RNA (Alexa 488 Ab - green), microtubules (Alexa 555 Ab - red) and actin (Alexa 633-phalloidin - gray). Bar: 10 μm. C, Quantification of newly-synthesized BrU-RNA signal (Alexa 488 Ab-BrU-RNA fluorescence intensity) along 45 μm from node of Ranvier towards internode of sciatic nerves axoplasm (incubated for 6 hours in BrU -black circles- or BrU plus 50μM colchicine -open circles). D, Quantification of newly-synthesized BrU-RNA signal (Alexa 488 Ab-BrU-RNA fluorescence intensity) in Schwann cell cytoplasm at node of Ranvier of sciatic nerves incubated for 6 hours in BrU (black column) or BrU plus 50μM colchicine (white column). E, Quantification of newly-synthesized BrU-RNA signal (Alexa 488 Ab-BrU-RNA fluorescence

intensity) in Schwann cell outer cytoplasm along 30 μm from nucleus of Schwann cells incubated for 6 hours in BrU (black circles) or BrU plus 50μM colchicine (open circles). F, Quantification of newly-synthesized BrU-RNA signal (Alexa 488 Ab-BrU-RNA fluorescence intensity) in Schwann cell outer cytoplasm along 30 μm from nucleus of Schwann cells incubated for 1 hour in BrU followed by 1 hour in BrU-free medium (black circles) or incubated 1 hour in BrU plus 50μM colchicine followed by 1 hour in BrU-free medium plus 50μM colchicine (open circles). Alexa 488-Ab BrU-RNA fluorescence intensity was measured along a line drawn on axoplasm, or Schwann cell cytoplasm. Fluorescence intensities were averaged between the 10 fibers every 2.5 μm along the axoplasm or Schwann cell cytoplasm. Data presented in all graphics are mean ± standard error. Statistical significance was determined by Student's t-test and is indicated when corresponds.

180x240mm (300 x 300 DPI)

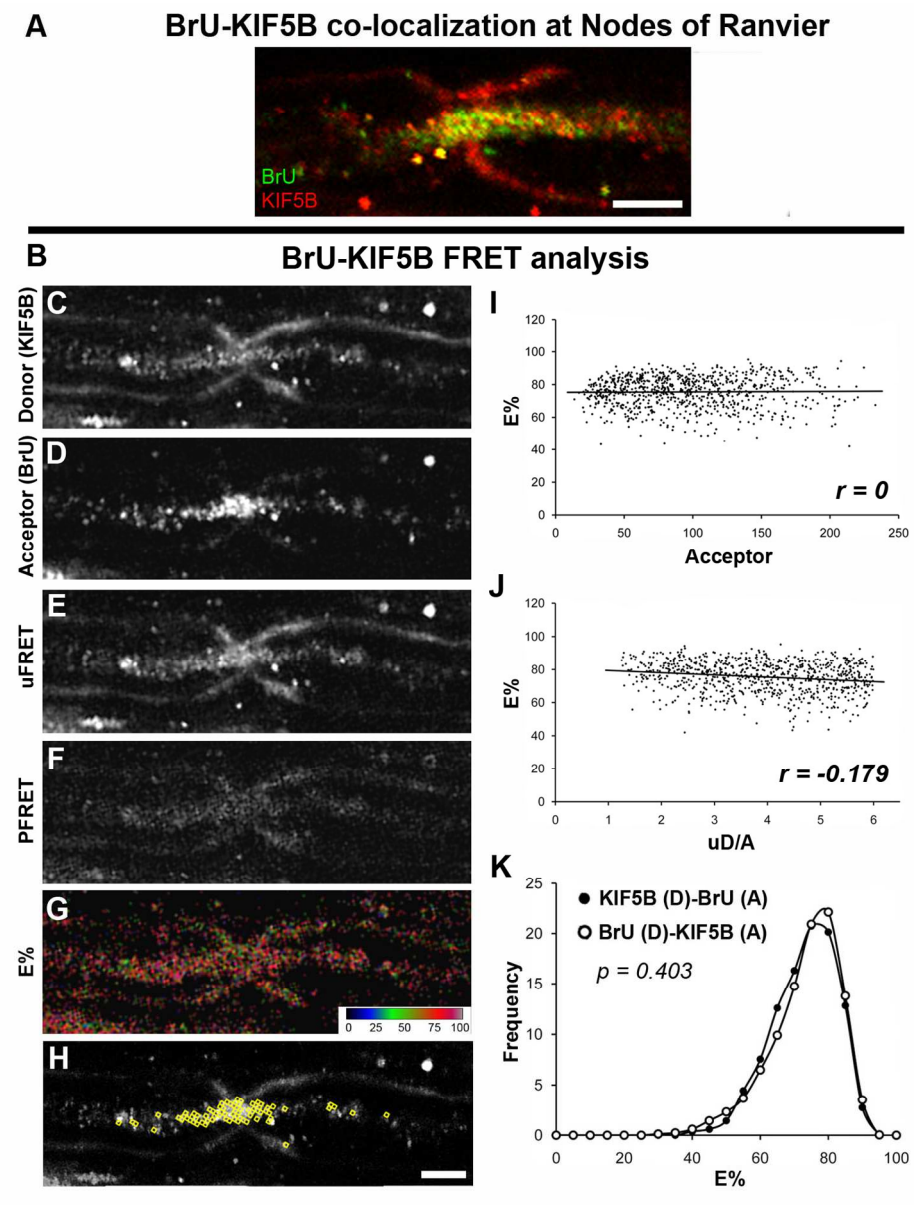

Figure 3. Newly-synthesized BrU-RNA co-localization and FRET analysis with KIF5B. Regenerating sciatic nerves were incubated in BrU-containing medium and immunostained to visualize newly-synthesized BrU-RNA as well as KIF5B. A, Single confocal plane at the axonal level of node of Ranvier showing Alexa 488 Ab-BrU-RNA signal (green) and Alexa 555 Ab-KIF5B signal (red). Bar: 10μm. B, FRET analysis. All images are single confocal planes of the same node of Ranvier at the axonal level. Bar: 10μm. C, donor excitation/donor channel shows the quenched donor (Alexa 488 Ab-KIF5) fluorescence intensity. D, acceptor excitation/acceptor channel shows acceptor fluorescence intensity (Alexa 555 Ab-BrU-RNA). E, donor excitation/acceptor channel shows the uncorrected FRET (uFRET) intensity, which includes energy transfer level, donor cross-talk and acceptor bleedthrough. F, corrected FRET image, where donor cross-talk and acceptor bleedthrough were removed from uFRET. The resulting image represents the energy transfer level (PFRET). G, E% pseudocolor image. Calibration bar = 0-100 grayscale. H, the same focal plane showing the localization of ROIs (plotted in I and J). I, J, ROIs located in axoplasm assayed for E% and acceptor levels (I) and E% and uD/A ratio (J) showing specific/clustered FRET behavior. Trend lines are

shown as visual helpers. Correlation coefficients are indicated (r). K, E% frequency histogram from Alexa 488 Ab-KIF5B as donor and Alexa 555 Ab-BrU-RNA as acceptor FRET analysis (filled circles) and Alexa 488 Ab-BrU-RNA as donor and Alexa 555 Ab-KIF5B as acceptor FRET analysis (open circles). Statistical significance between the two FRET analyses was determined by Student's t-test (p=0.403).

129x170mm (300 x 300 DPI)

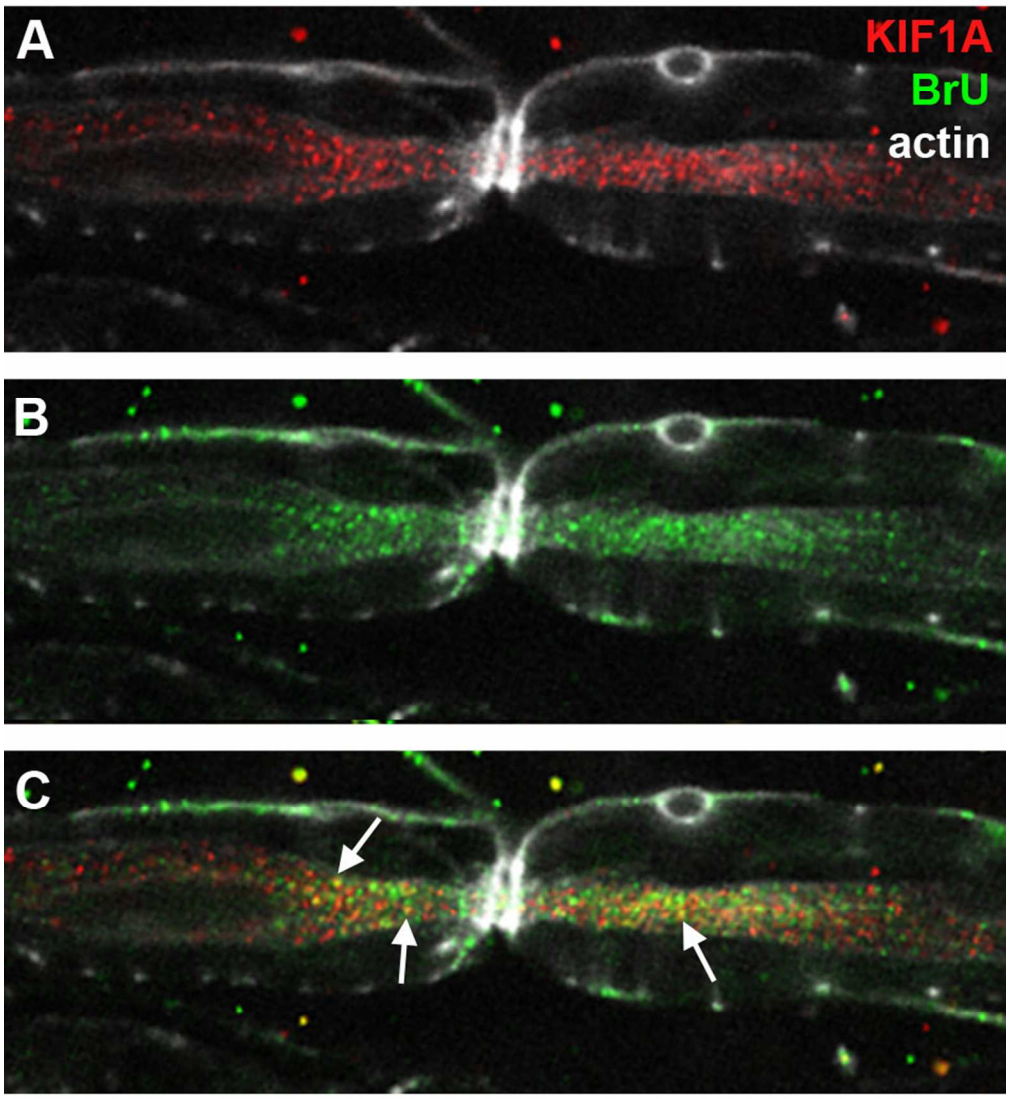

Figure 4. Newly-synthesized BrU-RNA co-localization analysis with KIF1A.
Regenerating sciatic nerves were incubated in BrU-containing medium and immunostained to visualize newly-synthesized BrU-RNA and KIF1A. A, Single confocal plane at the axonal level of node of Ranvier showing KIF1A signal (Alexa 555-Ab - red) and F-actin signal (Alexa 633-phalloidin - gray). B, Single confocal plane at the axonal level of the same node of Ranvier showing BrU signal (Alexa 488-Ab - green) and F-actin signal (Alexa 633-phalloidin - gray). C, Single confocal plane at the axonal level of node of Ranvier showing BrU-RNA signal (Alexa 488-Ab - green), KIF1A signal (Alexa 555-Ab - red) and F-actin signal (Alexa 633-phaloidin - gray). Arrows indicate co-localization signals between BrU-labeled RNA and KIF1A. Bar: 10μm.

80x90mm (300 x 300 DPI)

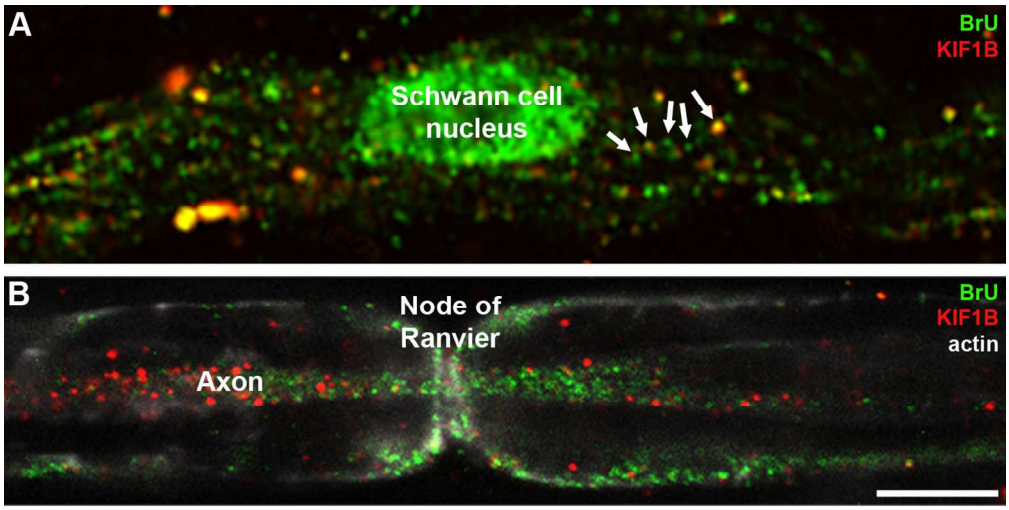

Figure 5. Newly-synthesized BrU-RNA co-localization analysis with KIF1B.
Regenerating sciatic nerves were incubated in BrU-containing medium and immunostained to visualize newly-synthesized BrU-RNA and KIF1B. A, Single confocal plane at Schwann cell outer cytoplasm next to the nucleus showing the KIF1B signal (Alexa 555-Ab - red) and BrU-RNA signal (Alexa 488-Ab - green). Arrows indicate ribonucleoparticles-like signals recognized by the anti-BrU antibody. B, Single confocal plane at the axonal level of node of Ranvier showing BrU-RNA signal (Alexa 488-Ab - green), KIF1B signal (Alexa 555-Ab - red) and F-actin signal (Alexa 633-phalloidin - gray). Bar: 10μm.

129x64mm (300 x 300 DPI)

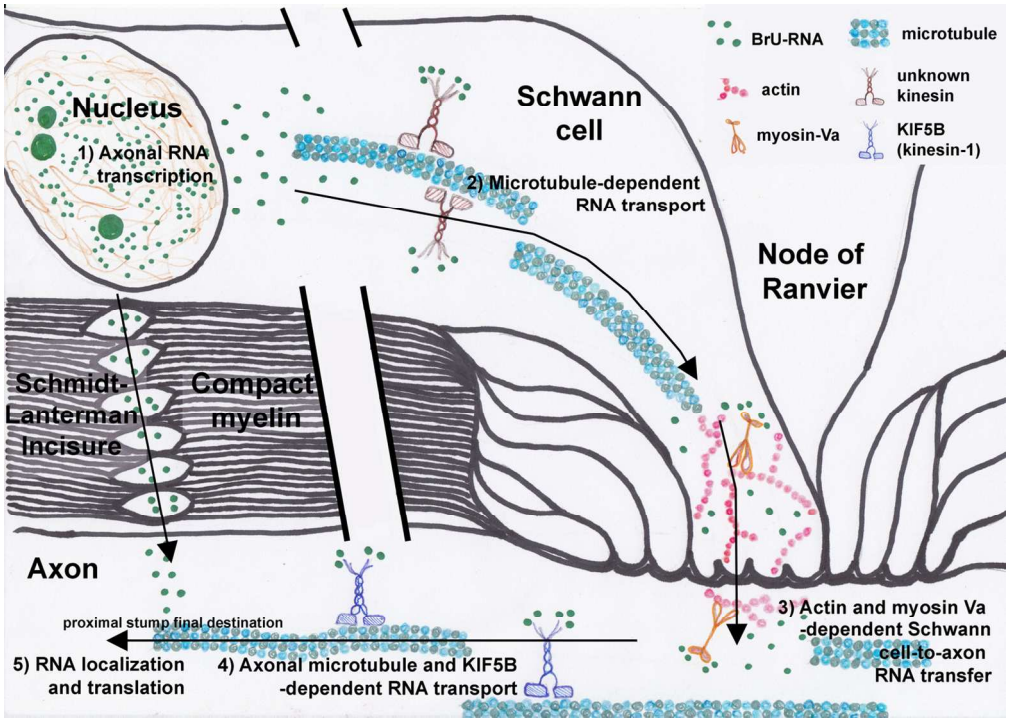

Figure 6. Model for RNA transfer from Schwann cell to axons.
128x91mm (300 x 300 DPI)

7.3. Capítulo III.

Identificación de los ARNm axonales transcritos en la célula de Schwann.

En los capítulos anteriores se presentaron los resultados que respondieron muchas de las preguntas planteadas en relación a la transferencia glia-axón de ARNs. Sin embargo, una de las interrogantes más interesantes quedaba todavía por responder: ¿cuál es la identidad de estos ARNs? Nuestra hipótesis sostenía que los ARN transferidos desde la célula de Schwann deberían incluir ARNm específicos neuronales y en particular axonales. En este capítulo se describen los experimentos llevados a cabo en la parte final de la tesis y que constituyen los primeros aportes que permitirán responder esta pregunta.

7.3.1. Inmunoprecipitación de los ARN-BrU y PCR.

Los ARNs transcritos en el núcleo de la célula de Schwann fueron marcados con BrU *in vitro* como se describió (ver capítulo I) y fueron purificados mediante inmunoprecipitación utilizando un anticuerpo anti-BrdU (de aquí en adelante nos referiremos a estas muestras como "ARN-BrU"). Se incluyó un grupo control en el cual los nervios ciáticos fueron incubados en medio sin BrU. Los ARNs provenientes de estos nervios fueron también sometidos a inmunoprecipitación utilizando el anticuerpo anti-BrdU (de aquí en adelante nos referiremos a estas muestras como "ARN control"). Se realizaron reacciones de PCR utilizando pares de cebadores diseñados para la amplificación de genes de expresión específica neuronal. Los tres marcadores seleccionados: NF-L, NF-M y ankirina G (Ank-G), dieron lugar a productos de amplificación del tamaño esperado en las muestras (sin realizar inmunoprecipitación) de ARN-BrU (carril 2, figura 6.1) y ARN control (carril 3, figura 6.1). Esto confirma la presencia de los tres ARNm en la población de ARNs que se purificaron a partir de los nervios ciáticos cultivados *in vitro*. Una vez ejecutada la inmunoprecipitación, las reacciones de PCR realizadas utilizando los ARN control no producen ningún fragmento amplificado (carril 5, figura 6.1). Esto significa que la inmunoprecipitación no da lugar a la purificación de ARNs no bromouridinados (los anticuerpos anti-BrdU no interactúan inespecíficamente con los ARNs) o por lo menos no purifican cantidades detectables por PCR de ARNs con los niveles de expresión de NF-L, NF-M y Ank-G. Por el contrario, las reacciones de PCR realizadas con los

ARN-BrU inmunoprecipitados, dan lugar a fragmentos del tamaño esperado para los tres marcadores neuronales (carril 4, figura 6.1). Es decir, que los ARNm que codifican para las subunidades liviana y mediana de los neurofilamentos y para la Ank-G, tres genes que supuestamente sólo se expresan en las neuronas, son neosintetizados en la célula de Schwann.

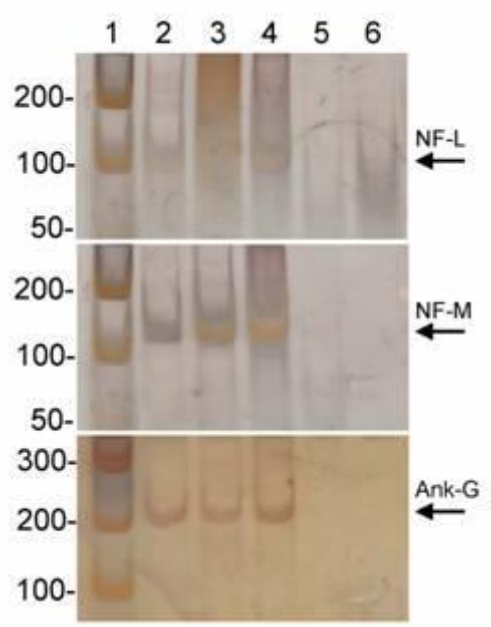

Figura 7.1. PCR para amplificar NF-L, NF-M y Ank-G.
Electroforesis en gel de poliacrilamida teñido con plata de los productos de la amplificación por PCR de los neurofilamentos liviano (NF-L), mediano (NF-M) o ankirina G (ank-G). El fragmento amplificado de tamaño esperado se indica con una flecha. 1- Marcador de peso molecular. A la izquierda se indica el tamaño de cada banda en pares de bases. En las reacciones de PCR se utilizó como molde ADNc retrotranscrito a partir de: 2- ARN-BrU sin inmunoprecipitar. 3- ARN control sin inmunoprecipitar. 4- ARN-BrU luego de la inmunoprecipitación. 5- ARN control luego de la inmunoprecipitación. 6- control negativo de la PCR (sin ADN molde)

7.3.2. Secuenciación masiva de los ARN-BrU

Los resultados preliminares obtenidos mediante PCR a tiempo final condujeron a realizar la secuenciación masiva de los ARNs purificados mediante inmunoprecipitación, para poder conocer la identidad de los ARNs neosintetizados en la célula de Schwann. Conociendo la identidad de los ARNm es posible, como primer paso, inferir cuáles son candidatos a integrar la población de ARNs transferidos de la glia al axón.

La secuenciación masiva de la muestra ARN-BrU y de la muestra ARN control se llevo a cabo utilizando la tecnología Ion Torrent. Los datos obtenidos se analizaron cualitativamente utilizando el programa *fastqc* y se resolvió hacer un recorte (*trimming*) de las secuencias obtenidas para mejorar su calidad. Para el *trimming* se utilizó el programa *sickle*, indicando que la calidad deseada debía ser mayor a 20 (q=20, donde $q=-10\log_{10}(P)$ en escala Phred, donde P es la probabilidad de error en la determinación de una base) y que el largo de las lecturas luego del recorte debía ser mayor a 50 pb. Se realizó un nuevo análisis de calidad (*fastqc*) de los datos obtenidos a partir del *trimming*, verificándose una mejora en la calidad de las secuencias por base, así como también en la distribución del largo de las secuencias y el contenido *k-mer*. El número de lecturas antes y después del *trimming* para ambas muestras se presenta en la Tabla I.

Tabla I. Número de lecturas de cada biblioteca antes y después del recorte.

Muestra	**Numero de lecturas**	
	Antes	**Después**
ARN-BrU	4.187.872	2.487.419
Control	93.510	54.602

Las lecturas procedentes de ambas muestras fueron alineadas al genoma de *Rattus norvegicus* con el programa *CLC Genomics Workbench 6.5* (CLC Bio), obteniéndose así listas de genes representados en cada una de ellas. El porcentaje de lecturas alineadas fue del 80 % para la muestra ARN-BrU y 66% para la muestra ARN control. Las listas fueron filtradas para conservar aquellos ARNm representados por más de 5 lecturas y con un RPKM mayor a 1.

Obtuvimos 8283 genes representados en la muestra ARN-BrU. Los genes representados en dicha lista están implicados en funciones biológicas muy diversas. Dentro de las categorías sobrerrepresentadas encontramos ARNm del transporte intracelular (343, $p=3.8\times10^{-43}$), de la localización de proteínas (421, $p=2.5\times10^{-39}$), de la respuesta celular al estrés (263, $p=6.1\times10^{-19}$), del procesamiento de ARN (217, $p=1.5\times10^{-15}$), de proteínas ribosomales

(69, $p=9.6x10^{-12}$), de la vía de señalización por neurotrofinas (90, $p=2.3x10^{-9}$), de la endocitosis (126, $p=4.4x10^{-8}$), de la vía de señalización por ErbB (63, $p=7.4x10^{-8}$), de la regulación del citoesqueleto de actina (127, $p=4.5x10^{-7}$) y de la fosforilación oxidativa (94, $p=1.1x10^{-8}$). A pesar de haber incluido un paso de eliminación de los ARN ribosomales durante la construcción de las bibliotecas de ADNc a secuenciar, entre las moléculas secuenciadas se encuentran los ARN ribosomales (Rn45S 141603 lecturas, Rn 28S 535 lecturas, Rn18S 737 lecturas y Rn5-8S 3052 lecturas). Esto indica que la depleción de los ARNr en las muestras no fue completa, pero por otro lado también indica que los ARNr son parte de la población de ARNs neosintetizados en la célula de Schwann y marcados con BrU.

Para evaluar cuántos de los ARNm identificados en los experimentos de secuenciación masiva, ya habían sido reportados en nervios ciáticos en regeneración (24 horas), nuestra lista se comparó con los datos obtenidos por Li *et al.*, (2013) mediante microarreglos. Se detectaron 5704 ARNm en común entre nuestra lista (ARN-BrU) y la lista de ARNm reportada por Li *et al.* en 2013 (p=0, figura 7.2). Los ARNm únicos para cada una de las listas pueden explicarse por las diferencias en las metodologías de identificación utilizadas, pero más aún por la diferencia entre las poblaciones de ARN analizadas. Li *et al.* analizaron mediante microarreglos la identidad del ARN total presente en nervios ciáticos en regeneración a las 24 horas de la lesión. En cambio en nuestro análisis se determinó mediante secuenciación masiva la identidad de los ARN neosintetizados en una ventana de tiempo entre las 18 y 24 horas post-lesión.

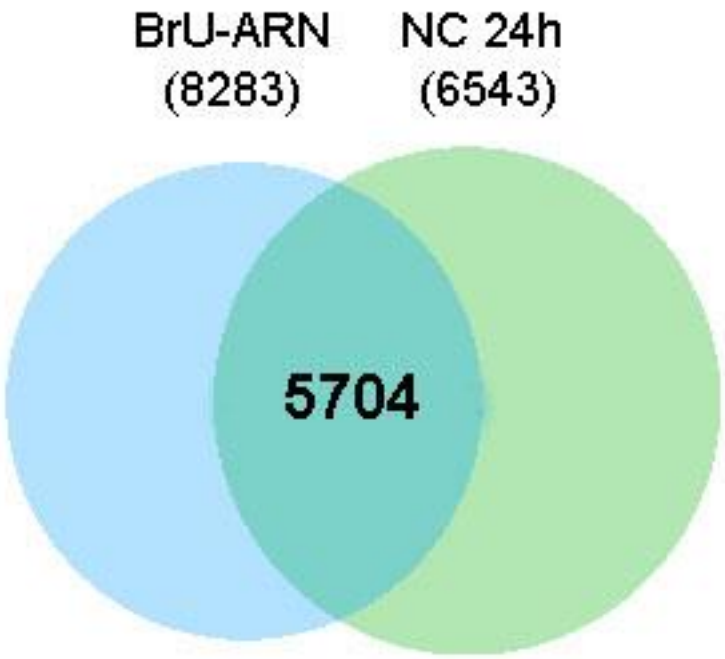

Figura 7.2. Diagrama de Venn ARN-BrU, NC 24h.
El diagrama de Venn muestra los genes compartidos (5704) entre la lista producida por secuenciación de la muestra ARN-BrU (8283 genes en total) y la lista de genes identificados por Li y cols. mediante microarreglos en nervios ciáticos 24 horas post-lesión (NC 24H, 6543 genes en total). p=0.

En la lista obtenida a partir de la muestra ARN-BrU se encuentran genes típicos marcadores de célula de Schwann (sólo se expresan en la célula de Schwann). Algunos de ellos se listan en la tabla II indicando el lugar que ocupan en la lista de ARN-BrU, el nivel de expresión (medido en RPKM) y el número de lecturas observadas para cada uno de ellos en las muestras ARN-BrU y ARN control. Queremos resaltar la diferencia en las lecturas obtenidas entre las muestras ARN-BrU y ARN control, que en todos los casos es de uno o dos órdenes de magnitud mayor en la primera con respecto a la segunda. Esto significa que algún grado de contaminación por ARNs se obtiene luego de la inmunoprecipitación con el anticuerpo anti-BrdU, pero esta contaminación es mínima y no explica las secuencias obtenidas a partir de la muestra ARN-BrU.

Tabla II. Genes típicos marcadores de célula de Schwann.

Gen	Posición	RPKM	n° de lecturas	
			ARN-BrU	ARN control
Mpz	2	2956	6000	100
Pmp22	14	827	3540	48
S100b	17	813	2576	44
Mbp	23	725	5867	156
Gsn	50	342	1901	39
Sdc4	113	156	771	21
Gldn	209	87	413	11
Gfap	324	57	381	NA
Cnp	448	42	212	NA
Plp1	569	33	227	8
Sdc3	3193	6	56	NA
Mag	4232	6	39	NA

NA: no aparece

La tabla III lista ARNm conocidos como de expresión específica neuronal que fueron identificados en nuestros análisis de secuenciación masiva de la muestra ARN-BrU. Indicamos para cada gen el lugar que ocupa en la lista de ARN-BrU, el nivel de expresión (medido en RPKM) y el número de lecturas observadas para cada uno de ellos en las muestras ARN-BrU y ARN control. La mayoría de los genes "neuronales" identificados codifican para proteínas del citoesqueleto, pero también puede observarse la presencia de genes que codifican para canales de potasio. Además de los genes listados, obtuvimos lecturas que mapean en otros genes conocidos como específicos neuronales. Entre ellos se encuentran dos canales de potasio (*Kcnq2* y *Kcnq3*) y los genes que codifican para las proteínas asociadas a microtúbulos MAP2 (*Map2*) y Tau (*Mapt*). Estos genes fueron eliminados de la lista definitiva luego de aplicar los filtros (RPKM>1, número de lecturas alineadas>5). Confiamos que cuando realicemos la secuenciación de los ARN-BrU a mayor profundidad estos genes permanecerán en la lista definitiva.

Tabla III. Genes típicos marcadores de neurona.

Gen	Posición	RPKM	n° de lecturas	
			ARN-BrU	ARN control
Sptan1	231	79	1237	93
Sptbn1	260	70	1943	87
Kcna1	584	32	112	NA
Kif1a	891	22	290	NA
Tubb3	1203	17	58	NA
Nefl	1163	17	69	NA
Ank3	1815	11	222	NA
Nefm	5059	3	21	NA
Ank2	5071	3	115	NA
Stau2	5485	3	20	NA
Nefh	7442	1	11	NA
Kcna2	7458	1	36	NA

NA: no aparece

Comparamos nuestra lista de ARN-BrU con los resultados obtenidos por Farías (Tesis de Maestría, "Análisis del transcriptoma de axones mielínicos mediante secuenciación masiva", PEDECIBA, Area Biología, Agosto 2014) mediante secuenciación masiva de ARN purificado a partir de axones maduros aislados, es decir libres de mielina. Se detectaron 429 ARNm en común entre ambas listas ($p=4.05x10^{-45}$, figura 7.3), así como 198 ARNm reportados por Farías que no fueron identificados en nuestro ensayo. Existen varias explicaciones posibles para este hecho. En primer lugar, la diferencia puede deberse al nivel de profundidad alcanzado en nuestros ensayos de secuenciación que puede ser insuficiente para identificar esos genes. En segundo lugar, Farías utilizó axones provenientes de las raíces medulares ventrales, mientras que nuestros ensayos fueron realizados a partir de nervios ciáticos. El transcriptoma de las fibras ventrales no necesariamente tiene que ser idéntico del transcriptoma del nervio ciático, el cual también incluye otras clases de fibras. Por último, tampoco podemos asumir que todos los ARNm del axón deban provenir de la célula de Schwann y esos 198 ARNm reportados por Farias podrían provenir únicamente del soma neuronal.

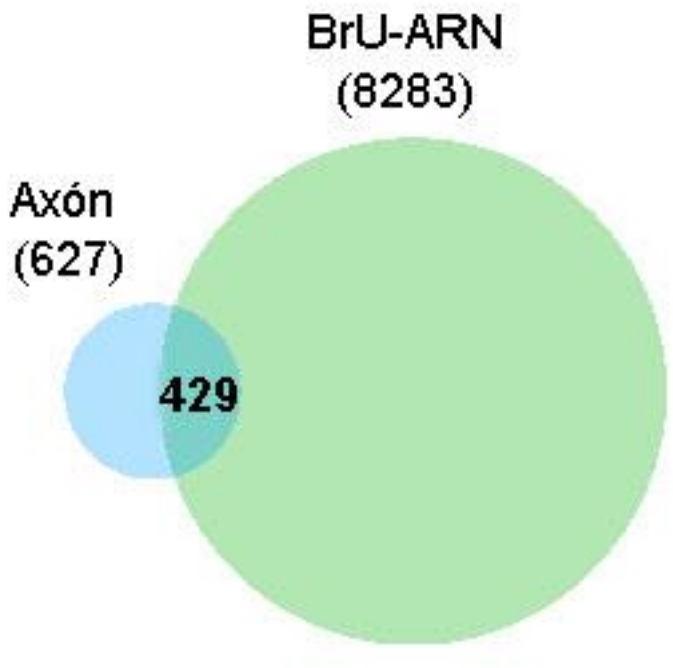

Figura 7.3. Diagrama de Venn BrU-ARN, Axón.
El diagrama de Venn muestra los genes compartidos (429) entre la lista producida por secuenciación de la muestra ARN-BrU (8283 genes en total) y la lista de genes identificados por Farias mediante secuenciación masiva de los ARNs presentes en axones maduros aislados (Axón, 627 genes en total). $p=4.05x10^{-45}$.

Por último, comparamos la lista de ARNm presentes en la muestra ARN-BrU con la lista de ARNs asociados a miosina Va (trabajo V), de la cual se sabe está implicada en la localización de ARNm en células de mamíferos (Ohashi *et al.*, 2002; Yoshimura *et al.*, 2006; Salerno *et al.*, 2008; Nalavadi *et al.*, 2012). Las listas de genes asociados a miosina Va fue generada por los Dres Calliari y Sotelo-Silveira mediante microarreglos. La muestra a hibridar procedió de la inmunoprecipitación de extractos de RNPs de cerebro de ratón, utilizando un anticuerpo anti-miosina Va. A partir de allí se purificaron los ARNm que co-inmunoprecipitan con miosina Va. Una vez comparada la lista de ARNm generada en el trabajo V con la lista de ARN-BrU, se identificaron 163 ARNm en común entre ambas listas ($p=5.01x10^{-14}$). Entre los coincidentes se encuentran casi todos los ARNm ubicados en los primeros lugares en la lista de ARN procedentes de la inmunoprecipitación con anti-miosina Va. Sin embargo, en la lista de los ARNm procedentes de la inmunoprecipitación con anti-miosina Va, no se observan los ARNm específicos neuronales presentes en nuestra

lista. Esto es sorprendente dado que la transferencia de ARN desde la glia al axón depende de la presencia de miosina Va. Dado que la inmunoprecipitación con anti-miosina Va fue realizada en extractos de cerebro de ratón, es necesario analizar si la población de ARNs que se asocian a miosina Va es diferente en el Sistema Nervioso Central con respecto a lo que sucede en los nervios ciáticos, y es esta la causa de la incongruencia encontrada.

A partir de los datos preliminares presentados en este capítulo consideramos que se abre un camino a explorar que permita un aporte consistente con los postulados de esta tesis. En primer lugar se deben secuenciar los ARN provenientes de la inmunoprecipitación con BrU con mayor profundidad intentando alcanzar unas 20.000.000 de lecturas y realizar un análisis más exhaustivo de las secuencias obtenidas. En segundo lugar, es necesario realizar ensayos (qPCR) que permitan confirmar la identidad y el valor de expresión de los ARNs identificados mediante secuenciación masiva. Por último, consideramos perentorio realizar experimentos de hibridación *in situ* contra ARNm de interés presentes en la lista ARN-BrU, que aporten información sobre su localización en el tejido y la existencia de co-localización de su señal con la correspondiente al anticuerpo anti-BrdU. Aunque estos experimentos ya han sido realizados eligiendo como candidato al ARNm de NFL (ver capítulo I, trabajo II), consideramos que los mismos deben ser realizados también para otros ARNm específicos neuronales identificados en nuestros experimentos de secuenciación masiva.

7.3.3. TRABAJO V

Calliari, A., Farias, J., Puppo, A., Canclini, L., Mercer, J. A., Munroe, D., Sotelo, J. R., Sotelo-Silveira, J. R. Myosin Va associates with mRNA in Ribonucleoprotein Particles present in myelinated Peripheral Axons and in the Central Nervous System. Developmental Biology, 74 (3), 382-396, 2014.

Myosin Va Associates With mRNA in Ribonucleoprotein Particles Present in Myelinated Peripheral Axons and in the Central Nervous System

Aldo Calliari,[1,2] Joaquina Farías,[3] Agostina Puppo,[1*] Lucía Canclini,[1] John A. Mercer,[4] David Munroe,[5] José R. Sotelo,[1] José R. Sotelo-Silveira[3,6]

[1] Department of Proteins and Nucleic Acids, Instituto de Investigaciones Biológicas Clemente Estable, Montevideo, Uruguay

[2] Department of Molecular and Cellular Biology, School of Veterinary-UdelaR, Montevideo, Uruguay

[3] Department of Genetics, Instituto de Investigaciones Biológicas Clemente Estable, Montevideo, Uruguay

[4] McLaughlin Research Institute, Great Falls MT, USA, and Institute for Stem Cell Biology and Regenerative Medicine, National Centre for Biological Sciences, Bangalore, India

[5] Cancer Research Technology Program, Leidos Biomedical Research, Inc.-Frederick National Laboratory for Cancer Research, Frederick, Maryland

[6] Department of Cell and Molecular Biology, School of Sciences-UdelaR, Montevideo, Uruguay

Received 22 May 2013; revised 17 November 2013; accepted 19 November 2013

ABSTRACT: **Sorting of specific mRNAs to particular cellular locations and regulation of their translation is an essential mechanism underlying cell polarization. The transport of RNAs by kinesins and dyneins has been clearly established in several cell models, including neurons in culture. A similar role appears to exist in higher eukaryotes for the myosins. Myosin Va (Myo5a) has been described as a component of ribonucleoprotein particles (RNPs) in the adult rat nervous system and associated to ZBP1 and ribosomes in ribosomal periaxoplasmic plaques (PARPs), making it a likely candidate for mediating some aspects of RNA transport in neurons. To test this hypothesis, we have characterized RNPs containing Myo5a in adult brains of rats and mice. Microarray analysis of RNAs co-immunoprecipitated with Myo5a indicates that this motor may associate with a specific subpopulation of neuronal mRNAs. We found mRNAs encoding α-synuclein and several proteins with functions in translation in these RNPs. Immunofluorescence analyses of RNPs showed apparent co-localization of Myo5a with ribosomes, mRNA and RNA-binding proteins in discrete structures present both in axons of neurons in culture and in myelinated fibers of medullary roots. Our data suggest that PARPs include RNPs bearing the mRNA coding for Myo5a and are equipped with kinesin and Myo5a molecular motors. In conclusion, we suggest that Myo5a is involved in mRNA trafficking both in the central and peripheral nervous systems.** © 2013 Wiley Periodicals, Inc. Develop Neurobiol 74: 382–396, 2014

Keywords: **RNA transport; ribonucleoprotein complexes; RNP; myosin Va; axon**

INTRODUCTION

The sorting of specific mRNAs to particular cell locations and the spatial regulation of their translation is

Additional Supporting Information may be found in the online version of this article.

**Present address:* Telethon Institute of Genetics and Medicine, Naples, Italy.

Correspondence to: J.R. Sotelo-Silveira (jsotelosilveira@iibce.edu.uy).

Contract grant sponsor: I+D Grants of the University of the Republic (CSIC- UdelaR, Uruguay), the Program for the Development of Basic Sciences (PEDECIBA, Uruguay), and the National Agency for Research and Innovation (ANII, Uruguay).

Published online 22 November 2013 in Wiley Online Library (wileyonlinelibrary.com).
DOI 10.1002/dneu.22155

essential to establish cell polarity and thus proper function (Gagnon and Mowry, 2011; Jung et al., 2011). In neurons, mRNA targeting to postsynaptic domains and regulated translation is important in synaptic plasticity (Costa-Mattioli et al., 2007; Westmark and Malter, 2007; Bear et al., 2008). On the presynaptic side, impaired axonal targeting of $\beta-$actin mRNA has been postulated to be responsible for spinal motor atrophy in humans (Rossoll et al., 2003). *In vivo*, the 3′ UTR of the mRNA coding for β-actin is sufficient to target a GFP transgene into axons (Willis et al., 2011) while the availability of ZBP1, an mRNA binding protein, modulates axonal regeneration (Donnelly et al., 2011). Although the adult axonal transcriptome remains to be characterized, genomic studies revealed a surprising diversity of mRNAs (for review, see Canclini et al., 2012; Deglincerti and Jaffrey, 2013). Recent observations from regenerating unmyelinated axons *in vitro* (Andreassi et al., 2011; Gumy et al., 2011; Zivraj et al., 2011) clearly broaden the possible functionality of the axonal compartment, including a contribution of axonal protein synthesis to neuronal polarity.

While the existence of microtubule-dependent transport of mRNA in neuronal axons is well established (Yoo et al., 2009; Gagnon and Mowry, 2011), the involvement of actin-based motors in RNA transport and localization is less understood. The first, and probably best example of myosin-dependent transport of mRNA was originally described in yeast by Long et al. (1997), where there is an absolute requirement of the class V myosin Myo4p for the transport and localization of ASH1 mRNA to the bud site (Kruse et al. 2002; for recent review see Paquin and Chartrand, 2008; Gonsálvez and Long, 2012). In metazoans, Myo5a has been implicated in β-actin mRNA localization in cultured fibroblasts (Salerno et al., 2008) but its direct involvement in RNA transport has not been established. More direct evidence was obtained in hippocampal neurons *in vitro*, in which Myo5a was shown to be actively involved in RNA localization through association with specific RNA-binding proteins (Yoshimura et al., 2006; Nalavadi et al., 2012).

In brain extracts, both Myo5a and myosin IIB were found to co-sediment in sucrose gradients and co-immunoprecipitated with the RNA-binding protein Pur-alpha, the S6 ribosomal protein, and mRNAs (Ohashi et al., 2002). In this regard, one of the first characterizations of Myo5a in the axons of the peripheral nervous system showed that this protein is abundant in the axoplasm and in the cytoplasm of the surrounding glia (Calliari et al., 2002). A more detailed study of Myo5a distribution in axons was carried out by Sotelo-Silveira et al. (2004) using axons of medullary roots, in which it was enriched in periaxoplasmic plaques (PARPs) and co-localizing with ribosomes. Interestingly PARPs also contained ZBP1, the β-actin mRNA-binding protein, together with β-actin mRNA (Sotelo-Silveira et al., 2008). More recently, a Myo5a-dependent Schwann cell-to-axon transfer of RNA was shown (Sotelo et al., 2013).

This evidence strongly supports the hypothesis that the actin cytoskeleton and myosins are involved in RNA compartmentalization in many cell types, including neurons. To better characterize Myo5a-dependent RNA compartmentalization in the nervous system, we have focused on identifying mRNAs associated with Myo5a in both brain and peripheral axons. Combining immunoprecipitation of ribonucleoprotein particles (RNPs) purified from mouse brain with an anti-Myo5a antibody with microarray studies, we identified hundreds of mRNAs associated with Myo5a. These code for proteins that function in multiple pathways. In addition, we used biochemical and immunofluorescence approaches to characterize the association of Myo5a to axonal RNPs *in vitro* and *in vivo*. In the axons forming the rat dorsal medullary roots, RNA was found packed as kinesin-associated RNPs, as evidenced by fluorescence microscopy and immunoprecipitation of Myo5a-containing RNPs. Besides the 18S rRNA, we identified other axonally transported mRNAs (Gumy et al., 2011) included in Myo5a-bearing granules: actb (β-actin) and Snrpg (nuclear ribonucleoprotein). We also detected the mRNA coding for Myo5a in these RNPs, an observation confirmed by in situ hybridization in myelinated axons where it was found co-localizing with ribosomes in PARP domains. Taken together, these findings support the hypothesis that the biochemical identity and the steady state of the axonal compartment rely on a regulated mechanism of selective transport of mRNA, at least partially dependent on Myo5a.

METHODS

Subcellular Fractionation

Purification of RNPs. RNPs were purified from whole brains of young adult Sprague-Dawley rats and C57BL6 mice, as described by Ohashi et al. (2002). Briefly, the brain of a rat or mouse slaughtered by decapitation was immediately washed in ice-cold buffer (Tris pH 7.5, $MgCl_2$ 2 m*M*, KCl 50 m*M*, EGTA 0,1 m*M*, cycloheximide 1 μg/mL, and sucrose 0.32*M*) chopped in small pieces, and homogenized using a Teflon pestle glass homogenizer. The

homogenate (~10 mL) was centrifuged at 10,000*g* for 15 min. The resulting supernatant was further ultracentrifuged at 120,000*g* for 1 h. The pellet was resuspended in 2 mL of the homogenization buffer but with KCl increased to 150 m*M*. The sample was incubated 15 min on ice to complete the solubilization and finally clarified by centrifugation at 10,000*g* for 15 min. The supernatant represents the RNP fraction referred below and further used for fractionation by ultracentrifugation in sucrose gradients, Western blot, and immunoprecipitation experiments.

RNP Fractionation by Ultracentrifugation in Sucrose Gradients. Five hundred microliter of the RNP fraction obtained from rat brain was applied onto the top layer of a 15–45% continuous sucrose gradient (4.5 mL). The sucrose was dissolved in 25 m*M* Tris pH 7.5, 25 m*M* NaCl, and 5 m*M* $MgCl_2$. To avoid the formation of a pellet at the bottom of the tube, a 200 μL cushion of 60% sucrose was added before applying the gradient. The RNP fraction was centrifuged for 1 h at 160,000 g. After centrifugation, the gradient was collected in 300 μL fractions using a peristaltic pump and absorbance at 280 nm was continuously monitored.

Medullary Roots Homogenates. Rat dorsal medullary roots were collected immediately after animal sacrifice and kept on ice. About 200 mg of tissue was collected per animal. If not immediately used, the tissue was kept frozen at −80 degrees. The homogenization buffer was the same as described above, with the addition of 100 μ*M* leupeptin and 50 units per mL of aprotinin. Dorsal roots were resuspended in 1.5 mL of buffer and sonicated for 6 s (three cycles of 2 s). To complete RNP extraction, the tissue was further homogenized using a Teflon pestle homogenizer. The homogenate (about 1 mL) was centrifuged at 10,000 g for 30 min. The resultant supernatant was used for the immunoprecipitation experiments or for protein detection by Western blot.

Immunoprecipitation

Immunoprecipitation experiments were carried out using Protein A/G agarose (30 μL of 2 % per 500 μL of homogenate) and 1 m*M* PMSF for 4 hours at 4°C. Before immunoprecipitation, total protein concentration in tissue extracts was adjusted to 1 mg/mL.

For microarrays, we used RNPs obtained from whole brain of mice (see "Purification of RNPs," more above). Then, each RNP fraction was divided into thirds: the first immunoprecipitated using anti-Myo5a antibodies (5 μg of anti-Myo5a), the second immunoprecipitated with an antibody against poly(A) binding protein (PABP, 2 μg of antibody) and the last used for a negative control of immunoprecipitations. Because most eukaryotic mRNAs of nuclear origin interact with PABP at their 3′ ends (Kahvejian et al., 2005), we assumed that those mRNAs pulled down with PABP should be representative of the total mRNA population associated with RNPs. As negative control, we tested two different conditions: an antibody against a protein no related with RNPs (anti-diphtheria toxin; 2 μg of antibody) or no antibody during the immunoprecipitation. The experiments were carried out in triplicate.

For Western blot and qPCR studies, we pulled down Myo5a and ribosomal P proteins from RNP extracted from mouse brain (Ohashi et al., 2002) and homogenates of medullary roots of rats. Myo5a was immunoprecipitated as described above, while ribosomes were immunoprecipitated using 10 μL of anti-P antiserum (10 mg/mL; Immunovision) which recognizes the ribosomal P proteins P0, P1 and P2. As a negative control for Western blot and immunoprecipitates, we used non specific rabbit or human IgGs. After 4 h at 4°C, the Protein A/G Agarose beads were washed with PBS and processed for Western blot or RNA extraction.

Microarray Analysis

A total of three independent microarrays experiments were carried out for each immunoprecipitation condition (anti Myo5a, anti PABP, anti-diphtheria toxin and beads alone; see Supporting Information Fig. 2). The RNA extracted from mouse brain immunoprecipitates was processed for hybridization with GeneChip 3′ IVT Express (Affymetrix), in accordance with the manufacturer's instructions. Briefly, cDNA was synthesized from immunoprecipitated RNA using reverse transcriptase followed by second-strand synthesis to generate double-stranded cDNA. An *in vitro* transcription reaction was used to generate biotinylated cRNA. After purification and fragmentation, cRNA was hybridized to the GeneChip® Affymetrix Mouse Genome 430 2.0 Array. Post-hybridization washes were preformed on an Affymetrix GeneChip Fluidics Station 450. Arrays were scanned on an Affymetrix GeneChip Scanner 3000. Scanned arrays were normalized using GCRMA in Partek software (Partek Incorporated). Ratios of signal intensity were calculated and genes that had fold change (IP-Myo5a/IP-control) and (IP-PABP/IP control) > 1.4 were listed. The list obtained was used as the input to ingenuity pathways analysis (IPA) to obtain indications of the functional relationships (Network Functions) of the enriched genes. All microarray data were submitted to the gene expression omnibus (GEO) database.

Real Time PCR

qRT-PCR of mRNAs isolated from immunoprecipitated brain RNPs was used to validate the microarray results and was carried out in triplicate. qRT-PCR of mRNAs sampled from medullary roots immunoprecipitates were performed (in quadruplicate) to study the MyoVa-RNA association in mature axons. The RNAqueous®-Micro kit (Ambion) was used to isolate RNA from immunoprecipitates of brain RNPs, medullary roots and the total RNPs fraction. After DNAse treatment, 0.5 μg of the purified RNA was reverse transcribed using standard conditions and oligo dT_{20} as primers or random primers to retain ribosomal RNAs. First

strand cDNA was obtained by reverse transcription using the SuperScript® III reverse transcriptase (Invitrogen), according to the instructions of the manufacturer. Candidate genes of interest for qRT-PCR were chosen from the list of genes enriched in immunoprecipitates of Myo5a yielded by the microarrays experiments (see Supporting Information Table 1). Quantitative real-time PCR (qPCR) was performed using iQ™ SYBR® Green Supermix kit (BioRad) and Rotor Gene 6000 and relative gene expression levels were calculated in regards to control conditions (control immunoprecipitations).

Sequences of each primer were designed as follows: Snca forward primer: CATCTTTAGCCATGGATGTGT TC and reverse primer: CACACCCTGCTTGGTTTTCT, Stt3a forward primer: TCTAAAGCTCCTCATCCTGTCG and reverse primer: TGAGCACAGCAAAAAGACGA, Hsp90aa1 forward primer: GGAGATAAATCCTGATC ACTCCA, and reverse primer: CAAGATGACCAGATCC TTCACA, Rnf139 forward primer: ACGTCTGCTCGGA TTACACC and reverse primer: TCTTGAATGTACAGC CATTTCC, Cpeb4 forward primer: CCAACCATCAAG GATAAACCA and reverse primer: ATATCGTTTTCC GTGGGTCA, Eef1g forward primer: CTGAGTACCGCT TCCCTGAA and reverse primer: TCAGTTTGTCCAAT CGCTGA, Skap2 forward primer: ATCTGTGCTCCCGA TAAACG, and reverse primer: CGTCAGATCCCATGT CTTGTAA, Ndufv2 forward primer: CGTTCCCTGTC AGCCTAGAG, and reverse primer: TGCACTGCTGTCT TATGCAA, Snrpg forward pimer: CTCACTCCTTCGC CGTTG, and reverse primer: AGGGTGGGCTTTGCT CAT, Sfxn1 forward primer: GCCACCCAACATTAA CATCA, and reverse primer: CTGGGATCAGTAACCGT GAAG, Pmp22 forward primer: GAATTCCTGTTCCT GTTCTTCTGCCAGCTC, and reverse primer: AAGCTTG TAGATGGCCGCTGCACTCATC, Actb forward primer: TATGTTGCCCTAGACTTCGAGC, and reverse primer: CAGCTCATAGCTCTTCTCCAGG, 18S ribosomal RNA forward primer: CCGCAGCTAGGAATAATGGA and reverse primer: GGACGCCGAATTAAACTGAG, Myo5a forward primer: TGTCAGCATGGCATGGAACCCAG, and reverse primer: ATGGCTTCCGCGTTCATCGTCAG.

Immunodetection of Proteins. Labeling of Nucleic Acids

Cell Culture. Dorsal root ganglia from young (30 days old) mice were collected in Hanks' Salt Balanced Solution (HBSS) and treated with collagenase 0.25% w/v for 45 min at 37°C. After collagenase digestion, DRGs were washed with HBSS free of calcium and magnesium and treated with trypsin 0.25% w/v for 15 min at 37°C. Mechanical dissociation of neurons was achieved by triturating the ganglia using a fire polished Pasteur pipette to obtain a homogeneous cell suspension. The cells were then applied onto a 30% Percoll solution in HBSS in a 15 mL conical centrifuge tube and centrifuged at 1200 rpm for 10 min. The neurons were recovered from the bottom of the tube, washed with culture medium (Ham's F12 with supplements and 50 ng/mL of NGF) and plated onto poly-L-lysine coated coverslips.

Isolation of Axoplasmic Wholemounts From Myelinated Dorsal Spinal Root Fibers. Dorsal medullary roots used in the present study were dissected from euthanized rats according to the study by Koenig et al. (2000). The tissues (several nerve root/rootlet) were suspended in a modified gluconate-substituted calcium-free Cortland salt solution (Koenig and Martin, 1996) containing 132 m*M* Na-gluconate, 5 m*M* KCl, 20 m*M* HEPES, 10 m*M* glucose, 3.5 m*M* MgSO4, and 2 m*M* EGTA, pH 7.2, stored at 4°C. A nerve root/rootlet, 3–5 mm, was immersed in a solution of 30 m*M* zinc acetate, 0.1*M* N-tris[hydroxymethyl]methylglycine (Tricine; Sigma, St. Louis, MO), pH 4.8, for 10 min and then was placed in a 35 mm plastic culture dish containing 2 mL of a "pulling" solution (i.e., a solution in which axoplasm was translated out from its myelin sheath). The composition of the pulling solution was 40 m*M* aspartic acid neutralized by 0.04*M* Tris at pH 5.5, 1 m*M* NaN_3, and 0.01% Tween 20 (Bio-Rad, Hercules, CA) to reduce surface tension. For each test, plaques were identified after staining with YOYO-1 (see below). Isolated axoplasmic whole mounts were attached with the aid of eyebrow hair tools to a N° 1 coverslip coated with 1% 3-aminopropyltriethoxysilane (Polysciences, Warrington, PA) in ethanol.

Immunofluorescent Labeling. DRG neurons or axoplasmic wholemounts attached to a coverslip were fixed by immersion in 4% paraformaldehyde in phosphate buffer saline and 0.01% triton X-100, adjusted to pH 7.2 with NaOH, for 15 min. They were washed in PBS (cells) or 0.15*M* ammonium acetate and 0.1% Tween 20, pH 7.2 (axons wholemounts), three times for 5 min each and then immersed in an immunoblocking solution, composed of 5% normal goat serum in PBS, and 5 m*M* NaN_3 for 30 min. Incubation with primary antibody was 1 h. Coverslips were washed three times with PBS and incubated for 60 min with a secondary antibody conjugated to one of three Alexa fluorophores (Invitrogen) having an excitation maximum at either 488 nm, 546 nm, or 555 nm. The immunostained specimens were washed three further times for 5 min each before being mounted.

YOYO-1 Staining of Axoplasmic Wholemounts. One microliter of a 1:10 stock of YOYO-1 iodide in DMSO (491/509, Invitrogen-Molecular Probes) was added to the pulling medium (final concentration, 1:5000) for 15 min. The dye was washed out by brief immersion in acidified 0.15*M* ammonium acetate (pH-adjusted to 4.5 with acetic acid) and 0.1% Tween 20. For fluorescence microscopy, the coverslip with axoplasmic sprays was mounted on a flow-thru chamber. The chamber was constructed by inverting the coverslip over spacers (0.5–1 mm thick) made of Silastic elastomer (Dow Corning, Midland, MI) attached to a large glass coverslip (35 × 50 mm) taped to a thin, U-shaped metal plate, and the well was filled with acidified ammonium acetate solution.

Antibodies. The immunoreagents used were (1) human polyclonal antibody against human ribosomal P antigen (Immunovision; Springdale, AR), obtained by ammonium sulphate precipitation of immunoglobulins present in whole serum; (2) rabbit affinity-purified polyclonal against a recombinant protein containing the Myo5a head domain (amino acids 5–752), a generous gift of Roy Larson (Espreafico et al., 1992); (3) goat polyclonal affinity-purified anti-Myo5a against the N-terminal domain (sc-17706 from Santa Cruz Biotechnology); (4) rabbit affinity puried polyclonal antibody against a synthetic peptide unique of HuD protein (Mobarak et al., 2000), a generous gift of Nora Perrone-Bizzozero; (5) monoclonal IBII from Sigma-Aldrich that recognizes the heavy chain of Kif5 and Kif3 families of kinesins (Sotelo-Silveira et al., 2004); (6) polyclonal rabbit antibody against poly (A) binding protein (sc-67017, from Santa Cruz Biotechnology); and (7) polyclonal anti-diphtheria toxin from Abcam (Ab 151222). Alexa-conjugated secondary antibodies were obtained from Invitrogen and used according to the manufacturer's instructions in dilutions ranging from 1/2000 to 1/3000.

Probes for Myo5a and In Situ Hybridization. A fragment (nucleotides 3171–6599) of the chicken Myo5a cDNA (clone 32a, kindly provided by Enilza Espreafico) was cloned into pBluescript SK +/−. ISH was carried out according to Sotelo-Silveira et al. (2011) for axonal whole mounts and Sotelo-Silveira et al. (2000) for sciatic nerves. The plasmid was digested at the HPA site and transcribed using the T7 promoter at the 5′ end. Transcription was carried out for 30 min using 10 units of T7 polymerase under the conditions provided by the manufacturer (Boehringer Mannheim). To label the probe, we used digoxigenin 11-UTP. The antisense sequence (1027 nucleotides) includes the 3′-UTR and the region coding for the globular tail domain of the protein (COOH end). Residual DNA was eliminated by adding two units of DNAse for 30 min at 37°C. Histological sections and naked wholemount axons were equilibrated in hybridization solution composed by 50% formamide, 500 μg/μL denatured salmon DNA, 250 μg/μL of yeast tRNA Denhardt's solution (0.1% w/v Ficoll, 0.1% w/v polyvinylpyrrolidone, 0.1% w/v BSA Fraction V) and SSC 4× (0.6*M* NaCl, 60 m*M* sodium citrate, pH 7) for 15 min at 42°C. New hybridization solution containing 1–2 ng/μL of Myo5a antisense probe was added and incubated at 42°C for 4 h (axons) or overnight (histological sections) in a humidity chamber. After that, samples were washed with SSC 4× to 0.25× in 15-min cycles at 42°C. Endogenous peroxidase activity was blocked with 0.01% hydrogen peroxide in PBS for 30 min, followed by blocking unspecific binding sites with 0.5% w/v of Promega blocking reagent for 30 min. Finally, the probe was detected using HRP-labeled anti-DIG antibody (Boehringer Mannheim) and tyramide-Cy3 reagent as substrate.

Microscopy and Image Processing. Epifluorescence imaging was performed with an Olympus BX61 microscope coupled to a DP70 digital camera (Olympus). The confocal system used consisted in an Olympus FV 300 equipped with krypton 488, HeNe 543, and HeNe 633 lasers in combination with an upright Olympus BX61 microscope. High-resolution images were captured using an oil immersion objective Plan Apo x60, with 1.42 NA lens. Co-localization studies were carried out using the Fluoview co-localization tool. Quantization of signal co-localization was performed using MIPAV software (http://mipav.cit.nih.gov/) and expressed as orthogonal correlation coefficients among variables.

Study of 3′-UTR Sequences Present in mRNAs Immunoprecipitated With Myo5a

To determine whether cis-acting zipcodes were present in the 3′-UTRs of mRNAs immunoprecipitated with Myo5a, we compared their 3′UTRs with two axonal cis-acting zipcodes: tau (Aranda-Abreu et al., 1999, 2005) and *β*-actin (Kislauskis et al., 1994; Ross et al., 1997; Patel et al., 2012), and with the dendritic zipcode present in the CaMKII mRNA (Mori et al., 2000). We used ClustalW (Thompson et al., 1994) for pairwise alignments between the mentioned zipcodes and the 3′-UTRs present in our set of mRNAs. Alignments with scores above the 75th percentile were used to create sequence logos (Schneider and Stephens, 1990), predict secondary structures (RNAfold from the Vienna RNA Package, Hofacker, 2003) and common structural motifs (RNApromo program; Rabani et al., 2008).

RESULTS

Myo5a Associates With a Subset of mRNAs in RNPs Obtained From Mouse Brains

To study the quantitative and qualitative extent of the putative association of Myo5a with mRNAs, we performed microarray studies. Messenger RNAs bound to Myo5a, PABP, and negative control immunoprecipitations were purified and identified using microarrays. RNAs with signals at least 1.4-fold increase over control and a p value less than 0.05 by one-way ANOVA were scored as positive associations. A total of 1358 and 255 mRNAs associated with PABP and Myo5a respectively were selected under this criterion. Figure 1(A) summarizes these data as a cluster analysis of mRNAs contained in both immunoprecipitates, suggesting that they are different RNA populations. Also, both groups of mRNAs were different from those obtained in negative control conditions. A selected group of genes among those most represented in the array were validated by qPCR [see Fig. 1(C,D) and Table 2]. A Gene Ontology detailed analysis of primary results was performed using

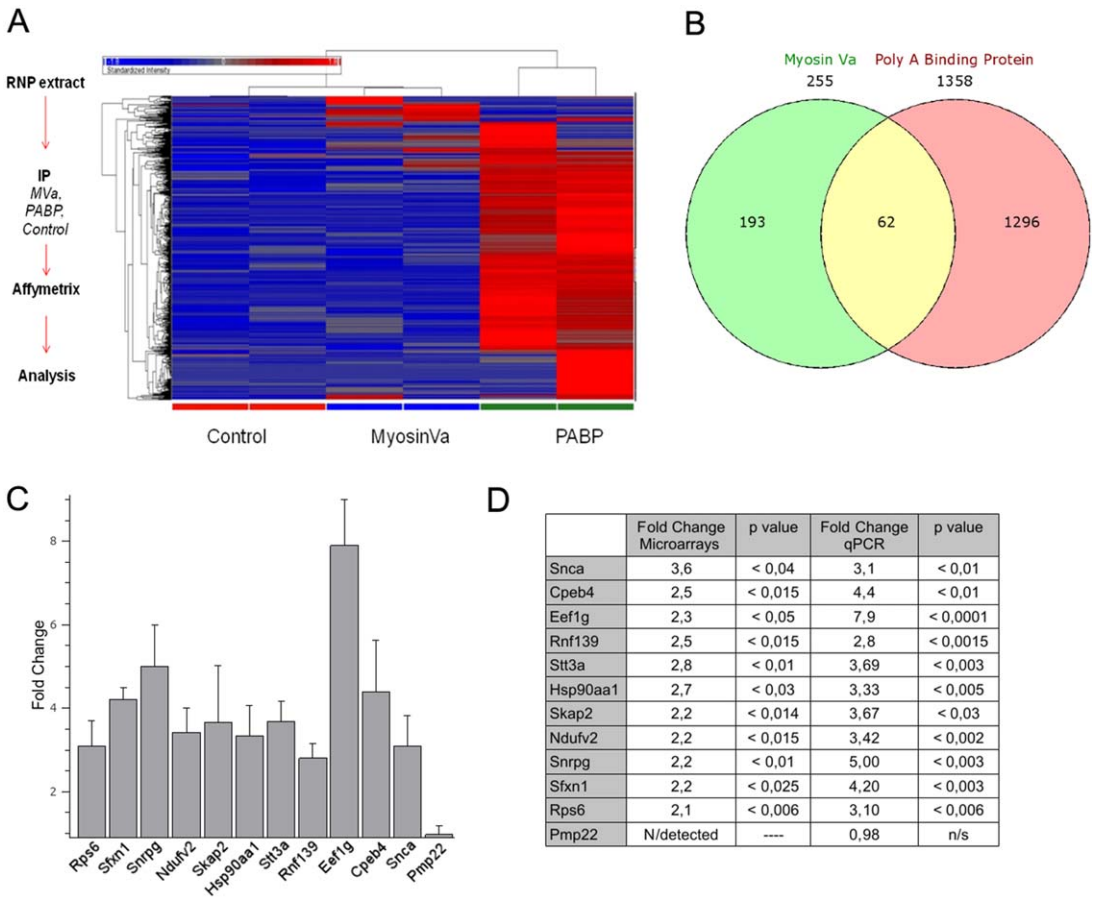

	Fold Change Microarrays	p value	Fold Change qPCR	p value
Snca	3,6	< 0,04	3,1	< 0,01
Cpeb4	2,5	< 0,015	4,4	< 0,01
Eef1g	2,3	< 0,05	7,9	< 0,0001
Rnf139	2,5	< 0,015	2,8	< 0,0015
Stt3a	2,8	< 0,01	3,69	< 0,003
Hsp90aa1	2,7	< 0,03	3,33	< 0,005
Skap2	2,2	< 0,014	3,67	< 0,03
Ndufv2	2,2	< 0,015	3,42	< 0,002
Snrpg	2,2	< 0,01	5,00	< 0,003
Sfxn1	2,2	< 0,025	4,20	< 0,003
Rps6	2,1	< 0,006	3,10	< 0,006
Pmp22	N/detected	----	0,98	n/s

Figure 1 Myo5a associates with a subset of mRNAs in brain RNPs. Microarrays studies of immunoprecipitated fraction using anti-Myo5a and anti-PABP antibodies, respectively demonstrate that each protein associate with a different mRNA population. (A) Cluster analysis of the mentioned group of genes. (B) Venn diagram. (C) A selected group of genes highly represented in the microarray of genes pulled down with Myo5a was validated by qPCR. To further asses the correlation between the microarrays and qPCR results, we included Pmp22 as a negative control. This gene did not meet the cut off criteria for detected genes in microarrays studies and therefore was considered as absent (not associated with Myosin Va). Error bars are SEM of triplicates. (D) The fold change and *p* values of the validated genes are compared with the results yielded by microarrays for the same messengers. [Color figure can be viewed in the online issue, which is available at wileyonlinelibrary.com.]

Ingenuity software, which assigned the mRNAs associated with Myo5a to network functions mainly related with RNA post-transcriptional modification, neurological disease, skeletal and muscular disorders, cellular assembly and organization, cellular function and maintenance, and protein trafficking. Some of these functions overlap with those assigned to the mRNAs associated with PABP (Table 1). However, only one-third of the genes pulled down by Myo5a were included among those immunoprecipitated with PABP, [Venn diagram in Fig. 1(B)]. While it is difficult to know if a full representation of associated mRNA was provided by the array, these results suggested that Myo5a associates with a subpopulation of mRNAs.

Myo5a is a Component of RNPs of Different Size and Composition

RNPs isolated from rat brains (Ohashi et al., 2002) were fractionated by sucrose gradient. The RNA peaks shown in the chromatogram of Figure 2(A) suggest that our RNPs are structurally heterogeneous. Our profile is very similar to that reported by Krichevsky and Kosik (2001) using RNPs obtained from primary neurons in culture.

Table 1 Gene Assignment to Canonical Network Functions

Top Networks		
A - *PABP*		
ID	Associated Network Functions	Score
1	RNA Post-Transcriptional Modification, Neurological Disease, Skeletal and Muscular Disorders	57
2	Cellular Assembly and Organization, Cellular Function and Maintenance, Protein Trafficking	44
3	Cellular Assembly and Organization, Hair and Skin Development and Function, DNA Replication, Recombination, and Repair	37
4	DNA Replication, Recombination, and Repair, Energy Production, Nucleic Acid Metabolism	34
5	Cell Morphology, Cellular Assembly and Organization, Cellular Development	28
B - *Myosin Va*		
ID	Associated Network Functions	Score
1	Hematological Disease, Hereditary Disorder, Cell Morphology	48
2	RNA Post-Transcriptional Modification, Dermatological Diseases and Conditions, Developmental Disorder	42
3	Developmental Disorder, Hereditary Disorder, Metabolic Disease	39
4	RNA Post-Transcriptional Modification. Cellular Assembly and Organization. Cellular Function and Maintenance	39
5	DNA Replication, Recombination, and Repair, Energy Production, Nucleic Acid Metabolism	38

Selected list of genes associated either with Myo5a or PABP were analyzed using *Ingenuity* software. *A*, correspond to Myo5a and *B* to PABP.

Because HuD is a neuronal RNA-binding protein that stabilizes labile mRNAs with AU-rich instability elements, we used it as a marker to identify RNPs in the sucrose fractions. Interestingly, a polyclonal antibody raised against this protein revealed the presence of HuD only in particles found in the top layers of the sucrose gradient. Second, we determined the distribution of Myo5a amongst the RNA-containing fractions. Western blot analysis showed that this motor is concentrated both in the heavier as well as in the lighter fractions, being less abundant in the intermediate fractions [Fig. 2(A)]. The ribosome marker P0 also was detected in the heavier fractions. To test for a Myo5a–ribosome association, we pulled down Myo5a from RNPs and thus probed for ribosomal markers in the immunoprecipitate fraction. As Figure 2(B) shows, ribosomes were pulled down with Myo5a. Moreover, the presence of both S6 and P0 ribosomal proteins (belonging to the small and large ribosomal subunits respectively) suggested the presence of assembled ribosomes. To confirm the putative Myo5a-ribosome interaction, we carried out the converse immunoprecipitation experiment, using anti-ribosomal P protein antibody and detecting Myo5a and S6 [Fig. 2(B)]. Interestingly, under these conditions we also detected two kinesin heavy chains, Kif3 and Kif5, among the immunoprecipitated proteins [Fig. 2(C)].

Subcellular Localization of RNPs Containing Myo5a in Mature Axons

The association of ribosomes with HuD in neurites and growth cones of PC12 cells differentiated into neurons has previously been reported (Smith et al., 2004). We observed that such organization appears to be preserved in axons and growth cones of DRG neurons in culture (Supporting Information Figs. S1 and S2). On the other hand, immunoprecipitation of RNPs obtained from brain suggested that kinesin and Myo5a may be associated with ribosomes. Thus, we investigated if RNPs found in peripheral axons had a similar pattern. Because it was extremely difficult to obtain pure axonal samples in a sufficient amount to do immunoprecipitation experiments, we took advantage of the axonal wholemount preparation in combination with fluorescence microscopy. Axonal wholemounts obtained by our methods are essentially free of glial contamination (Koenig and Martin, 1996; Keonig et al., 2000). We therefore probed for Myo5a and RNPs in axonal wholemounts obtained from medullary dorsal roots. We found co-localization of Myo5a, kinesin and ribosomes [Fig. 3(A)]. Triple co-localization of these three markers in discrete granular structures (arrows) was suggested in the axoplasm and in the peripheral region of PARPs. We also noticed what appeared to be a gradient of granular components from the PARP to the axoplasm. This was particularly evident when particles were labeled using the anti-ribosomal P protein antibody [Fig. 3(A), second row]. Myo5a also co-localized with HuD and the YOYO-1 nucleic acid probe [arrows in Fig. 3(B)]. Some discrete triple and many double (Myo5a-HuD) co-localizations were detected both in axoplasm and PARPs [asterisk in Fig. 3(B), Yoyo-1]. The latter raises the possibility of

Table 2 A Representative List of mRNAs Enriched in the Immunoprecipitate Fraction of Myo5a From Mouse Brain

Gene Symbol	Gene Title	RefSeq Transcript ID	Fold-Change
Snca	synuclein, alpha	NM_001042451 *III* NM_009221	3.6
E2f8	E2F transcription factor 8	NM_001013368	3.0
Atp6ap2	ATPase, H+ transporting, lysosomal accessory protein 2	NM_027439	2.7
Hsp90aa1	heat shock protein 90, alpha (cytosolic), class A member 1	NM_010480	2.7
Cpeb4	cytoplasmic polyadenylation element binding protein 4	NM_026252	2.5
Eif3e	eukaryotic translation initiation factor 3, subunit E	NM_008388	2.4
Eef1g	eukaryotic translation elongation factor 1 gamma	NM_026007	2.3
Ndufv2	NADH dehydrogenase (ubiquinone) flavoprotein 2	NM_028388	2.2
Sfxnl	sideroflexin 1	NM_027324	2.2
Rps6	40S ribosomal protein S6	NM_009096	2.1
Cox4i1	cytochrome c oxidase subunit IV isoform 1	NM_009941	2.1
Pfn1	profilin 1	NM_011072	2.1
Mdh2	malate dehydrogenase 2, NAD (mitochondrial)	NM_008617	2.0
Cetn4	centrin 4	NM_145825	1.9
Ptp4a2	protein tyrosine phosphatase 4a2	NM_001164745 /// NM_008974	1.9
Rpl22l1	ribosomal protein L22 like 1	NM_026517	1.9
Ptp4a1	protein tyrosine phosphatase 4a1	NM_011200	1.9
Vdac3	voltage-dependent anion channel 3	NM_011696	1.9
Ubb	ubiquitin B	NM_011664	1.9
Rps27	ribosomal protein S27	NM_027015	1.9
Rpn1	ribophorin I	NM_133933	1.9
Kcnn4	potassium intermediate/small conductance calcium-activated channel, subfamily N,	NM_001163510 /// NM_008433	1.8
Selplg	selectin, platelet (p-selectin) ligand	NM_009151	1.8
Sf3b1	splicing factor 3b, subunit 1	NM_031179	1.8

Selected group of genes obtained from the complete list depicted in Supporting Information Table T1. The present list illustrates the nature and relative abundance of prototypical genes; i.e., those engaged with protein processing pathways and ribosome integrity.

the existence of a HuD-bearing particle lacking RNA.

Myo5a Associates With Axonal mRNAs

We then focused on the putative association of Myo5a with mRNA in mature axons. To do so, we pulled down Myo5a from dorsal medullary root homogenates, then performed qPCR of the immunoprecipitate using specific primers to amplify several mRNAs [Fig. 4(A,C)]. Transcripts were selected among those previously identified as associated to Myo5a in RNPs from brain (Fig. 1, Supporting Information Table 1). In addition, to demonstrate the axonal origin of the mRNAs co-precipitated by Myo5a, we looked for mRNAs that also were expressed in axons (Gumy et al. 2011). Evidence for co-immunoprecipitation of ribosomes (18S RNA pulled down together with P proteins) was also found [Fig. 4(A,C)].

The axonal localization of the mRNA coding for Myo5a was further confirmed by hybridization. These experiments revealed that Myo5a mRNA primarily co-localized with PARPs [Fig. 5(A,B)]. When hybridization was combined with immunolabeling of ribosomes, some punctate signals positive for both signals were detected not only on PARPs but also in the axoplasm [Fig. 5(A) inset]. Images from cross sections of sciatic nerve show that the mRNA encoding Myo5a was present in periaxoplasmic cortical regions, where the contribution of glia or axons as a source of label was difficult to discriminate (*bottom left*, thin arrows); however, an abundant labeling of clearly axonal origin could be occasionally observed (*bottom left*, inset). In addition, re-analysis of the data obtained by Gumy and cols (2011) suggested that Myo5a is a prominent mRNA present in cultured DRG axons among the mRNAs coding for motor proteins [Fig. 5(D) for myosins and E for kinesins].

Tau and β-actin 3′-UTR Zipcodes are Present in mRNAs Associated With Myosin Va

To detect sequences that may direct axonal or dendritic targeting in the 3′-UTR of mRNAs immunoprecipitated by Myo5a, we aligned these 3′-UTRs with the

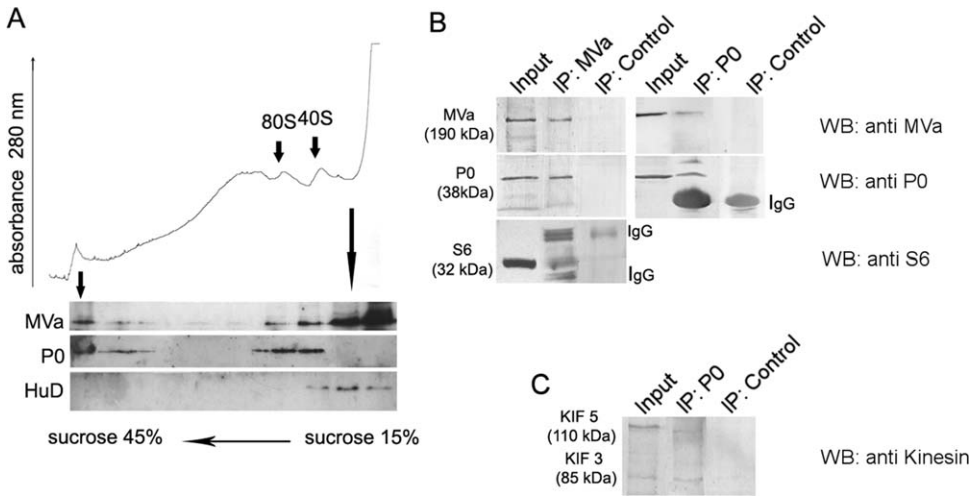

Figure 2 Ribonucloprotein particles (RNPs) are heterogeneous in size and composition. (A) RNPs purified from whole rat brain were sedimented through a 15–45% sucrose gradient; fractions were collected with continuous monitoring at 280 nm. Anti-Myo5a, ribosomal P0 and HuD proteins antibodies were probed in each fraction by Western blot. The peak on the left (tube bottom) corresponds to the heaviest RNPs with ribosomes and Myo5a protein. The less dense particles (right part of the chromatogram) are rich in Myo5a and HuD proteins. 80 and 40S denote the peaks corresponding to free ribosomes, according to their sedimentation coefficient and P0 detection in Western blots. (B) Myo5a and ribosomal P0 proteins co-immunoprecipitated from the RNP fraction obtained from brain using anti-Myo5a as well as anti-P0 antibodies. Besides P0, the ribosomal S6 protein could also be detected in the immunoprecipitated fractions. IP controls were done using non-specific IgGs. (*C*) The microtubule based motors kif 5 and 3 were pulled down using anti-ribosomal proteins antibodies. IP control was done similarly as in *B*.

cis-acting zipcodes present in the mRNAs coding for tau, β-actin, and CAMKII. A total of 17 3′-UTRs had scores greater than the 75th percentile in alignments with β-actin and tau zipcodes. Interestingly, the zipcode that targets CAMKII to dendrites was not found among this set of mRNAs. To evaluate the conservation of the zipcodes in these sequences we constructed sequence logos [Fig. 6(A–C)]. To find common structural motifs among the selected set of 17 3′-UTRs, we used the program RNApromo (Rabani et al., 2008). As a result, we identified a significant motif (AUC = 1, p-value < 0.01), predicted to fold into a stem-loop structure with a relatively short loop [Supporting Information Fig. 4(A)]. An extended set of generated secondary structures are displayed in Supporting Information Fig. 4(B–R), with the conserved motif highlighted circled.

DISCUSSION

The presence of RNA in the axonal compartment of mature axons, once extremely controversial, is now largely accepted (for comprehensive reviews, see Giuditta et al., 2002, Twiss and van Minnen, 2006, Sotelo-Silveira et al., 2006, and others in this special issue). Currently, it is known that axons of neurons grown *in vitro* contain all the components of the translational machinery and that local translation of at least some mRNAs indeed occurs (Eng et al., 1999; Willis et al., 2005). According to recent reports, a large variety and number of mRNAs are present in axons. By microarray analyses of cortical axons in culture, Taylor et al. (2009) detected the presence of more than 300 different transcripts, while other studies suggested that this population is probably larger (Willis et al., 2005, Gumy et al., 2011). While considerable progress has been made in characterizing the axonal transport of RNA along microtubule tracks (Olink-Coux and Hollenbeck, 1996; Bassell et al., 1998), much less is known about the involvement of myosins and microfilaments in RNA mobilization along axons. Previous studies have suggested that Myo5a is important for proper localization of mRNA and the RNA-binding proteins TLS and ZBP-1 in hippocampal neurons in culture (Yoshimura, et al., 2006; Nalavadi et al., 2012). Myo5a also was identified in RNPs immunoprecipitated from brain extracts (Ohashi et al., 2002) and as component of P-bodies in multiple cell lines (Lindsay and McCaffrey, 2011).

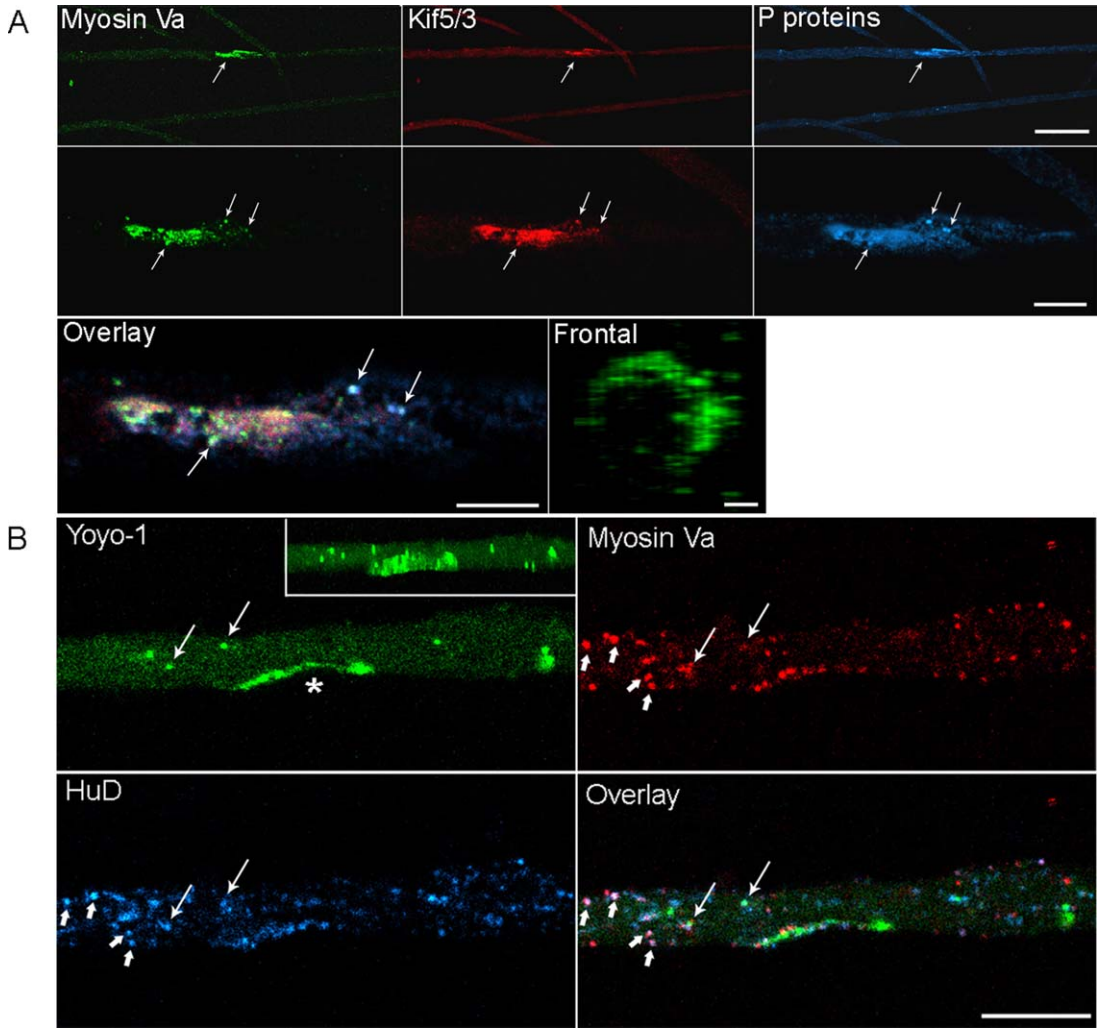

Figure 3 High-resolution confocal microscopy of RNPs in myelinated axons. (A) RNPs containing ribosomal and motor proteins are structurally related with the Peri Axoplasmic Ribosomal Domains (PARPs). *Upper row*; low magnification images of axoplasmic wholemounts labeled for Myo5a, Kinesin 5/3 and ribosomal P proteins, respectively. Arrow depicts two axonal PARPs. Bar is 20 μm. *Middle row*; confocal single optical plane containing one of the PARPs shown by the arrows above. Arrows show visible individual granules labeled by the three different antibodies. Bar is 5 μm. *Overlay*; merged image. Bar is 5 μm. *Frontal*; a 3D reconstruction of the PARP labeled with anti-Myo5a antibody. Bar is 1 μm. (B) *YOYO-1* labeling of a single optical Z-plane image of an isolated axoplasm labeled with the YOYO-1 probe. Positive granules (arrows) are RNA rich structures (PARP, asterisk). Inset: A 3D reconstruction of the same axoplasm; The Z-stack was slightly rotated onto its *X* axis to better appreciate the PARP domain. *Myosin Va* and *HuD*; anti-myosin Va and anti-ELAV HuD protein antibodies labeling of axoplasm. Long arrows depict those particles where YOYO, Myo5a and HuD apparently co-localize, whereas the short arrows designate positive particles for Myo5a and HuD only. Such double and triple co-localizations are better appreciated in the *Overlay* frame. Bar is 10 μm. [Color figure can be viewed in the online issue, which is available at wileyonlinelibrary.com.]

Here, we present data demonstrating that myosin-Va is a component of a heterogeneous population of RNPs of different sizes and composition, both in brain and PNS. The extent of this association was assessed using microarrays hybridized to cRNA made from mRNA present in RNPs immunoprecipitated with Myo5a. Ingenuity software analysis clustered the identified transcripts in network functions dealing mainly with RNA post-transcriptional modification, neurological disease, cellular assembly and

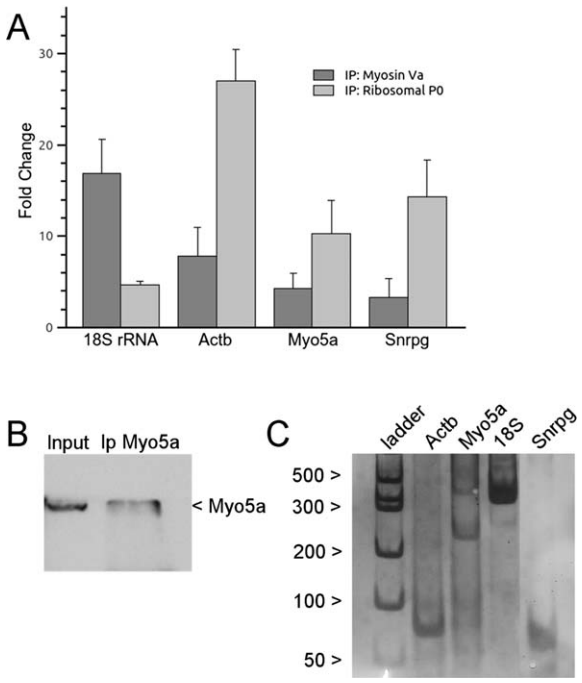

Figure 4 Quantitative PCR of RNA extracted from immunoprecipitates of Myosin Va and ribosomes from homogenates of medullary roots. (A) Biochemical analysis of myosin Va-bearing RNPs reveals that this fraction contains ribosomes (18S rRNA) and mRNAs. The results are expressed as fold change with respect to the negative control condition (immunoprecipitation using non-specific IgGs). The 18S rRNA as well as the same mRNAs can be detected in immunoprecipitates obtained using anti-ribosomal P proteins antibody. (B) Western blot showing that Myo5a protein is immunoprecipitated from homogenated dorsal roots, using anti-Myo5a antibodies. (C) The PCR products were identified according their expected size (in base pairs).

organization, cellular function and maintenance, and protein trafficking (Table 1). The association of Myo5a with these groups of mRNAs suggests that this motor protein participates in the localization of a specific subset of mRNAs (Table 2 and Supporting Information Table 1). Alpha-synuclein was the most enriched mRNA among those associated with Myo5a. Although this finding requires a great deal of further study, it implies that RNA localization and local protein synthesis may be involved in neurodegenerative disorders such as Parkinson disease. Interestingly, mRNAs encoding proteins involved in protein translation and processing, molecular transport, and mitochondrial maintenance were major categories in previous independent screens using neurons from different sources (Taylor et al., 2009; Zivraj et al., 2010; Gumy et al., 2011). Further work and additional experimental approaches (i.e., RNA sequencing) will be needed to exhaustively evaluate the extent and identity of the mRNA population associated with myosin Va in neurons.

When subjected to velocity sedimentation through sucrose gradients, the isolated RNPs were a heterogeneous population of particles [Fig. 2(A)]. These particles resembled the "RNA granules" and the "messenger ribonucleoprotein complexes" described in cultured neurons by Krichevsky and Kosik (2001). Here we showed that RNPs purified from brains and immunoprecipitated using anti-Myo5a antibodies contained ribosomes, RNA-binding proteins (HuD protein), kinesins [Fig. 2(A,C)] and mRNAs (Fig. 1). The presence of mRNAs in the immunoprecipitated fractions suggests that Myo5a may participate in the transport or localization of mRNAs subjected to arrest during translation.

Because we are especially interested in the dynamics of RNA transport in mature axons, we next investigated the interaction of motor proteins with RNPs in this neuronal territory. Again, Myo5a co-localized at least partially with structures containing RNA (in some cases identified as ribosomes) but also with the RNA-binding protein HuD and mRNA (Fig. 3). This was similar to what we observed in axons and growth cones of DRG neurons in culture (Supporting Information Figs. S1 and S2). In this regard, previous reports demonstrated that besides binding and stabilizing the mRNA coding for GAP43, HuD also associates with ribosomal protein S6 in neurites of differentiated PC12 cells (Smith et al., 2004). This study also showed that the localization of this complex in grown cones is dependent on F-actin. In this regard, Myo5a arose as a potentially relevant molecule for ribosome translocation or localization. Evidence supporting this hypothesis was obtained upon metaanalysis of the raw data provided by Gumy et al. (2011), in which the transcript coding for Myo5a was one of the most abundant myosin mRNAs [Fig. 5(D)].

To better understand the role of Myo5a in mRNA localization, we analyzed the localization sequences (zipcodes) in the 3′-UTRs of the mRNAs pulled down with Myo5a. β-actin mRNA was identified in RNPs containing Myo5a. Both β-actin and tau zipcodes have been experimentally demonstrated to be responsible for mRNA targeting to axons (Willis et al., 2011; Aranda-Abreu et al., 1999) and the zipcode of CAMKII to dendrites (Mori et al., 2000). Thus, we looked for similar zipcodes present in the 3′-UTR of mRNAs enriched in the immunoprecipitate of Myo5a. Interestingly, we found a good alignment for the case of tau and β-actin, but negative results for dendrite targeting sequences. While these

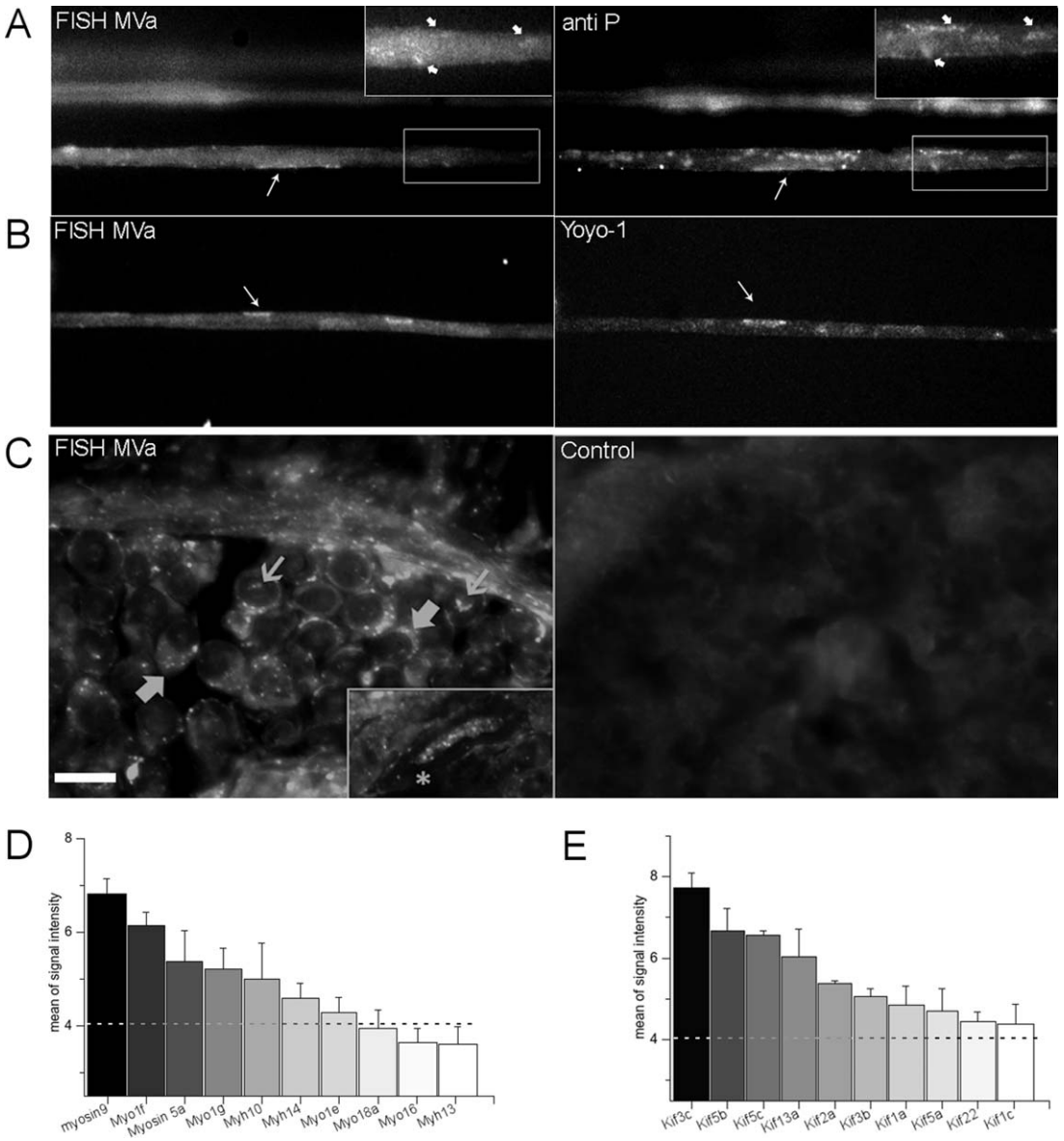

Figure 5 The mRNA coding for Myo5a is detected both in RNPs and PARPs by *in situ* hybridization in axons of the peripheral nervous system. (A) *Upper row*, The same PARP present in an individualized axon is evidenced with an antisense digoxigenin labeled probe (arrow, left) or anti-ribosomal P antibody (*right*). The reaction is mainly concentrated on PARPs, but some granular reaction is also observed in the axoplasm (arrows in the insets). (B) Labeling of a group of PARPs in a single selected axoplasm using fluorescence in situ hybridization (left) and YOYO-1 staining (*right*). (C) The mRNA for Myo5a was also detected in sciatic nerve (*left*). The signal is compartmentalized between axoplasm (thin arrows) and glial cells (thick arrows). The inset displays a semi longitudinal section of a nerve fiber which axoplasm was heavily labeled; the asterisk depicts the myelin sheath. *Right*; Negative control experiment done without probe. Bar is 10 μm. (D) and (E) the data from Gumy et al. (2011) were reanalyzed to determine the relative abundance of specific mRNAs in the context of the total transcripts coding for myosins or kinesins heavy chains. Only the 10 most abundant are displayed. The dashed line indicates the background level of signal for Affimetrix chips.

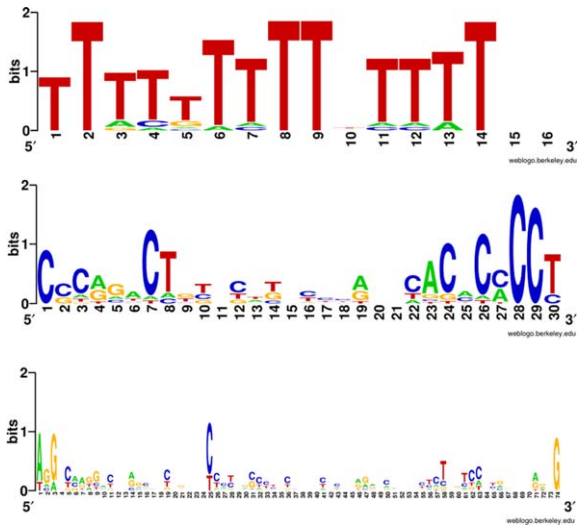

Figure 6 Tau and β-actin zipcodes are present in Myo5a-associated mRNAS. Sequence logos obtained after the alignment of 3′UTRs of the mRNA immunoprecipited with Myo5a against tau (A), β-actin (B), and CamKII (C) zipcode sequences. [Color figure can be viewed in the online issue, which is available at wileyonlinelibrary.com.]

data do not address direct or indirect interaction among Myo5a and messengers, they further suggest the involvement of Myo5a in RNA mobilization/tethering in mature axons. It is worth noting that the RNA-binding proteins HuD [Fig. 3(B)] and ZBP1 zipcodes have been found in mature myelinated axons (Sotelo-Silveira et al., 2008).

Despite its processivity, Myo5a appears to function only along short distances (Langford, 2002). Thus, its presence in RNPs is likely insufficient to explain how these structures can be transported to axonal regions localized millimeters or even centimeters away from the soma. The co-immunoprecipitation of the kinesin heavy chain together with Myo5a in brain RNPs, coupled with the co-localization of kinesin with Myo5a on the same RNPs in axons of medullary roots [Fig. 3(A)], is consistent with the hypothesis of an interdependent role of microtubules and microfilaments for RNA localization in the axonal territory. Moreover, using hippocampal neurons in culture, Nalavadi et al. (2012) demonstrated that when Myo5a is knocked down with RNAi, the speed of anterograde transport of RNPs is increased. This result strongly suggests that Myo5a acts more as an anchor or tether, a phenomenon previously observed with myosin Vb for endosomal compartments in fibroblasts (Provance et al., 2008). In this hypothesis, large distances are covered by kinesins while the myosins are specially needed to localize the particle in actin-rich regions. This dual motor complex hypothesis for the transport of cargoes was initially advanced by Langford (Langford, 1995) and further evidence has been found in multiple models (Langford, 2002; Muslimov et al., 2002). In mammalian axons, this type of RNP was found concentrated on the PARP itself as well as in the axoplasmic regions surrounding it, suggesting that PARPs are dynamic structures able to interchange components with other regions of the axoplasm. In this regard, we have recently demonstrated that Myo5a is necessary for the cell-to-cell transfer of RNA from the adaxonal Schwann cell to axons of the sciatic rat nerve (Sotelo et al., 2013, see also a review by Sotelo et al., 2014). This observation provides an alternative origin of PARPs and axonal RNPs and contributes to our understanding of the role of the actin-based transport of RNA in mature axons.

REFERENCES

Amrute-Rayak M, Bullock SL. 2012. Single-molecule assays reveal that RNA localization signals regulate dynein-dynactin copy number on individual transcript cargoes. Nat Cell Biol 14:416–423.

Andreassi C, Zimmermann C, Mitter R, Fusco S, Devita S, Saiardi A, Riccio A. 2010. An NGF-responsive element targets myo-inositol monophosphatase-1 mRNA to sympathetic neuron axons. Nat Neurosci 13:291–301.

Aranda-Abreu GE, Behar L, Chung S, Furneaux H, and Ginzburg I. 1999. Embryonic lethal abnormal vision-like RNA-binding proteins regulate neurite outgrowth and Tau expression in PC12 cells. J Neurosci 19:6907–6917.

Aranda-Abreu GE, Hernández ME, Soto A, Manzo J. 2005. Possible Cis-acting signal that could be involved in the localization of different mRNAs in neuronal axons. Theor Biol Med Model 2:33–42.

Bassell GJ, Zhang H, Byrd AL, Femino AM, Singer RH, Taneja KL, Lifshitz LM, Herman IM, Kosik KS. 1998. Sorting of β-actin mRNA and protein to neurites and growth cones in culture. J Neurosci 18:251–265.

Bear MF, Dölen G, Osterweil E, Nagarajan N. 2008. Fragile X: Translation in action. Neuropsychopharmacology 33:84–87.

Calliari A, Sotelo-Silveira J, Costa MC, Nogueira J, Cameron LC, Kun A, Benech J, Sotelo JR. 2002. Myosin Va is locally synthesized following nerve injury. Cell Motil Cytoskeleton 51:169–176.

Canclini L, Kun Alejandra, Calliari A, Mercer JA, Sotelo JR, Sotelo-Silveira JR. 2011. The axonal transcriptome: RNA localization and function. Curr Chem Biol 5:99–107.

Costa-Mattioli M, Gobert D, Stern E, Gamache K, Colina R, Cuello C, Sossin W, Kaufman R, Pelletier J, Rosenblum K, Krnjević K, Lacaille JC, Nader K, Sonenberg N. 2007. eIF2alpha phosphorylation

bidirectionally regulates the switch from short- to long-term synaptic plasticity and memory. Cell 129:195–206.

Deglincerti A, Jaffrey SR. 2012. Insights into the roles of local translation from the axonal transcriptome. Open Biol 2:120079.

Donnelly CJ, Willis DE, Xu M, Tep C, Jiang C, Yoo S, Schanen NC, Kirn-Safran CB, van Minnen J, English A, Yoon SO, Bassell GJ, Twiss JL. 2011. Limited availability of ZBP1 restricts axonal mRNA localization and nerve regeneration capacity. EMBO J 30: 4665–4677.

Eng H, Lund K, Campenot RB. 1999. Synthesis of beta-tubulin, actin, and other proteins in axons of sympathetic neurons in compartmented cultures. J Neurosci 19:1–9.

Espreafico EM, Cheney RE, Matteoli M, Nascimento AA, De Camilli PV, Larson RE, and Mooseker MS. 1992. Primary structure and cellular localization of chicken brain myosin-V (p190), an unconventional myosin with calmodulin light chains. J Cell Biol 119:1541–57.

Gagnon JA, Mowry KL. 2012. Molecular motors: Directing traffic during RNA localization. Crit Rev Biochem Mol Biol 46:229–239.

Giuditta A, Kaplan BB, van Minnen J, Alvarez J, Koenig E. 2002. Axonal and presynaptic protein synthesis: New insights into the biology of the neuron. Trends Neurosci 25:400–404.

Gonsalvez GB, Long RM. 2012. Spatial regulation of translation through RNA localization. F1000 Biol Rep 2012;4:16.

Gumy LF, Yeo GSH, Tung Y-CL, Zivraj KH, Willis D, Coppola G, Lam BY, Twiss JL, Holt CE, Fawcett JW. 2011. Transcriptome analysis of embryonic and adult sensory axons reveals changes in mRNA repertoire localization. RNA 17:85–98.

Hofacker IL. 2003. Vienna RNA secondary structure server. Nucleic Acids Res 31:3429–3431.

Jung H, O'Hare CM, Holt CE. 2011. Translational regulation in growth cones. Curr Opin Genet Dev 21:458–464.

Kahvejian A, Svitkin YV, Sukarieh R, M'Boutchou M-N, Sonenberg N. 2005. Mammalian poly(A)-binding protein is a eukaryotic translation initiation factor, which acts via multiple mechanisms. Genes Dev 19:104–113.

Kislauskis EH, Zhu X, Singer RH. 1994. Sequences responsible for intracellular localization of β-actin messenger RNA also affect cell phenotype. J Cell Biol 127:441–451.

Koenig E, Martin R. Cortical plaque-like structures identify ribosome-containing domains in the Mauthner cell axon. 1996. J Neurosci 16:1400–1411.

Koenig E, Martin R, Titmus M, Sotelo-Silveira JR. Cryptic peripheral ribosomal domains distributed intermittently along mammalian myelinated axons. 2000. J Neurosci 20:8390–8400.

Krichevsky AM, Kosik KS. 2001. Neuronal RNA granules: A link between RNA localization and stimulation-dependent translation. Neuron 32:683–696.

Kruse C, Jaedicke A, Beaudouin J, Bohl F, Ferring D, Guttler T, Ellenberg J, Jansen RP. 2002. Ribonucleoprotein-dependent localization of the yeast class V myosin Myo4p. J Cell Biol 159:971–982.

Langford GM. 1995. Actin- and microtubule-dependent organelle motors: Interrelationships between the two motility systems. Curr Opin Cell Biol 7:82–88.

Langford GM. Myosin-V. 2002. a versatile motor for short-range vesicle transport. Traffic 3:859–865.

Lindsay AJ, McCaffrey MW. 2011. Myosin Va is required for P body but not stress granule formation. J Biol Chem 286:11519–11528.

Long RM, Singer RH, Meng X, Gonzalez I, Nasmyth K, Jansen RP. 1997. Mating type switching in yeast controlled by asymmetric localization of ASH1 mRNA. Science 277:383–387.

Mobarak CD, Anderson KD, Morin M, Beckel-Mitchener A, Rogers SL, Furneaux H, King P, Perrone-Bizzozero NI. 2000. The RNA-binding protein HuD is required for GAP-43 mRNA stability, GAP-43 gene expression, and PKC-dependent neurite outgrowth in PC12 cells. Mol Biol Cell 11:3191–203.

Mori Y, Imaizumi K, Katayama T, Yoneda T, Tohyama M. 2000. Two cis-acting elements in the 3Ç untranslated region of α-CaMKII regulate its dendritic targeting. Nat Neurosci 3:1079–1084.

Muslimov I, Titmus M, Koenig E, Tiedge H. 2002. Transport of neuronal BC1 RNA in mauthner axons. J Neurosci 22:4293–4301.

Nalavadi VC, Griffin LE, Picard-Fraser P, Swanson AM, Takumi T, Bassell GJ. 2012. Regulation of zipcode binding protein 1 transport dynamics in axons by myosin Va. J Neurosci 32:15133–15141.

Ohashi S, Koike K, Omori A, Ichinose S, Ohara S, Kobayashi S, Sato TA, Anzai K. 2002. Identification of mRNA/protein (mRNP) complexes containing Puralpha, mStaufen, fragile X protein, and myosin Va and their association with rough endoplasmic reticulum equipped with a kinesin motor. J Biol Chem 277:37804–37810.

Olink-Coux M, Hollenbeck PJ. 1996. Localization and active transport of mRNA in axons of sympathetic neurons in culture. J Neurosci 16:1346–1358.

Paquin N, Chartrand P. 2008. Local regulation of mRNA translation: New insights from the bud. Trends Cell Biol 18:105–111.

Patel VL, Mitra S, Harris R, Buxbaum AR, Lionnet T, Brenowitz M, Girvin M, et al. 2012. Spatial arrangement of an RNA zipcode identifies mRNAs under post-transcriptional control. Genes Dev 26:43–53.

Provance DW Jr, Addison EJ, Wood PR, Chen DZ, Silan CM, Mercer JA. 2008. Myosin-Vb functions as a dynamic tether for peripheral endocytic compartments during transferrin trafficking. BMC Cell Biol 9:44.

Rabani M, Kertesz M, Segal E. 2008. Computational prediction of RNA structural motifs involved in posttranscriptional regulatory processes. PNAS 105:14885–14890.

Ross AF, Oleynikov Y, Kislauskis EH, Taneja KL, Singer RH. 1997. Characterization of a β-actin mRNA Zipcode-binding protein. Mol Cell Biol 17:2158–2165.

Rossoll W, Jablonka S, Andreassi C, Kröning AK, Karle K, Monani UR, Sendtner M. 2003. Smn, the spinal muscular

atrophy–determining gene product, modulates axon growth and localization of β-actin mRNA in growth cones of motoneurons. J Cell Biol 163:801–812.

Salerno VP, Calliari A, Provance DW Jr, Sotelo-Silveira JR, Sotelo JR, Mercer JA. 2008. Myosin-Va mediates RNA distribution in primary fibroblasts from multiple organs. Cell Motil Cytoskeleton 65:422–433.

Schneider TD, Stephens RM. 1990. Sequence logos: A new way to display consensus sequences. Nucleic Acids Res 18:6097–6100.

Smith CL, Afroz R, Bassell GJ, Furneaux HM, Perrone-Bizzozero NI, Burry RW. 2004. GAP-43 mRNA in growth cones is associated with HuD and ribosomes. J Neurobiol 61:222–235.

Sotelo JR, Canclini L, Kun A, Sotelo-Silveira JR, Calliari A, Cal K, Bresque M, et al. 2014. Glia to axon RNA transfer. Dev Neurobiol 74:292–302.

Sotelo JR, Canclini L, Kun A, Sotelo-Silveira JR, Xu L, Wallrabe H, Calliari A, et al. 2013. Myosin-Va-dependent cell-to-cell transfer of RNA from Schwann cells to axons. PLoS ONE 8;e61905.

Sotelo-Silveira JR, Calliari A, Kun A, Elizondo V, Canclini L, Sotelo JR. 2011. Localization of mRNA in vertebrate axonal compartments by in situ hybridization. Methods Mol Biol 714:125–138.

Sotelo-Silveira JR, Calliari A, Kun A, Benech JC, Sanguinetti C, Chalar C, Sotelo JR. 2000. Neurofilament mRNAs are present and translated in the normal and severed sciatic nerve. J Neurosci Res 62:65–74.

Sotelo-Silveira JR, Calliari A, Cárdenas M, Koenig E, Sotelo JR. 2004. Myosin Va and kinesin II motor proteins are concentrated in ribosomal domains (periaxoplasmic ribosomal plaques) of myelinated axons. J Neurobiol 60:187–196.

Sotelo-Silveira JR, Calliari A, Kun A, Koenig E, Sotelo JR. 2006. RNA trafficking in axons. Traffic 7:508–515.

Sotelo-Silveira J, Crispino M, Puppo A, Sotelo JR, Koenig E. 2008. Myelinated axons contain beta-actin mRNA and ZBP-1 in periaxoplasmic ribosomal plaques and depend on cyclic AMP and F-actin integrity for in vitro translation. J Neurochem 104:545–557.

Taylor AM, Berchtold NC, Perreau VM, Tu CH, Li Jeon N, Cotman CW. Axonal mRNA in uninjured and regenerating cortical mammalian axons. 2009. J Neurosci 29:4697–4707.

Thompson JD, Higgins DG, Gibson TJ. 1994. CLUSTAL W: Improving the sensitivity of progressive multiple sequence alignment through sequence weighting, position-specific gap penalties and weight matrix choice. Nucleic Acids Res 22:4673–4680.

Twiss JL, van Minnen J. 2006. New insights into neuronal regeneration: The role of axonal protein synthesis in pathfinding and axonal extension. J Neurotrauma 23:295–308.

Mikl M, Vendra G, Klieber MA. 2011. Independent localization of MAP2, CaMKIIα and β-actin RNAs in low copy numbers. EMBO Rep 12:1077–1084.

Westmark CJ, Malter JS. 2007. FMRP mediates mGluR5-dependent translation of amyloid precursor protein. PLoS Biol 5:e52.

Willis D, Li KW, Zheng JQ, Chang JH, Smit AB, Kelly T, Merianda TT, et al. 2005. Differential transport and local translation of cytoskeletal, injury-response, and neurodegeneration protein mRNAs in axons. J Neurosci 25:778–791.

Willis DE, Xu M, Donnelly CJ, Tep C, Kendall M, Erenstheyn M, English AW, et al. 2011. Axonal Localization of transgene mRNA in mature PNS and CNS neurons. J Neurosci 31:14481–14487.

Yoo S, van Niekerk EA, Merianda TT, Twiss JL. 2010. Dynamics of axonal mRNA transport and implications for peripheral nerve regeneration. Exp Neurol 223:19–27.

Yoshimura A, Fujii R, Watanabe Y, Okabe S, Fukui K, Takumi T. 2006. Myosin-Va facilitates the accumulation of mRNA/protein complex in dendritic spines. Curr Biol 16:2345–2351.

Zivraj KH, Tung YCL, Piper M, Gumy L, Fawcett JW, Yeo GSH, Holt CE. 2010. Subcellular profiling reveals distinct and developmentally regulated repertoire of growth cone mRNAs. J Neurosci 30:15464–15478.

8. DISCUSION

Hemos demostrado la existencia de una transferencia de ARNs desde la glía al axón en el SNP de roedores, tanto en condiciones normales como de regeneración axonal. Durante la regeneración, esta transferencia parece ser importante para el crecimiento de los brotamientos axonales, dado que en estas estructuras los ARN-BrU son muy abundantes tanto a las 24 horas de la lesión como a los 7 días (Apéndice 10.1, figura 1). Tenemos además indicios de que la transferencia de ARNs también ocurre en el nervio sural de seres humanos (Kun, comunicación personal), por lo que proponemos que la transferencia de ARNs desde la célula de Schwann al axón es un evento que tiene lugar en fibras mielínicas del SNP de mamíferos. En el transcurso de la presente tesis hemos recabado datos que nos permiten proponer el siguiente modelo (figura 8.1) para la transferencia glía-axón de ARNs:

1) Transcripción de genes con destino axonal en el núcleo de la célula de Schwann y empaquetamiento en ribonucleopartículas (RNPs).

2) Transporte de las RNPs con destino axonal desde las inmediaciones del núcleo hasta los *microvilli* nodales de la célula de Schwann (y al límite entre ambas células en las incisuras de Schmidt-Lanterman), por medio de los microtúbulos.

3) Transferencia propiamente dicha de las RNPs desde la glia al axón a través de las membranas plasmáticas de ambas células, mediante un mecanismo desconocido que involucra el citoesqueleto de actina y el motor miosina Va.

4) Transporte de las RNPs dentro del axón a través de los microtúbulos.

5) Localización de las RNPs en el sitio donde serán traducidos los ARNm.

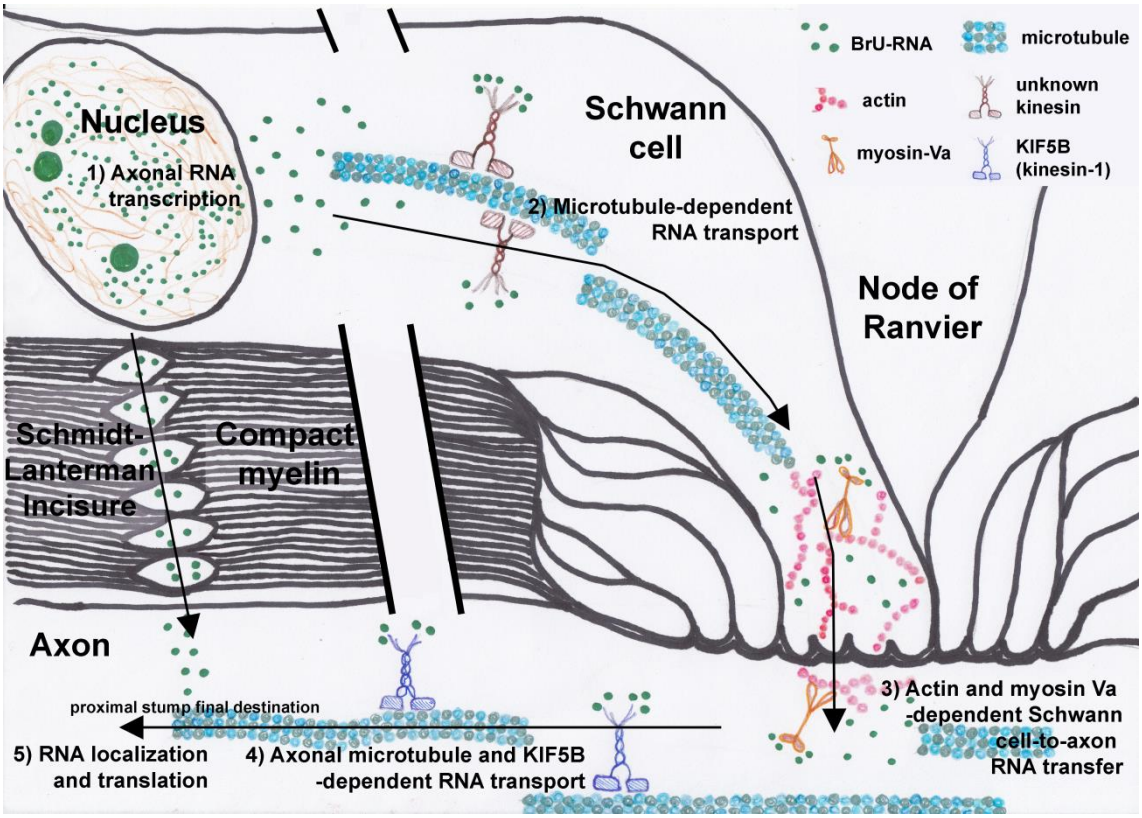

Figura 8.1. Modelo propuesto para el mecanismo del transporte y la transferencia de ARNs de la célula de Schwann al axón (tomado de Canclini *et al*., manuscrito enviado para su publicación, trabajo IV de la presente tesis).

Discutiremos a continuación cada uno de los pasos del mecanismo propuesto para la transferencia de ARN desde la célula de Schwann al axón.

8.1. Transcripción y empaquetamiento de ARNs con destino axonal

En el núcleo de la célula de Schwann (fibras mielínicas) se transcriben ARNs que serán utilizados para el metabolismo propio de esta célula, pero también ARNs que serán transferidos al axón (trabajo II). Esto sucede en condiciones normales, en todas las células de Schwann a lo largo de la fibra mielínica. Queda por determinar si esta síntesis de ARNs con destino axonal está regulada intrínsecamente en la célula de Schwann o se activa y regula por señales provenientes del axón. La síntesis de ARNs que serán transferidos al axón aumenta luego de una injuria y son las células de Schwann del cabo proximal más cercanas al sitio lesionado las que muestran este comportamiento (trabajo II). Este aumento debe responder a señales del

entorno inmediato, ya sean señales provenientes del axón o señales del ambiente inflamatorio que se genera luego de una lesión (Dubový *et al.*, 2013).

La población de ARNs transcritos en el núcleo de la célula de Schwann que serán transferidos incluye ARNs ribosomales y mensajeros. Los ARNs ribosomales son transferidos en forma de ribosomas, como hemos determinado mediante ensayos de co-localización entre las señales de un anticuerpo que reconoce ribosomas y del anticuerpo que reconoce los ARN-BrU (trabajo II). Las pruebas de la transferencia de ribosomas también han sido aportadas por Li *et al.* (2005a; b), Kun *et al.* (2007) y Court *et al.* (2008, 2011), tanto en nervios normales como en regeneración. Determinamos que la población de ARN transferidos incluye mensajeros mediante estrategias experimentales diferentes. Realizamos experimentos de secuenciación masiva de los ARNs neosintetizados en el núcleo de la célula de Schwann (capítulo III) e identificamos varios ARNm que codifican para proteínas de expresión neuronal y que no se traducen en la célula de Schwann mielínica (Izant and McIntosh, 1980; Iwanaga *et al.*, 1989; Lee *et al.*, 1990; Shin *et al.*, 1991; Portier *et al.*, 1993; Dehmelt and Halpain, 2005; Faivre-Sarrailh and Devaux, 2013). Si bien aún no determinamos la transferencia para la mayoría de ellos, el hecho de que las proteínas que codifican no sean traducidas en la célula de Schwann los hace candidatos promisorios para ser transferidos. Sí hemos confirmado la presencia axonal del ARNm que codifica para la subunidad liviana de los neurofilamentos, sintetizado en el núcleo de la célula de Schwann, mediante experimentos de hibridación *in situ* contra dicho ARNm e inmunocitoquímica contra BrU (trabajo II). Por último, la inhibición de la transcripción a partir de la ARN polimerasa II, mediante α-amanitina, da lugar a una importante reducción de la cantidad de ARN transferidos desde la glia al axón (trabajo II). El resultado de estos experimentos fue inesperado dado que la reducción de la señal de los ARNs transferidos fue alrededor del 50%. Debemos determinar si esta reducción se debe a que realmente la población de ARNs transferidos contiene un 50% de ARNm, o bien si la inhibición de la transcripción afecta la expresión de algún factor importante para el transporte y/o la transferencia de los ARN desde la célula de Schwann al axón. Sin embargo existe también otra posibilidad. Los microARNs son transcritos, dependiendo del promotor que dirija su expresión, por la ARN polimerasa II (Lee *et al.*, 2004) o ARN

polimerasa III (Borchert *et al.*, 2006). Puede ser entonces, que la disminución observada de ARNs transferidos en las fibras tratadas con α-amanitina se deba a la suma de la disminución de ARNm y microARN transferidos. No hemos realizado ningún ensayo específico para determinar si existen microARNs transferidos desde la célula de Schwann al axón, pero esta es una posibilidad altamente probable, dado que existen varios ejemplos en la literatura de transferencia de microARNs entre células (Ramachandran and Palanisamy; Valadi *et al.*, 2007; Ekström *et al.*, 2012; McDonald *et al.*, 2013).

Una vez transcritos los ARNs deben ser empaquetados en ribonucleopartículas (RNPs) para ser transportados. En este sentido, una de las cuestiones más interesantes que no hemos abordado aún es cómo se diferencian los ARNs que permanecerán en la célula de Schwann de aquellos que serán transferidos. ¿Existen señales diferentes codificadas en cada una de las poblaciones de ARNs? O bien ¿cada población se empaqueta en RNPs con composiciones proteicas diferentes? Tenemos resultados preliminares que indican que hnRNPA2 podría ser parte de las RNPs transferidas desde la célula de Schwann al axón (Apéndice 10.1, figura 2). hnRNPA2 es una proteína de unión a ARN que co-inmunoprecipita con miosina Va (Larson, comunicación personal), por lo que podría estar involucrada en el transporte de los ARN-BrU. En nuestros experimentos preliminares observamos la co-localización entre las señales del anti-hnRNPA2 y el anticuerpo que reconoce los ARN-BrU en el axón y también en el citoplasma y el núcleo de la célula de Schwann. Es posible entonces, que los ARNm que serán transferidos al axón se empaqueten en RNPs que contienen hnRNPA2 en el núcleo de la célula de Schwann. No toda la señal de ARN-BrU que se observa en el citoplasma de la célula de Schwann, co-localizan con la señal del anti-hnRNPA2, indicando que esta proteína no es necesariamente el único factor que se une a los ARNs transferidos de la célula de Schwann al axón. Por otra parte, identificamos el ARNm que codifica hnRNPA2 como parte de la población de ARN-BrU.

8.2. Transporte dentro del citoplasma de la célula de Schwann

Los ARNs que serán transferidos al axón (y los que residirán en regiones alejadas del núcleo de la célula de Schwann) son transportados a través de los

microtúbulos (trabajo IV). Este resultado está en concordancia con la velocidad de transporte que observamos para los ARN-BrU desde el núcleo de la célula de Schwann hasta el límite entre la misma y el axón (trabajo III), unas 200 µm/h. La velocidad reportada para el transporte basado en microtúbulos es 300 a 500 µm/h (Kiebler and Bassell, 2006).

En el transcurso de esta tesis, no hemos podido determinar cuál es el motor molecular implicado en este transporte. Basándonos en la información bibliográfica disponible en el momento, realizamos experimentos de inmunocitoquímica para reconocer KIF1B al mismo tiempo que los ARN-BrU (trabajo IV). Esta es, en nuestro conocimiento, la única KIF para la que se ha reportado alguna función en células gliales (Lyons *et al.*, 2009). Determinamos que los ARNs transferidos desde la glia al axón no son transportados mediante este miembro de la familia de las kinesinas. Pese a ser un resultado negativo, constituye una información muy interesante. KIF1B es responsable del transporte del ARNm de MBP (*Myelin Basic Protein*) hacia la mielina de los oligodendrocitos (Lyons *et al.*, 2009). El hecho que un motor molecular que transporta ARNs residentes en la glia no esté involucrado en el transporte de los ARNs que serán transferidos al axón es una prueba adicional de que la transferencia de ARNs glia-axón es un evento específico y regulado.

A partir de la secuenciación de los ARN-BrU que realizamos (capítulo III) identificamos la expresión de 16 genes que codifican KIFs (Apéndice 10.1, tabla 2). Además, Li *et al.* (2013) mediante ensayos de microarreglos determinaron la expresión de 21 genes que codifican para KIFs (Apéndice 10.1, tabla 2). Aunque no sabemos si la expresión de estos mensajeros realmente significa que sus productos proteicos sean expresados en la célula de Schwann, estas KIFs son candidatos que deberemos analizar (salvo KIF1A, ver sección 8.3) en la búsqueda de la kinesina responsable del transporte dentro del citoplasma de la célula de Schwann.

8.3. Transferencia a través de las membranas plasmáticas

Una vez alcanzada la región de los *microvilli* en el nodo de Ranvier (o el límite con el axón en las incisuras de Schmidt-Lanterman), los ARN que serán transferidos deben atravesar dos membranas plasmáticas para llegar al axón.

No sabemos cuál es el mecanismo por el cual los ARNs atraviesan ambas membranas, pero determinamos que cualquiera sea este, es dependiente del citoesqueleto de actina y de la actividad de la miosina Va (trabajo II y III). Al ser necesario atravesar dos membranas el mecanismo probablemente involucre vesículas. Las células de mamíferos secretan dos tipos de vesículas extracelulares para la comunicación entre diferentes células y que contienen ARNm y microARNs: los exosomas y los ectosomas (Choi *et al.*, 2013). Ambas formas de vesículas se diferencian en su tamaño (50-100 nm los exosomas, 100-1000 nm los ectosomas) y el mecanismo de biogénesis (Cocucci *et al.*, 2009; Simons and Raposo, 2009). Sin embargo, existe una gran controversia en la literatura con respecto a las diferencias y similitudes en la composición de cada clase de partícula (Choi *et al.*, 2013). En el contexto de esta tesis se realizaron algunos experimentos para saber si los exosomas podrían estar involucrados en la transferencia de ARNs desde la glia al axón. Se realizó inmunocitoquímica de las fibras para reconocer una de las pocas proteínas marcadora exclusivas de exosomas (tsg101, http://evpedia.info, http://exocarta.org) al mismo tiempo que los ARN-BrU (datos no mostrados). Al no encontrar co-localización entre las marcas, la posibilidad de que los exosomas estén implicados en la transferencia glia-axón de ARNs es dudosa. De todas formas, la secreción de vesículas, ya sea exosomas o ectosomas, requiere la función del citoesqueleto de actina (Mittelbrunn *et al.*, 2015), de la misma manera que la transferencia de los ARN-BrU. El mecanismo de transporte de los ARN-BrU a través de las membranas plasmáticas que deben atravesar es un tema que queda pendiente en la presente tesis.

8.4. Transporte dentro del axón, localización y traducción de los ARNm

Los ARNs transferidos desde la glia se transportan dentro del axón por los microtúbulos, mediante KIF5B (trabajo IV). Las KIF5s parecen ser los motores moleculares que dirigen el "transporte axonal lento" (4-125 µm/h)(Hirokawa and Noda, 2008), una forma de transporte basado en microtúbulos, que es lento, no por la velocidad a la que se mueven los motores, sino por la existencia de pausas prolongadas en su movimiento (Trivedi *et al.*, 2007; Li *et al.*, 2014). Los resultados que indican que el transporte de los ARN-

BrU en el axón está mediado por KIF5B (trabajo IV) están de acuerdo con la medida de la velocidad del transporte de los ARN-BrU dentro del axón (6 µm/h, trabajo III). Queda por determinar si las RNPs que llevan los ARNs transferidos hacen realmente pausas o simplemente se descargan de los motores en los sitios donde se localizan definitivamente. Cuáles son esos sitios también es una incógnita a develar. Tenemos evidencias de que los brotamientos axonales son uno de los sitios donde se localizarán los ARN transferidos desde la glia al axón durante la regeneración post-lesión, pero nada sabemos del destino final de los ARNs transferidos dentro del axón de las fibras en regeneración o de la fibra normal. En este sentido, una de las preguntas más interesantes a responder es si los ARNs transferidos tienen como destino las placas periaxoplásmicas ribosomales (PPAR) descritas por Koenig and Martin (1996). Finalmente, entendemos fundamental responder si los ARNm transferidos son traducidos en el axón, ya sea en las PPAR o en otros sitios del axoplasma.

9. CONCLUSIONES Y PERSPECTIVAS

A partir de los datos presentados en la presente tesis de Doctorado podemos concluir que:

1) En las células de Schwann se transcriben ARNs que son transferidos al axón en condiciones normales.

2) La transferencia de ARNs desde la célula de Schwann al axón tiene lugar durante la regeneración axonal en mayor cantidad.

3) Los microtúbulos están implicados en el transporte de los ARN-BrU tanto dentro del citoplasma de la célula de Schwann como en el dominio axonal. Dentro del axón los ARN-BrU son transportados por KIF5B.

4) Los filamentos de actina están implicados en la transferencia de los ARN-BrU en el límite entre la célula de Schwann y el axón. El motor molecular asociado a actina implicado en este proceso es la miosina Va.

En el transcurso de esta tesis hemos recabado mucha información acerca de la transferencia de ARNs desde la glia al axón en el SNP, pero cada respuesta ha abierto nuevas interrogantes, por lo que queda mucho trabajo por hacer. Como perspectiva a corto plazo debemos secuenciar a mayor profundidad los ARN-BrU y confirmar mediante PCR cuantitativa e hibridación *in situ* los resultados obtenidos para ARNm seleccionados en términos de nivel de expresión y localización en el tejido. Deberemos además dilucidar el mecanismo responsable de la transferencia *per se* a través de las membranas citoplasmáticas de la célula de Schwann y el axón. En este sentido, creemos que la aplicación de microscopía electrónica de transmisión e inmunomicroscopía electrónica de transmisión es una buena estrategia para avanzar en este aspecto. A más largo plazo nos interesa identificar cuáles son las señales que median la comunicación entre el axón y la célula de Schwann que dirigen la síntesis, transporte y transferencia de los ARN que se transcriben en el núcleo de la célula de Schwann pero que serán utilizados para el metabolismo del axón. En este sentido también nos parece importante encontrar cuales son las señales que distinguen a los ARNs que serán transferidos al axón de aquellos que son residentes de la célula de Schwann. ¿Son estructuras secundarias particulares de los ARNm? ¿Es la unión diferencial de los mismos a proteínas accesorias que dirigen su transporte y localización? Con respecto a la localización, sabemos que es axonal, pero nada sabemos de la localización específica de los ARNs transferidos dentro del

dominio axonal. Los ARN transferidos desde la célula de Schwann al axón, ¿se distribuyen homogéneamente en todo el axoplasma? O bien ¿existen sitios específicos (que pueden ser las PPAR, entre otros) de localización final para los ARNs transferidos? Indiscutiblemente también es importante conocer si estos ARNs son realmente funcionales una vez llegan a su destino axonal, si los ARNm son traducidos, los ARNr están incorporados en ribosomas "traductores", etc. Por otra parte, la mayoría de los datos que fuimos recabando en la presente tesis se refieren a la transferencia de ARNs desde la célula de Schwann al axón en condiciones de regeneración nerviosa. Sabemos que la transferencia sucede en condiciones normales, pero mucho falta saber de este evento en una fibra no lesionada. ¿La identidad de los ARNs transferidos es la misma? ¿Varía la transferencia de ARNs, ya sea cuanti como cualitativamente según las condiciones de vida del animal? ¿Es diferente en animales sedentarios que en animales ejercitados? ¿Es dependiente de la dieta? ¿Varía según la edad del organismo?

Como ya hemos dicho, las preguntas que quedan por contestar son muchas y a nuestro entender muy interesantes. Sin embargo, nuestra meta más ambiciosa es, sin lugar a dudas, poder visualizar la transferencia *in vivo*, siguiendo el viaje de un ARNm desde al núcleo de la célula de Schwann hasta su traducción en el axón. En este sentido, planeamos realizar experimentos marcando de manera fluorescente (color 1) un ARNm endógeno que codifique para una proteína de expresión específica neuronal y de fusión a una proteína fluorescente (color 2). De esta manera podremos visualizar el "viaje" de dicho ARNm y su traducción en su destino final.

10. REFERENCIAS GENERALES

Alvarez J, Giuditta A, Koenig E. 2000. Protein synthesis in axons and terminals: significance for maintenance, plasticity and regulation of phenotype. With a critique of slow transport theory. Prog Neurobiol [Internet] 62:1–62. Available from: http://www.ncbi.nlm.nih.gov/pubmed/10821981

Alvarez J. 2001. The autonomous axon: a model based on local synthesis of proteins. Biol Res [Internet] 34:103–9. Available from: http://www.ncbi.nlm.nih.gov/pubmed/11715201

Amrute-Nayak M, Bullock SL. 2012. Single-molecule assays reveal that RNA localization signals regulate dynein-dynactin copy number on individual transcript cargoes. Nat Cell Biol [Internet] 14:416–23. Available from: http://www.pubmedcentral.nih.gov/articlerender.fcgi?artid=3343632&tool=pmcentrez&rendertype=abstract

Bassell GJ, Oleynikov Y, Singer RH. 1999. The travels of mRNAs through all cells large and small. FASEB J [Internet] 13:447–54. Available from: http://www.ncbi.nlm.nih.gov/pubmed/10064611

Benech C, Sotelo JR, Menéndez J, Correa-Luna R. 1982. Autoradiographic study of RNA and protein synthesis in sectioned peripheral nerves. Exp Neurol [Internet] 76:72–82. Available from: http://www.ncbi.nlm.nih.gov/pubmed/6177544

Bishop B. 1982. Neural plasticity: Part 3. Responses to lesions in the peripheral nervous system. Phys Ther [Internet] 62:1275–82. Available from: http://www.ncbi.nlm.nih.gov/pubmed/7051055

Black MM, Lasek RJ. 1977. The presence of transfer RNA in the axoplasm of the squid giant axon. J Neurobiol [Internet] 8:229–37. Available from: http://www.ncbi.nlm.nih.gov/pubmed/874479

Black MM, Lasek RJ. 1979. Axonal transport of actin: slow component b is the principal source of actin for the axon. Brain Res [Internet] 171:401–13. Available from: http://www.ncbi.nlm.nih.gov/pubmed/89886

Black MM, Lasek RJ. 1980. Slow components of axonal transport: two cytoskeletal networks. J Cell Biol [Internet] 86:616–23. Available from: http://www.pubmedcentral.nih.gov/articlerender.fcgi?artid=2111498&tool=pmcentrez&rendertype=abstract

Borchert GM, Lanier W, Davidson BL. 2006. RNA polymerase III transcribes human microRNAs. Nat Struct Mol Biol [Internet] 13:1097–101. Available from: http://dx.doi.org/10.1038/nsmb1167

Brittis PA, Lu Q, Flanagan JG. 2002. Axonal protein synthesis provides a mechanism for localized regulation at an intermediate target. Cell [Internet] 110:223–35. Available from: http://www.ncbi.nlm.nih.gov/pubmed/12150930

Brown A. 2003. Axonal transport of membranous and nonmembranous cargoes: a unified perspective. J Cell Biol [Internet] 160:817–21. Available from: http://www.pubmedcentral.nih.gov/articlerender.fcgi?artid=2173776&tool=pmcentrez&rendertype=abstract

Buchan JR. 2014. mRNP granules: Assembly, function, and connections with disease. RNA Biol [Internet] 11. Available from: http://www.ncbi.nlm.nih.gov/pubmed/24866467

Bunge RP. 1994. The role of the Schwann cell in trophic support and regeneration. J Neurol [Internet] 242:S19–21. Available from: http://www.ncbi.nlm.nih.gov/pubmed/7699403

Buttermore ED, Thaxton CL, Bhat MA. 2013. Organization and maintenance of molecular domains in myelinated axons. J Neurosci Res [Internet] 91:603–22. Available from: http://www.pubmedcentral.nih.gov/articlerender.fcgi?artid=4049519&tool=pmcentrez&rendertype=abstract

Calliari A, Sotelo-Silveira J, Costa MC, Nogueira J, Cameron LC, Kun A, Benech J, Sotelo JR. 2002. Myosin Va is locally synthesized following nerve injury. Cell Motil Cytoskeleton [Internet] 51:169–76. Available from: http://www.ncbi.nlm.nih.gov/pubmed/11977091

Campenot RB, Eng H. Protein synthesis in axons and its possible functions. J Neurocytol [Internet] 29:793–8. Available from: http://www.ncbi.nlm.nih.gov/pubmed/11466471

Carson JH, Worboys K, Ainger K, Barbarese E. 1997. Translocation of myelin basic protein mRNA in oligodendrocytes requires microtubules and kinesin. Cell Motil Cytoskeleton 38:318–28.

Chen Y, Periasamy A. 2006. Intensity range based quantitative FRET data analysis to localize protein molecules in live cell nuclei. J Fluoresc 16:95–104.

Ching W, Zanazzi G, Levinson SR, Salzer JL. Clustering of neuronal sodium channels requires contact with myelinating Schwann cells. J Neurocytol [Internet] 28:295–301. Available from: http://www.ncbi.nlm.nih.gov/pubmed/10739572

Choi D-S, Kim D-K, Kim Y-K, Gho YS. 2013. Proteomics, transcriptomics and lipidomics of exosomes and ectosomes. Proteomics [Internet] 13:1554–71. Available from: http://www.ncbi.nlm.nih.gov/pubmed/23401200

Chun JT, Gioio AE, Crispino M, Eyman M, Giuditta A, Kaplan BB. 1997. Molecular cloning and characterization of a novel mRNA present in the squid giant axon. J Neurosci Res [Internet] 49:144–53. Available from: http://www.ncbi.nlm.nih.gov/pubmed/9272637

Cocucci E, Racchetti G, Meldolesi J. 2009. Shedding microvesicles: artefacts no more. Trends Cell Biol [Internet] 19:43–51. Available from: http://www.ncbi.nlm.nih.gov/pubmed/19144520

Court FA, Hendriks WTJ, MacGillavry HD, Alvarez J, van Minnen J. 2008. Schwann cell to axon transfer of ribosomes: toward a novel understanding of the role of glia in the nervous system. J Neurosci 28:11024–9.

Court FA, Midha R, Cisterna BA, Grochmal J, Shakhbazau A, Hendriks WT, Van Minnen J. 2011. Morphological evidence for a transport of ribosomes from Schwann cells to regenerating axons. Glia 59:1529–39.

Crispino M, Capano CP, Kaplan BB, Giuditta A. 1993. Neurofilament proteins are synthesized in nerve endings from squid brain. J Neurochem [Internet] 61:1144–6. Available from: http://www.ncbi.nlm.nih.gov/pubmed/8360679

Crispino M, Chun JT, Cefaliello C, Perrone Capano C, Giuditta A. 2014. Local gene expression in nerve endings. Dev Neurobiol [Internet] 74:279–91. Available from: http://www.ncbi.nlm.nih.gov/pubmed/23853157

Cutillo V, Montagnese P, Gremo F, Casola L, Giuditta A. 1983. Origin of axoplasmic RNA in the squid giant fiber. Neurochem Res [Internet] 8:1621–34. Available from: http://www.ncbi.nlm.nih.gov/pubmed/6200785

Dehmelt L, Halpain S. 2005. The MAP2/Tau family of microtubule-associated proteins. Genome Biol [Internet] 6:204. Available from: http://www.pubmedcentral.nih.gov/articlerender.fcgi?artid=549057&tool=pmcentrez&rendertype=abstract

Dictenberg JB, Swanger SA, Antar LN, Singer RH, Bassell GJ. 2008. A direct role for FMRP in activity-dependent dendritic mRNA transport links filopodial-spine morphogenesis to fragile X syndrome. Dev Cell 14:926–39.

Donnelly CJ, Fainzilber M, Twiss JL. 2010. Subcellular communication through RNA transport and localized protein synthesis. Traffic [Internet] 11:1498–505. Available from: http://www.pubmedcentral.nih.gov/articlerender.fcgi?artid=3058479&tool=pmcentrez&rendertype=abstract

Dubový P, Jančálek R, Kubek T. 2013. Role of inflammation and cytokines in peripheral nerve regeneration. Int Rev Neurobiol [Internet] 108:173–206. Available from: http://www.ncbi.nlm.nih.gov/pubmed/24083435

Ekström K, Valadi H, Sjöstrand M, Malmhäll C, Bossios A, Eldh M, Lötvall J. 2012. Characterization of mRNA and microRNA in human mast cell-derived exosomes and their transfer to other mast cells and blood CD34 progenitor cells. J Extracell vesicles [Internet] 1. Available from: http://www.pubmedcentral.nih.gov/articlerender.fcgi?artid=3760639&tool=pmcentrez&rendertype=abstract

Elangovan M, Wallrabe H, Chen Y, Day RN, Barroso M, Periasamy A. 2003. Characterization of one- and two-photon excitation fluorescence resonance energy transfer microscopy. Methods 29:58–73.

Eng H, Lund K, Campenot RB. 1999. Synthesis of beta-tubulin, actin, and other proteins in axons of sympathetic neurons in compartmented cultures. J Neurosci [Internet] 19:1–9. Available from: http://www.ncbi.nlm.nih.gov/pubmed/9870932

Eyman M, Cefaliello C, Ferrara E, De Stefano R, Lavina ZS, Crispino M, Squillace A, van Minnen J, Kaplan BB, Giuditta A. 2007. Local synthesis of axonal and presynaptic RNA in squid model systems. Eur J Neurosci [Internet] 25:341–50. Available from: http://www.ncbi.nlm.nih.gov/pubmed/17284174

Faivre-Sarrailh C, Devaux JJ. 2013. Neuro-glial interactions at the nodes of Ranvier: implication in health and diseases. Front Cell Neurosci [Internet] 7:196. Available from: http://www.pubmedcentral.nih.gov/articlerender.fcgi?artid=3810605&tool=pmcentrez&rendertype=abstract

Fischer S, Gariglio P, Tarifeño E. 1969. Incorporation of H3-uridine and the isolation and characterization of RNA from squid axon. J Cell Physiol [Internet] 74:155–62. Available from: http://www.ncbi.nlm.nih.gov/pubmed/5358252

Friede RL, Bischhausen R. 1980. The fine structure of stumps of transected nerve fibers in subserial sections. J Neurol Sci [Internet] 44:181–203. Available from: http://www.ncbi.nlm.nih.gov/pubmed/7188775

Ghabriel MN, Allt G. 1979. The role of Schmidt-Lanterman incisures in Wallerian degeneration. I. A quantitative teased fibre study. Acta Neuropathol [Internet] 48:93–93. Available from: http://www.ncbi.nlm.nih.gov/pubmed/506700

Ghabriel MN, Allt G. 1980. Schmidt-Lanterman incisures. II. A light and electron microscope study of remyelinating peripheral nerve fibres. Acta Neuropathol [Internet] 52:97–104. Available from: http://www.ncbi.nlm.nih.gov/pubmed/7435169

Ghabriel MN, Allt G. 1981. Incisures of Schmidt-Lanterman. Prog Neurobiol [Internet] 17:25–58. Available from: http://www.ncbi.nlm.nih.gov/pubmed/7323300

Gioio AE, Chun JT, Crispino M, Capano CP, Giuditta A, Kaplan BB. 1994. Kinesin mRNA is present in the squid giant axon. J Neurochem [Internet] 63:13–8. Available from: http://www.ncbi.nlm.nih.gov/pubmed/8207422

Giuditta A, Chun JT, Eyman M, Cefaliello C, Bruno AP, Crispino M. 2008. Local gene expression in axons and nerve endings: the glia-neuron unit. Physiol

Rev [Internet] 88:515–55. Available from: http://www.ncbi.nlm.nih.gov/pubmed/18391172

Giuditta A, Cupello A, Lazzarini G. 1980. Ribosomal RNA in the axoplasm of the squid giant axon. J Neurochem [Internet] 34:1757–60. Available from: http://www.ncbi.nlm.nih.gov/pubmed/7381500

Giuditta A, Kaplan BB, van Minnen J, Alvarez J, Koenig E. 2002. Axonal and presynaptic protein synthesis: new insights into the biology of the neuron. Trends Neurosci [Internet] 25:400–4. Available from: http://www.ncbi.nlm.nih.gov/pubmed/12127756

Giuditta A, Menichini E, Perrone Capano C, Langella M, Martin R, Castigli E, Kaplan BB. 1991. Active polysomes in the axoplasm of the squid giant axon. J Neurosci Res [Internet] 28:18–28. Available from: http://www.ncbi.nlm.nih.gov/pubmed/1904102

Giuditta A, Metafora S, Felsani A, Del Rio A. 1977. Factors for protein synthesis in the axoplasm of squid giant axons. J Neurochem [Internet] 28:1393–5. Available from: http://www.ncbi.nlm.nih.gov/pubmed/874504

Gumy LF, Katrukha EA, Kapitein LC, Hoogenraad CC. 2014. New insights into mRNA trafficking in axons. Dev Neurobiol [Internet] 74:233–44. Available from: http://www.ncbi.nlm.nih.gov/pubmed/23959656

Gumy LF, Yeo GSH, Tung Y-CL, Zivraj KH, Willis D, Coppola G, Lam BYH, Twiss JL, Holt CE, Fawcett JW. 2011. Transcriptome analysis of embryonic and adult sensory axons reveals changes in mRNA repertoire localization. RNA [Internet] 17:85–98. Available from: http://www.pubmedcentral.nih.gov/articlerender.fcgi?artid=3004069&tool=pmcentrez&rendertype=abstract

Hirokawa N, Niwa S, Tanaka Y. 2010. Molecular motors in neurons: transport mechanisms and roles in brain function, development, and disease. Neuron 68:610–38.

Hirokawa N, Noda Y. 2008. Intracellular transport and kinesin superfamily proteins, KIFs: structure, function, and dynamics. Physiol Rev 88:1089–118.

Holt CE, Bullock SL. 2009. Subcellular mRNA localization in animal cells and why it matters. Science 326:1212–6.

Huang DW, Sherman BT, Lempicki RA. 2009a. Bioinformatics enrichment tools: paths toward the comprehensive functional analysis of large gene lists. Nucleic Acids Res [Internet] 37:1–13. Available from: http://www.pubmedcentral.nih.gov/articlerender.fcgi?artid=2615629&tool=pmcentrez&rendertype=abstract

Huang DW, Sherman BT, Lempicki RA. 2009b. Systematic and integrative analysis of large gene lists using DAVID bioinformatics resources. Nat Protoc [Internet] 4:44–57. Available from: http://www.ncbi.nlm.nih.gov/pubmed/19131956

Iwanaga T, Takahashi Y, Fujita T. 1989. Immunohistochemistry of neuron-specific and glia-specific proteins. Arch Histol Cytol [Internet] 52 Suppl:13–24. Available from: http://www.ncbi.nlm.nih.gov/pubmed/2510778

Izant JG, McIntosh JR. 1980. Microtubule-associated proteins: a monoclonal antibody to MAP2 binds to differentiated neurons. Proc Natl Acad Sci U S A [Internet] 77:4741–5. Available from: http://www.pubmedcentral.nih.gov/articlerender.fcgi?artid=349922&tool=pmcentrez&rendertype=abstract

Jansen R-P, Niessing D. 2012. Assembly of mRNA-protein complexes for directional mRNA transport in eukaryotes--an overview. Curr Protein Pept Sci 13:284–93.

Kanai Y, Dohmae N, Hirokawa N. 2004. Kinesin transports RNA: isolation and characterization of an RNA-transporting granule. Neuron 43:513–25.

Kaplan BB, Gioio AE, Capano CP, Crispino M, Giuditta A. 1992. beta-Actin and beta-Tubulin are components of a heterogeneous mRNA population present in the squid giant axon. Mol Cell Neurosci [Internet] 3:133–44. Available from: http://www.ncbi.nlm.nih.gov/pubmed/19912853

Kaplan BB, Gioio AE, Hillefors M, Aschrafi A. 2009. Axonal protein synthesis and the regulation of local mitochondrial function. Results Probl Cell Differ [Internet] 48:225–42. Available from: http://www.pubmedcentral.nih.gov/articlerender.fcgi?artid=2786086&tool=pmcentrez&rendertype=abstract

Kar AN, MacGibeny MA, Gervasi NM, Gioio AE, Kaplan BB. 2013. Intra-axonal synthesis of eukaryotic translation initiation factors regulates local protein synthesis and axon growth in rat sympathetic neurons. J Neurosci [Internet] 33:7165–74. Available from: http://www.pubmedcentral.nih.gov/articlerender.fcgi?artid=3685850&tool=pmcentrez&rendertype=abstract

Khawaja S, Gundersen GG, Bulinski JC. 1988. Enhanced stability of microtubules enriched in detyrosinated tubulin is not a direct function of detyrosination level. J Cell Biol 106:141–9.

Kiebler MA, Bassell GJ. 2006. Neuronal RNA granules: movers and makers. Neuron [Internet] 51:685–90. Available from: http://www.ncbi.nlm.nih.gov/pubmed/16982415

Kislauskis EH, Zhu X, Singer RH. 1997. beta-Actin messenger RNA localization and protein synthesis augment cell motility. J Cell Biol [Internet] 136:1263–

70. Available from: http://www.pubmedcentral.nih.gov/articlerender.fcgi?artid=2132521&tool=pmcentrez&rendertype=abstract

Koenig E, Giuditta A. 1999. Protein-synthesizing machinery in the axon compartment. Neuroscience [Internet] 89:5–15. Available from: http://www.ncbi.nlm.nih.gov/pubmed/10051213

Koenig E, Martin R, Titmus M, Sotelo-Silveira JR. 2000. Cryptic peripheral ribosomal domains distributed intermittently along mammalian myelinated axons. J Neurosci [Internet] 20:8390–400. Available from: http://www.ncbi.nlm.nih.gov/pubmed/11069946

Koenig E, Martin R. 1996. Cortical plaque-like structures identify ribosome-containing domains in the Mauthner cell axon. J Neurosci [Internet] 16:1400–11. Available from: http://www.ncbi.nlm.nih.gov/pubmed/8778291

Koenig E. 1979. Ribosomal RNA in Mauthner axon: implications for a protein synthesizing machinery in the myelinated axon. Brain Res [Internet] 174:95–107. Available from: http://www.ncbi.nlm.nih.gov/pubmed/487126

Kun A, Otero L, Sotelo-Silveira JR, Sotelo JR. 2007. Ribosomal distributions in axons of mammalian myelinated fibers. J Neurosci Res [Internet] 85:2087–98. Available from: http://www.ncbi.nlm.nih.gov/pubmed/17520748

Lawrence JB, Singer RH. 1986. Intracellular localization of messenger RNAs for cytoskeletal proteins. Cell [Internet] 45:407–15. Available from: http://www.ncbi.nlm.nih.gov/pubmed/3698103

Lee MK, Tuttle JB, Rebhun LI, Cleveland DW, Frankfurter A. 1990. The expression and posttranslational modification of a neuron-specific beta-tubulin isotype during chick embryogenesis. Cell Motil Cytoskeleton [Internet] 17:118–32. Available from: http://www.ncbi.nlm.nih.gov/pubmed/2257630

Lee Y, Kim M, Han J, Yeom K-H, Lee S, Baek SH, Kim VN. 2004. MicroRNA genes are transcribed by RNA polymerase II. EMBO J [Internet] 23:4051–60. Available from: http://www.pubmedcentral.nih.gov/articlerender.fcgi?artid=524334&tool=pmcentrez&rendertype=abstract

Li J. 2008. Hypothesis of double polarization. J Neurol Sci [Internet] 275:33–6. Available from: http://www.ncbi.nlm.nih.gov/pubmed/18706661

Li S, Liu Q, Wang Y, Gu Y, Liu D, Wang C, Ding G, Chen J, Liu J, Gu X. 2013. Differential gene expression profiling and biological process analysis in proximal nerve segments after sciatic nerve transection. PLoS One [Internet] 8:e57000. Available from: http://www.pubmedcentral.nih.gov/articlerender.fcgi?artid=3578805&tool=pmcentrez&rendertype=abstract

Li Y, Brown A, Jung P. 2014. Deciphering the axonal transport kinetics of neurofilaments using the fluorescence photoactivation pulse-escape method. Phys Biol [Internet] 11:026001. Available from: http://www.ncbi.nlm.nih.gov/pubmed/24632540

Li Y-C, Cheng C-X, Li Y-N, Shimada O, Atsumi S. 2005a. Beyond the initial axon segment of the spinal motor axon: fasciculated microtubules and polyribosomal clusters. J Anat [Internet] 206:535–42. Available from: http://www.pubmedcentral.nih.gov/articlerender.fcgi?artid=1571525&tool=pmcentrez&rendertype=abstract

Li Y-C, Li Y-N, Cheng C-X, Sakamoto H, Kawate T, Shimada O, Atsumi S. 2005b. Subsurface cisterna-lined axonal invaginations and double-walled vesicles at the axonal-myelin sheath interface. Neurosci Res [Internet] 53:298–303. Available from: http://www.ncbi.nlm.nih.gov/pubmed/16129504

Lyons DA, Naylor SG, Scholze A, Talbot WS. 2009. Kif1b is essential for mRNA localization in oligodendrocytes and development of myelinated axons. Nat Genet 41:854–8.

Martin KC, Ephrussi A. 2009. mRNA localization: gene expression in the spatial dimension. Cell 136:719–30.

McDonald MK, Capasso KE, Ajit SK. 2013. Purification and microRNA profiling of exosomes derived from blood and culture media. J Vis Exp [Internet]:e50294. Available from: http://www.ncbi.nlm.nih.gov/pubmed/23792786

Minis A, Dahary D, Manor O, Leshkowitz D, Pilpel Y, Yaron A. 2014. Subcellular transcriptomics-dissection of the mRNA composition in the axonal compartment of sensory neurons. Dev Neurobiol [Internet] 74:365–81. Available from: http://www.ncbi.nlm.nih.gov/pubmed/24127433

Mittelbrunn M, Vicente Manzanares M, Sánchez-Madrid F. 2015. Organizing polarized delivery of exosomes at synapses. Traffic [Internet]. Available from: http://www.ncbi.nlm.nih.gov/pubmed/25614958

Nalavadi VC, Griffin LE, Picard-Fraser P, Swanson AM, Takumi T, Bassell GJ. 2012. Regulation of zipcode binding protein 1 transport dynamics in axons by myosin Va. J Neurosci [Internet] 32:15133–41. Available from: http://www.pubmedcentral.nih.gov/articlerender.fcgi?artid=3508068&tool=pmcentrez&rendertype=abstract

Natera-Naranjo O, Aschrafi A, Gioio AE, Kaplan BB. 2010. Identification and quantitative analyses of microRNAs located in the distal axons of sympathetic neurons. RNA [Internet] 16:1516–29. Available from: http://www.pubmedcentral.nih.gov/articlerender.fcgi?artid=2905752&tool=pmcentrez&rendertype=abstract

Natera-Naranjo O, Kar AN, Aschrafi A, Gervasi NM, Macgibeny MA, Gioio AE, Kaplan BB. 2012. Local translation of ATP synthase subunit 9 mRNA alters ATP levels and the production of ROS in the axon. Mol Cell Neurosci [Internet] 49:263–70. Available from: http://www.ncbi.nlm.nih.gov/pubmed/22209705

Ohashi S, Koike K, Omori A, Ichinose S, Ohara S, Kobayashi S, Sato T-A, Anzai K. 2002. Identification of mRNA/protein (mRNP) complexes containing Puralpha, mStaufen, fragile X protein, and myosin Va and their association with rough endoplasmic reticulum equipped with a kinesin motor. J Biol Chem 277:37804–10.

Peles E, Salzer JL. 2000. Molecular domains of myelinated axons. Curr Opin Neurobiol [Internet] 10:558–65. Available from: http://www.ncbi.nlm.nih.gov/pubmed/11084317

Piper M, Holt C. 2004. RNA translation in axons. Annu Rev Cell Dev Biol [Internet] 20:505–23. Available from: http://www.pubmedcentral.nih.gov/articlerender.fcgi?artid=3682640&tool=pmcentrez&rendertype=abstract

Poliak S, Peles E. 2003. The local differentiation of myelinated axons at nodes of Ranvier. Nat Rev Neurosci [Internet] 4:968–80. Available from: http://www.ncbi.nlm.nih.gov/pubmed/14682359

Portier MM, Escurat M, Landon F, Djabali K, Bousquet O. 1993. Peripherin and neurofilaments: expression and role during neural development. C R Acad Sci III [Internet] 316:1124–40. Available from: http://www.ncbi.nlm.nih.gov/pubmed/8076208

Provance DW, Addison EJ, Wood PR, Chen DZ, Silan CM, Mercer JA. 2008. Myosin-Vb functions as a dynamic tether for peripheral endocytic compartments during transferrin trafficking. BMC Cell Biol [Internet] 9:44. Available from: http://www.pubmedcentral.nih.gov/articlerender.fcgi?artid=2533098&tool=pmcentrez&rendertype=abstract

Ramachandran S, Palanisamy V. Horizontal transfer of RNAs: exosomes as mediators of intercellular communication. Wiley Interdiscip Rev RNA [Internet] 3:286–93. Available from: http://www.pubmedcentral.nih.gov/articlerender.fcgi?artid=3263325&tool=pmcentrez&rendertype=abstract

Rapallino M V, Cupello A, Giuditta A. 1988. Axoplasmic RNA species synthesized in the isolated squid giant axon. Neurochem Res [Internet] 13:625–31. Available from: http://www.ncbi.nlm.nih.gov/pubmed/2457819

Rios JC, Rubin M, St Martin M, Downey RT, Einheber S, Rosenbluth J, Levinson SR, Bhat M, Salzer JL. 2003. Paranodal interactions regulate expression of sodium channel subtypes and provide a diffusion barrier for

the node of Ranvier. J Neurosci [Internet] 23:7001–11. Available from: http://www.ncbi.nlm.nih.gov/pubmed/12904461

Roberson MD, Toews AD, Goodrum JF, Morell P. 1992. Neurofilament and tubulin mRNA expression in Schwann cells. J Neurosci Res [Internet] 33:156–62. Available from: http://www.ncbi.nlm.nih.gov/pubmed/1453479

Rodriguez AJ, Shenoy SM, Singer RH, Condeelis J. 2006. Visualization of mRNA translation in living cells. J Cell Biol [Internet] 175:67–76. Available from: http://www.pubmedcentral.nih.gov/articlerender.fcgi?artid=2064499&tool=pmcentrez&rendertype=abstract

Rosenbluth J, Dupree JL, Popko B. 2003. Nodal sodium channel domain integrity depends on the conformation of the paranodal junction, not on the presence of transverse bands. Glia [Internet] 41:318–25. Available from: http://www.ncbi.nlm.nih.gov/pubmed/12528185

Rosenbluth J, Mierzwa A, Shroff S. 2013. Molecular architecture of myelinated nerve fibers: leaky paranodal junctions and paranodal dysmyelination. Neuroscientist [Internet] 19:629–41. Available from: http://www.ncbi.nlm.nih.gov/pubmed/24122820

Salerno VP, Calliari A, Provance DW, Sotelo-Silveira JR, Sotelo JR, Mercer JA. 2008. Myosin-Va mediates RNA distribution in primary fibroblasts from multiple organs. Cell Motil Cytoskeleton [Internet] 65:422–33. Available from: http://www.pubmedcentral.nih.gov/articlerender.fcgi?artid=2633925&tool=pmcentrez&rendertype=abstract

Salzer JL, Brophy PJ, Peles E. 2008. Molecular domains of myelinated axons in the peripheral nervous system. Glia [Internet] 56:1532–40. Available from: http://www.ncbi.nlm.nih.gov/pubmed/18803321

Salzer JL, Bunge RP. 1980. Studies of Schwann cell proliferation. I. An analysis in tissue culture of proliferation during development, Wallerian degeneration, and direct injury. J Cell Biol [Internet] 84:739–52. Available from: http://www.pubmedcentral.nih.gov/articlerender.fcgi?artid=2110577&tool=pmcentrez&rendertype=abstract

Salzer JL. 1997. Clustering sodium channels at the node of Ranvier: close encounters of the axon-glia kind. Neuron [Internet] 18:843–6. Available from: http://www.ncbi.nlm.nih.gov/pubmed/9208851

Salzer JL. 2003. Polarized domains of myelinated axons. Neuron [Internet] 40:297–318. Available from: http://www.ncbi.nlm.nih.gov/pubmed/14556710

Sasaki Y, Gross C, Xing L, Goshima Y, Bassell GJ. 2014. Identification of axon-enriched microRNAs localized to growth cones of cortical neurons. Dev Neurobiol [Internet] 74:397–406. Available from: http://www.ncbi.nlm.nih.gov/pubmed/23897634

Scheib J, Höke A. 2013. Advances in peripheral nerve regeneration. Nat Rev Neurol [Internet] 9:668–76. Available from: http://www.ncbi.nlm.nih.gov/pubmed/24217518

Scherer SS, Arroyo EJ. 2002. Recent progress on the molecular organization of myelinated axons. J Peripher Nerv Syst [Internet] 7:1–12. Available from: http://www.ncbi.nlm.nih.gov/pubmed/11939347

Sherman DL, Brophy PJ. 2005. Mechanisms of axon ensheathment and myelin growth. Nat Rev Neurosci [Internet] 6:683–90. Available from: http://www.ncbi.nlm.nih.gov/pubmed/16136172

Shin RW, Iwaki T, Kitamoto T, Tateishi J. 1991. Hydrated autoclave pretreatment enhances tau immunoreactivity in formalin-fixed normal and Alzheimer's disease brain tissues. Lab Invest [Internet] 64:693–702. Available from: http://www.ncbi.nlm.nih.gov/pubmed/1903170

Simons M, Raposo G. 2009. Exosomes--vesicular carriers for intercellular communication. Curr Opin Cell Biol [Internet] 21:575–81. Available from: http://www.ncbi.nlm.nih.gov/pubmed/19442504

Singer M, Green MR. 1968. Autoradiographic studies of uridine incorporation in peripheral nerve of the newt, Triturus. J Morphol [Internet] 124:321–44. Available from: http://www.ncbi.nlm.nih.gov/pubmed/5657935

Son YJ, Thompson WJ. 1995a. Nerve sprouting in muscle is induced and guided by processes extended by Schwann cells. Neuron [Internet] 14:133–41. Available from: http://www.ncbi.nlm.nih.gov/pubmed/7826631

Son YJ, Thompson WJ. 1995b. Schwann cell processes guide regeneration of peripheral axons. Neuron [Internet] 14:125–32. Available from: http://www.ncbi.nlm.nih.gov/pubmed/7826630

Sotelo JR, Benech CR, Kun A. 1992. Local radiolabeling of the 68 kDa neurofilament protein in rat sciatic nerves. Neurosci Lett [Internet] 144:174–6. Available from: http://www.ncbi.nlm.nih.gov/pubmed/1436698

Sotelo JR, Kun A, Benech JC, Giuditta A, Morillas J, Benech CR. 1999. Ribosomes and polyribosomes are present in the squid giant axon: an immunocytochemical study. Neuroscience [Internet] 90:705–15. Available from: http://www.ncbi.nlm.nih.gov/pubmed/10215172

Sotelo-Silveira J, Crispino M, Puppo A, Sotelo JR, Koenig E. 2008. Myelinated axons contain beta-actin mRNA and ZBP-1 in periaxoplasmic ribosomal plaques and depend on cyclic AMP and F-actin integrity for in vitro

translation. J Neurochem [Internet] 104:545–57. Available from: http://www.ncbi.nlm.nih.gov/pubmed/17961153

Sotelo-Silveira JR, Calliari A, Cárdenas M, Koenig E, Sotelo JR. 2004. Myosin Va and kinesin II motor proteins are concentrated in ribosomal domains (periaxoplasmic ribosomal plaques) of myelinated axons. J Neurobiol [Internet] 60:187–96. Available from: http://www.ncbi.nlm.nih.gov/pubmed/15266650

Sotelo-Silveira JR, Calliari A, Kun A, Benech JC, Sanguinetti C, Chalar C, Sotelo JR. 2000. Neurofilament mRNAs are present and translated in the normal and severed sciatic nerve. J Neurosci Res [Internet] 62:65–74. Available from: http://www.ncbi.nlm.nih.gov/pubmed/11002288

Sotelo-Silveira JR, Calliari A, Kun A, Koenig E, Sotelo JR. 2006. RNA trafficking in axons. Traffic 7:508–15.

Taylor AM, Berchtold NC, Perreau VM, Tu CH, Li Jeon N, Cotman CW. 2009. Axonal mRNA in uninjured and regenerating cortical mammalian axons. J Neurosci [Internet] 29:4697–707. Available from: http://www.pubmedcentral.nih.gov/articlerender.fcgi?artid=3632375&tool=pmcentrez&rendertype=abstract

Terenghi G. 1999. Peripheral nerve regeneration and neurotrophic factors. J Anat [Internet] 194 (Pt 1:1–14. Available from: http://www.pubmedcentral.nih.gov/articlerender.fcgi?artid=1467889&tool=pmcentrez&rendertype=abstract

Thaxton C, Bhat MA. 2009. Myelination and regional domain differentiation of the axon. Results Probl Cell Differ [Internet] 48:1–28. Available from: http://www.pubmedcentral.nih.gov/articlerender.fcgi?artid=2824168&tool=pmcentrez&rendertype=abstract

Trivedi N, Jung P, Brown A. 2007. Neurofilaments switch between distinct mobile and stationary states during their transport along axons. J Neurosci [Internet] 27:507–16. Available from: http://www.pubmedcentral.nih.gov/articlerender.fcgi?artid=1933499&tool=pmcentrez&rendertype=abstract

Valadi H, Ekström K, Bossios A, Sjöstrand M, Lee JJ, Lötvall JO. 2007. Exosome-mediated transfer of mRNAs and microRNAs is a novel mechanism of genetic exchange between cells. Nat Cell Biol [Internet] 9:654–9. Available from: http://www.ncbi.nlm.nih.gov/pubmed/17486113

Wallrabe H, Chen Y, Periasamy A, Barroso M. 2006. Issues in confocal microscopy for quantitative FRET analysis. Microsc Res Tech 69:196–206.

Wallrabe H, Elangovan M, Burchard A, Periasamy A, Barroso M. 2003. Confocal FRET microscopy to measure clustering of ligand-receptor complexes in endocytic membranes. Biophys J 85:559–71.

Weiner OD, Zorn AM, Krieg PA, Bittner GD. 1996. Medium weight neurofilament mRNA in goldfish Mauthner axoplasm. Neurosci Lett [Internet] 213:83–6. Available from: http://www.pubmedcentral.nih.gov/articlerender.fcgi?artid=2830807&tool=pmcentrez&rendertype=abstract

Willis D, Li KW, Zheng J-Q, Chang JH, Smit AB, Smit A, Kelly T, Merianda TT, Sylvester J, van Minnen J, Twiss JL. 2005. Differential transport and local translation of cytoskeletal, injury-response, and neurodegeneration protein mRNAs in axons. J Neurosci [Internet] 25:778–91. Available from: http://www.ncbi.nlm.nih.gov/pubmed/15673657

Willis DE, van Niekerk EA, Sasaki Y, Mesngon M, Merianda TT, Williams GG, Kendall M, Smith DS, Bassell GJ, Twiss JL. 2007. Extracellular stimuli specifically regulate localized levels of individual neuronal mRNAs. J Cell Biol [Internet] 178:965–80. Available from: http://www.pubmedcentral.nih.gov/articlerender.fcgi?artid=2064621&tool=pmcentrez&rendertype=abstract

Yoshimura A, Fujii R, Watanabe Y, Okabe S, Fukui K, Takumi T. 2006. Myosin-Va facilitates the accumulation of mRNA/protein complex in dendritic spines. Curr Biol [Internet] 16:2345–51. Available from: http://www.ncbi.nlm.nih.gov/pubmed/17141617

Zivraj KH, Tung YCL, Piper M, Gumy L, Fawcett JW, Yeo GSH, Holt CE. 2010. Subcellular profiling reveals distinct and developmentally regulated repertoire of growth cone mRNAs. J Neurosci [Internet] 30:15464–78. Available from: http://www.pubmedcentral.nih.gov/articlerender.fcgi?artid=3683943&tool=pmcentrez&rendertype=abstract

11. APENDICE

11. 1. RESULTADOS PRELIMINARES ADICIONALES

En esta sección presentaremos resultados que por ser preliminares consideramos no deben formar parte de los capítulos centrales de la presente tesis.

En los experimentos de inmunocitoquímica descritos en la presente tesis nos abocamos a observar el fenómeno de transferencia de ARNs desde la glia al axón, centrándonos en lo que sucedía en el nodo de Ranvier. Sin embargo, existen otras regiones de la fibra en regeneración donde el fenómeno parece tener un rol y que son sumamente interesantes de estudiar. Un ejemplo son los brotamientos axonales. Hemos observado que los brotamientos están repletos de ARNs transferidos, tanto a las 24 horas de realizada una lesión (figura 10.1A), como a los 7 días (figura 10.B). Cuáles son los ARNs que se localizan en los brotamientos y cuál es su función son dos aspectos del fenómeno que serán abordados en el futuro.

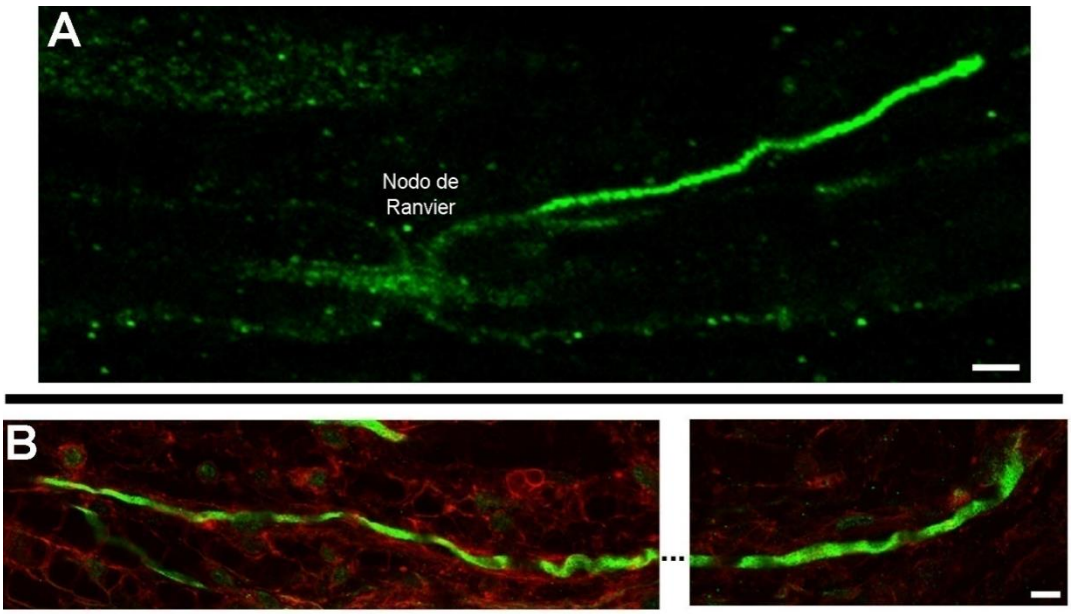

Figura 10.1. Brotamientos axonales.
Se muestran brotamientos axonales de fibras de nervio ciático en regeneración 24 horas (A) y 7 días (B) post-lesión. **A,** Nodo de Ranvier en el plano del axón, mostrando los ARN-BrU en verde. **B,** Brotamiento axonal mostrando los ARN-BrU en verde y la actina filamentosa en rojo. Las interrupciones de la señal de los ARN-BrU se deben a que el brotamiento queda por fuera del plano focal fotografiado. Barras: 5 µm.

La figura 10.2 muestra el resultado de los experimentos preliminares de inmunocitoquímica realizados para evaluar si hnRNPA2 co-localiza con los ARN-BrU. En estos experimentos encontramos co-localización entre las señales del anti-hnRNPA2 (figura 10.2, rojo) y el anticuerpo que reconoce los ARN-BrU (figura 10.2, verde) en el axón (figura 10.2A, flechas) y también en el citoplasma (figura 10.2B, flechas) y el núcleo de la célula de Schwann (figura 10.2B, cabezas de flechas).

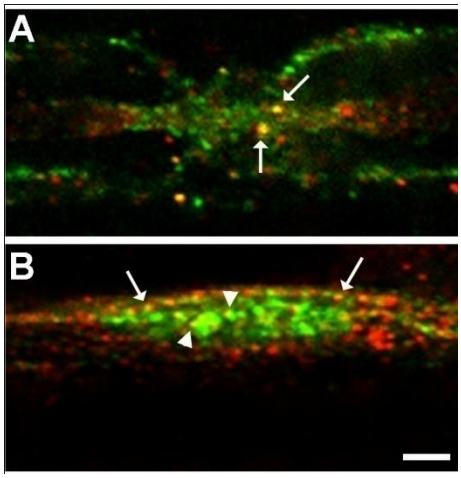

Figura 10.2. Co-localización de los ARN-BrU con hnRNPA2.
La figura muestra planos confocales de un nodo de Ranvier en el plano del axón (A) y de un núcleo de la célula de Schwann (B) de fibras inmunoteñidas con un anticuerpo que reconoce los ARN-BrU (verde) y un anticuerpo que reconoce hnRNPA2 (rojo). Las flechas señalan puntos de co-localización entre los ARN-BrU y hnRNPA2 en el axoplasma (A) y el citoplasma externo de la célula de Schwann (B). Las cabezas de flechas señalan ejemplos de puntos de co-localización entre ambas moléculas en el núcleo de la célula de Schwann. Barra: 5 µm.

Tabla I. ARNm que codifican KIFs expresados en nervio ciático.

Gen	**Identificado en la muestra BrU-ARN**	**Identificado por Li y cols.**
kif1a	x	
kif1b	x	x
kif1c	x	x
kif2a	x	
kif2c		x
kif3a	x	
kif3b	x	x
kif3c	x	x
kif5a	x	x
kif5b	x	x
kif5c	x	x
kif12		x
kif13a	x	x
kif13b	x	x
kif15		x
kif16b	x	x
kif18a		x
kif19	x	
kif20a		x
kif20b		x
kif21a	x	x
kif21b		x
kif22		x
kif23		x
kif26b	x	
kif27		x

11. 2. OTRAS PUBLICACIONES GENERADAS VINCULADAS A LA PRESENTE TESIS

7.1.2. TRABAJO VI.

Kun A.; Canclini L.; Rosso G.; Bresque, M.; Romeo C.; Hanusz, A.; Cal K.; Calliari, A.; Sotelo-Silveira, J.R.; Sotelo J. R. F-actin distribution at nodes of Ranvier and Schmidt-Lanterman incisures in mammalian sciatic nerves. Cytoskeleton, 69, 486-495, 2012

Mi participación formal en este trabajo incluyó el diseño y realización de los experimentos que dieron lugar a las figuras 4, 5, 6, 7, 8 y 9, y la redacción del manuscrito en colaboración con la Dra. Kun y el Dr. Sotelo. En este trabajo analizamos la distribución del citoesqueleto de actina en fibras mielínicas normales y en regeneración de nervios ciáticos de rata. También indagamos la estabilidad de la actina filamentosa frente a dos drogas que desestabilizan dicho citoesqueleto: citocalasina D y latrunculina A. Los resultados obtenidos así aportaron datos fundamentales para la realización de los experimentos vinculados con el citoesqueleto de actina presentados en el capítulo II de la presente tesis.

RESEARCH ARTICLE
Cytoskeleton, July 2012 69:486–495 (doi: 10.1002/cm.21011)

F-Actin Distribution at Nodes of Ranvier and Schmidt-Lanterman Incisures in Mammalian Sciatic Nerves

Alejandra Kun,[1,2] Lucía Canclini,[1] Gonzalo Rosso,[1] Mariana Bresque,[1,3] Carlos Romeo,[1,3] Alicia Hanusz,[1] Karina Cal,[1] Aldo Calliari,[1,4] José Sotelo Silveira,[5,6] and José R. Sotelo[1]*

[1]*Department of Proteins and Nucleic Acids, Instituto de Investigaciones Biológicas Clemente Estable (IIBCE), Av. Italia 3318, Montevideo, Uruguay*
[2]*Department of Biochemistry, School of Science, Universidad de la República (UdelaR), Montevideo, Uruguay*
[3]*Project of the Comisión Sectorial de Investigación Científica (CSIC, UdelaR), Montevideo, Uruguay*
[4]*Area Biofísica, School of Veterinary, UdelaR, Montevideo, Uruguay*
[5]*Department of Cell and Molecular Biology, School of Science, UdelaR, Montevideo, Uruguay*
[6]*Department of Genetics, IIBCE, Montevideo, Uruguay*

Received 8 November 2011; Revised 18 January 2012; Accepted 18 January 2012
Monitoring Editor: Peter Baas

Very little is known about the function of the F-actin cytoskeleton in the regeneration and pathology of peripheral nerve fibers. The actin cytoskeleton has been associated with maintenance of tissue structure, transmission of traction and contraction forces, and an involvement in cell motility. Therefore, the state of the actin cytoskeleton strongly influences the mechanical properties of cells and intracellular transport therein. In this work, we analyze the distribution of F-actin at Schmidt-Lanterman Incisures (SLI) and nodes of Ranvier (NR) domains in normal, regenerating and pathologic Trembler J (TrJ/+) sciatic nerve fibers, of rats and mice. F-actin was quantified and it was found increased in TrJ/+, both in SLI and NR. However, SLI and NR of regenerating rat sciatic nerve did not show significant differences in F-actin, as compared with normal nerves. Cytochalasin-D and Latrunculin-A were used to disrupt the F-actin network in normal and regenerating rat sciatic nerve fibers. Both drugs disrupt F-actin, but in different ways. Cytochalasin-D did not disrupt Schwann cell (SC) F-actin at the NR. Latrunculin-A did not disrupt F-actin at the boundary region between SC and axon at the NR domain. We surmise that the rearrangement of F-actin in neurological disorders, as presented here, is an important feature of TrJ/+ pathology as a Charcot-Marie-Tooth (CMT) model. © 2012 Wiley Periodicals, Inc

*Address correspondence to: Dr. José R. Sotelo, Head of the Department of Proteins and Nucleic Acids, Instituto de Investigaciones Biológicas Clemente Estable (IIBCE), Av. Italia 3318, Montevideo, Uruguay. E-mail: sotelo@iibce.edu.uy or sotelotalibo@gmail.com

Published online 9 March 2012 in Wiley Online Library (wileyonlinelibrary.com).

Key Words: F-actin, Trembler J, sciatic nerve, CMT, neurodegenerative disease

Introduction

In the peripheral nervous system (PNS), each axon in the mature myelinated fiber is ensheathed by numerous Schwann cells (SCs). Myelinated fibers exhibit a striking longitudinal polarity that is centered about nodes of Ranvier (NR), which are myelin gaps of about 1 μm, occupied by outer SC cytoplasm [Salzer, 2003]. Each of the successive node structures are contacted by hundreds of interdigitating microvilli that project from the end of the SC to closely appose the nodal axolemma.

Internodes are myelin segments which extend between nodes and are characterized by two different structural myelin regions: compact and non-compact myelin. The latter is represented by paranodal loops and Schmidt-Lanterman incisures (SLIs). SLIs are prominent, regular features of myelinated peripheral nerve fibers [Ghabriel and Allt, 1979]. These structures have been reported to include a single microtubule within each spiral loop, desmosome-like bands, actin filaments, mitochondria and smooth endoplasmic reticulum [Singer and Green, 1968, Blakemore, 1969, Hall and Williams 1970, Landon and Hall, 1976]. They also contain a variety of cellular proteins, such as alkaline phosphatase, myelin-associated glycoprotein (MAG) and P2 basic protein, as well as a variety of cytoskeletal proteins like connexin 32, S-100 and tubulin [Pinner et al., 1964; Novikoff, 1967; Trapp et al., 1979; Schober et al., 1981; Xu et al., 2000; Erb et al., 2006].

Several roles have been proposed for these structures, including a metabolic function for the maintenance of the

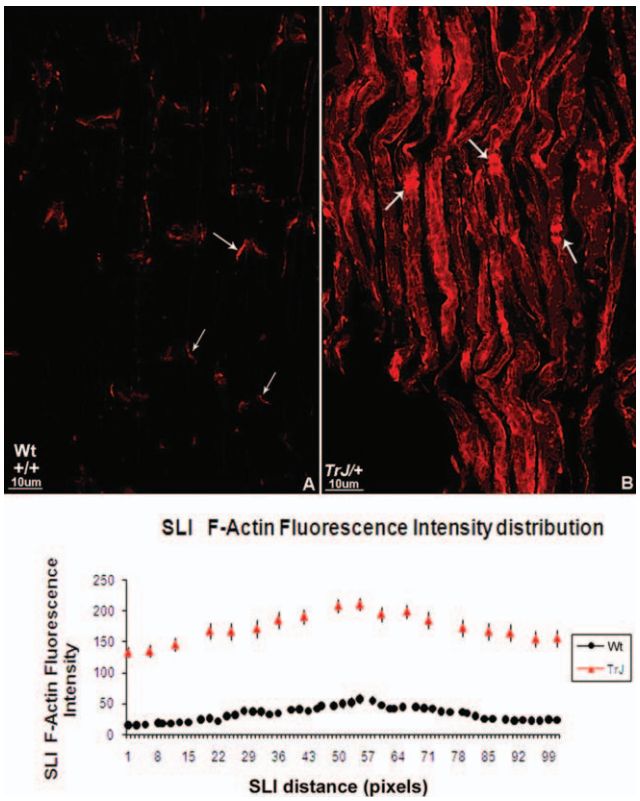

Fig. 1. The Schmidt Lanterman Incisure' F-actin has different fluorescence intensity in Wild type and Trembler-J peripheral mouse fibers. F-actin fluorescence intensity distribution (arbitrary units) was obtained using Alexa-546 Phalloidin (Invitrogen) for staining wild type (Wt+/+) and Trembler-J (TrJ/+) sciatic nerve cryosections. **A** and **B**, single confocal stacks (250 nm thick) of Wt+/+ and TrJ/+ sciatic nerve sections. TrJ/+ fibers were highly stained and had an irregular F-actin distribution (B), whereas the Wt fibers show a well-structured actin distribution (A), especially evident at the SLI. **C**, Actin microfilaments have different distribution and abundance in each genotype. The fluorescence intensity distribution of F-actin is higher in TrJ/+ SLI (red triangles) compared to F-actin intensity distribution of Wt+/+ (black circles). To normalize and compare de intensity/μm the line length crossing each SLI were considered as a 100 pixels. The intensity was expressed in function of this distance.

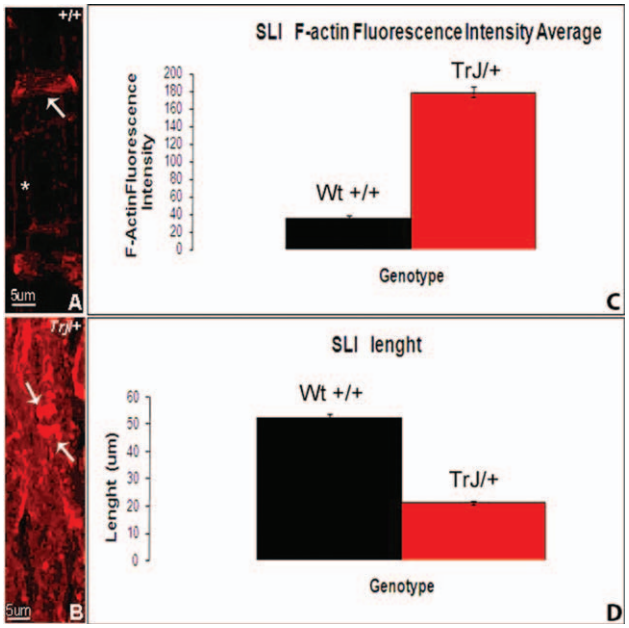

Fig. 2. Comparison of F-actin fluorescence intensity average between SLI of Wt and Trembler-J. A and **B**, Same areas of Wild type (Wt+/+) and Trembler-J (TrJ/+) (532X824 pixels) sciatic nerve 10-μm cryosection were recorded under the same confocal condition. Settings were: HV: 620; Gain: 0%; Offset: 0%; 250 nm stack thickness, 30 stacks by area; 10 different areas each genotype. **C**, the average fluorescence intensity (arbitrary units) of F-actin by linear micron in SLI shows a 5 fold more intense signal in the Trembler-J (TrJ/+) than Wt+/+ ($P < 0.001$). **D**, Length of SLI determined was also statistical significantly different ($P < 0.01$) between TrJ/+ and Wt+/+ fibers.

myelin sheath, interchanging metabolites between all the membranes surface of myelin and the cytoplasmic matrix of the SC [Robertson, 1962; Krishnan and Singer, 1973].

Other authors suggest a potential role as a communications shortcut across SC myelin sheets, from external regions of SC cytoplasm to the inner compartments, until reaching the axonal plasma membrane [Singer and Salpeter, 1966; Singer and Green, 1968; Hall and Williams, 1971; Singer et al., 1972; Rawlins, 1973].

Under different pathological conditions, the appearance of SLIs can be altered, suggesting that these structures might play a role in myelin maintenance [Berger and Gupta, 2006]. In human inherited peripheral neuropathies (i.e., Charcot-Marie-Tooth type 1A disease), the organization of myelinated nerve fibers is altered. CMT1A is the

Table I. F-Actin Fluorescence Intensity in Schmidt Lanterman Incisures and Nodes of Ranvier

Genotype	SLI F-actin intensity* average	SLI (TrJ/+)/(Wt+/+) F-actin, intensity* average ratio	SLI length average (μm)	SLI (Wt+/+)/(TrJ/+), length average ratio	NR (TrJ/+)/(Wt+/+) F-actin, intensity* average ratio
TrJ/+	179±6,2	4.97 ($P < 0.001$)	3.5 ± 0.1	2.49 ($P < 0.01$)	1.79 ($P < 0.001$)
Wt+/+	36±2.1		8.7 ± 0.2		

*Arbitrary units; Number of SLI by phenotype = 30.
Wild-type (Wt+/+) is compared with Trembler J (TrJ/+) mice.

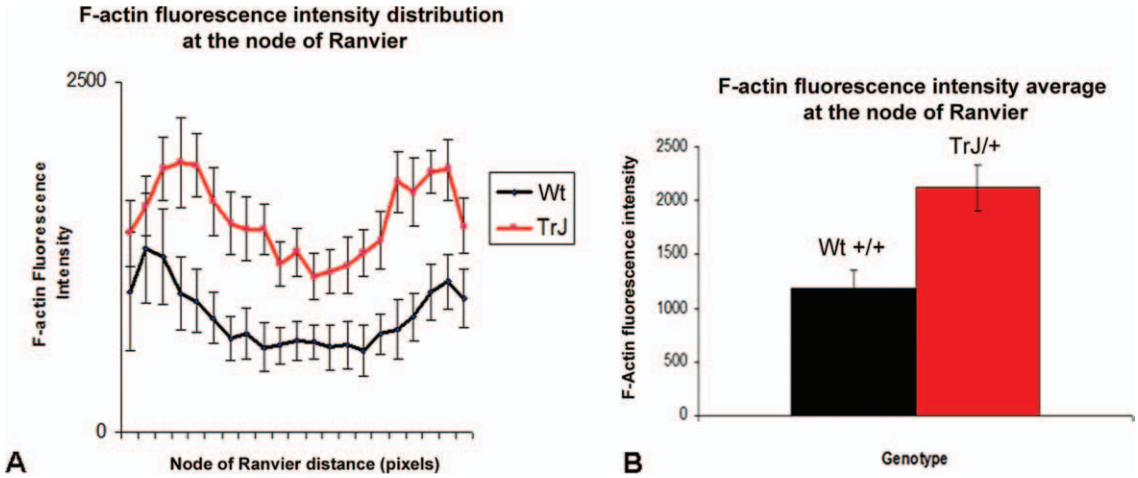

Fig. 3. F-actin fluorescence distribution in Wt+/+ NR is similar to TrJ/+ NR, but fluorescence intensity is higher in TrJ/+ compared to Wt+/+. Sciatic nerve cryosections were incubated with Alexa-546 phalloidin and analyzed by confocal microscopy. **A**, F-actin fluorescence intensity (arbitrary units) distribution across NR. **B**, the averages of NR F-actin fluorescence intensity (arbitrary units) is 1.7 folds higher in TrJ/+ compared to Wt+/+ ($P < 0.001$). Lines crossing each node of Ranvier were divided in 100 pixels to avoid variation in nodal width.

most frequent human hereditary demyelinating neuropathy (prevalence 1:2500) involving the *pmp22* gene (encodes peripheral myelin protein, PMP-22). PMP-22 is a transmembrane tetraspan glycoprotein, highly expressed by myelinating SCs and involved in myelin formation and maintenance, among other functions [Kitamura et al., 1976; Schneider et al., 1988; Manfioletti et al., 1990; Zoidl et al., 1995; Spreyer et al., 1991; Welcher et al., 1991; Müller et al., 1997]. The *pmp22* duplication is associated with most cases of CMT1A [Patel et al., 1992]. Nevertheless, single point mutations in *pmp22* have also been identified in CMT1A human families [Valentijn et al., 1992; Suter and Snipes 1995a]. The same mutation is present in Trembler-J mice (TrJ), which are therefore considered to be an animal model of human CMT1A [Suter and Snipes 1995a; Suter and Snipes 1995b]. This *pmp22* allele results in a non-conservative leucine-to-proline (L16P) replacement in the final PMP-22 protein, preventing its normal folding, myelin insertion, and normal myelination. In addition to the intrinsic *pmp22* mutation effects, other structural modifications have been observed in Trembler-J mouse nerve fibers [Kun et al.,

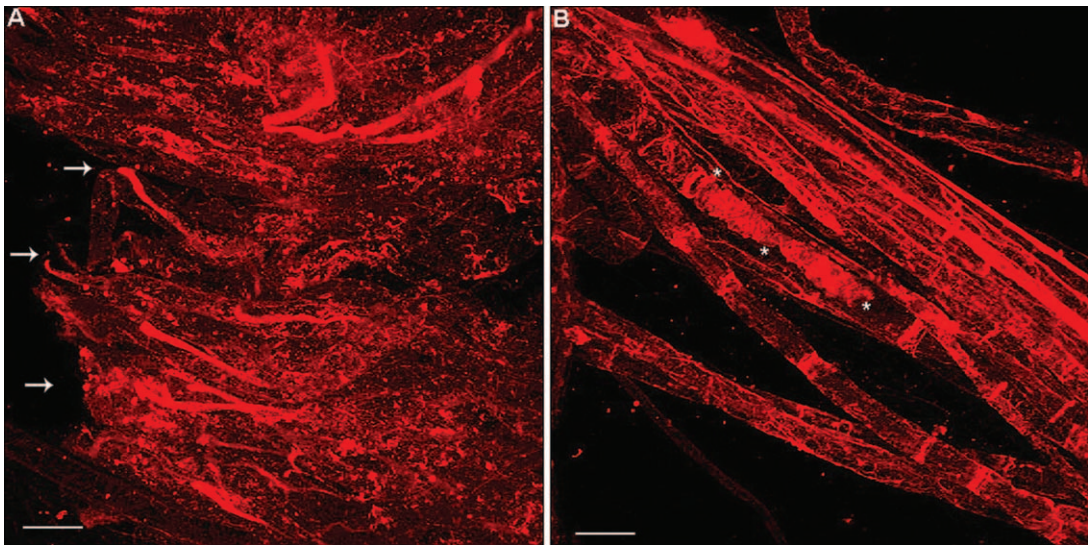

Fig. 4. The F-actin fluorescence distribution is different at the place of injury (proximal stump) when compared to a segment of nerve 100-μm upstream. Rat sciatic nerves were transected and after 18 h regeneration were fixed and stained with Alexa-546 phalloidin. **A** and **B** show confocal Z-projections of 32 stacks (0.25-μm optical sections). **A**, the place of injury (white arrows) shows the stronger signal of F-actin fluorescence and that distribution is not homogeneous. Nodal and SLI domains could not be clearly detected in the proximal stump region. **B**, The F-actin fluorescence 100-μm upstream, shows a normal distribution (asterisks). (Bars = 10 μm).

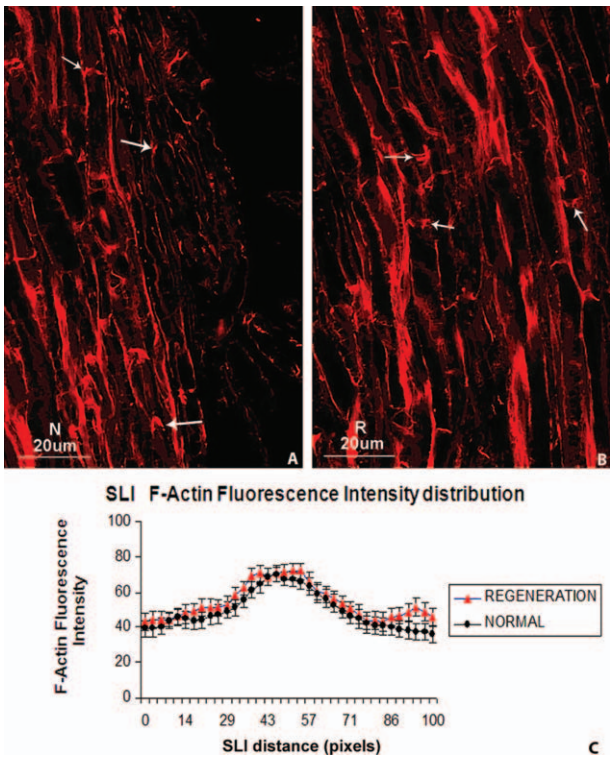

Fig. 5. SLI F-actin distribution during regeneration in normal (N) and transected regenerating (R) rat sciatic nerve fibers. The F-actin fluorescence distribution (arbitrary units) was determined using specific Alexa-546 Phalloidin probe staining in normal (N) and 18 h regenerating (R) rat sciatic nerve fibers. **A** and **B**, show single confocal-stacks (250-nm thick) of normal and regenerating sciatic nerve fibers. Actin microfilaments have approximately the same arrangement in each condition. **C**, Eighteen hours after injury no significant differences ($P < 0.15$) between regenerating (red triangles) and normal fibers (black circles) have been found. To normalize and compare F-Actin fluorescence intensity distribution by micrometer, the line length crossing each SLI were considered as 100 pixels. The intensity was expressed in function of this distance. [Color figure can be viewed in the online issue which is available at wileyonlinelibrary.com]

2011]. These degenerative changes have global influence on nerve fiber structure and function. These alterations define a specific architectural phenotype that characterizes these pathological nerve fibers.

Despite all the proposed roles for SLIs, their function and participation during normal and pathological processes in the PNS are not yet completely understood. In this study, the structural organization of the F-actin cytoskeleton in Schmidt Lanterman Incisures and Nodes of Ranvier was analyzed under normal and pathological conditions by confocal microscopy. Moreover, different regenerative early process (transected nerve) and chronic (Trembler-J mouse) conditions were studied and analyzed. Our results indicate that F-actin organization and expression in SLIs and NR is altered under normal and pathological conditions. These data suggest the presence of an underlying compensatory mechanism that involves effecting changes in actin expression at SLIs and nodes. These changes in SLI and NR might be an important component in the maintenance of peripheral nerve health.

Materials and Methods

Animal Care and Maintenance

Rattus norvegicus (Sprague Dawley) were obtained from the IIBCE colony. Our Trembler-J *(B6. D2-Pmp22 ⟨Tr-j⟩/J*, Jackson Laboratory, USA) mouse colony was started in 2008. These mice carry a spontaneous mutation in Peripheral Myelin Protein 22 (PMP-22). All mice are recorded, numbered and genotyped following the method previously described [Rosso et al., 2010]. All animals live under controlled temperature and 12-h light/dark cycle. Rats and mice are fed *ad libitum*. The animal housing conditions are in agreement with the National Committee for Animal Care and Maintenance (CHEA-Universidad de la República-Uruguay, www.chea.udelar.edu.uy)

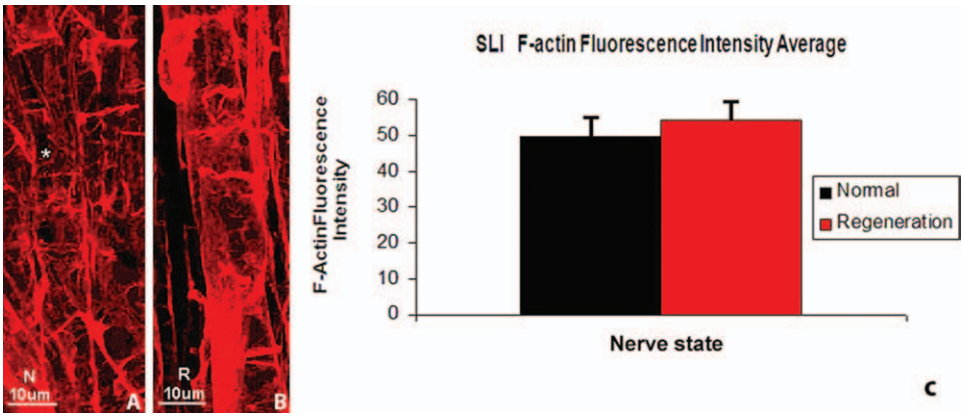

Fig. 6. SLI F-Actin Fluorescence intensity average in normal (N) and regenerating (R) rat sciatic nerve fibers. A and **B**, show 532 × 824 areas of Normal (N) and regenerating (R) confocal projections of rat sciatic fibers. **C**, The average of F-actin fluorescence intensity (arbitrary units) determined in 30 SLI was compared between normal and regenerating sciatic nerve fibers. The considered areas have the same dimensions. No statistical significant differences between normal and regenerating fibers were found ($P < 0.15$). [Color figure can be viewed in the online issue which is available at wileyonlinelibrary.com]

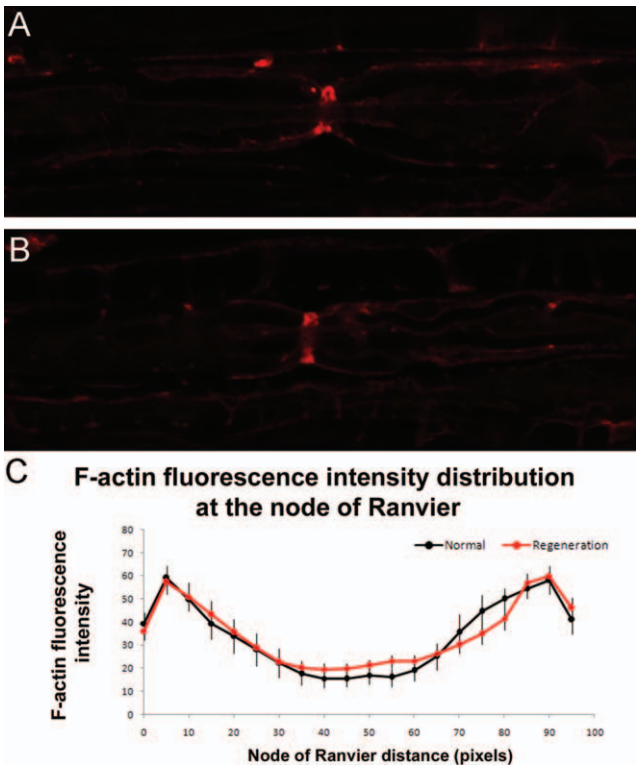

Fig. 7. F-actin fluorescence intensity distribution in NR is not altered during regeneration. The F-actin fluorescence intensity distribution in NR was determined in both, normal (N) and regenerating (R) sciatic nerve fibers (100-µm upstream the proximal stump). **A** and **B**, representative single focal planes of normal (A) and regenerating (B) rat sciatic nerve teased fibers. NR showing actin labeled cytoskeleton are shown in the center of the picture. **C**, F-actin fluorescence intensity distribution across the NR show no significant statistically differences ($P < 0.2$) between N and R fibers. Lines crossing each node of Ranvier were divided in 100 pixels to avoid variations in width. The intensities are expressed in arbitrary units. [Color figure can be viewed in the online issue which is available at wileyonlinelibrary.com]

Trembler-J Mice Genotyping

Genotyping was carried out as described in Kun et al. [2011]. Briefly, after DNA extraction and PCR amplification using specific primers, the products were digested with *Bfa*I (Fermentas) and the digestion products size were evaluated in a 6% PAGE system. The digestion products were stained with $AgNO_3$. The *Bfa*I digestion produced two fragments (221 and 500 bp). The TrJ mutation, where the *Bfa*I recognition site is lost, produced a single band of 721 bp.

Sciatic Nerve Transection and F-Actin Disruption Treatment

Adult Sprague-Dawley rats were anesthetized with 50-mg/kg pentobarbital. An incision was made at mid-thigh and the sciatic nerve was exposed and completely transected. Incisions were closed with cyanoacrylate glue. After 18-h recovery, the rats were euthanized and a ~2-cm sciatic nerve segment proximal to the transection was removed. The segment was incubated in Neurobasal medium (Invitrogen, control condition) or Neurobasal medium containing Latrunculin-A or Cytochalasin-D for 6 h at 37°C and 5% CO_2.

Fixation

Mouse and rat sciatic nerves were immersed in fixative solution (3% paraformaldehyde in PHEM buffer, 25-mM HEPES, 60-mM PIPES, 10-mM EGTA, 2-mM $MgCl_2$, pH 7.2–7.6) at 4°C, 30 min, then washed in PHEM for 30 min (gentle stirring), changing the solution every 5 min.

Samples Processes

1. Rat sciatic nerves. Epineuria from intact nerves were dissected and the extracellular matrix was unstructured by collagenase digestion with Collagenase XII (Sigma), 0.3 mg/ml dissolved in PHM (25-mM HEPES, 60-mM PIPES, 2-mM $MgCl_2$, pH 7.2–7.6) with 5-mM $CaCl_2$ final concentration, 1 h, at 37°C. The enzymatic activity was stopped by cold washing in buffer PHEM (3 × 10 min). After collagenase digestion, rat sciatic nerves were placed on a cold slide and were mechanically teased under stereoscopic microscope using blunt needles to prevent fibers from tearing. Successive treatments were performed in floating fibers.
2. Mice sciatic nerves. Sciatic nerves were cryoprotected with successive passages in solutions of increasing concentrations of sucrose-to-sucrose rising 30%, dissolved in PHEM buffer, at 4°C with stirring, to complete imbibition of sucrose. The samples were then quickly frozen and cryosectioned at 20°C.

Staining with Phalloidin Probe

Cell membranes were permeabilized once with 0.1% Triton X-100 in PHEM, 30 min with stirring at room temperature (RT). Excess detergent was removed by successive washes in buffer PHEM (3 × 5 min). In the procedures that follow no detergent was used. Fibers were blocked using 5% goat normal serum dissolved in incubation buffer (IB, 0.15-mM glycine, 1% Bovine Serum Albumin in PHEM), 30 min at 37°C. After that, the tissue was immediately incubated with Alexa 546-phalloidin (working dilution 1/150, Invitrogen) 1 h at RT in IB, and washed 6 × 5 min, at RT with IB. The material was mounted with Prolong Gold Antifade (Invitrogen).

Microscopy and Image Analysis

Teased rat sciatic nerve and mouse sciatic nerve cryosections were imaged in an Olympus FV300 confocal microscope. In every case, all the microscope and software settings (laser intensity, high voltage photomultiplier, image depth) were the same for imaging comparing samples. Fluorescence intensity quantification was assessed

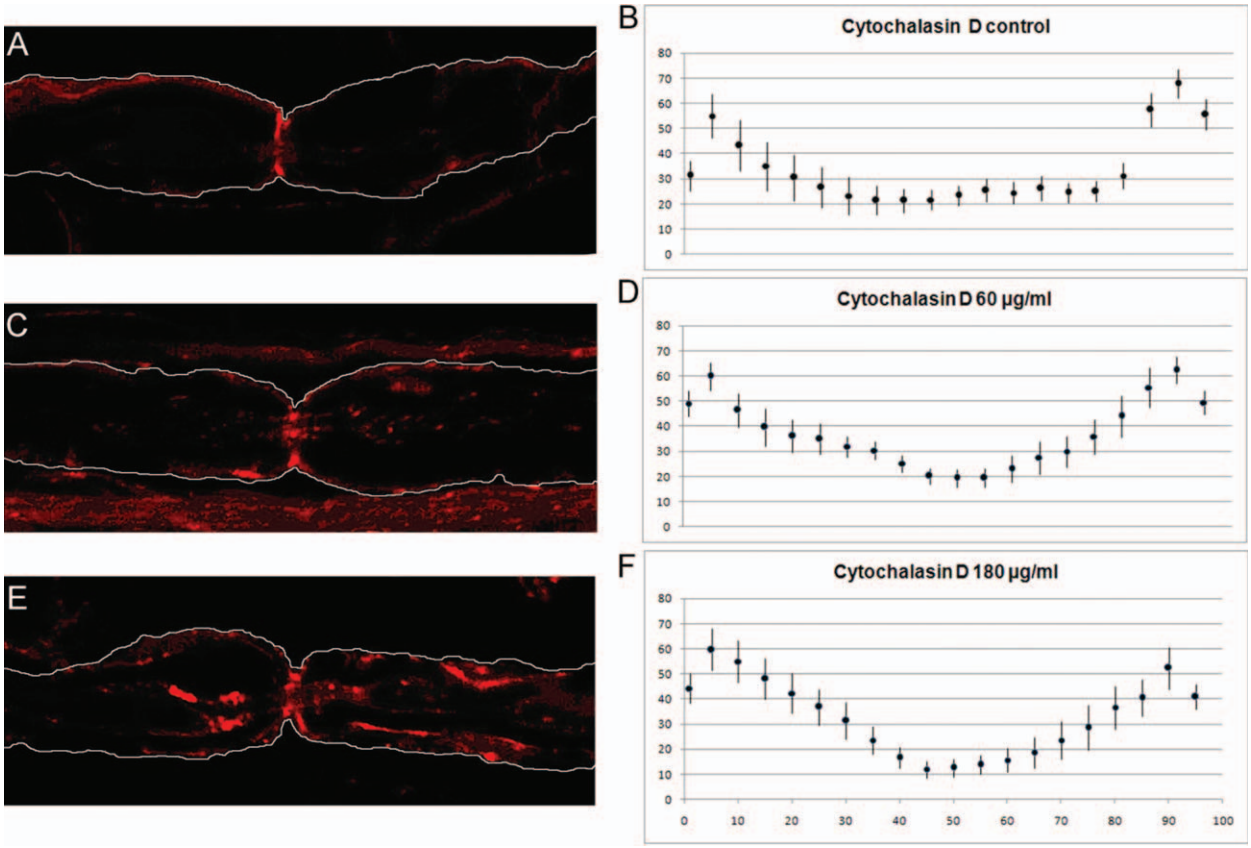

Fig. 8. Cytochalasin-D treatment of rat sciatic nerve fibers do not affect F-actin fluorescence intensity distribution in NR. A, **C**, and **E**: single confocal planes of rat sciatic nerve teased fibers, showing F-actin fluorescence (Alexa-546 Phalloidin). Fibers were incubated in absence (**A**) or in presence of 60 µg/ml (**C**) and 180 µg/ml (**E**) of cytochalasin D for 6 h. External border of Schwann cells are indicated by white lines. **B**, **D**, **F**: graphic representation of F-Actin fluorescence quantification across NR of at least 10 fibers. Lines crossing each node of Ranvier were divided in 100 pixels to avoid variations in nerve fiber width. Cytochalasin D concentration used in each experiment is indicated above graphics. *X*-axis: pixels; *Y*-axis: fluorescence intensity average. Standard deviation is indicated. [Color figure can be viewed in the online issue which is available at wileyonlinelibrary.com]

using ImageJ and Fluoview softwares. In the case of Schmidt-Lanterman incisures (SLIs) quantification was done on 10 Z-stacks projection. Fluorescence intensity was measured throughout a line following the axonal longitudinal axis, including the complete length of the SLI.

Results

F-Actin Expression in Peripheral Neurodegenerative Disease (CMT, Trembler-J mice)

a. The Trembler-J Mice nerve fibers show different SLI size and F-actin expression. The F-actin fluorescence intensity distribution of TrJ/+ sciatic nerve fibers stained by Alexa-546 Phalloidin was compared to F-actin fluorescence intensity of sciatic nerve fibers of Wild type (Wt+/+) littermates. F-actin fluorescence intensity was measured using the same confocal conditions for both genotypes (see material and methods). The high voltage was selected to avoid saturation in TrJ/+ fiber images, but maintaining visible Wt+/+ F-actin fluorescence. The registered intensities were plotted in Fig. 1C (TrJ/+: triangles; Wt+/+: circles). F-actin fluorescence intensity in TrJ/+ Schmidt-Lanterman Incisures (SLIs) was higher than F-actin fluorescence intensity in Wt+/+ SLIs (Fig. 1C). Compact myelin domain is empty of fluorescence, (Fig. 2A, asterisk). When total F-actin fluorescence intensity was averaged for each Wt+/+ SLI the mean value was below 50 fluorescence arbitrary units (Fig. 2C, black column). On the other hand, TrJ/+ sciatic fibers show a higher F-actin fluorescence intensity average, that reaches up to 180 arbitrary units (Fig. 2C, red column). The TrJ/+ F-actin fluorescence intensity mean was 4.97 times higher than the Wt+/+ mean. Student-t test between both means was statistically significant ($P < 0.001$). Schmidt-Lanterman Incisures mean length was calculated in each genotype. This analysis yielded a statistically significant difference ($P < 0.01$) between SLI F-actin fluorescence length of TrJ/+ as compared to Wt+/+ (Fig. 2D, Table I).

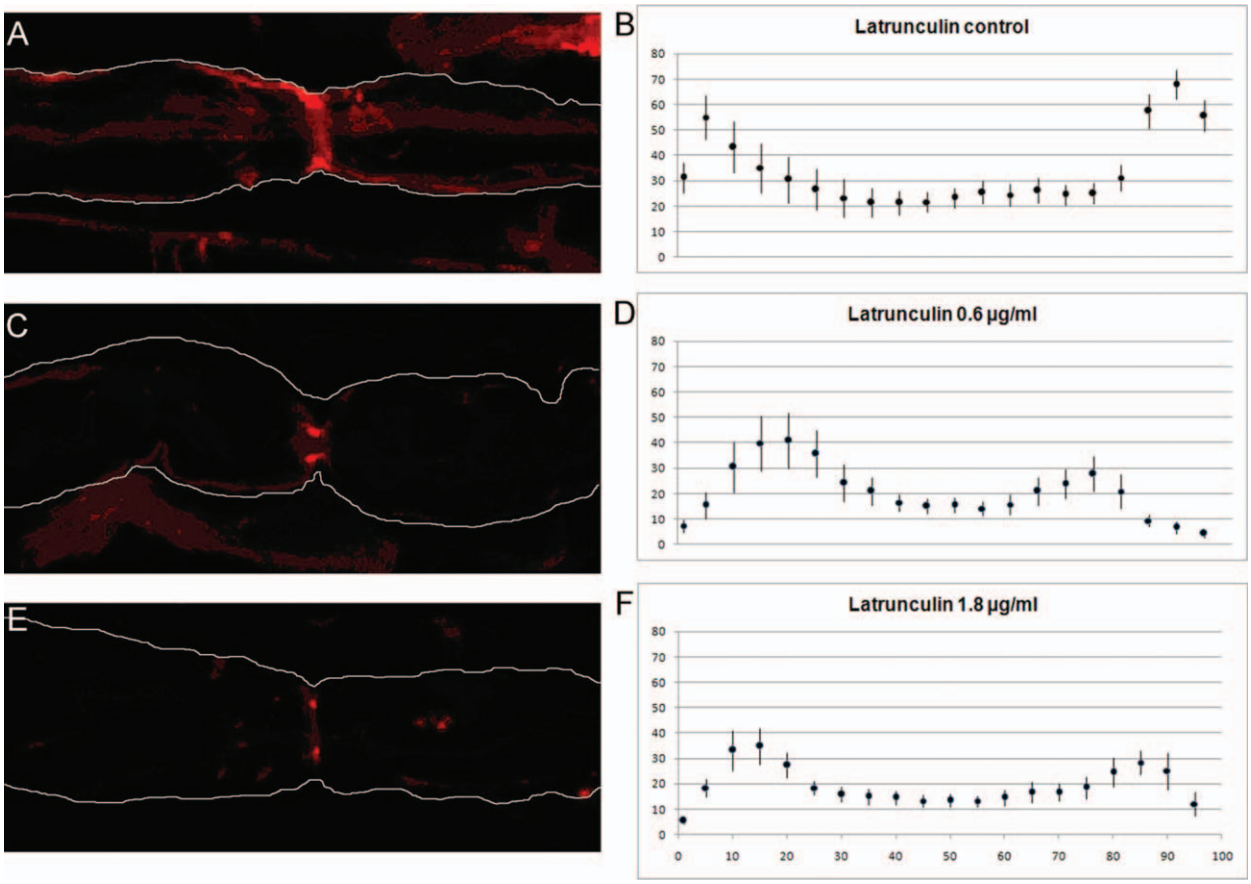

Fig. 9. Latrunculin-A treatment of rat sciatic nerves fibers. A, **C**, and **E** single confocal planes of rat sciatic nerve teased fibers showing F-actin fluorescence (Alexa-546 Phalloidin). Fibers were incubated in absence (A) or in presence of 0.6 µg/ml (C) and 1.8 µg/ml (E) of latrunculin-A for 6 h. External border of Schwann cells are indicated by white lines. **B**, **D**, and **F**, graphic representation of F-Actin fluorescence intensity is shown across NR. Lines crossing each node of Ranvier were divided in 100 pixels to avoid variations in nerve fiber width. Latrunculin-A concentration used in each experiment is indicated above graphics. *X*-axis: pixels; *Y*-axis: fluorescence intensity average. Standard deviation is indicated. [Color figure can be viewed in the online issue which is available at wileyonlinelibrary.com]

b. Trembler-J NR Regions show an increased F-actin fluorescence intensity. F-actin fluorescence intensities distribution on NR of TrJ/+ and Wt+/+ show a statistically significant difference ($P < 0.001$, Fig. 3A). When the average of nodal fluorescence intensities was compared between TrJ/+ and Wt+/+, it showed that the former has over 1.7 fold more F-actin fluorescence intensity than Wt+/+ ($P<0.001$, Fig. 3B).

F-actin Fluorescence Intensity During Early Nerve Regeneration

a. Nodes of Ranvier and Schmidt-Lanterman Incisure Domains. Actin cytoskeleton structure was also evaluated in normal and regenerating rat sciatic nerve fibers. F-actin in normal fibers is distributed in outer Schwann cell cytoplasm, Schmidt-Lanterman Incisures, inner Schwann cell cytoplasm/subcortical axonal region and is enriched in paranodal and nodal regions of SCs, corresponding to paranodal loops and microvilli structures (Figs. 4–7).

After nerve transection, the processes of regeneration start in the proximal stump, while distal stump degenerates [Cajal, 1923]. These regeneration/degeneration events have an intense action domain in the boundary near the transected zone. When actin cytoskeleton is analyzed in this region, the intensity and distribution of F-actin show two gradients going from the proximal stump to the neuronal cell body: (1) a decreasing gradient of F-actin fluorescence intensity, and (2) an increasing gradient of organization of structured F-actin fiber domains (Fig. 4A and B). Nodal and SLI domains could not be clearly detected in the proximal stump region (Fig. 4A). However, a short distance upstream, in the direction of the neuronal cell body, these glial domains begin to restore their normal organization (Fig. 4B). We analyzed F-actin fluorescence distribution and arrangement in a region about 100-μm upstream from the proximal stump. The normal F-actin distribution is not significantly changed in early regeneration fibers 18 h after injury, even at SLIs

($P < 0.15$, Figs. 5 and 6) or NR ($P < 0.2$, Fig. 7) at this region.

b. F-Actin Disruption in Regenerating Fibers. Actin cytoskeleton stability in regenerating PNS fibers was assessed by Cytochalasin-D and Latrunculin-A treatment at different concentrations over 6 h. Cytochalasin-D treatment alters the actin cytoskeleton. The continuity of phalloidin label in the outer Schwann cell cytoplasm and inner Schwann cell cytoplasm/subcortical axonal actin cytoskeleton is disrupted as Cytochalasin-D concentration increases. However, there are regions where F-actin remains polymerized even with a high concentration of Cytochalasin-D, when treated fibers are compared to control nerves (Figs. 8A, 8C, and 8E). Surprisingly, paranodal and nodal F-actin cytoskeleton of SCs are completely resistant to Cytochalasin-D. The distribution and amount of F-actin fluorescence in this region are unaltered despite Cytochalasin-D treatment (Figs. 8B, 8D, and 8F). As shown in Fig. 9, Latrunculin-A has a strong effect in altering the distribution of F-actin in rat sciatic nerve fibers. Outer Schwann cell cytoplasm and inner Schwann cell cytoplasm/subcortical axonal actin cytoskeleton disappears as Latrunculin-A concentration increases (Figs. 9A, 9C, and 9E). Paranodal and nodal F-actin cytoskeleton of SCs are also disrupted by Latrunculin-A. However, there is a portion of F-actin in the nodal region that is resistant to Latrunculin-A treatment. Distribution and amount of F-actin in the microvilli region close to Schwann cell/axon boundary remains constant in spite Latrunculin-A treatment, compared to control experiments (Figs. 9B, 9D, and 9F). Concentrations of Latrunculin-A higher than 1.8 μg/ml, did not reduce the F-actin ring at the node of Ranvier (data not shown).

Discussion

The F-actin cytoskeleton is localized at the cortical axoplasm in peripheral nerve fibers [Kalil et al., 2011]. In SCs, the cytoplasm contains a filamentous actin meshwork that provides structural plasticity, and motility. This meshwork is in close association with cell membrane [Cingolani and Goda, 2008]. The close relationship between SC and the axon generates structures and functions in common, frequently related to the F-actin cortical cytoskeleton. The nodal regions have been identified as the initial organizer of this "bi-cellular" organization [Salzer, 2003, 2008]. The SC cytoplasmic region, free of compact myelin (nodal microvillis, paranodal loops, SLI) seems to have the cytoskeleton for intracellular transport (i.e., actin, tubulin and associated molecular motors) [Ghabriel and Allt, 1979a,b, 1980a,b, 1981, 1987; Hall and Williams, 1970]. Cytoskeletal homeostasis may be altered in pathological regeneration/degeneration conditions.

Trembler-J mouse suffers a hereditary, chronic, and progressive disease. The alteration [also described in a human CMT family by Valentij et al., 1992], is a punctual mutation in *pmp22* gene that prevents the normal insertion of PMP-22 protein into myelin [Suter, 1992]. Trembler-J nerve fibers have diminished myelin sheaths and fiber diameters [Sereda and Nave, 2006]. PMP-22 accumulates in cytoplasmic aggregates with other proteins in lysosomal and endosomal vesicles [Suter and Snipes, 1995a,b]. We have recently communicated that this protein is also present in Schwann cell nuclei; the signals are granular, similar to those described as cytoplasmic aggresomes-like in SC cytoplasm [Kun et al., 2011]. The presence of aggresomes has been found in association with the redistribution of cytoskeletal components. Intermediate filaments play a key role in forming a condensed cage surrounding pericentriolar aggregates of ubiquitinated proteins [Notterpek et al., 1999]. On the other hand, our findings of increased increments of F-actin at Schmidt Lanterman Incisures (5 fold higher in TrJ/+ compared to Wt+/+), as well as in NR (1.7-fold higher in TrJ/+, compared to Wt+/+, Fig. 3), have not been described until now. Excluding the compact myelin domains, NR and SLI are the most extensive cytoplasmic Schwann cell to axon contact, with a specific role in fiber maintenance. Why do these particular regions increase F-actin under chronic pathological regeneration/degeneration like CMT1A conditions? SLI have been described as a SC shortcut to myelin maintenance [Hiscoe, 1947; Robertson, 1958; Ghabriel, et al., 1979a,b, 1980a,b, 1981, 1987; MacKenzie et al., 1984]. Might it mean that the structure of this region must be preserved for its important functional value? The voltage-dependent sodium channels (Nav) are concentrated at Ranvier's nodes, anchored to the actin cytoskeleton by specific forms of ankyrin-G and spectrin IV.

Recently, we have characterized the molecular expression of actin, tubulin, vimentin, MAG, nucleic acid, ribosomes, and multivesicular bodies in SLI [Kun et al., 2011], and local expression of heavy neurofilament subunit RNA in SLI under normal and pathological conditions (manuscript in redaction). Thus, SLIs seem to be prepared not only for local traffic, but also for communication between Schwann cell domains. Other possible roles related to axon-glia homeostasis and axonal maintenance has also been proposed [Sotelo-Silveira et al., 2006; Kun et al., 2007; Court et al., 2008]. However, under chronic pathological conditions, these functions would be permanently active, but never reach "normal" equilibrium operating levels. The surprisingly high level of F-actin in SLIs and increased level in nodal areas, in TrJ/+ fibers may be a protective mechanism, ensuring the permanence of a structural domain essential not only for SCs, but also for axonal maintenance and survival.

During early regeneration, these functions are activated as a physiological repair mechanism. Thus, the normal fiber structure is restored by the normal physiological mechanisms. F-actin fluorescence intensity in both SLI and NR were not significantly different between normal and regenerating fibers (Figs. 5–7). That may mean that this process differs from those occurring under neurodegenerative conditions. They are repair processes that are included in the genetic information of normal animals.

We used both Latrunculin-A and Cytochalasin-D to disrupt the F-actin cytoskeleton. However, the underlying mechanism of each drug is different. Latrunculin-A associates with actin monomers and modifies the kinetics of actin-filament polymerization at both the barbed and pointed ends [Morton et al., 2000]. During Latrunculin-A treatment, the actin cytoskeleton disappears proportionally as Latrunculin-A concentration increases. However, at the node of Ranvier, there is an F-actin rich domain that continually shows F-actin signals regardless of the Latrunculin-A concentration used. This F-actin rich domain is located at the Schwann cell microvilli level, but could also correspond to the subaxolemal region, since it is not possible to determine the exact boundary between Schwann cell and axon at the optical level. Moreover, this F-actin rich region is not the entire F-actin ring observed in NR of control rats, but it is in the proximity of the Schwann cell-axon boundary. Despite this, it must be considered that the region could have other associated proteins that may promote actin polymerization, such as profilin [Yarmola et al., 2000; Hertzog et al., 2002; Kudryashov et al., 2010].

Cytochalasin-D binds to plus ends of growing F-actin filaments, blocking the incorporation of new actin monomers. During regeneration, the inhibitory effect of Cytochalasin-D was evident at the central axoplasmic domain, where the incorporation of actin monomers clearly diminishes with the drug concentration increment. Nevertheless, F-actin at perimembranous axonal and Schwann cell domains seems to be unaltered or even increased (Fig. 8). The turnover of actin monomers would therefore seem to be stopped or slowed at this region. The valuable nodal structure (microfilament organization at the nodal microvillis and external perinodal F-actin SC domains) seems to be protected against Cytochalasin-D inhibition.

In hereditary peripheral neurodegenerative pathologies (CMTs in humans; Trembler-J in mice) the "normal" equilibrium between degeneration and regeneration would never be attained, because reparation mechanisms and the degenerative process should always be simultaneously active.

Conclusions

1. F-actin levels are increased 5-fold in SLI and 1.7-fold in Nodes of Ranvier TrJ/+ murine sciatic nerve fibers compared to Wt+/+.
2. F-actin levels are not increased at the SLI or in the NR during regeneration (if the region considered is situated at 100-μm upstream to the proximal stump).
3. Latrunculin-A inhibits microfilament polymerization at the nodal domains, on the SC side and in most of the axoplasm, but a ring of F-actin always remains.
4. Cytochalasin-D inhibits microfilament polymerization at the central axoplasmic domain, but has no effect at the perimembranous SC-axon domain.

Acknowledgments

We thank CSIC-Facultad de Ciencias-Universidad de la República-Uruguay, FIRCA-USA, PEDECIBA-Uruguay, IIBCE-MEC-Uruguay. Also we especially thank Dr. John Mercer for his valuable reading of the manuscript.

References

Berger BL, Gupta R. 2006. Demyelination secondary to chronic nerve compression injury alters Schmidt Lanterman incisures. J Anat 209(1):111–118.

Blakemore WF. 1969. Schmidt-Lanterman incisures in the central nervous system. J Ultrastruc Res 29(5):496–498.

Cajal SRY. 1928. Degeneration and regeneration of the nervous system. Vol. I and II. London: Oxford University Press.

Cingolani LA, Goda Y. 2008. Differential involvement of β3-integrin in pre- and postsynaptic forms of adaptation to chronic activity deprivation. Neuron Glia Biol 4(3):179–187.

Court FA, Hendriks WT, MacGillavry HD, Alvarez J, van Minnen J. 2008. Schwann cell to axon transfer of ribosomes: toward a novel understanding of the role of glia in the nervous system. J Neurosci 28(43):11024–11029.

Erb M, Flueck B, Kern F, Erne B, Steck AJ, Schaeren-Wiemers N. 2006. Unraveling the differential expression of the two isoforms of myelin-associated glycoprotein in a mouse expressing GFP-tagged S-MAG specifically regulated and targeted into the different myelin compartments. Mol Cell Neurosci 31(4):613–627.

Ghabriel MN, Allt G. 1979a. The role of Schmidt-Lanterman incisures in Wallerian degeneration. II. An electron microscopic study. Acta Neuropathol 48(2):95–103.

Ghabriel MN, Allt G. 1979b. The role of Schmidt-Lanterman incisures in Wallerian degeneration. I. A quantitative teased fiber study. Acta Neuropathol 48:83–93.

Ghabriel MN, Allt G. 1980a. Schmidt-Lanterman incisures. II. A light and electron microscope study of remyelinating peripheral nerve fibers. Acta Neuropathol 52(2):97–104.

Ghabriel MN, Allt G. 1981. Incisures of Schmidt-Lanterman. Prog Neurobiol. 7(1–2):25–58.

Ghabriel MN, Allt G. 1987. Incisures of Schmidt-Lanterman. Prog Neurobiol 17:25–58.

Ghabriel MN, Allt G. 1980b. Schmidt-Lanterman incisures I. A light an electron microscopy study of remyelinating peripheral nerve fibres. Acta Neuropathol 52:85–95.

Hall SM, Williams PL. 1971. The distribution of electron-dense tracers in peripheral nerve fibres. J Cell Sci 8(2):541–555.

Hertzog M, Yarmola EG, Didry D, Bubb MR, Carlier MF. 2002. Control of actin dynamics by proteins made of β-thymosin repeats: the actobinding family. J Biol Chem 277(17):14786–14792.

Hiscoe HB. 1947. Distribution of nodes and incisures in normal and regenerated nerve fibers. Anat Rec 99:447–475.

Kalil K, Li L, Hutchins BI. 2011. Signaling mechanisms in cortical axon growth, guidance and branching. Front Neuroanat 5:62–78.

Kitamura K, Suzuki M, Uyemura K. 1976. Purification and partial characterization of two glycoproteins in bovine peripheral nerve myelin membrane. Biochim Biophys Acta 455(3):806–816.

Krishnan N, Singer M. 1973. Penetration of peroxidase into peripheral nerve fibers. Am J Anat 136(1):1–14.

Kudryashov DS, Grintsevich EE, Rubenstein PA, Reisler E. 2010. A nucleotide state-sensing region on actin. J Biol Chem 285(33): 25591–25601.

Kun A, Otero L, Sotelo-Silveira JR, Sotelo JR. 2007. Ribosomal distributions in axons of mammalian myelinated fibers. J Neurosc 85: 2087–2098.

Kun A, Rosso G, Canclini L, Bresque M, Romeo C, Cal K, Calliari A, Hanusz A, Sotelo-Silveira JR, Sotelo JR. 2011.The Schwann cell-axon link in normal condition or neuro-degenerative diseases: an immunocytochemical approach. In: Ferdowski HD, editor. Immunocytochemistry. Rijeka, Croatia: InTech; ISBN 978-953-308-18-9 (http://www.intechweb.org).

Landon DN, Hall S. 1976. The Myelinated Nerve Fiber. In: Landon DN, editor. The Peripheral Nerve; London: Chapman and Hall. pp 1–105.

MacKenzie ML, Ghabriel MN, Allt G. 1984. Nodes of Ranvier and Schmidt-Lanterman incisures: an in vivo lanthanum tracer study. J Neurocytol 13(6):1043–1055.

Manfioletti G, Ruaro ME, Del Sal G, Philipson L, Schneider C. 1990. A growth arrest-specific (gas) gene codes for a membrane protein. Mol Cell Biol 10(6):2924–2930.

Morton WM, Ayscough KR, McLaughlin PJ. 2000 Latrunculin alters the actin-monomer subunit interface to prevent polymerization. Nat Cell Biol 2(6):376–378.

Müller HW, Suter U, Van Broeckhoven C, Hanemann CO, Nelis E, Timmerman V, Sancho S, Barrio L, Bolhuis P, Dermietzel R, Frank M, Gabreëls-Festen A, Gillen C, Haites N, Levi G, Mariman E, Martini R, Nave K, Rautenstrauss B, Schachner M, Schenone A, Schneider C, Schröder M, Willecke K. 1997. Advances in Charcot-Marie-Tooth disease research: cellular function of CMT-related proteins, transgenic animal models and pathomechanisms. Neurobiol Dis 4:206–211.

Notterpek L, Ryan MC, Tobler AR, Shooter EM. 1999. PMP22 accumulation in aggresomes: implications for CMT1A pathology. Neurobiol Dis 6(5):450–460.

Novikoff AB. 1967. Enzyme localizations with Wachstein-Meisel procedures: real or artifact. J Histochem Cytochem 15(6):353–354.

Patel I, Roa B, Welcher A, Schoener-Scott R, Trask J, Pentao L, Snipes J, Garcia A, Francke U, Shooter M, Lupski R, Suter U. 1992. The gene for the peripheral myelin protein PMP-22 is a candidate for Charcot-Marie-Tooth disease type 1A. Nat Genet 1:159–165.

Pinner B, Davison JF, Campbell JB. 1964. Phosphatase in peripheral nerves. Science 145:936–938.

Rawlins FA. 1973. A time-sequence autoradiographic study of the in vivo incorporation of (1,2–3H) cholesterol into peripheral nerve myelin. J Cell Biol 58(1):42–53.

Robertson JD. 1958. The ultrastructure of Schmidt Lanterman clefts and related shearing defects of the myelin sheath. J. Biophis Biochem Cytol 4:39–46.

Robertson JD. 1962. The unit membrane of cells and mechanisms of myelin formation. Res Publ Assoc Res Nerv Ment Dis 40:94–158.

Rosso G, Cal K, Canclini L, Damián JP, Ruiz P, Rodríguez H, Sotelo JR, Vazquez C, Kun A. 2010. Early phenotypical diagnoses in Trembler-J mice model. J Neurosci Meth 190:14–19.

Salzer Jl, Brophy PJ, Peles E. 2008. Molecular domains of myelinated axons in the peripheral nervous system. Glia 56:1532–1540.

Salzer JL. 2003. Polarized domains of myelinated axons. Neuron 40(2):297–318.

Schneider C, King RM, Philipson L. 1988. Genes specifically expressed at growth arrest of mammalian cells. Cell 54(6): 787–793.

Schober R, Itoyama Y, Sternberger NH, Trapp BD, Richardson EP, Asbury AK, Quarles RH, Webster HD. 1981. Immunocytochemical study of P0 glycoprotein, P1 and P2 basic proteins, and myelin-associated glycoprotein (MAG) in lesions of idiopathic polyneuritis. Neuropathol Appl Neurobiol 7(6):421–434.

Sereda MW, Nave KA. 2006. Animal models of Charcot-Marie-Tooth disease type 1A. Neuromolecular Med 8(1–2):205–216.

Singer M, Green MR. 1968. Autoradiographic studies of uridine incorporation in peripheral nerve of the newt, Triturus. J Morphol 124(3):321–344.

Singer M, Krishnan N, Fyfe DA. 1972. Penetration of ruthenium red into peripheral nerve fibers. Anat Rec 173(4):375–389.

Singer M, Salpeter MM. 1966. Transport of tritium-labelled l-histidine through the Schwann and myelin sheaths into the axon of peripheral nerves. Nature 210(5042):1225–1227.

Sotelo-Silveira JR, Calliari A, Kun A, Koenig E, Sotelo JR. 2006. RNA trafficking in axons. Traffic 7(5):508–515.

Spreyer P, Kuhn G, Hanemann CO, Gillen C, Schaal H, Kuhn R, Lem ke G, Müller HW. 1991. Axon-regulated expression of a Schwann cell transcript that is homologous to a 'growth arrest-specific' gene. EMBO J 10(12):3661–3668.

Suter U, Moskow JJ, Welcher AA, Snipes GJ, Kosaras B, Sidman RL, Buchberg AM, Shooter EM. 1992. A leucine-to-proline mutation in the putative first transmembrane domain of the 22-kDa peripheral myelin protein in the trembler-J mouse. Proc Natl Acad Sci 89(10):4382–4386.

Suter U, Snipes J. 1995a. Biology and genetics of hereditary motor and sensory neuropathies. Annu Rev Neurosci 18:45–75.

Suter U, Snipes J. 1995b. Peripheral myelin protein 22: facts and hypothesis. J Neurosci Res 40:145–151.

Trapp BD, McIntyre LJ, Quarles RH, Sternberger NH, Webster HD. 1979. Immunocytochemical localization of rat peripheral nervous system myelin proteins: P2 protein is not a component of all peripheral nervous system myelin sheaths. Proc Natl Acad Sci U S A 76(7):3552–3556.

Valentijn LJ, Baas F, Wolterman RA, Hoogendijk JE, van den Bosch NH, Zorn I, Gabreëls-Festen AW, de Visser M, Bolhuis PA. 1992. Identical point mutations of PMP-22 in Trembler-J mouse and Charcot-Marie-Tooth disease type 1A. Nat Genet 2:288–291.

Welcher AA, Suter U, De Leon M, Snipes GJ, Shooter EM. 1991. A myelin protein is encoded by the homologue of a growth arrest-specific gene. Proc Natl Acad Sci U S A 88(16):7195–7199.

Xu W, Manichella D, Jiang H, Vallat JM, Lilien J, Baron P, Scarlato G, Kamholz J, Shy ME. 2000. Absence of P0 leads to the deregulation of myelin gene expression and myelin morphogenesis. J Neurosci Res 60(6):714–724.

Yarmola EG, Somasundaram T, Boring TA, Spector I, Bubb MR. 2000. Actin-latrunculin A structure and function. Differential modulation of actin-binding protein function by latrunculin A. J Biol Chem 275(36):28120–28127.

Zoidl G, Blass-Kampmann S, D'Urso D, Schmalenbach C, Müller HW. 1995. Retroviral-mediated gene transfer of the peripheral myelin protein PMP22 in Schwann cells: modulation of cell growth. EMBO J 14(6):1122–1128.

11.2.2. TRABAJO VII

Sotelo, J. R., Canclini, L., Kun, A., Sotelo-Silveira, J. R., Calliari, A., Cal, K., Bresque, M., Di Paolo, A., Farias, J., Mercer, J. A. Glia to axon RNA transfer. Developmental Biology, 74 (3), 292-302, 2014. Revisión bibliográfica.

Glia to Axon RNA Transfer

José Roberto Sotelo,[1] Lucía Canclini,[1] Alejandra Kun,[1,2] José Roberto Sotelo-Silveira,[3,4] Aldo Calliari,[5] Karina Cal,[1] Mariana Bresque,[1] Andrés DiPaolo,[1] Joaquina Farias,[2] John A. Mercer[6,7]

[1] Department of Proteins and Nucleic Acids, Instituto de Investigaciones Biológicas Clemente Estable, Montevideo, Uruguay

[2] Biochemistry Section, School of Sciences, Universidad de la Republica, Montevideo, Uruguay

[3] Department of Genetics, Instituto de Investigaciones Biológicas Clemente Estable, Montevideo, Uruguay

[4] Department of Cell Biology, School of Sciences, Universidad de la Republica, Montevideo, Uruguay

[5] Department of Biochemistry, Biophysics Area, Molecular and Cell Biology, School of Veterinary, Universidad de la República, Montevideo, Uruguay

[6] Professor, McLaughlin Research Institute, Great Falls, Montana 59405-4900

[7] Cardiovascular Biology and Disease, Cardiomyopathies, Institute for Stem Cell Biology and Regenerative Medicine, National Center for Biological Sciences, Tata Institute for Fundamental Research, Bangalore 560065, India

Received 14 May 2013; revised 21 August 2013; accepted 22 August 2013

ABSTRACT: **The existence of RNA in axons has been a matter of dispute for decades. Evidence for RNA and ribosomes has now accumulated to a point at which it is difficult to question, much of the disputes turned to the origin of these axonal RNAs. In this review, we focus on studies addressing the origin of axonal RNAs and ribosomes. The neuronal soma as the source of most axonal RNAs has been demonstrated and is indisputable. However, the surrounding glial cells may be a supplemental source of axonal RNAs, a matter scarcely investigated in the literature. Here, we review the few papers that have demonstrated that glial-to-axon RNA transfer is not only feasible, but likely. We describe this process in both invertebrate axons and vertebrate axons. Schwann cell to axon ribosomes transfer was conclusively demonstrated (Court et al. [2008]: J. Neurosci 28:11024–11029; Court et al. [2011]: Glia 59:1529–1539). However, mRNA transfer still remains to be demonstrated in a conclusive way. The intercellular transport of mRNA has interesting implications, particularly with respect to the integration of glial and axonal function. This evolving field is likely to impact our understanding of the cell biology of the axon in both normal and pathological conditions. Most importantly, if the synthesis of proteins in the axon can be controlled by interacting glia, the possibilities for clinical interventions in injury and neurodegeneration are greatly increased.** © 2013 Wiley Periodicals, Inc. Develop Neurobiol 74: 292–302, 2014

Keywords: **axon, Schwann cell; RNA cell-to-cell transfer; myosin Va; ribosomes; axonal protein synthesis**

Corresponding to: J.R. Sotelo (jsotelo@iibce.edu.uy).
Contract grant sponsor: ANII.
Contract grant sponsor: PEDECIBA.
Contract grant sponsor: CSIC.
Contract grant sponsor: MEyC.
Contract grant sponsor: FIRCA-NIH; contract grant number: 1 R03 TW007220-01A2.

Published online 30 August 2013 in Wiley Online Library (wileyonlinelibrary.com).
DOI 10.1002/dneu.22125

INTRODUCTION

The failure of conventional electron microscopy to consistently show the presence of ribosomes in axons led to several arguments against the idea of endogenous protein synthesis. Therefore, most investigators concentrated on axoplasmic transport as the most important mechanism for supplying proteins to the axon. A major problem is the extreme difficulty of dissecting axons from Schwann cells to reliably demonstrate that RNA obtained from axons was not the result of contamination from surrounding glia.

A small group of investigators undertook the analysis of the RNA content of axoplasm (Edstrom et al., 1962; Koenig, 1967, 1991; Steward and Ribak, 1986; Sotelo et al., 1992; Koenig and Martin, 1996; Bassell et al., 1998; Eng et al., 1999; Zhang et al., 1999; Koenig et al., 2000; Sotelo-Silveira et al., 2000, 2004, 2008; Zhang et al., 2001; Willis et al., 2005, 2007; Kun et al., 2007; Aschrafi et al., 2008; Kaplan et al., 2009; Taylor et al., 2009; Natera-Naranjo et al., 2010; Zivraj et al., 2010; Gumy et al., 2011). Recent findings using multiple methods have converged to better support the hypothesis of axonal protein synthesis (Koenig and Giuditta, 1999; Alvarez et al., 2000; Giuditta et al., 2002, 2008; Piper and Holt, 2004; Eyman et al., 2007). In addition to functions already proposed for mRNA translation in axons, including growth, maintenance, and regeneration, other functions related to presynaptic plasticity and axonal guidance have recently been proposed (Martin et al., 1997; Brittis et al., 2002; Martin, 2004; Piper and Holt, 2004; Preitner and Flanagan, 2012).

The transport of RNA from the neuronal soma to the axons has been documented in cortical dissociated neuron culture in microfluidic chambers in normal or regenerating conditions (Taylor et al., 2009), as well as in the terminal axon, showing β-catenin mRNA in recently formed boutons, where it is translated to regulate synaptic vesicle release dynamics (Taylor et al., 2013). Axonal mRNA has been found in embryonic, neonatal, and adult rat dissociated dorsal root ganglia neurons cultured in microfluidic chambers. Many axonal mRNAs encoding molecules known to be involved in axon growth and guidance were found, as well as mRNAs encoding β-tubulin, β-actin, and several proteins involved in actin dynamics (Vogelaar et al., 2009; Gumy et al., 2011). An important feature of dissociated neuron culture is that any of axonal mRNAs could only originate in the neuronal soma.

Sequences involved in targeting of mRNAs to axons have been identified. β-Actin's 3′-UTR is sufficient to cause axonal localization of a chimeric green fluorescent protein (GFP) mRNA into mouse sciatic nerve axons, whereas a γ-actin 3′-UTR had no effect. Sciatic nerve injury increased axonal accumulations of β-actin's 3′-UTR-GFP-mRNA (Willis et al., 2011). Transcription factors are translated in adult axons and retrogradely transported to the neuronal soma, apparently for transmitting information about axonal injury (Ben-Yaakov et al., 2012). We will not review these papers exhaustively, because they are covered in other articles in this same issue.

If all the components required for protein synthesis (mRNA, ribosomes, tRNA, microRNAs and associated enzymes, and factors) are present in axons, an important question needs to be addressed: might associated glia transfer RNA to axons? Considering the close proximity of Schwann cells and oligodendrocytes to axons and the distance required for transport from neuronal soma *in vivo*, it is appealing to hypothesize that this glia may provide ribosomes, mRNAs, and other translational components under at least some conditions. Recent publications have provided significant support for this hypothesis. Schwann cell-to-axon ribosome transfer has been well-documented (Court et al. 2008, 2011). However, whether mRNA is part of this transfer is still not conclusive (Sotelo et al. 2013).

CELL-TO-CELL RNA TRANSFER

Starting in the Peripheral Nervous System (PNS), cell-to-cell RNA transfer in myelinated axons was generally disregarded in the past, in spite of some interesting, decades-old observations (Singer and Green, 1968). Slowly but persistently, more data have accumulated to support the hypothesis of cell-to-cell transfer. These include transfer of RNA between cultured PC12 cells connected by nanotubes (Rustom et al., 2004), between *Drosophila* follicle cells and oocytes (Palacios, 2002), and between human and mouse mast cells (Valadi et al., 2007). Other cases of cell-to-cell transfer of organelles are better understood and accepted, including melanosomes from melanocytes to keratinocytes (Boissy, 2003) and mitochondria in a lung epithelial cell line (Spees et al., 2006).

Any technical approach to distinguishing between glial and axonal material must deal with the issue of glia-derived contamination of axoplasm. For this reason, model systems have exploited large axons, such as the 100-μm-diameter goldfish Mauthner axon, as well as the 300 to 1000-μm-diameter squid giant axon. Edward Koenig, studying extruded axoplasm from rat and rabbit axons, demonstrated synthesis of proteins that are transported in the slow axonal

transport component. Koenig and colleagues also discovered new axonal structures and termed as periaxoplasmic ribosomal plaques (PARPs; Koenig, 1991; Koenig and Martin, 1996; Koenig et al., 2000; Sotelo-Silveira et al., 2004, 2006, 2008). PARPs are embedded in an actin network containing ribosomes, mRNAs (including those encoding beta-actin and myosin-Va). Sciatic nerve PARPS contain the ZBP-1 protein, known to have a major role in mRNA transport. PARPs also contain molecular motors (myosin-Va and kinesin) (Sotelo-Silveira et al., 2004, 2008).

ZBP-1 and related proteins interact with 3′ or 5′ UTRs of mRNAs and adaptor proteins, which in turn link to motor proteins (Long et al., 1997, 2000) and target mRNAs to the place where they will be translated, but also regulate translation (Iakova et al., 2004; Spence et al., 2006). In fibroblasts, ZBP-1 protein determines the final location to which the beta-actin mRNA will be transported (Bassell et al., 1999). Following transport, mRNAs normally are unpackaged and translated. It seems likely that these proteins would serve the same function in axons (Sotelo-Silveira et al., 2008).

The association of ZBP-1 with PARPs raises some additional questions: Are PARPs places for storing mRNAs? Are mRNAs translated at PARPs? Where are the mRNAs coming from? Are they transcribed in the neuronal soma or in Schwann cells and then transferred to axons? The axonal transport of ribosomes and mRNA from the neuronal soma to the axon has been demonstrated mainly in cultured neurons (Giuditta et al., 2008). Meanwhile, in spite of the experiments performed in invertebrate squid giant axons (Rapallino et al., 1988), the matter of glia-to-axon mRNA transfer in mammal nerves is still unsettled.

The same questions can be asked about axonal ribosomes, first described by Zelena (Zelena, 1970, 1972a,b) who found them near the dorsal root ganglia and near nodes of Ranvier of sciatic nerve fibers. The origin of axonal ribosomes was first addressed by Li et al (2005a,b). Using Transmission Electron Microscopy (TEM) of spinal cord, they found finger-like vesicles protruding from Schwann cells to axons, surrounded by double membranes. To deal with the difficulties in determining topologies from static images, they analyzed serial sections following vesicles in thousands of sections, interpreting their observations as evidence for cell-to-cell transfer. Another TEM analysis of normal rat sciatic nerve axons described protruding axonal vesicles containing ribosomes that were decorated by an anti-ribosome antibody (Kun et al., 2007). The authors avoided traditional lead citrate and uranyl acetate staining to better show the contrast of peroxidase immunoreactivity (Fig. 1). This study clearly showed ribosomal clusters in the central core of the axon, corresponding to the microtubule-rich zone. Of course, from static images, one cannot conclude that ribosomes were being transported along microtubules by axonal transport, but the data were suggestive. In the same paper, it was shown that Schwann cells had ribosome-containing vesicles that interrupted myelin sheaths and protruded into axons, suggesting that these may coincide with Schmidt–Lanterman incisures (Fig. 1). Ribosomal RNA was detected throughout compact myelin-interrupting structures by immunocytochemistry EM and Light Microscopy (LM) *in situ* hybridization.

GLIA-TO-AXON RNA TRANSFER IN INVERTEBRATES

Two groups had a long discussion in the literature over transfer between glia and the squid giant axon. The first group was led by Harold Gainer and Raymond Lasek and the second by Antonio Giuditta. The former group tested the hypothesis that axonal proteins were synthesized in the glia and transferred to the giant axon. The axoplasm was extruded and the glial sheath was labeled with [^{3}H]leucine. The empty glial tube was perfused, and they recovered radioactive proteins in the perfusion medium. They also hypothesized that the giant axon does not contain the complete protein synthesis machinery, only tRNA (Lasek et al., 1974, 1977; Gainer et al., 1977).

Giuditta's group, using the same experimental methodology (extruding axoplasm) but offering radioactive nucleosides to glia instead of leucine, recovered labeled, newly synthesized RNAs in the axon perfusion medium. They hypothesized that these RNAs are synthesized in the glial sheath surrounding the giant axon and transferred to the axon for translation (Rapallino et al., 1988; Kaplan et al., 1992; Giuditta et al., 2008) They also built a library from the giant axon containing more than 100 mRNAs and demonstrated the capability for cycloheximide-sensitive protein synthesis in isolated presynaptic terminals. The presence of ribosomes and polyribosomes in these large terminals was suggested in foci containing high phosphorous signal by electron spectroscopic phosphorous imaging (Crispino et al., 1997).

RNA TRANSFER TO VERTEBRATE AXONS

Vertebrate glia-to-axon RNA transfer was first proposed by Singer and Green based on quantitative autoradiography of distal stumps of severed sciatic nerve

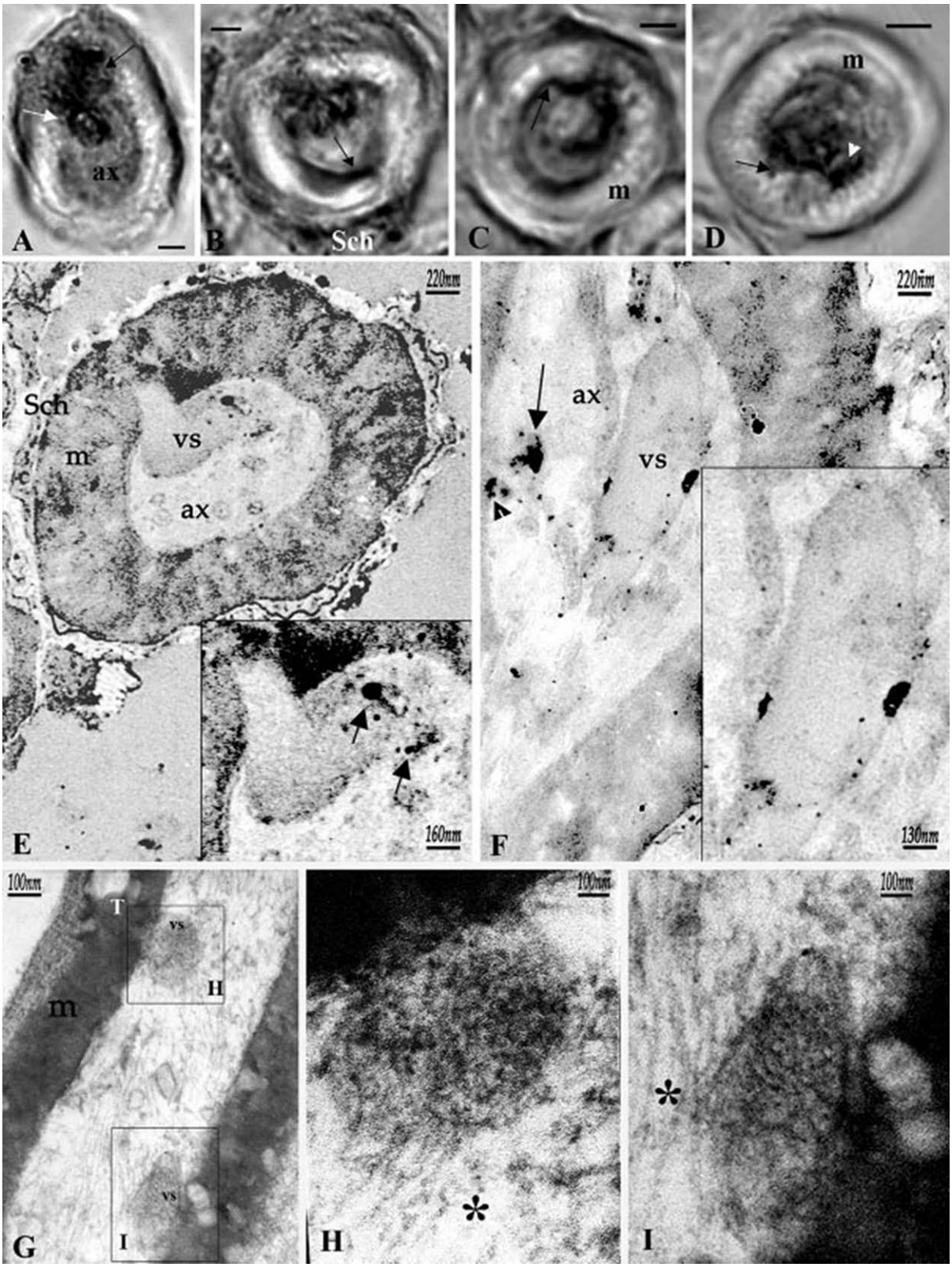

Figure 1 (See legend on following page.)

after intraperitoneal injection of ^{3}H-uridine to label newly synthesized RNA. The distribution of radioactivity revealed a gradient from Schwann cells to axons, suggesting that glial nuclei were the origin of most of these RNAs (Singer and Green, 1968). Some years later, Gambetti et al. (1973) found similar results by quantitative autoradiography of rabbit optic nerve after intraocular injection of ^{3}[H]-uridine. Schwann cell-to-axon RNA transfer was demonstrated by autoradiography in severed rat sciatic nerve (Benech et al., 1982). Both sciatic nerves were severed 4.5 cm away from the dorsal root ganglion. A trough sealed with silicon grease was built around the proximal stumps. Tritiated uridine in saline solution was offered to the right sciatic nerve proximal stump for 30 min, while the left control trough was filled with saline solution. Label was found over Schwann cells, myelin, and axoplasm. It is important to note that this experimental design all but eliminated the possibility that RNA could have been transcribed in the neuronal soma and conveyed to the axoplasm at the proximal stump, because it was labeled for only 30 min. At known speeds of fast axonal transport, 2.5 h would have been required for transport of any newly synthesized RNA to the proximal stump of both nerves (right and left) from the neuronal soma. The control contralateral proximal stump (left nerve) had no label. Furthermore, the upstream nerve segment (in the neuronal soma direction, separated 1 cm from the right sciatic-labeled segment), was not labeled. The authors concluded that RNA was transcribed in the Schwann cell and transferred to the axon. Using this methodology, it was not possible to identify which kinds of RNA were labeled. In the section below, we review three recent papers demonstrating RNA Schwann cell-to-axon transfer in detail.

WALLERIAN DEGENERATION SLOW MUTANT MICE AS A MODEL FOR SCHWANN CELL-TO-AXON TRANSFER OF RNA

The *Wld*^{s} allele is a spontaneous autosomal-dominant mutation in which a rearrangement in mouse

Figure 1 Ribosome immunocytochemistry of myelinated fiber sections. (A–D) Cryosections of sciatic nerve fibers (5–10-μm thick) were incubated with the ribosome polyclonal antibody (anti-rib) and developed using the HRP-DAB system. Immunoreactivity was observed in perimyelin regions of Schwann cell cytoplasm (B, Sch) and periaxoplasmic domains (B–D, black arrows). Immunoreactivity also was present within the axonal core (D, white arrow head). Occasionally, novel structures that originated in the myelin sheath and that protruded into periaxonal space had immunoreactivity associated with the protruding tip (A, white arrow), bridging myelin, and axonal structures. ax, axoplasm; m, myelin. Optical magnification 100X. Scale bar 2.5 μm. (E,F) Immunoelectron microscopy of ribosomes in myelinated fibers in absence of EM uranyl counterstaining (only 20-s lead citrate staining). Ribosomal immunoreactivity was observed at the subcellular level in transverse sections of myelinated axons. (E) A myelinated fiber in transverse section showing a vesicular-like structure (vs), bridging the axonal core and the outer half of the myelin sheath. The contrast is sufficient to suggest that it may comprise an internal vesicular structure. Clusters of immunoprecipitates of different sizes and single reaction signals are associated with it (inset, arrow). (F) An area of axoplasm sectioned diagonally contains immunoprecipitates of varying sizes (arrow and arrow head). A large inclusion vesicular structure (vs) is present in the axon, which is distinguishable from surrounding axoplasm, despite the low contrast due to the absence of osmium tetroxide and uranyl acetate staining. This structure contains clusters of immunoprecipitates localized along its periphery. (G) Immunoelectron microscopy of myelinated fibers using conventional EM counterstaining (uranyl acetate þ lead citrate). Myelinated fiber longitudinally sectioned showing vesicle-like structures (vs) protruding from myelin into the axon. The two vesicle-like structures are seen in opposite sites of the axon. The protruding vesicles contain ribosomal immunoreactivity and apparent RiboNucleoProteins (RNP). The connection of the vesicles with myelin shows what seems to be a tubular structure (white T) bridging the Schmidt–Lanterman cleft. The normal compact myelin structure (membrane layers) is disrupted (T). [H (inset)] Enlargement of the left protruding vesicle-like structure (vs). The content is clearly immunostained. Around the vesicle can be seen immunostained ribosomes in the axoplasm. Axoplasmic fibers were observed (H, asterisk) in conjunction with the vesicle-like structure. [H (inset)] Left vesicle-like structure. In (I) (right vesicle-like structure), the same content as the left vesicle-like structure can be seen. The enhanced contrast used for these two micrographs make less evident the tubular structures (white T) described in (G). (Reproduced with permission from Kun et al. J Neurosci Res 2007 85:2087–2098, © Wiley.)

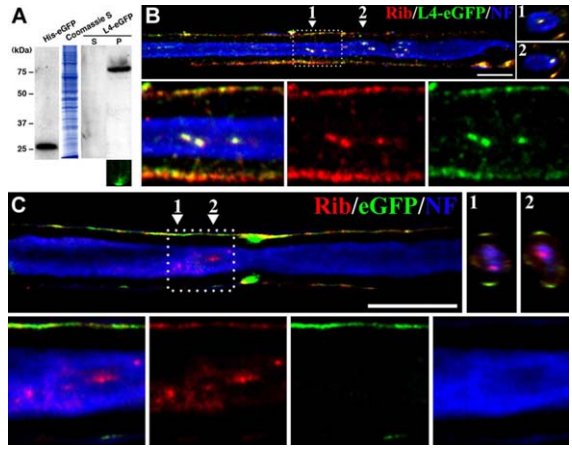

Figure 2 Transfer of ribosomes from Schwann cell to axon. *A*, Western blot showing incorporation of the L4-eGFP fusion protein into ribosomes. HEK cells were infected with LV-L4-eGFP, fractionated, after which the blot was stained with anti-eGFP. First lane, Histidine-tagged eGFP; second lane, coomassie-stained supernatant of pellet fraction; third lane, supernatant of pellet fraction; fourth lane, sucrose gradient of purified ribosomal fraction. The antibody recognizes a single band that corresponds to the molecular weight of His-eGFP (first lane) and the fusion protein (fourth lane), respectively. In the supernatant (third lane), no signal is detected, indicating that the cytosol contains little if any L4-eGFP. Bottom image, the ribosomal pellet shows intense eGFP fluorescence after sucrose gradient purification. *B*, *C*, *Wld*^{s} teased fibers, 7 d after crush; the distal segment of the nerve was injected immediately after the crush with LV-L4-eGFP (*B*), or with LV-eGFP (*C*). Color codes indicate the antibodies used. *B*, Top, Triple immunostaining and Z-projections at the corresponding numbers; in the neurofilament space, puncta are seen in which ribosomal and L4-eGFP fluorescent markers colocalize. Bottom, higher magnification of boxed area shows in detail colocalization of signals in both Schwann cell cytoplasm and axoplasm (merged signals, left), ribosome signal (middle), and L4-eGFP signal (right). *C*, as in *B*, except that the encoded protein lacked the ribosomal protein L4. Ribosomal signals are present in Schwann cells and axoplasm, but eGFP is present only in the Schwann cell. These results suggest that the transfer mechanism between Schwann cells and axons is selective. Scale bars, 10 μm. (Reproduced with permission from Court et al. J Neurosci 2008, 28, 11024–11029, © Wiley). [Color figure can be viewed in the online issue, which is available at wileyonlinelibrary.com.]

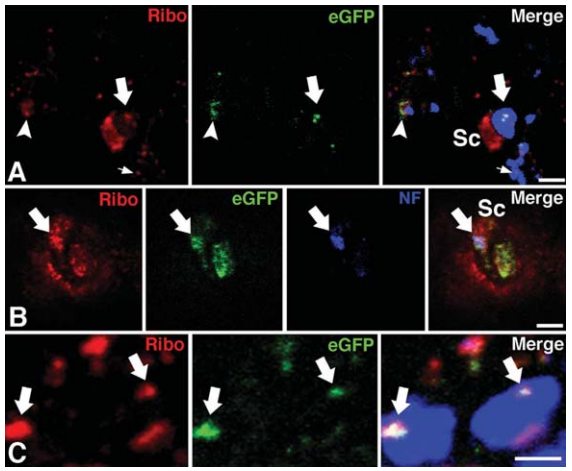

Figure 3 Schwann cells transfer L4-eGFP fluorescent ribosomes to regenerating axons. (A) 16-day graft, the arrow shows an L4-eGFP/ribosome immunopositive punctum in the axon, arrowhead shows immunoreactivity in periaxonal Schwann cell cytoplasm, but not in the axon. Small arrow points at ribosome immunoreactivity in axon that does not colocalize with L4-eGFP immunoreactivity. (B) 3-week-old graft, showing a small axon containing L4-eGFP-positive ribosomes (arrows). (C) 8-week-old graft. Arrows point to colocalized ribosome and L4-eGFP immunoreactivity in two separate and adjacent axons. Ribo, ribosome, NF, neurofilament, and eGFP, L4-eGFP immunoreactivity. Scale bars, 2 μm in (A), (B), and 5 μm in (C). (Reproduced with permission from Court et al. RNA 2011, 59, 1529–1539, © Wiley.) [Color figure can be viewed in the online issue, which is available at wileyonlinelibrary.com.]

Chromosome 4 produced a fusion protein (Coleman et al., 1998). The function of the mutant fusion protein is unknown, but its expression delays normal Wallerian degeneration for 3 weeks (Lunn et al., 1989; Mack et al., 2001). Recent studies suggest that the fusion protein protects axons by a mechanism that is still poorly understood (Araki et al., 2004; Conforti et al., 2007).

Van Minnen and colleagues used the distal portion of transected *Wld*^{s} sciatic nerves to test for cell-to-cell ribosome transfer in desomatized axons (Court et al., 2008). Enhanced GFP (eGFP)-tagged L4 ribosomal protein was expressed exclusively in Schwann cells of *Wld*^{s} mice using a lentivirus. Subsequently, eGFP fluorescence was found in the desomatized axons (Fig. 2). Furthermore, they also found that the L4-eGFP fluorescence colocalized with human anti-ribosomal antibody signal (Massardo et al., 2002). Because the desomatized axon could not obtain ribosomes from the neuronal cell body and the axoplasm does not synthesize RNA, the increase of axonal ribosomes should only be provided by Schwann cells. Consistent with this hypothesis, immunocytochemistry revealed that protrusions of Schwann cells positive for the anti-ribosome signal occasionally invaginated into the axon in internodes and paranodes.

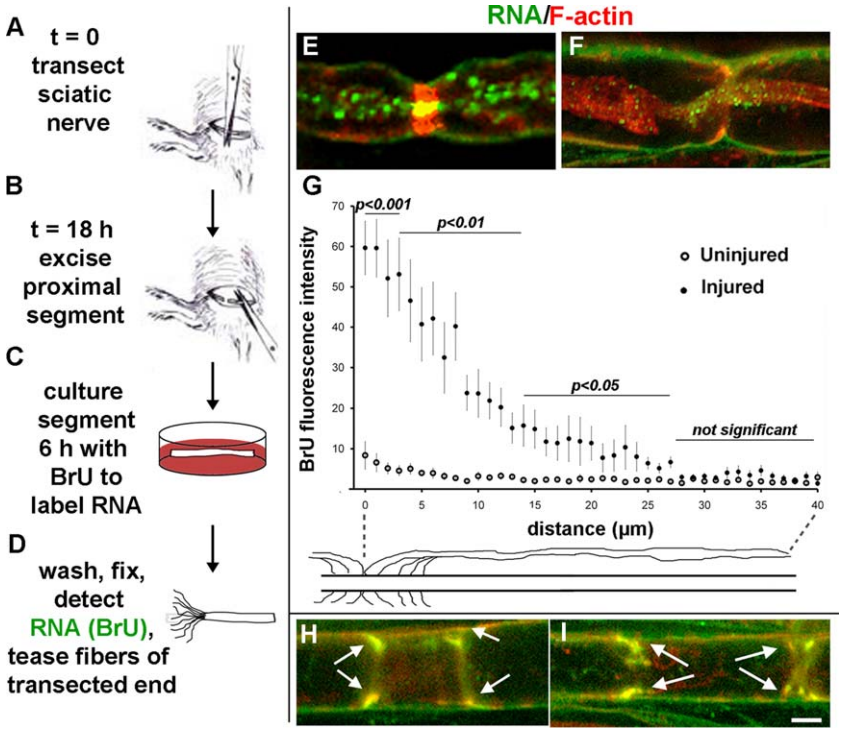

Figure 4 Newly synthesized RNA is transferred from Schwann cells to axons after sciatic nerve transection. (A–D) Experimental procedure. (E–F) Single confocal planes of fibers at nodes of Ranvier showing BrU incorporation (green) and F-actin (red). (G) Axonal BrU fluorescence intensity plotted as a function of distance from the node of Ranvier for uninjured control (open circles) and injured (closed circles) nerves. Statistical significance at each distance between injured and uninjured nerves was determined by Student's t-test. Error bars represent standard errors. (H–I) Single confocal planes showing BrU labeling (green) of F-actin-rich (red) Schmidt–Lanterman incisures (arrows). Bars = 5 μm. (Reproduced with permission from Sotelo et al. PLoS One, 2013, 8, e61905, © Wiley). [Color figure can be viewed in the online issue, which is available at wileyonlinelibrary.com.]

SCHWANN CELLS TRANSFER RIBOSOMES TO NORMAL AND REGENERATING AXONS

In 2011, the same group used the same lentivirus L4-eGFP expression strategy to study regenerating nerves of normal mice (Court et al., 2011). Two basic experiments were performed. First, cultured Schwann cells loaded with the LV-L4-eGFP were injected in the distal portion of the crushed sciatic nerves (Fig. 3). Second, decellularized nerve grafts were used to repair transected nerves. These grafts were filled with transduced Schwann cells expressing L4-eGFP tagged ribosomes. The grafts were surgically inserted between the proximal and distal stumps. In the first experiment, tagged ribosomes were found in axons of the injured nerves. In the second, regenerating axons were associated with transduced Schwann cells expressing tagged ribosomes. These Schwann cells wrapped the regenerating axons and tagged ribosomes were found in the regenerating axons (Fig. 3).

SCHWANN CELL-TO-AXON RNA TRANSFER IS DEPENDENT ON MYOSIN-VA

In our recent publication (Sotelo et al., 2013), we showed conclusively that after sciatic nerve injury, a significant amount of newly synthesized axonal RNA is transferred from Schwann cells to the axons they wrap. We also identified two necessary components of the transfer mechanism. We labeled newly synthesized RNA in sciatic nerve fragments explanted after injury with bromouridine, allowing identification with anti-BrU antibody (Fig. 4). Because this

insights into the biology of the neuron. Trends Neurosci 25:400–404.

Guescini M, Genedani S, Stocchi V, Agnati LF. 2010. Astrocytes and Glioblastoma cells release exosomes carrying mtDNA. J Neural Transm 117:1–4.

Gumy LF, Yeo GS, Tung YC, Zivraj KH, Willis D, Coppola G, Lam BY, et al. 2011. Transcriptome analysis of embryonic and adult sensory axons reveals changes in mRNA repertoire localization. RNA 17:85–98.

Iakova P, Wang GL, Timchenko L, Michalak M, Pereira-Smith OM, Smith JR, Timchenko NA. 2004. Competition of CUGBP1 and calreticulin for the regulation of p21 translation determines cell fate. Embo J 23: 406–417.

Kaplan BB, Gioio AE, Capano CP, Crispino M, Giuditta A. 1992. beta-Actin and beta-Tubulin are components of a heterogeneous mRNA population present in the squid giant axon. Mol Cell Neurosci 3:133–144.

Kaplan BB, Gioio AE, Hillefors M, Aschrafi A. 2009. Axonal protein synthesis and the regulation of local mitochondrial function. Results Probl Cell Differ 48:225–242.

Koenig E. 1967. Synthetic mechanisms in the axon. IV. In vitro incorporation of [3H]precursors into axonal protein and RNA. J Neurochem 14:437–446.

Koenig E. 1991. Evaluation of local synthesis of axonal proteins in the goldfish Mauthner cell axon and axons of dorsal and ventral roots of the rat in vitro. Mol Cell Neurosci 2:384–394.

Koenig E, Giuditta A. 1999. Protein-synthesizing machinery in the axon compartment. Neuroscience 89:5–15.

Koenig E, Martin R. 1996. Cortical plaque-like structures identify ribosome-containing domains in the Mauthner cell axon. J Neurosci 16:1400–1411.

Koenig E, Martin R, Titmus M, Sotelo-Silveira JR. 2000. Cryptic peripheral ribosomal domains distributed intermittently along mammalian myelinated axons. J Neurosci 20:8390–8400.

Kun A, Otero L, Sotelo-Silveira JR, Sotelo JR. 2007. Ribosomal distributions in axons of mammalian myelinated fibers. J Neurosci Res 85:2087–2098.

Lasek RJ, Gainer H, Barker JL. 1977. Cell-to-cell transfer of glial proteins to the squid giant axon. The glia-neuron protein transfer hypothesis. J Cell Biol 74:501–523.

Lasek RJ, Gainer H, Przybylski RJ. 1974. Transfer of newly synthesized proteins from Schwann cells to the squid giant axon. Proc Natl Acad Sci USA 71:1188–1192.

Li YC, Cheng CX, Li YN, Shimada O, Atsumi S. 2005a. Beyond the initial axon segment of the spinal motor axon: Fasciculated microtubules and polyribosomal clusters. J Anat 206:535–542.

Li YC, Li YN, Cheng CX, Sakamoto H, Kawate T, Shimada O, Atsumi S. 2005b. Subsurface cisterna-lined axonal invaginations and double-walled vesicles at the axonal-myelin sheath interface. Neurosci Res 53:298–303.

Long RM, Gu W, Lorimer E, Singer RH, Chartrand P. 2000. She2p is a novel RNA-binding protein that recruits the Myo4p-She3p complex to ASH1 mRNA. Embo J 19: 6592–6601.

Long RM, Singer RH, Meng X, Gonzalez I, Nasmyth K, Jansen RP. 1997. Mating type switching in yeast controlled by asymmetric localization of ASH1 mRNA. Science 277:383–387.

Lunn ER, Perry VH, Brown MC, Rosen H, Gordon S. 1989. Absence of Wallerian degeneration does not Hinder regeneration in peripheral nerve. Eur J Neurosci 1:27–33.

Mack TG, Reiner M, Beirowski B, Mi W, Emanuelli M, Wagner D, Thomson D, et al. 2001. Wallerian degeneration of injured axons and synapses is delayed by a Ube4b/Nmnat chimeric gene. Nat Neurosci 4:1199–1206.

Martin KC. 2004. Local protein synthesis during axon guidance and synaptic plasticity. Curr Opin Neurobiol 14: 305–310.

Martin KC, Casadio A, Zhu H, Yaping E, Rose JC, Chen M, Bailey CH et al. 1997. Synapse-specific, long-term facilitation of aplysia sensory to motor synapses: a function for local protein synthesis in memory storage. Cell 91:927–938.

Massardo L, Burgos P, Martinez ME, Perez R, Calvo M, Barros J, Gonzalez A, et al. 2002. Antiribosomal P protein antibodies in Chilean SLE patients: No association with renal disease. Lupus 11:379–383.

Natera-Naranjo O, Aschrafi A, Gioio AE, Kaplan BB. 2010. Identification and quantitative analyses of microRNAs located in the distal axons of sympathetic neurons. RNA 16:1516–1529.

Palacios IM. 2002. RNA processing: splicing and the cytoplasmic localisation of mRNA. Curr Biol 12:R50–R52.

Piper M, Holt C. 2004. RNA translation in axons. Annu Rev Cell Dev Biol 20:505–523.

Preitner N, Flanagan JG. Axonal mRNA translation: An unexpected link to axon survival and the mitochondrion. Neuron 73:629–631.

Rapallino MV, Cupello A, Giuditta A. 1988. Axoplasmic RNA species synthesized in the isolated squid giant axon. Neurochem Res 13:625–631.

Rustom A, Saffrich R, Markovic I, Walther P, Gerdes HH. 2004. Nanotubular highways for intercellular organelle transport. Science 303:1007–1010.

Singer M, Green MR. 1968. Autoradiographic studies of uridine incorporation in peripheral nerve of the newt, Triturus. J Morphol 124:321–344.

Skog J, Wurdinger T, van Rijn S, Meijer DH, Gainche L, Sena-Esteves M, Curry WT Jr, et al. 2008. Glioblastoma microvesicles transport RNA and proteins that promote tumour growth and provide diagnostic biomarkers. Nat Cell Biol 10:1470–1476.

Sotelo-Silveira J, Crispino M, Puppo A, Sotelo JR, Koenig E. 2008. Myelinated axons contain beta-actin mRNA and ZBP-1 in periaxoplasmic ribosomal plaques and depend on cyclic AMP and F-actin integrity for in vitro translation. J Neurochem 104:545–557.

Sotelo-Silveira JR, Calliari A, Cardenas M, Koenig E, Sotelo JR. 2004. Myosin Va and kinesin II motor proteins are concentrated in ribosomal domains (periaxoplasmic

mitochondrial DNA (Guescini et al., 2010) and glioblastoma-derived exosomes are characterized by the presence of mRNA, noncoding-RNA, retrotransposon elements, and cDNA derived from oncogenic sequences (Skog et al., 2008; Balaj et al., 2011). Although an exosomal mechanism for interchange between Schwann cells and axons has not been established, several vesicles with exosomal characteristics (Li et al., 2005a,b; Kun et al., 2007; Court et al., 2011; Canclini et al, unpublished results) have been found in Schwann cells and axons in both normal and regenerating conditions.

We believe that this field holds great promise for assisting in developing treatments for nervous system injury and degeneration.

The authors of this article have no conflict of interest.

REFERENCES

Alvarez J, Giuditta A, Koenig E. 2000. Protein synthesis in axons and terminals: significance for maintenance, plasticity and regulation of phenotype. With a critique of slow transport theory. Prog Neurobiol 62:1–62.

Araki T, Sasaki Y, Milbrandt J. 2004. Increased nuclear NAD biosynthesis and SIRT1 activation prevent axonal degeneration. Science 305:1010–1013.

Aschrafi A, Schwechter AD, Mameza MG, Natera-Naranjo O, Gioio AE, Kaplan BB. 2008. MicroRNA-338 regulates local cytochrome c oxidase IV mRNA levels and oxidative phosphorylation in the axons of sympathetic neurons. J Neurosci 28:12581–12590.

Balaj L, Lessard R, Dai L, Cho YJ, Pomeroy SL, Breakefield XO, Skog J. 2011. Tumour microvesicles contain retrotransposon elements and amplified oncogene sequences. Nat Commun 2:1–19, 180.

Bassell GJ, Oleynikov Y, Singer RH. 1999. The travels of mRNAs through all cells large and small. FASEB J 13: 447–454.

Bassell GJ, Zhang H, Byrd AL, Femino AM, Singer RH, Taneja KL, Lifshitz LM, Herman IM, Kosik KS. 1998. Sorting of beta-actin mRNA and protein to neurites and growth cones in culture. J Neurosci 18:251–265.

Ben-Yaakov K, Dagan SY, Segal-Ruder Y, Shalem O, Vuppalanchi D, Willis DE, Yudin D, et al. 2012. Axonal transcription factors signal retrogradely in lesioned peripheral nerve. Embo J 31:1350–1363.

Benech C, Sotelo JR Jr, Menendez J, Correa-Luna R. 1982. Autoradiographic study of RNA and protein synthesis in sectioned peripheral nerves. Exp Neurol 76:72–82.

Boissy RE. 2003. Melanosome transfer to and translocation in the keratinocyte. Exp Dermatol 12 Suppl 2:5–12.

Brittis PA, Lu Q, Flanagan JG. 2002. Axonal protein synthesis provides a mechanism for localized regulation at an intermediate target. Cell 110:223–235.

Canclini L, Wallrabe H, Di Paolo P, Kun A, Calliari A, Sotelo-Silveira JR, Sotelo JR. 2013. Association of Myosin Va and Schwann Cells-derived RNA in mammal myelinated axons, analyzed by immunocytochemistry and confocal FRET microscopy. Methods, in press.

Carsten F, Dominik F, Wen PK, Jesa A, Sebastian T, Aiman SS, Frank K, Wiebke Móbius, Sandra Goebbels, Klaus-Armin Nave, Anja Schneider, Mikael Simons, Matthias Klugmann, Jacqueline Trotter, Eva-Maria Krámer-Albers. 2013. Neurotransmitter-Triggered Transfer of Exosomes Mediates Oligodendrocyte-Neuron Communication. PLoS Biol 11:e1001604. doi: 10.1371/journal.pbio.1001604.

Coleman MP, Conforti L, Buckmaster EA, Tarlton A, Ewing RM, Brown MC, Lyon MF, et al. 1998. An 85-kb tandem triplication in the slow Wallerian degeneration (Wlds) mouse. Proc Natl Acad Sci USA 95:9985–9990.

Conforti L, Fang G, Beirowski B, Wang MS, Sorci L, Asress S, Adalbert R, et al. 2007. NAD(+) and axon degeneration revisited: Nmnat1 cannot substitute for Wld(S) to delay Wallerian degeneration. Cell Death Differ 14:116–127.

Court FA, Hendriks WT, MacGillavry HD, Alvarez J, van Minnen J. 2008. Schwann cell to axon transfer of ribosomes: toward a novel understanding of the role of glia in the nervous system. J Neurosci 28:11024–11029.

Court FA, Midha R, Cisterna BA, Grochmal J, Shakhbazau A, Hendriks WT, Van Minnen J. 2011. Morphological evidence for a transport of ribosomes from Schwann cells to regenerating axons. Glia 59:1529–1539.

Crispino M, Kaplan BB, Martin R, Alvarez J, Chun JT, Benech JC, Giuditta A. 1997. Active polysomes are present in the large presynaptic endings of the synaptosomal fraction from squid brain. J Neurosci 17:7694–7702.

Edstrom JE, Eichner D, Edstrom A. 1962. The ribonucleic acid of axons and myelin sheaths from Mauthner neurons. Biochim Biophys Acta 61:178–184.

Eng H, Lund K, Campenot RB. 1999. Synthesis of beta-tubulin, actin, and other proteins in axons of sympathetic neurons in compartmented cultures. J Neurosci 19:1–9.

Eyman M, Cefaliello C, Ferrara E, De Stefano R, Lavina ZS, Crispino M, Squillace A, et al. 2007. Local synthesis of axonal and presynaptic RNA in squid model systems. Eur J Neurosci 25:341–350.

Gainer H, Tasaki I, Lasek RJ. 1977. Evidence for the glia-neuron protein transfer hypothesis from intracellular perfusion studies of squid giant axons. J Cell Biol 74: 524–530.

Gambetti P, Autilio-Gambetti L, Shafer B, Pfaff LD. 1973. Quantitative autoradiographic study of labeled RNA in rabbit optic nerve after intraocular injection of (3H)uridine. J Cell Biol 59:677–684.

Giuditta A, Chun JT, Eyman M, Cefaliello C, Bruno AP, Crispino M. 2008. Local gene expression in axons and nerve endings: the glia-neuron unit. Physiol Rev 88:515–555.

Giuditta A, Kaplan BB, van Minnen J, Alvarez J, Koenig E. 2002. Axonal and presynaptic protein synthesis: new

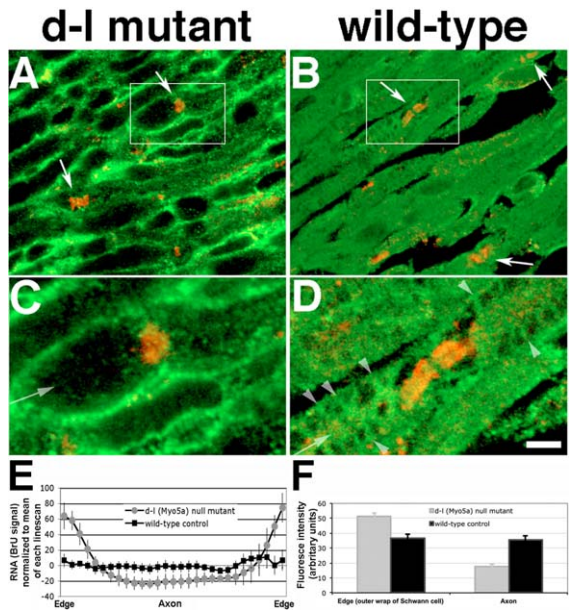

Figure 5 Myosin-Va function is required for transfer of RNA from Schwann cells to axons. Longitudinal 10-μm sections of transected sciatic nerves from null (*d-l*) Myo5a mutant mice have reduced axoplasmic levels of newly synthesized RNA. (A) and (C) null mutant; (B) and (D) wild-type control. RNA labeled by BrU is shown in green, the paranodal marker Caspr in red. Panels (C) and (D) show higher magnification views of boxed regions in panels (A) and (B), respectively. Arrows, nodes of Ranvier; arrowheads, bands of Cajal. Micrographs are single optical sections from Z-stacks imaged with a laser scanning confocal microscope. Bar = 5 μm. (E) Linescan quantitation of abundance of BrU-labeled RNA across fibers from *d-l* mutant and wild-type control mice. Edges are the outer wraps of Schwann cells; center approximates the location of the axon. Intensity measurements were normalized to the mean of each linescan. Bars represent standard deviations. (F) Absolute BrU-Ab fluorescence intensities in edges (as shown in E, 4 bins at each end combined; $n = 160$) and centers (10 central bins combined; $n = 200$). Error bars represent standard errors. (Reproduced with permission from Sotelo et al. PLoS One, 2013, 8, e61905, © Wiley.) [Color figure can be viewed in the online issue, which is available at wileyonlinelibrary.com.]

protocol separated axons from their cell bodies before exposure to BrU, it was impossible for the neuronal nucleus to be the source of any labeled RNA. BrU signal was concentrated in nodes of Ranvier and Schmidt–Lanterman incisures (Fig. 4). At lower magnification, BrU labeling shows a high concentration in axons at the transected end that decreases in the direction of the neuronal soma. RNA only partially colocalized with ribosomes detected by immunocytochemistry, suggesting that at least some RNA and ribosomes are transferred independently. Also, ribosomes may be at this place before BrU labeling, or they may be accumulated there by axonal transport, because ribosomes could be originated in the neuronal soma or in Schwann cell (Court et al., 2008). Newly synthesized BrU-RNA could be either mRNA, rRNA, tRNA, or miRNA. A mitochondrial origin of axonal BrU labeling was eliminated as BrU signal did not colocalize with mitochondria. BrU labeling in the presence of 10 mg/mL alpha-amanitin was reduced about twofold showing that a significant fraction of the signal was generated by RNA Polymerase II, suggesting that mRNA makes up a large fraction of the BrU-RNA.

Disruption of the actin cytoskeleton with latrunculin A decreased the BrU-RNA signal in the axon and prevented all accumulation at 1.8 μg/mL. Quantitative confocal FRET microscopy was used to track and determine the molecular association between newly synthesized BrU-RNA and Myosin Va. A rigorous deep analysis of FRET derived-data led us to establish that Myosin-Va interaction with BrU labeled RNA depends on what celular location we are analysing (Schwann cell cytoplasm at the Node of Ranvier, or axoplasm at the Node of Ranvier). This suggest that both molecules have different functional relationship depending on which cell location we are studying (Canclini et al., 2013). Finally, dilute-lethal *(Myo5ad-l20J/Myo5ad-l20J)* null mutant mice had detectable BrU-RNA labeling in Schwann cells but not in axons, clearly demonstrating that Schwann cell-to-axon RNA transfer is dependent on myosin-Va (Fig. 5). During the revision process of the present article, a paper was published in which the authors determined a neurotransmitter-triggered transfer of oligodendrocyte exosomes (containing RNA and proteins) into axons. This finding clearly support the results obtained about Schwann-cell-to axon RNA transfer in the PNS described in the present article (Carstein et al., 2013).

CONCLUSIONS

Any transfer of RNA and/or ribosomes between Schwann cells and axons would require the crossing of two lipid bilayers: the Schwann cell and axonal plasma membranes. Given the complex topology of myelination, the exact sequence of events will be extremely difficult to dissect. Vesicular transendocytosis and exosomes appear to be the most likely mechanisms. In the nervous system, exosomes have been documented to contain nucleic acids. Astrocyte-derived exosomes have been reported to contain

ribosomal plaques) of myelinated axons. J Neurobiol 60: 187–196.

Sotelo-Silveira JR, Calliari A, Kun A, Benech JC, Sanguinetti C, Chalar C, Sotelo JR. 2000. Neurofilament mRNAs are present and translated in the normal and severed sciatic nerve. J Neurosci Res 62:65–74.

Sotelo-Silveira JR, Calliari A, Kun A, Koenig E, Sotelo JR. 2006. RNA trafficking in axons. Traffic 7:508–515.

Sotelo JR, Benech CR, Kun A. 1992. Local radiolabeling of the 68 kDa neurofilament protein in rat sciatic nerves. Neurosci Lett 144:174–176.

Sotelo JR, Canclini L, Kun A, Sotelo-Silveira JR, Xu L, Wallrabe H, Calliari A, et al. 2013. Myosin-va-dependent cell-to-cell transfer of RNA from Schwann cells to axons. PLoS One 8:e61905.

Spees JL, Olson SD, Whitney MJ, Prockop DJ. 2006. Mitochondrial transfer between cells can rescue aerobic respiration. Proc Natl Acad Sci USA 103:1283–1288.

Spence J, Duggan BM, Eckhardt C, McClelland M, Mercola D. 2006. Messenger RNAs under differential translational control in Ki-ras-transformed cells. Mol Cancer Res 4:47–60.

Steward O, Ribak CE. 1986. Polyribosomes associated with synaptic specializations on axon initial segments: Localization of protein-synthetic machinery at inhibitory synapses. J Neurosci 6:3079–3085.

Taylor AM, Berchtold NC, Perreau VM, Tu CH, Li Jeon N, Cotman CW. 2009. Axonal mRNA in uninjured and regenerating cortical mammalian axons. J Neurosci 29: 4697–4707.

Taylor AM, Wu J, Tai HC, Schuman EM. 2013. Axonal translation of beta-catenin regulates synaptic vesicle dynamics. J Neurosci 33:5584–5589.

Valadi H, Ekstrom K, Bossios A, Sjostrand M, Lee JJ, Lotvall JO. 2007. Exosome-mediated transfer of mRNAs and microRNAs is a novel mechanism of genetic exchange between cells. Nat Cell Biol 9:654–659.

Vogelaar CF, Gervasi NM, Gumy LF, Story DJ, Raha-Chowdhury R, Leung KM, Holt CE, et al. Axonal mRNAs: Characterisation and role in the growth and regeneration of dorsal root ganglion axons and growth cones. Mol Cell Neurosci 42:102–115.

Willis D, Li KW, Zheng JQ, Chang JH, Smit A, Kelly T, Merianda TT, et al. 2005. Differential transport and local translation of cytoskeletal, injury-response, and neurodegeneration protein mRNAs in axons. J Neurosci 25:778–791.

Willis DE, van Niekerk EA, Sasaki Y, Mesngon M, Merianda TT, Williams GG, Kendall M, et al. 2007. Extracellular stimuli specifically regulate localized levels of individual neuronal mRNAs. J Cell Biol 178: 965–980.

Willis DE, Xu M, Donnelly CJ, Tep C, Kendall M, Erenstheyn M, English AW, et al. 2011. Axonal Localization of transgene mRNA in mature PNS and CNS neurons. J Neurosci 31:14481–14487.

Zelena J. 1970. Ribosome-like particles in myelinated axons of the rat. Brain Res 24:359–363.

Zelena J. 1972a. Ribosomes in myelinated axons of dorsal root ganglia. Z Zellforsch Mikrosk Anat 124:217–229.

Zelena J. 1972b. Ribosomes in the axoplasm of myelinated nerve fibres. Folia Morphol (Praha) 20:91–93.

Zhang HL, Eom T, Oleynikov Y, Shenoy SM, Liebelt DA, Dictenberg JB, Singer RH, et al. Neurotrophin-induced transport of a beta-actin mRNP complex increases beta-actin levels and stimulates growth cone motility. Neuron 31:261–275.

Zhang HL, Singer RH, Bassell GJ. 1999. Neurotrophin regulation of beta-actin mRNA and protein localization within growth cones. J Cell Biol 147:59–70.

Zivraj KH, Tung YC, Piper M, Gumy L, Fawcett JW, Yeo GS, Holt CE. 2010. Subcellular profiling reveals distinct and developmentally regulated repertoire of growth cone mRNAs. J Neurosci 30:15464–15478.

11.2.3. TRABAJO VIII

Kun A., Rosso G., Canclini L., Bresque, M., Romeo C., Cal K., Calliari, A., Hanuzs, A., Sotelo-Silveira, J.R., Sotelo J. R. The Schwann cell-axon link in normal condition or neuro-degenerative diseases: an immunocytochemical approach. Applications of immunocytochemistry, 249-266, InTech. 2012. Capítulo de libro.

12

The Schwann Cell-Axon Link in Normal Condition or Neuro-Degenerative Diseases: An Immunocytochemical Approach

Alejandra Kun[1,2] et al.[*]
Department of Proteins & Nucleic Acids,
Instituto de Investigaciones Biológicas Clemente Estable (IIBCE), Montevideo, Uruguay

1. Introduction

Peripheral nerve axons of mammals have been demonstrated to contain ribosomes (Court et al., 2008, 2011, Kun et al. 2007, Li et al. 2005a and 2005b, Sotelo et al. 1999), as well as specific mRNAs that have been shown to concentrate in specific peripheral axonal domains (Koenig & Martin 1996, Koenig et al., 2000, Sotelo-Silveira et al., 2006, 2008), the so called Periaxoplasmic-Ribosomal-Plaques (PARPs). Two possible origins have been proposed to supply mRNAs and ribosomes to axons and PARPs: a) from neuronal body axonal transport, or b) Schwann cell to axon trans-cellular transfer (Court et al. 2008, 2011, Sotelo-Silveira et al. 2006, Sotelo et al., to be published elsewhere). We showed that Schwann cell provide newly synthesized RNA (Bromouridine -BrU- labeled RNA) to the axon by a transcellular transfer process. This newly synthesized RNA was provided by Schwann cell nucleus and transported to the axon throughout Schmidt-Lanterman Incisures, and/or Nodes of Ranvier using the actin network, using molecular motors such as Myosin-Va. This was found in normal regenerating nerves disconnected from their neuronal body of origin, meaning that the only possible origin of this axonal RNA is the Schwann cell (to be published elsewhere).

The transfer of mRNAs and ribosomes from Schwann cell to the axon in normal or regenerating nerve fibers we found, make us think about which role it may play in neurodegenerative diseases. Mice models of Charcot-Marie-Tooth (CMT, Trembler-J mouse, Patel 1992, Suter 1992), as well as human nerve samples of CMT patients, were analyzed in

[*] Gonzalo Rosso[1], Lucía Canclini[1], Mariana Bresque[1], Carlos Romeo[1], Karina Cal[1], Aldo Calliari[1,3], Alicia Hanuz[1], José Roberto Sotelo-Silveira[4,5] and José Roberto Sotelo[1]
1 Department of Proteins & Nucleic Acids, Instituto de Investigaciones Biológicas Clemente Estable (IIBCE), Montevideo, Uruguay
2 Biochemical Section, School of Science, Universidad de la República (UdelaR), Montevideo, CSIC Project, UdelaR, Uruguay
3 Biophysics Area, School of Veterinary, (UdelaR), Montevideo, Uruguay
4 Cell and Molecular Biology Department, School of Sciences, (UdelaR), Montevideo, Uruguay
5 Department of Genetics, Instituto de Investigaciones Biológicas Clemente Estable (IIBCE), Montevideo, Uruguay

order to study the metabolic characteristics of this Schwann cell-axon relationship may have to the pathogenesis of this important human illness.

CMT is the most frequent genetic peripheral neuropathy (1/2500 prevalence, Berciano & Combarros, 2003, Inherited Peripheral Neuropathies Mutation Database: www.molgen.ua.ac.be/cmtmutations). This chronic progressive illness has two possible origins: axonal, CMT-II (neurofilament, KIF 1B or Rab7 protein mutations, among others), or Schwann cell, CMT-I (PMP-22, Conexin 32, P0 protein mutations, among others, Mersiyanova et al, 2000, Pérez-Ollé et al, 2002, Verhoeven et al, 2003, Zhao et al, 2001). Regardless the initial alteration, all CMT end in a functional axonopathy, which emphasize the importance of Schwann cell-axon relationship in the context of the gene expression of both cells. This local supply of transcripts may be altered in CMT, probably causing the final pathologic phenotype.

The histological analysis of CMT (I or II) patients' nerves showed the conventional myelin or axonal typical alterations (onion bulbs, axonal ovoids, internode shortening, fiber diameter variations, paranodal remyelination, etc.), plus a marked increase of axonal sprouting (myelinopathies). Molecular composition of CMT1 human patients, normal rats, PMP-22 mutant mice nerves, as well as mice organotypic dorsal root ganglia culture, was characterized here. More and more, mutant animals, transgenic animals, transfected cell culture, or cell culture obtained from any of these animal types are used to unravel the pathogenesis of important human diseases. The present paper contribute to the understanding of human Charcot-Marie-Tooth syndrome, because as we will describe below we found abnormal distribution of mutant PMP-22 transcript and protein, but also an irregular accumulation of ribosomes on altered Schwann cells and axons.

2. Schwann cell organization. Characterization of normal human and rat Schmidt Lanterman Incisures (SLI)

Whole mount of normal teased human and rat peripheral nerve fibers preparation let us know the normal interrelation between glia cell and axons in PNS. Teased fibers of Human Sural nerves and rat Sciatic nerves, (immunostained by floating), permitted to characterize the molecular expression of both nerve cells, Schwann cell and neuron (axonal domain). Internodal non-compact myelin mainly represented by Schmidt Lanterman Incisures (SLI) has been clearly characterized in this type of whole mount. Confocal single stacks show the SLI immunoreactivity with antibodies against tubulin, vimentin, Myelin Associated Glycoprotein (MAG) and ribosomes, in human sural nerve teased fibers (arrows in Figure 1, A green, B, C and F, respectively). Ribosomes are present in Schwann cell cytoplasm, Nodes of Ranvier and SLI (Figure 1, F). Nucleic acids have been also found in SLI of human fibers, identified by a fluorescent specific probe (Yoyo-1) as can be seen in Figure 1 D. Central axonal area in human longitudinal fiber appear strongly stained with anti-Neurofilament-200kDa (Figure 1, E,). Vimentin seems most evident in external Schwann cell and SLI cytoplasm (Figure 1, C). Filamentous actin, recognized by Phalloidin coupled to Alexa 546, shows a moderate signal in Schwann cell cytoplasm and axoplasm, and a more vigorous signal in SLI (Figure 1, A red). A similar signal pattern has been seen in rat sciatic teased fibers (Figure 1, J, K, L). A three dimensional reconstruction of confocal stacks series from a whole mount single fiber (rat), immunostained with anti-ribosomal antibody, let as to identify the spiral funnel-like path of

SLI. The whole reconstruction was 90º rotated to show the SLI image (Figure 1, M), enreached in ribosomes. The same SLI path image is outlined in Figure 1, N. The fine structure of myelinated sural human fibers show a well organized SLI (Figure 1 H, clear arrow). The compact myelin (Figure 1 H, white asterisk), surround the non compact myelin of SLI (Figure 1, H clear arrow). The external SLI domain is characterized by a well structured autotypical adherents type junction (Figure 1, H asterisk). Near this region, it can be seen the external mesaxón (Figure 1, H, black arrow). The external Schwann cell cytoplasm (Figure 1, H, eSc) appear clear, with evident cytoskeleton. Boxed area in H is enlarged in I. Close to the axolema, Schwann cell cytoplasm among the non compact myelin membranes of the SLI (Figure 1, I, asterisk), show the presence of a Multivesicular Body (Figure 1, I arrow). Near this region, the compact myelin, appear devoid of cytoplasm. Internodal regions constitute the largest domain of contact between the glial cell and axon. However, the molecular characterization of internodal transcellular interactions is barely known. Non-compact myelin is found in paranodal regions and Schmidt-Lanterman Incisures, which traverse diagonally compact myelin. It is postulated that, under normal conditions, the presence of cytoplasm in SLI would ensure protein turnover and vesicular trafficking (lysosomes, vesicles of endoplasmic reticulum) for the homeostasis of essential myelin and cell domains distant within the glial cell itself. These glial "shortcut" have been largely described in literature. The internodes SLI's number varies, depending on the species, axonal diameter and physiological conditions (Cajal, 1928, Ghabriel, et al., 1979a and b, 1980a and b, 1981, 1987; Hiscoe, 1947; MacKenzie et al., 1984; Robertson, 1958,). In the present work SLI have been characterized throughout the molecular expression of cytoskeleton components (actin, tubulin, vimentin) and adhesion molecules (MAG), showing that the SLI cytoplasm have well organized "roads" devoted to traffic. The presence of multi-vesicular bodies at the SLI have been seen in the past (Hall &Williams, 1970) as has been also described here, revealing an active vesicular metabolism in the cytoplasm of non compact internodal myelin. The expression of nucleic acid especially ribosomal RNA, indicate that SLI and Nodes of Ranvier have local traffic of translational machinery. Why ribosomes could be transported to these domains? One of the possible answer is the local synthesis of glial and myelin proteins. However, we noted other possible roles related to axon-glia homeostasis and axonal maintenance (Court et al., 2008; Kun et al., 2007, Sotelo-Silveira et al., 2006), which could be altered in pathological conditions. Some of our more recent results contribute to this hypothesis. Indeed, we found a SLI local expression of heavy neurofilament subunit mRNA and his final product, the corresponding protein, in normal and pathological conditions (manuscript en redaction). However it is important to highlight that trans-cellular traffic between Schwann cell and axon especially through SLI implies vesicular transport system inside SLI and a trans-endocytosis mechanism between both nerve cells. That would mean a different set of adhesion and signaling molecules in each part of this process, where MAG seems to be one of the candidates molecules involved. MAG expression is specific to myelin-forming cells in the early process of myelination. One of its functions is to promote initial interactions in the process of fastening the first layer of myelin around axons (inner mesaxon), and further development of myelin. But the level expression of MAG is relatively high, suggesting other possible roles. Among them, a particularly important role for MAG is the receptor binding axonal ligand (protein-ganglioside complex), which could activate intra-axonal signal transduction cascades necessary for the maintenance and survival of myelinated axons (Quarles, 2007).

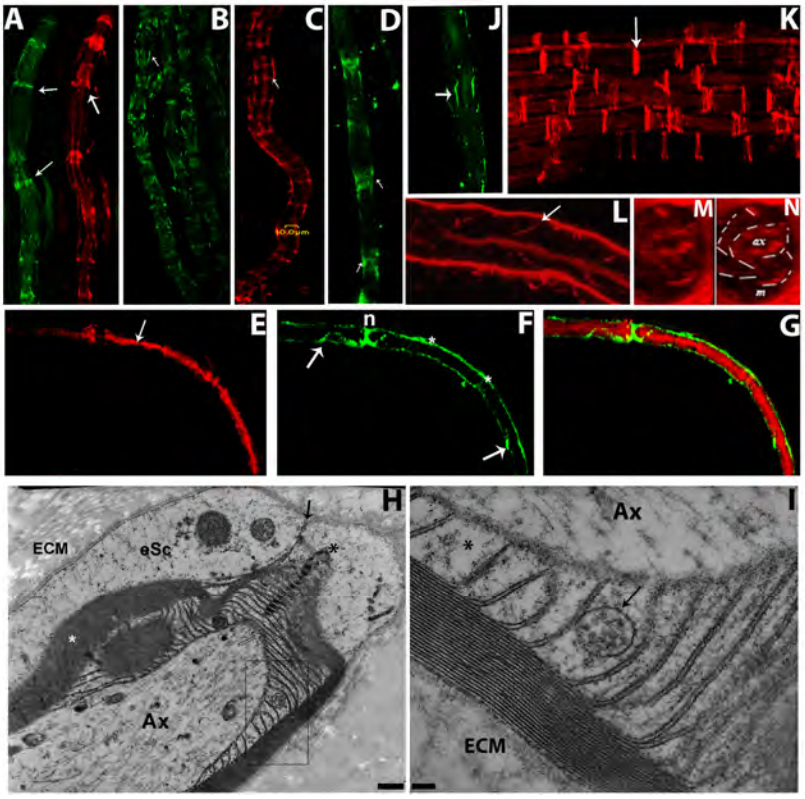

Fig. 1. Molecular characterization of normal Schmidt Lanterman Incisures (SLI) and Nodes of Ranvier (NR), in human and rat peripheral fibers.

Human SLI have been studied by immuno-confocal microscopy (A-G) and conventional electron microscopy (H and I). Human sural teased fibers were immunostained and observed by confocal microscopy. Single confocal planes show SLI (arrows) enriched in Myelin Associated Glycoprotein (A, green), Actin (A, red), Tubulin (B) Vimentin (C) and nucleic acid (D, Yoyo-1) and a few NR. Among them, the ribosomes (F, green) are present in Schwann cell cytoplasm (asterisk), in Nodes of Ranvier (F, n) and SLI (arrows). Central axonal domain appear strongly stained with anti-Neurofilament -200 kDa (E in red, arrow), merged image is shown in G showing how ribosomes are entering to the axon throughout NR (demonstraded by Z stacks analysis, not shown here) and SLI. Actin (K, in red), nucleic acids (J, YoYo-1, in green) and ribosomes (L in red) are also present in SLI of rat sciatic teased fibers. Three dimensional reconstruction of panel L, in which Z-stacks series was rotated 90º to show the SLI funnel spiral path image in M, enriched in ribosomes. The SLI path is outlined, in the same image, in N (ax, axoplasm; m, myelin). TEM, the ultrastructure of semi-longitudinal section of human sural fiber reveal a well organized SLI (H, clear arrow). In H, black asterisk shows the external part of SLI adherens junction, black arrow indicates the external mesaxon and white asterisk indicate compact myelin. The external Schwann cell cytoplasm (H, eSc) and the extra cellular matrix (H, ECM) are also indicated. Boxed area in H is enlarged in I. The presence of

Schwann cell cytoplasm among the non compact myelin membranes of the SLI (I, asterisk) might be observed, meanwhile it is completely absent in adjacent compact myelin. A Multivesicular Body (MVB) is present in the SLI cytoplasm (I, arrow). Bar in H represents 400nm, bar in I represents 100nm.

3. Schwann cell and axonal ribosomes have been identified in normal rat sciatic nerve fibers. Post-embedding immuno-gold staining

Normal rat sciatic nerve fibers have been explored to highlight the distribution of translational machinery, based on ribosomal recognition. An expected pattern of Schwann cell ribosomes (internal positive control) has been found by indirect postembedding immunogold staining (Figure 2, B), where it is possible to recognize immunocomplex in Schwann cell cytoplasm (Figure 2, B, box 8) and in myelinic region (Figure 2, B, boxes 8 and 9). Immunocomplex, recognized by gold particles are also present in the axoplasmic domains (Figure 2, A and B, box 10). Axoplasmic immunogold complexes (Figure 2, A, box 1) have a diverse distribution involving mitochondria (Figure 2, A, M) and their proximity (Figure 2, A, box 6). The immunocomplex seems to be associated to the cytoskeleton (Figure 2, A, boxes 2, 4 and 6), or in a multivesicular like-body (Figure 2, A, box 5). Axoplasmic polysomes not associated to cytoskeleton, has been found linked to immunogold particles (Figure 2, A, box 3). The samples were not osmificated previously to LRW inclusion, but exposed to osmium vapor, after immunostaining. Because that, the membranes are poorly countersained in LRW. The ultrathin sections were incubated with uranyl acetate and lead citrate as usual in Transmission Electron Microscocopy (TEM).The uranyl solution recognize the amino and phosphate groups of proteins and nucleic acid, while lead citrate is osmium-enhancing and bind to hydroxyl groups (also including phosphate groups). The absence of osmium staining before the inclusion, also result in a weak lead salt counterstaining. The Nano-gold particles have 15 nm in diameter.

TEM experimental evidences have demonstrated the presence of ribosomes in normal peripheral axons in different species including invertebrates (Kun et al., 1998 and 2007; Koenig and Martin, 1996; Zelena, 1972a, 1972b and 1970; Martin et al., 1989; Sotelo et al, 1999;). Axonal translational machinery could play an important role in structural and physiological maintenance, especially considering renewal and turn-over of proteins. Considering the Schwann cell as a positive internal control (as well as mitochondria, since the polyclonal antibody recognized also prokaryotic ribosomes), comparing their ribosome immunoreactions, axonal ribosomes appear associated to cytoskeleton in free polysomes-like complex. We have proposed that the axoplasmic ribosomes could have two possibles origins: the neuronal cell body and the neighbor Schwann cell (Kun et al. 2007; Sotelo-Silveira et al., 2006,). Peripheral normal axons run unusual long distances in cellular scale. However, its unusual geometry does not affect the homogeneity of the axoplasm. Cajal (1928), proposed that Wallerian degeneration was somehow in equilibrium with axon regeneration, and now we know that the axon is a dynamic steady state. Meanwhile, in hereditary peripheral neurodegenerative diseases (CMT, the most frequent peripheral human neuropathy), there is a chronic condition where the "normal" equilibrium is never reached. In addition, the chronic condition makes the displacement of the equilibrium always worst, because cellular repair mechanisms are insufficient to reverse the illness progress. In those conditions, the repair mechanisms are permanently activated. The resultant neuro-pathological phenotype, as occur with the normal phenotype, emerges from the integration of both Schwann cell and the axons (Aguayo et al, 1977; Salzer et al., 2008; Suter and Scherer, 2003,).

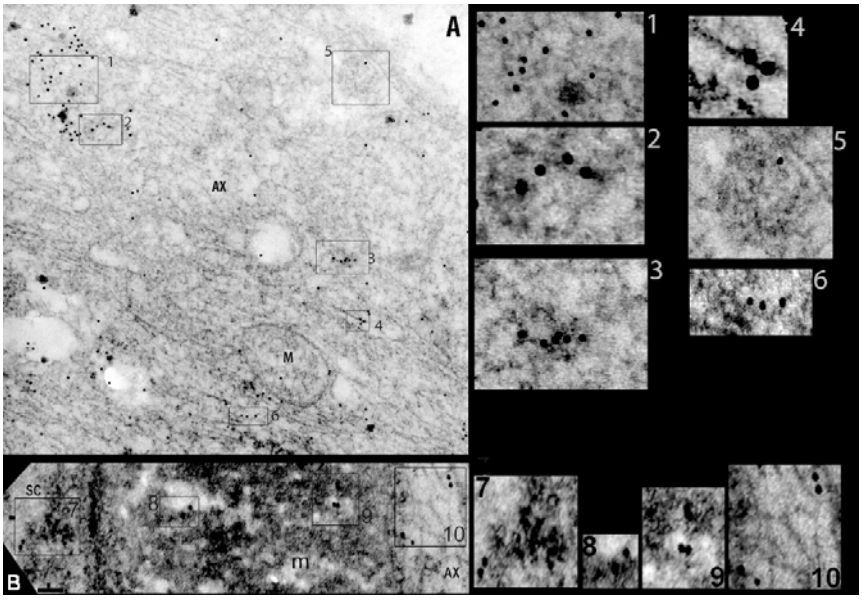

Fig. 2. TEM, normal rat sciatic nerve, postembedding ribosome immuno-gold staining.

Ultrathin transversal sections of rat sciatic nerve included in LRW hydrophilic resin was immunostained using a specific polyclonal antibody against ribosomes (raised in rabbit Kun et al. 2007), recognized in time by a goat-antirabbit gold conjugated antibody. It can be observed in A the presence of single or grouped axoplasmic immunocomplex, recognized by gold particles. The immunocomplex are framed in different boxes (boxes 1, 2, 3, 4, 5 and 6), some close to mitochondria (box 6) and within it (M, mitochondria), associated to the cytoskeleton (boxes 2, 4, 5 and 6), or in a Multivesicular like-Body (box 5). The polysomes domain are clearly decorated by immunogold particles (box 3).The boxed areas in A are enlarged in numbered boxes on the right hand (1 to 6). Different transversal fiber domains show immunogold staining (B, box 7, 8, 9 and 10). The material was included without conventional posfixation or staining in block (osmium tetroxide, uranil acetate). After imunostaining, the ultrathin sections were exposed to osmium vapors (to specially emphasize the membrane structure) and counterstained with uranyl acetate and lead citrate as usually used in TEM. The bar in A and B represent 100nm, each gold particle has 15nm in diameter. AX, axoplasm; M, mitochondria; m, myelin; SCc, Schwann cell cytoplasm.

4. Schwann cells' ribosomes are involved in axonal sprouting of human CMT-1 sural nerve fibers. Axonal sprouting is promoted by myelin compaction decrease

The presence of ribosomes has been used to recognize the Schwann cell citoplasmic domains in CMT-1 human patient whole mount of sural nerve teased fibers, immunostained by floating. A longitudinal confocal tridimensional reconstruction of one of that fibers is showed in Figure 3, A and B (original image is showed in A, but specific cellular domains have been outlined in B). Delaminated myelin (dM) let the Schwann cell

cytoplasm (Figure 3, B, SCc) expand among their de-compacted layers, that appears strongly stained with ribosomes (Figure 3 A and B, red signal). Some of the ribosomal signals are also present at the axoplamic region (Figure 3B, merged yellow, asterisks) in the main axon (Figure 3 B, mAx) and in the origin of the new-born axon-sprout 1 (Figure 3B, oS1). Next to the main axon, a bulk of ribosomes also surround axonal sprouting path (Figure 3B, R). The axonal domains are identified by phosphorylated neurofilament protein (NF-P) signal (Figure 3, green). An inhomogeneous arrangement of NF-P signal distribution (characteristic of this pathology) is showed in the main axon (Figure 3B, mAx) and in the lateral sprout axons 1 and parallel axon sprout 2 and 3 (Figure 3 B, S1, S2 and S3). A similar pattern of expression is showed in other single human CMT-1 sural teased fiber showed in Figure 3 C, D and E. A most homogeneous distribution of NF-P signal is observed in that fiber. The main axon and their sprouting, NF-P signaled (Figure 3 C, green), also expand among the delaminated myelin, highly decorated by ribosomes (Figure 3 D, red signal). It is a longitudinal image of a conventional "onion bulb" typical diagnosis image, with specific molecule expression.

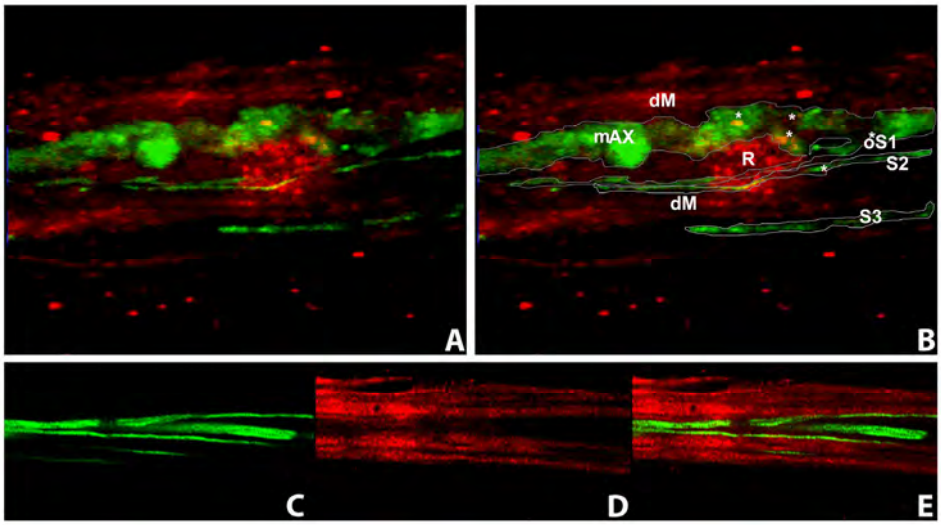

Fig. 3. Ribosomes and Phosphorylated Neurofilaments in Human CMT-1 sural teassed fiber. A. The original image is shown in A, while the specific cellular domains and components have been outlined and indicated in B. The image show a longitudinal single teased fiber from a human CMT1 sural nerve (confocal tridimensional reconstruction). The main axon (mAx) shows an inhomogeneous distribution of phosphorylated neurofilaments (green) and a lateral axoplasmic sprouting (S1) originated from the main axon (oS1). The delaminated myelin (dM) allows the Schwann cell cytoplasm (SCc) to expand among their membranes strongly inmunostained by the ribosomal antibody (red). The presence of ribosomes are also evident at the axoplasmic level (asterisks, merged color) in the main axoplasm and in the new-born axoplasm (sprouting, S1). A big conglomerate of ribosomes (R) appears close to the main axoplasm and it is crossed by the (S1). Sproutings running in parallel to the main axon can be also seen in the same image (S2, S3). A human teased sural fiber from other

CMT1 patient is showed in C, D and E. The axoplasm is also identified by the phosphorylated neurofilament (green, C) and the Schwann cell cytoplasm by the ribosomes (red, D). The image shows a longitudinal "onion bulb"-like organization (E, merged image). Also are evident the thin sprouts originated from the main axon, passing throughout the layers of delaminated myelin.

Alteration in PMP-22 represent 70% of myelinopathy (Young et al., 2003), in demyelinating human peripheral fibers, we observed axonal sprouting consequently with the lack of inhibitory effect of myelin and normal Schwann cell (Shen et al., 1998; De Bellard et al., 1996). This axonal growing is in close relation with structural and functional changes, as observed among myelin disassembly, axonal sprouting. Trembler-J mice (*Tr-J*) develop a neurodegenerative phenotype that is validated as an animal model of CMT1A (Devaux and Scherer, 2005; Sereda and Nave, 2006; Sidman et al, 1979). Gene mapping indicates that the primary defect is a mutation resulting in a leucine (16) to proline substitution in PMP-22 (Suter et al, 1992). The same amino acid substitution was found in a human family who suffered CMT1A (Valentijn et al, 1992). This substitution prevents normal protein folding, insertion into the membrane and normal myelination. Heterozygous mice (Trj/+) show a spastic paralysis and generalized tremor. While homozygous mice (TrJ/TrJ), show more severe peripheral myelin deficiency, causing death before weaning (Henry et al, 1983; Henry and Sidman, 1983; Suter et al, 1992). The main changes affecting the SNP, begins to be evident from post-natal day 20 (P20), showing a characteristic body tremor and the impossibility of abduction and extension of the hind legs (from P11), as we recently described (Rosso et al, 2010). Typically the mutation is confirmed by individual genotyping of mice (mainly by PCR-RFLP; Notterpek et al, 1997; Fortun et al, 2005; Khajavi et al, 2007, Rosso et al, 2010).

5. Schwann cell express a mutate pmp22 gen in CMT-1A animal model (Trembler mouse). Peripheral Myelin Protein-22 in vitro distribution is altered in Trembler J mice

The PMP-22 is a myelin protein whose mutation is characteristic of CMT1A human peripheral illness. Trembler J mice is an animal model to study CMT1A caused by *pmp22* mutation. The Schwann cell expression of *pmp22* (green) has been observed in normal (Figure 4, WT, A and B) and heterozygous (Figure 4, TrJ, D and E) organotypic culture of embryonic dorsal root ganglion (DRG). The wild type (WT, +/+) Schwann cell *pmp22* RNA is observed at cytoplasm and in perinuclear domains, excluding the nucleoplasm, that appear mostly empty of ISH signal (Figure 4, asterisk in A and B). The opposite is observed in Trembler J heterozygous (HZ, TrJ/+) DRG, where the *pmp22* expression is mostly concentrated into nuclear and perinuclear domains (Figure 4, asterisk in D and E). When the PMP-22 expression was analyzed in adult sciatic nerves, the immunocytochemical signal also appears concentrated in the nucleoplasm of HZ teased fibers (Figure 4F, green, asterisk). The adult WT teased sciatic fibers showed a cytoplasmic and perinuclear distribution, excluding the nucleoplasm (Figure 4C). Axoplasmic and Schwann cell domains are also counter stained with anti NF-68 antibody (blue signal) and Phalloidin-Alexa 546 (red signal) in Figure 4, C and F. In TrJ/+ mice the whole expression of *pmp22* is concentrated at Schwann cell nuclei region (Figure 4D, 4E and 4F).

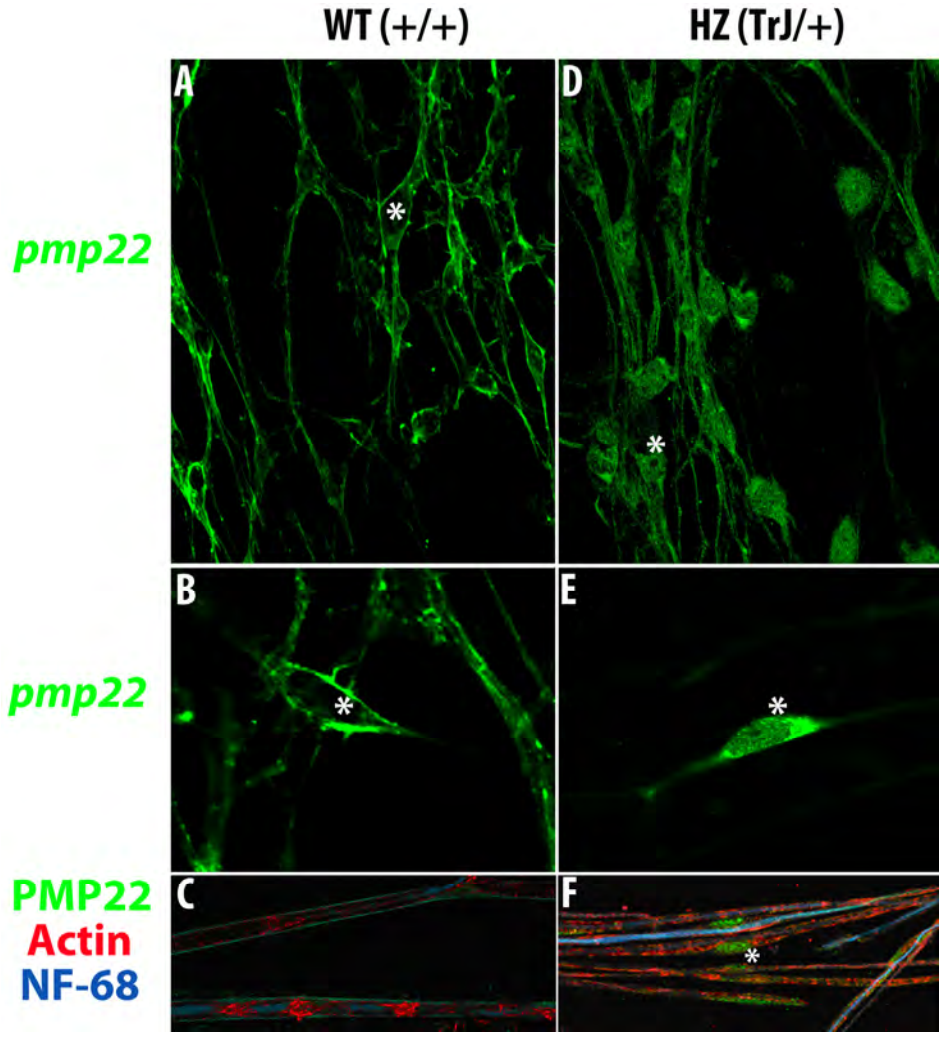

Fig. 4. Peripheral *pmp22* expression. The expression of peripheral myelin proteín 22 gene might be observed in normal (WT, +/+, A and B) and heterozygous (HZ TrJ/+, D and E) cultured E13 DRGs. In normal genotype (+/+), the Schwann cell transcript distribution show a peri-nuclear cytoplasmic arrangement, remaining the nucleoplasm almost empty of In Situ Hybridization (ISH) signal (asterisk in A and B); meanwhile in the Schwann cell from mutants (TrJ/+), the whole nuclear domain appear filled of *pmp22* ISH signal (asterisk in D and E). B and E are different regions at higher magnification. C and F show immunocytochemical recognition of proteins: PMP-22 (green), Actin (red) and Neurofilament 68kDa subunit (blue) in WT +/+ (C) and HZ TrJ/+ (F) in teased sciatic nerve fibers from adult mice. As we showed for *pmp22* transcript the mutant HZ TrJ/+ Schwann cell nuclei not only contain the RNA, but the product of its translation PMP-22 protein (F, green). The opposite occurs in WT (A, B and C).

In myelinating Schwann cells from adult Trembler-J mice, PMP-22 protein accumulates in cytoplasmic aggregates, ER-Golgi compartments and is associated with other proteins in endosomes and lysosomes suggesting high levels of protein degradation (Suter and Snipes, 1995a, 1995b). In normal Schwann cells, ~80% of the newly-synthesized PMP-22 is degraded within 30 min by the proteasome, likely due to inefficient folding (Notterpek et al 1999a; Ryan et al., 2002). The proteasome is a multi-catalytic complex involved in a variety of cellular processes, including the degradation of short-lived proteins (Goldberg, 2003). PMP-22 is a short-live molecule, that form aggregates when the proteasome is inhibited or the protein is mutated (Fortun et al., 2007). It is conceivable that the amount of PMP-22 targeted for degradation is increased in the gene duplication and point mutations disease, which could overwhelm the proteasome and lead to the accumulation of miss-folded proteins along the secretory pathway. Removal of pre-existing PMP-22 aggregates is assisted by autophagy, and chaperones/autopaghy induction can suppress accumulation of PMP-22 aggregates. The expression of *pmp22*, observed in WT (+/+) DRG cultures, occurs from early stages of culture, showing a discrete distribution in any glia cytoplasm, including perinuclear region, correlating strongly with PMP-22 expression (data not shown). Adjacent axons show the presence of phosphorylated neurofilament, typically with discontinuous distribution (data not shown). However, in HZ (TrJ/+) DRGs, the *pmp22* distribution is concentrated almost exclusively in glial nuclear and perinuclear regions, being absent from the glial myelin domains along the axon. In adults TrJ/+ fibers the nuclear and perinuclear PMP-22 expression confirm a pattern of mutated *pmp22* expression conserved from early myelination to adult stage. PMP-22 signals are granular and form a bulk of molecules, similars to those described as aggresomes. It has been described that aggresome formation is accompanied by redistribution of cytoskeleton components. Intermediate filaments, play key role forming a condense cage surrounding a pericentriolar aggregated and ubiquitinated proteins. A growing number of disease-associated proteins have been found to accumulate in aggresomes, including peripheral myelin protein 22 (PMP-22) (Notterpek et al., 1999; Ryan et al., 2002), huntingtin (Waelter et al., 2001), parkin, and alpha-synuclein (Junn et al., 2002). However, the presence of *pmp22* transcript and PMP-22 protein signals in nuclear domains during myelinogenesis and in TrJ/+ adult fibers, respectively (Fig. 4), suggest other type of alterations. Would they be, a) an altered post-transcriptional regulation, and/or b) an altered motor protein link, potentially involved in pathogenesis and illness consolidation.

6. Experimental procedures

6.1 Animal care and maintenance

Rattus norvegicus (Sprague Dawley) were obtained from the IIBCE colony. TremblerJ (B6. D2-Pmp22 <Tr-j>/J, Jackson Laboratory, USA) mice colony was started in 2008 (CSIC Grant-Universidad de la República 2005-2009). These mice carries a spontaneous mutation in Peripheral Myelin Protein-22 (PMP-22). All mice are recorded, numbered and genotyped following the method previously described (Rosso et al, 2010). Harems are formed after determining the stage of the female estral cycle. Pregnancy starts is determined by the examination of vaginal exudates and controlled by weekly weight of females. The colony, have now 100 animals, living in isolated cages, stored in isolated rooms.

All animals are maintained under controlled temperature and light cycle. Water and food are supplied *ad libitum*. The animal housing conditions are in agreement with the National

Committee for Animal Care and Maintenance (CHEA-Universidad de la República-Uruguay, *www.chea.udelar.edu.uy*)

6.2 Trembler J mice genotyping

Genomic DNA was extracted using a phenol–chloroform based method. DNA concentration was determined by spectrophotometry. PCR was performed on 200ng of DNA using specific primers (forward: 5′-GTTCCAAAGGCAAAAGATGTTC-3′; reverse: 5′-AACAATAAT CCCAAACCACACTTC-3′) that flanked the mutation site. PCR products were digested with BfaI (Fermentas) for 2h at 37 ◦C and separated by 6% polyacrylamide gel electrophoresis (PAGE). The digestion products were stained with AgNO3. The BfaI digestion of the amplified fragment from the wild-type allele produced two fragments of 221 and 500 basepairs (bp).The TrJ mutation results in a loss of the BfaI site. Consequently, the amplified fragment obtained using the TrJ allele as template was visualized as a single band of 721bp**.**

6.3 DRGs organotypic culture

Thirteen day mice embryos (E-13) were euthanized and Dorsal Root Ganglia were collected for organotypic culture in appropriated media (Neurobasal (Invitrogen) complemented by 0,20 ml/ml B27, 0,01μg/ml Nerve Growth Factor (NGF) and 2mM glutamax). The culture was done at 37ºC under 5% CO_2 controlled atmosphere. The cultured medium was changed every 48 hours. At 16 days of dorsal root ganglia culture, the culture media was complemented with 50μg/ml Ascorbic Acid, to promote *in vitro* myelination.

6.4 Fixation

Rats and mice were euthanized under pentobarbital anesthesia following the Uruguayan Committee for Ethical Animal Experimentation (CHEA in Spanish). Rats were euthanized by intracardiac perfusion of fixative (4% paraformaldehyde (PFA) for confocal microscopy and 0.25% glutaraldehyde was added for Electron Microscopy (EM) in PHEM (25mM HEPES, 10 mM EGTA, 60 mM PIPES, 2mM MgCl2 , adjusted to pH 7,2- 7,6, with KOH) after heparinization. Sciatic nerves were excised immediately after perfusion (cut in 2-mm pieces), pre-immersed in the same fixative solution for 2 hr, then washed in PHEM for 2 hr (gentle stirring), changing solution every 10 min. Mice sciatic nerves were excized and fixed by immersion in 3% PFA in PHEM, 30 minutes, at 4ºC. The samples were then washed 6X5 minutes with gentle stirring. Cultured ganglia were fixed by 10 min immersion in 2% PFA in PHEM. Throughly washed in PHEM 1 hour (6 X 10 min). The samples followed different pre-treatement before in situ molecular studies.

6.5 Human samples

Clinically diagnosed patients with a family history of polyneuropathy, presenting a chronic sensory-motor polyneuropathy were included in the present study. Electrophysiological studies were performed to confirm the nature of the demyelinating neuropathy prior to their inclusion. Alcoholics, diabetics, exposed to toxic or neurotoxic drugs and/or bearers of

systemic diseases patients were specifically excluded. Electrophysiological studies were: nerve conduction velocity analysis, electromyogram and quantification of motor units. Patients meeting the inclusion criteria have been informed of the study and samples were taken only after they signed an Informed Consent to participate in the CSIC I+D (2005-2009) Project (Grant from Universidad de la República, Uruguay). Human control was obtained from Human whole donors from the "Instituto Nacional de Donantes y Trasplantes de células, Tejidos y Organos (INDT)". Briefly, a portion of each sural nerve biopsy from human CMT patient, used for histopathological diagnosis was fixed in 3% PFA diluted in PHEM, 30 minutes at 4ºC with stirring. Fixative was washed with PHEM (6X10 minutes). When it was possible, the epineuria was removed to facilitate the ulterior treatments.

6.6 Electron Microscopy

Nerves pieces were processed for postembedding immunostaining. (Bozzola & Russel, 1998; Vazquez Nin, 2001). Briefly, nerve pieces were dehydrated increasing concentration of alcohol, until pure alcohol. Thereafter were embedded in hydrophilic resine LR-white (LRW) by increasing its concentration. When they were in pure LRW (overnight at room temperature), the blocks were polymerized, under anhydrous conditions, in two steps: 24 hs at 45ºC and 24 hours at 60ºC. Ultrathin sections (60-100 nm) were obtained by ultramicrotomy and collected in nickel grids, without film. Indirect immunostaining was followed. The grids were placed exposing the ultrathin section to different series of drops on Parafilm extended layer. The general processes are described under "*Immunostaining*". After that, sections were exposed to Osmium Tetroxide vapours and counterstained with Uranyl Acetate and Lead Citrate as usual in Transmission Electron Microscopy (TEM).

7. Immunocytochemistry

7.1 Pre treatment

7.1.1 Collagen digestion

Epineuria from intact nerve mice were dissected and the extracellular matrix was unstructured by collagenase digestion with Collagenase XII (Sigma), 0.3mg/ml dissolved in PHEM without EGTA (25mM HEPES, 60 mM PIPES, MgCl2, pH 7,2- 7,6) with 5mM CaCl2 final concentration, 1 hour, at 37ºC. The enzymatic activity was stopped by cold washing in buffer PHEM (3X10 minutes).

7.1.2 Teasing

After collagenase digestion, rat and mouse sciatic nerves were placed on a cold slide and were mechanically teased under stereoscopic microscope using blunt needles to prevent fibers tearing. Further treatments were performed over floating fibers.

7.1.3 Resin relaxing

Ultrathin LRW sections were incubated 10 minutes in sodium periodate 0.56M in water at room temperature (RT) to relaxing the resin and washed thereafter with PHEM (6X5 minutes), to remove resins.

7.1.4 Permeabilization

The permeabilization must be a single event that will balance the benefit of increased accessibility of intracellular epitopes for immunocytochemistry or ISH with the hindrance of the consequent deterioration of the structure to be recognized. Cell membranes were permeabilized once with Triton X-100 0.1% in PHEM, at variable times (10 minutes for cell cultures to 30 minutes for whole fibers and LRW ultrathin sections), stirring at RT. Excess detergent was removed by successive washes in buffer PHEM (3x5 minutes). In the procedures that follows no detergent was used. No detergent was used in human samples.

7.1.5 Aldehyde blocking

To reduce background from aldehydes and ketones free groups (generated by fixative or belonging to the cellular structure) they were blocked by incubation with sodium borohydride 0.1% in water for 10 minutes (in cell cultures) or 20 minutes (in intact nerve), at RT. The remains of borohydride are eliminated by repeated washings with buffer PHEM at RT and gentle stirring.

7.1.6 Unspecific antigen blocking

In indirect immunostaining, nonspecific antigen reactions were blocked using 5% normal serum from the animal species in which the anti antibody was raised, dissolved in incubation buffer (IB, 0.150 mM glycine, 0.1% Bovine Serum Albumin in PHEM), 30 minutes at 37°C. After that, the tissue or cells were immediately incubated with the specific antibody.

7.1.7 Immunostaining

After pre-treatment, the procedure was done basically as described by Kun et al (2007) and Sotelo et al. (1999), with some modifications. The sections were incubated 1 h at 37ºC with the specific antibodies in IB (see above) in a wet chamber. Washed 3X5 min, at 37ºC with IB and incubated over 45 minutres at 37ºC with the anti-antibodies. Fluorophores photobleaching was avoided maintaining the slices in dark. The non binding antibodies were eliminated by washing with IB (3X5 min) at 37ºC and PHEM (3X5 minutes) at RT. Slides for confocal microscopy were mounted with Prolong Gold Antifade (Invitrogen). The ultrathin sections were counter-stained as described in "*Electron Microscopy Section*".

7.1.8 Specific antibodies and fluorescent probes

The specific antibodies used in the present work, were: polyclonal anti-Ribosomes antibody (Kun et al, 2007) work dilution 1:500, monoclonal anti phosphorylated Neurofilament (Stemberger) work dilution 1:2500; monoclonal anti-Neurofilament-200 (phosphorylated and non phosphorylated) from Sigma, working dilution 1:800. Human anti-P ribosomal protein (Immunovision) working dilution 1:100, polyclonal anti-Myelin Associated Glycoprotein S/L (MAG, Chemicon) working dilution 1:150; monoclonal anti-Vimentin (Sigma) working dilution 1:400; Alexa-546 Phaloidin (Invitrogen) working dilution 1:40. YoYo-1 (Invitrogen) 1:1000; DAPI (Sigma) working dilution 1:1000.

7.1.9 Secondary-antibodies

The anti-antibodies used in the present work were: Goat anti-Mouse Alexa 488 (A11029, Invitrogen), working dilution 1:2000, Goat anti Rabbit Alexa 546 (A11030, Invitrogen), working dilution 1:2000, Goat anti-Mouse CY5 (Chemicon) working dilution 1:800; Goat anti-Rabbit 15nm gold conjugated (Aurion) working dilution 1:80.

7.2 *In situ* hybridization

The cDNA encoding mouse *pmp-22* mRNA region (425-538) was cloned in the PST-19 plasmid. The plasmid was linearized with HindIII or EcoRI and used as template by *in vitro* transcription reactions. Single-stranded RNA probes were transcribed using SP6 or T7 RNA polymerase according to manufacturer's instructions and labeled with digoxigenin-UTP (Roche). The samples were first permeabilized as indicated in "Permeabilization Section". The endogenous peroxidase was blocked with 0.03% H_2O_2 diluted in PHEM during 1 hour at RT, changing the solution every 15 minutes to refresh the offer of hydrogen peroxide. The samples were then washed with PHEM (3X5 min). The pre-hybridization condition was performed to avoid unspecific probe binding. The prehybridization and hybridization was done in the same condition: incubation with hybridization solution (10% dextran sulfate, 0.1mg/ml tRNA, 0.5mg/ml salmon sperm DNA, 50% formamide, 4XSSC) during two hours at 50ºC without probes (prehybridization) or with sense/antisense probes. Immediately before hybridization, digoxigenin labeled transcripts were denatured 3 min at 95ºC and fast returning to 4ºC thereafter; 5 min to denature the RNA, avoiding the RNA folding. The non hybridized RNA probes were eliminated by repeated washing with decreasing saline concentration (stringency increase), until 0,25X SSC. After that, the hybrid was fixed with fresh prepared 2% PFA in PHEM and gently washed with PHEM (3X5minutes). The hybrid was recognized by sheep anti-digoxigenin antibody conjugated to peroxidase. The immunocomplex were developed by the Tyramide labelling kit (Roche) giving a fluorescent complex (in 520 nm). General methods were adapted and applied to our conditions (Morel, et al. 2001 Sambrook & Russell, 2001). After that, immunostaining was applied as described in "Immunostaining".

8. Conclusions

1. Schmidt-Lanterman Incisures and Nodes of Ranvier are pathways for ribosomes and RNAs to be related to axonal function.

2. CMT human patients' nerves showed inhomogeneous neurofilament arrangements in axons. Myelin is delaminated. Big groups of ribosomes are present near the irregular newborn axonal sprouting. Ribosomes have been found also in axoplasm.

3. The presence of *pmp22* transcript and PMP-22 protein signals in nuclear domains during myelinogenesis and in TrJ/+ adult fibers described here (Fig. 4), suggest other type of alterations. They would be, a) altered post-transcriptional regulation? and/or b) altered motor protein link, both potentially involved in pathogenesis and illness consolidation.

9. Acknowledgements

CSIC-Universidad de la República, Montevideo, Uruguay, PEDECIBA, MEyC, ANII, FIRCA-NIH. The authors especially thank Dr. Timothy De Voogd (Professor at the University of Cornell, NY, USA) for his careful reading and correction of the present manuscript.

10. References

Aguayo, AJ, Atiwell, M, Trecarten, J, Perkins, S, Bray, M. 1977. Abnormal myelination in transplanted Trembler mouse Schwann cells. Nature 265: 73-75.

Berciano, J. and Combarros, O. 2003. Hereditary Neuropathies. Current Opinion in Neurology, 16: 613-622.

Bozzola, JJ & Russell, LD, 1998. Electron Microscopy. Principles and techniques for Biologists, ISBN 0763701920. 2nd edition, Jones & Bartlett Publischers, Sudbury, Massachusetts.

Depillar ME, Tang S, Mukhopadhyay G, Shen YJ, Filbin MT. 1996.

Myelin-associated glycoprotein inhibits axonal regeneration from a variety of neurons via interaction with a sialoglycoprotein. Mol Cell Neurosci.;7(2):89-101.

Cajal, SRY. 1928. Degeneration and regeneration of the nervous system, volumenes I y II Oxford University Press London.

Cornbrooks CJ, Mithen F, Cochran JM, Bunge RP.1982.Factors affecting Schwann cell basal lamina formation in cultures of dorsal root ganglia from mice with muscular dystrophy. Brain Res. ;282(1):57-67.

Court FA, Hendriks WT, MacGillavry HD, Alvarez J, van Minnen J. 2008. Schwann cell to axon transfer of ribosomes: toward a novel understanding of the role of glia in the nervous system. J Neurosci.;28(43):11024-9.

Court FA, Midha R, Cisterna BA, Grochmal J, Shakhbazau A, Hendriks WT, Van Minnen J. 2011.Morphological evidence for a transport of ribosomes from Schwann cells to regenerating axons. Glia. 2011 Oct;59(10):1529-39. doi: 10.1002/glia.21196. Epub 2011 Jun 8.

Devaux J.J. & Scherer SS , 2005 .Altered Ion Channels in an Animal Model of Charcot-Marie-Tooth Disease Type IA, The Journal of Neuroscience, February 9, • 25(6):1470 – 1480.Fortun J, Li J, Go J, Fenstermaker A, Fletcher BS, Notterpek L. 2005- Impaired proteasome activity and accumulation of ubiquitinated substrates in a hereditary neuropathy model. J Neurochem. ;92:1531–1541.

Fortun J, Verrier JD, Go JC, Madorsky I, Dunn WA, Notterpek L. 2007.The formation of peripheral myelin protein 22 aggregates is hindered by the enhancement of autophagy and expression of cytoplasmic chaperones.Neurobiol Dis. ;25(2):252-65.

Ghabriel, MN and Allt G. 1987. Incisures of Schmidt-Lanterman, Progress in Neurobiology vol 17,25-58.

Ghabriel MN, Allt G. 1981. Incisures of Schmidt-Lanterman. Prog Neurobiol1,7(1-2):25-58.

Ghabriel MN, Allt G. 1980a. Schmidt-Lanterman incisures. II. A light and electron microscope study of remyelinating peripheral nerve fibres.Acta Neuropathol. 52(2):97-104.

Ghabriel, MN and Allt G. 1980b Schmidt-Lanterman incisures I. A light an electron microscopy study of remyelinating peripheral nerve fibres. Acta Neuropathol.52, 85-95.

Ghabriel MN, Allt G. 1979a. The role of Schmidt-Lanterman incisures in Wallerian degeneration. II. An electron microscopic study.Acta Neuropathol. 48(2):95-103.

Ghabriel, MN and Allt G. 1979b. The role of Schmidt-Lanterman ncisures in Wallerian degeneration. I. A quantitative teased fibre study. Acta Neuropathol. 48, 83-93.

Goldberg AL. 2003. Protein degradation and protection against misfolded or damaged proteins. Nature.;426(6968):895-9. Review.

Hall, SM & Williams, PL. 1970. Studies on the incisures of Schmidt and Lanterman. J. Cell Sci. 6, 767-791.

Inherited Peripheral Neuropathies Mutation Database, http://www.molgen.ua.ac.be/cmtmutations/

Henry, E.; Cowen, J.; Sidman, R. (1983) Comparison of Trembler and Trembler- J Phenotypes: varying severity of peripheral hypomyelination. Journal of Neuropathology and Experimental Neurology, 42, 688-706.

Henry EW, Sidman RL. 1983.The murine mutation trembler-J: proof of semidominant expression by use of the linked vestigial tail marker.J Neurogenet.;1(1):39-52.

Hiscoe, HB, 1947. Distribution of nodes and incisures in normal and regenerated nerve fibers. Anat. Rec 99, 447-475.

Junn E, Lee SS, Suhr UT, Mouradian MM. 2002. Parkin accumulation in aggresomes due to proteasome impairment.J Biol Chem 6;277(49):47870-7.

Khajavi M, Shiga K, Wiszniewski W, He F, Shaw CA, Yan J, Wensel TG, Snipes GJ, Lupski JR. 2007- Oral curcumin mitigates the clinical and neuropathologic phenotype of the Trembler-J mouse: a potential therapy for inherited neuropathy. Am J Hum Genet.;81(3):438-53.

Koenig E & Martin R. 1996. Cortical plaque-like structures identify ribosome-containing domains in the Mauthner cell axon. J Neurosci.;16(4):1400-11.

Koenig E, Martin R, Titmus M, & Sotelo-Silveira J. 2000. Cryptic Peripheral Ribosomal Domains Distributed Intermittently along Mammalian Myelinated Axons. The Journal of Neuroscience, November 15, 2000, *20*(22):8390–8400.

Kun A, J. C. Benech, A. Giuditta & J.R. Sotelo. 1998. Polysomes are present in the squid giant axon: an Immuno Electron Microscopy. ICEM-14, Electron Microscopy, 1998, Vol. I:825-826.

Kun, A, Otero, L., Sotelo-Silveira, J. & Sotelo, J. 2007. Ribosomal distribution in axón of mammalian myelinated fibers. J.Neuroscience Research 85:2087-2098

Li YC, Li YN, Cheng CX, Sakamoto H, Kawate T, Shimada O & Atsumi S .2005. Subsurface cisterna-lined axonal invaginations and double-walled vesicles at the axonal-myelin sheath interface. Neurosci Res.;53(3):298-303.

Li YC, Cheng CX, Li YN, Shimada O, & Atsumi S. 2005.Beyond the initial axon segment of the spinal motor axon: fasciculated microtubules and polyribosomal clusters. J Anat; 206(6):535-42.

MacKenzie ML, Ghabriel MN & Allt G. 1984. Nodes of Ranvier and Schmidt-Lanterman incisures: an in vivo lanthanum tracer study.J Neurocytol. 13(6):1043-55.–

Martin R, Fritz W & Giuditta A. 1989. Visualization of polyribosomes in the postsynaptic area of the squid giant synapse by electron spectroscopic imaging. J Neurocytol.; 18(1):11-8.

Mersiyanova IV, Perepelov AV, Polyakov AV, Sitnikov VF, Dadali EL, Oparin RB, Petrin AN & Evgrafov OV, 2000. A new variant of Charcot-Marie-Tooth disease type 2 is probably the result of a mutation in the neurofilament-light gene. Am J Hum Genet 67: 37-46.

Morel G, Cavalier A & Williams L. 2001. In situ hybridization in electron microscopy CRC Press Boca New York Washington, D.C. ISBN 0849300444, 9780849300448. Editors Morel G, Cavalier A, Williams L.

Notterpek L, Ryan MC, Tobler AR & Shooter EM. 1999. PMP-22 accumulation in aggresomes: implications for CMT1A pathology. Neurobiol Dis. ;6(5):450-60.

Notterpek L, Shooter EM & Snipes GJ. 1997. Upregulation of the endosomal-lysosomal pathway in the trembler-J neuropathy. J Neurosci.;17(11):4190-200.

Patel PI, Roa BB, Welcher AA, Schoener-Scott R, Trask BJ, Pentao L, Snipes GJ, Garcia CA, Francke U, Shooter EM, Lupski JR & Suter U. 1992.The gene for the peripheral myelin protein PMP-22 is a candidate for Charcot-Marie-Tooth disease type 1A. Nat Genet.;1(3):159-65.

Pérez-Ollé, R, Leung, CL, Liem, RKH. 2002. Effects of Charcot-Marie-Tooth linked mutation of the neurofilament light subunit on intermediate filament formation. Journal of Cell Science 115:4937-4946.

Quarles RH. 2007.Myelin-associated glycoprotein (MAG): past, present and beyond.J Neurochem.100(6):1431- 48.

Ryan TE, Patterson SD. 2002.Proteomics: drug target discovery on an industrial scale.Trends Biotechnol.;20(12 Suppl):S45-51. Review.

Robertson JD. 1958. The ultrastruture of Schmidt Lanterman clefts and related shearing defects of the myelin sheath. J. Biophis. Biochem. Cytol., 4, 39-46. 48.

Rosso G, Cal K, Canclini L, Damián JP, Ruiz P, Rodríguez H, Sotelo JR, Vazquez C, Kun A. 2010. Early phenotypical diagnoses in Trembler-J mice model. J Neurosci Methods;190(1):14-9.

Salzer JL, Brophy PJ, Peles E. 2008. Molecular Domains of Myelinated Axons in the Peripheral Nervous System. Glia 56:1532–1540

Sambrook Y, Russell DW. 2006. Molecular Cloning A laboratory manual. Third edition. Cold Spring Harbor Laboratory Press. ISBN 0879697717

Sereda M, Griffiths I, Pühlhofer A, Stewart H, Rossner MJ, Zimmerman F, Magyar JP, Schneider A, Hund E, Meinck HM, Suter U, Nave KA. 1996. A transgenic rat model of Charcot-Marie-Tooth disease. Neuron.;16(5):1049-60.

Shen YJ, DeBellard ME, Salzer JL, Roder J, Filbin MT. 1998.Myelin-associated glycoprotein in myelin and expressed by Schwann cells inhibits axonal regeneration and branching.Mol Cell Neurosci. 1998 Sep;12(1-2):79-91.

Sidman, R.; Cowen, J.; Eicher, E. 1979. Inheredit muscle and nerve diseases in mice: A tabulation with commentary. Ann NY Academy Science, 317, 497-505.

Small JR, Ghabriel MN, Allt G 1987. The development of Schmidt-Lanterman incisures: an electron microscope study.J Anat.150:277-86.

Snipes GJ, Suter U.1995. Molecular basis of common hereditary motor and sensory neuropathies in humans and in mouse models.Brain Pathol. ;5(3):233-47.

Snipes GJ, Suter U. 1995.Molecular anatomy and genetics of myelin proteins in the peripheral nervous system. J Anat.;186 (Pt 3):483-94. Review.

Sotelo JR, Kun A, Benech JC, Giuditta A, Morillas J, Benech CR.1999. Ribosomes and polyribosomes are present in the squid giant axon: an immunocytochemical study.Neuroscience.; 90(2):705-15.

Sotelo-Silveira JR, Calliari A, Kun A, Koenig E, Sotelo JR. 2006.RNA trafficking in axons.Traffic.;7(5):508-15. Review.

Suter,U. and Scherer, S. 2003, Disease mechanisms in inherited neuropathies. Nature Rev Neurosc 4:714-726.

Suter U, Moskow JJ, Welcher AA, Snipes GJ, Kosaras B, Sidman RL, Buchberg AM, Shooter EM.1992. A leucine-to-proline mutation in the putative first transmembrane domain of the 22-kDa peripheral myelin protein in the trembler-J mouse.Proc Natl Acad Sci U S A.; 15;89(10):4382-6.

Valentijn LJ, Baas F, Wolterman RA, Hoogendijk JE, van den Bosch NH, Zorn I, Gabreëls-Festen AW, de Visser M, Bolhuis PA. 1992.Identical point mutations of PMP-22 in Trembler-J mouse and Charcot-Marie-Tooth disease type 1A. Nat Genet. ;2(4):288-91.

Vallat JM, Funalot B. 2010 Charcot-Marie-Tooth (CMT) disease: an update.Med Sci (Paris). 2010 Oct;26(10):842-7.

Verhoeven K, De Jonghe P, Coen K, Verpoorten N, Auer-Grumbach M, Kwon JM, FitzPatrick D, Schmedding E, De Vriendt E, Jacobs A, Van Gerwen V, Wagner K, Hartung HP, Timmerman V. 2003. Mutations in the Small GTP-ase Late Endosomal Protein RAB7 Cause Charcot-Marie-Tooth Type 2B Neuropathy. Am J Hum Genet 72: 722-727

Waelter S, Boeddrich A, Lurz R, Scherzinger E, Lueder G, Lehrach H, Wanker EE. 2001. Accumulation of mutant huntingtin fragments in aggresome-like inclusion bodies as a result of insufficient protein degradation. Mol Biol Cell.;12(5):1393-407.

Young P, Suter U. 2003.The causes of Charcot-Marie-Tooth disease.

Cell Mol Life Sci. ;60(12):2547-60.

Zelená J. 1970.Ribosome-like particles in myelinated axons of the rat. Brain Res.; 1;24(2):359-63.

Zelená J. 1972. Ribosomes in the axoplasm of myelinated nerve fibres.Folia Morphol (Praha).;20(1):91-

Zelená J. 1972. Ribosomes in myelinated axons of dorsal root ganglia. Z Zellforsch Mikrosk Anat. 1972;124(2):217-29.

Zhao C, Takita J, Tanaka Y, Setou M, Nakagawa T, Takeda S, Yang HW, Terada S, Nakata T, Takei Y, Saito M, Tsuji S, Hayashi Y, Hirokawa N. 2001. Charcot-Marie-Tooth disease type 2A caused by mutation in a microtubule motor KIF1Bbeta. Cell, 1;105(5):587-97.

11.2.4. TRABAJO IX

Sotelo-Silveira, J.R.; Calliari, A.; Kun A., Elizondo V., Canclini L., Sotelo J. R. Localization of mRNA in vertebrate axonal compartments by in situ hybridization. RNA detection and visualization, 714, 125-138, Humana Press. 2011. Capítulo de libro.

Chapter 8

Localization of mRNA in Vertebrate Axonal Compartments by In Situ Hybridization

José Roberto Sotelo-Silveira, Aldo Calliari, Alejandra Kun, Victoria Elizondo, Lucía Canclini, and José Roberto Sotelo

Abstract

The conclusive demonstration of RNA in vertebrate axons by in situ hybridization (ISH) has been elusive. We review the most important reasons for difficulties, including low concentration of axonal RNAs, localization in specific cortical domains, and the need to isolate axons. We demonstrate the importance of axon micro-dissection to obtain a whole mount perspective of mRNA distribution in the axonal territory. We describe a protocol to perform fluorescent ISH in isolated axons and guidelines for the preservation of structural and molecular integrity of cortical RNA-containing domains (e.g., Periaxoplasmic Ribosomal Plaques, or PARPs) in isolated axoplasm.

Key words: ISH, Axons, Confocal ISH, PARPs, Trans-acting factors, TAF, RNA binding proteins

1. Introduction

Since the first communications describing the localization of an rRNA in an oocyte (1, 2), uses for in situ hybridization (ISH) have widened and the protocols improved to answer particular questions. Advances in detecting low copy number transcripts and spatial organization of the transcriptome helped advance the evolution of ISH techniques (3). Increasing sensitivity was one of the main goals in efforts to improve the different protocols used especially in cells where structural issues and the subcellular distribution of mRNA was not the main issue in question. In the case of neuronal cells, ISH was broadly used to detect and even semiquantify the levels of a variety of mRNAs in the cell perikaryon. Focusing on the cell body alone would leave more than 95% of the neuronal cytoplasm, comprised in many cases mainly by

Jeffrey E. Gerst (ed.), *RNA Detection and Visualization: Methods and Protocols*, Methods in Molecular Biology, vol. 714,
DOI 10.1007/978-1-61779-005-8_8,

dendrites and/or axons (4), uncharted. Furthermore, since mRNAs are of high abundance in the cell body, setting up protocols to detect mRNAs in these areas will lead to a default decrease in sensitivity for neuronal projections where mRNA localization is not uniform and is less concentrated. In the latter, if the user employs "cell body" ISH labeling times needed to accumulate detectable color precipitates or "cell body" parameters to detect fluorescently labeled probes, it will be difficult to obtain reliable signals. On the other hand, very long labeling times are not recommended to avoid increase background in axons.

Distribution of the protein synthesis machinery and its activity pointed out that mRNAs were being transported and localized in dendrites (and the postsynaptic densities) and axons (5, 6). mRNAs were first demonstrated to be in invertebrate unmyelinated axons or vertebrate myelinated axons by ISH (7–9). Despite a broad range of evidence showing protein synthesis activity in myelinated vertebrate axons, mRNA localization studies supporting these data only appeared in the last decade of the century (6–10). Among the main reasons for these late findings we could find the need for adaptation of ISH methods to reach sensitivity and spatial resolution to cope with the neuron and nervous tissue structural complexity. Regarding axons in the peripheral nervous system, our group demonstrated the presence of the mRNA coding for the small subunit of neurofilaments in axons of the sciatic nerve using colorimetric ISH methods (8) and the presence of beta actin mRNA with its RNA binding protein in motor axons of the lumbar ventral roots (9), but also ribosomal RNA in sciatic nerve (11). Different studies showed that mRNAs could be also detected in axons of the central nervous system like the hypothalamic–hypophyseal tract (12) where oxytocin- and vasopressin-coding mRNAs were found, or in axons of the olfactory tract where mRNAs coding for olfactory receptors were localized (13). In several studies, neuronal cell culture models were chosen to isolate axons from their complex surroundings (14, 15). Bassell and colleagues showed that axons in culture could localize beta actin mRNAs into growth cones by fast axonal transport of mRNAs embedded in ribonucleoprotein particles (RNPs) (16, 17). These studies used different approaches to gain sufficient resolution and sensitivity to answer the question of mRNA distribution in neurons. When examining an intact tissue, a balance of structural preservation coupled with the penetration of large labeled nucleic acids into the cryo-sections, combined with digoxigenin detection using alkaline phosphatase, is required (8). As the fluorescent techniques are more available and reliable, the use of laser confocal microscopy combined with either fluorescent oligos or amplification of the fluorescent signal with enzymatic methods is now preferred (9, 11).

It is possible to increase probe accessibility and resolution of axons if the user selects culture systems to perform ISH, however the main disadvantage of this approach is that the distribution of mRNAs in the animal model is not accurately assessed in this way, since axons do not fully develop in culture and the glial microenvironment is not preserved in such conditions. To solve this problem, the user can choose conventional cryo-sections or use microdissected axons from adult animals. Using methods formerly developed by Koenig and colleagues (18–23), is possible to isolate the giant axon (50–100 μm) of the Mauthner neuron, a myelinated axon from the central nervous system derived from a single cell that runs through the spinal cord of goldfish and other bony fishes. A variation of the method could be used to dissect motor neuron and sensory axons of ventral and dorsal roots of different mammals like mouse, rat, or rabbit. In both cases myelin is not present in the preparation, which allows for the fast penetration of probes and clear visualization of different probes in a stretch of up to 1,000 μm of axoplasm. In this chapter we describe methods used to detect mRNAs in micro-dissected axons from different vertebrate species and locations. mRNA may be transported as RNPs, structures also named endoaxoplasmic ribosomal plaques (EARPs) (10), via core cytoskeletal elements and then localized at cortical actin-rich Periaxoplasmic ribosomal plaque (PARP) domains (9, 18, 20, 23, 24). Therefore special attention will be given on how to preserve cortical axonal areas. Since different sources of evidences are indicating that the RNA complexity (25), either in immature (26), or mature (27) axons, is higher than previously expected, we consider ISH in single microdissected axons as a valuable tool for confirmation and/or discovery of the intra-axonal distribution and interactions of messenger RNA in neuronal projections.

2. Materials

2.1. Whole Mount Axonal Preparation in Goldfish, Rats, Mice, or Rabbits (see Note 1)

1. Cortland solution: 132 mM Na-gluconate, 5 mM KCl, 20 mM HEPES, 10 mM glucose, 3.5 mM MgSO4, and 2 mM EGTA (ethylene glycol tetraacetic acid) at pH 7.2, stored at 4°C.
2. Ammonium acetate 0.15 M at pH 4.0, Tween-20 0.01%, and NaN_3 5 mM.
3. Ethyl m-aminobenzoate (MS-222).
4. Denaturing solution: 30 mM zinc acetate and 0.1 M Tricine (*N*-tris(hydroxymethyl) methylglycine).
5. Axon pulling solution (stock solution): (a) 0.2 M aspartate acid, and (b) 0.192 M Tris–HCl at pH 5.5.

6. Axon pulling solution (working solution): prepare a series of 30–90 mM aspartate solutions by diluting the stock aspartate solution (2.1.5) with RNAse free water as needed.
7. 1% 3-aminopropyltriethoxysilane (Polysciences, Warrington, PA) in 100% ethanol.
8. 3.75% Paraformaldehyde in PBS.
9. Tween-20.
10. #1 coverslips.
11. #5 Forceps.
12. Petri dishes (35 mm).
13. Stereoscopic microscope with fiber optics illumination source.
14. Eyebrow tool (An eyebrow attached to the tip of a Pasteur pipette).
15. YOYO-1 iodide (491/509) or POPO-1 iodide (434/456) (Invitrogen). Stock solution of YOYO-1 or POPO-1 in DMSO (1:10).
16. Epifluorescence or Confocal Microscope.

2.2. Probe Preparation

1. DIG RNA Labeling Kit (SP6/T7) (Boehringer-Mannheim, Cat. No. 1 175 025). Concentrated RNA Labeling Mix contains 10 mM each of ATP, CTP, and GTP; 6.5 mM UTP; 3.5 mM Digoxigenin-UTP; pH 7.5 (20°C).
2. Transcription Buffer (400 mM Tris–HCl (pH 8.0, 20°C), 60 mM $MgCl_2$, 100 mM Dithiothreitol (DTT), and 20 mM spermidine).
3. RNA Polymerases (SP6, T7, or T3).
4. RNasin ribonuclease inhibitor (Promega).
5. Restriction enzymes (single cut 5′ and 3′ of insert).
6. Phenol and chloroform.
7. LiCl 4 M.
8. Ethanol 70, 95, and 100%.
9. Water – RNAse/DNAse Free (with no traces of DEPC).
10. Agarose electrophoresis system.
11. Plasticware RNAse/DNAse Free.

2.3. In Situ Hybridization

1. Phosphate Buffered Saline (PBS).
2. 3.75% Paraformaldehyde in PBS.
3. 0.1 mol/L sodium diethylmalonate buffer at pH 7.0, with 0.1% Tween 20.
4. 20× SSC stock solution (0.3 M NaCl and 0.3 M sodium citrate).
5. 50% formamide.

6. 4× SSC.
7. 0.2× SSC.
8. Hybridization solution (4× SSC, 500 µg/µL salmon sperm DNA, 250 µg/µL yeast tRNA, 1× Denhardt, and 10% (w/v) dextran sulfate).
9. Bovine serum albumin.

2.4. Detection

1. Antibody anti-digoxigenin HRP conjugated antibody (Cat. No. 1-207-733 Boehringer-Mannheim).
2. 0.3% H_2O_2 in PBS.
3. TSA Plus Fluorescence Systems NEL744 (Cyanine 3) (Perkin Elmer).
4. DMSO (dimethyl sulfoxide – molecular biology or HPLC-grade).
5. Blocking reagent (Perkin Elmer Cat. No. FP1020).
6. TNT Wash Buffer (0.1 M Tris–HCl, pH 7.5, 0.15 M NaCl, and 0.05% Tween® 20).
7. TNB Blocking Buffer (0.1 M Tris–HCl, pH 7.5, and 0.15 M NaCl 0.5% Blocking Reagent).
8. Sodium peroxide.
9. 10% of dextran sulfate.
10. Fluorophore tyramide, Plus Amplification Diluent (NEN Life Science Products).
11. Prepare fluorophore tyramide Stock Solution. Each vial must be reconstituted with 0.15 mL DMSO before use. The fluorophore tyramide stock solution, when stored at 4°C, is stable for at least 3 months.
12. Prepare fluorophore tyramide working solution. Before each procedure, dilute the Fluorophore Tyramide Stock Solution 1:50 using 1× Plus Amplification Diluent to make the fluorophore tyramide working solution (28). Approximately 100–300 µL is required per slide. Discard any unused portion of working solution.
13. ProLong antifade (Invitrogen).

3. Methods

3.1. Probe Preparation

1. Linearize DNA with an appropriate restriction enzyme that does not leave 3′ end overhangs.
2. Extract with phenol–chloroform and precipitate. Resuspend in sterile water at 1 mg/mL.
3. Add the following, in the order shown:

- 1 μg of purified, linearized plasmid DNA or 100–200 ng of purified PCR fragment.
- 2 μL of 10× concentrated DIG RNA Labeling Mix.
- 2 μL of 10× concentrated Transcription Buffer (see Note 2).
- 2 μL of RNA polymerase (SP6, T7, or T3).
- Enough sterile, redistilled RNAse free water to make a total reaction volume of 20 μL.

4. Mix gently, do not vortex, spin down drops in microfuge (see Note 3).
5. Incubate at 37°C for 2–6 h.
6. Check 1 μL on a 1% agarose gel (see Note 4), and in the meantime, purify the probe using precipitation: Add 100 μL water, 10 μL 4 M LiCl, 300 μL ethanol, and 1 μL glycogen (4 mg/mL). Place at −80°C for at least 1 h. Spin and resuspend the pellet in 30 μL of water; add 15 μL of 7.8 M ammonium acetate, 1 μL glycogen and 100 μL of ethanol. Place at −80°C for at least 1 h. Spin and resuspend pellet in 30 μL of water. Store at −80°C (see Note 5).

3.2. Whole-Mount Axon Preparation

3.2.1. Mauthner Axons: Tissue Dissection

1. Anesthetize common goldfish, *Carassius auratus* (6–8 cm in length), for 30 min in ice/water bath containing MS-222 (0.01%). The isolation of brain and spinal cord tissue requires about 5 min.
2. The lower portion of the brain is exposed and severed in situ along the anterior border of the cerebellum.
3. The spinal cord and lower brainstem are rapidly dissected and placed on ice-cold Cortland medium.
4. As a next step, the brainstem is cut about midway through cerebellum; dorsal structures, including vagal lobes, facial lobe, and cerebellar crests are then excised in order to expose the rostral course of M-cell axons. The M-cell axons run superficially in the floor of the ventricle and their course can be visualized under a dissecting microscope either by reflected light or transillumination (see Fig. 1a, b).
5. Approximately 5 mm portions of brainstem and spinal cord are cut and left in ice-cold Cortland solution in a 35-mm Petri dish, waiting for denaturation step.

3.2.2. Mauthner Axon: Axon Pulling

1. CNS segments are transferred to a dish containing denaturing solution and incubated for 10 min at room temperature.
2. The spinal cord segments are transferred to a Petri dish containing axon pulling solution and a #1 coverslip previously coated with 1% 3-aminopropyltriethoxysilane.
3. After 1 min of incubation use #5 forceps to start pulling out the axoplasm while observing through a stereoscopic microscope

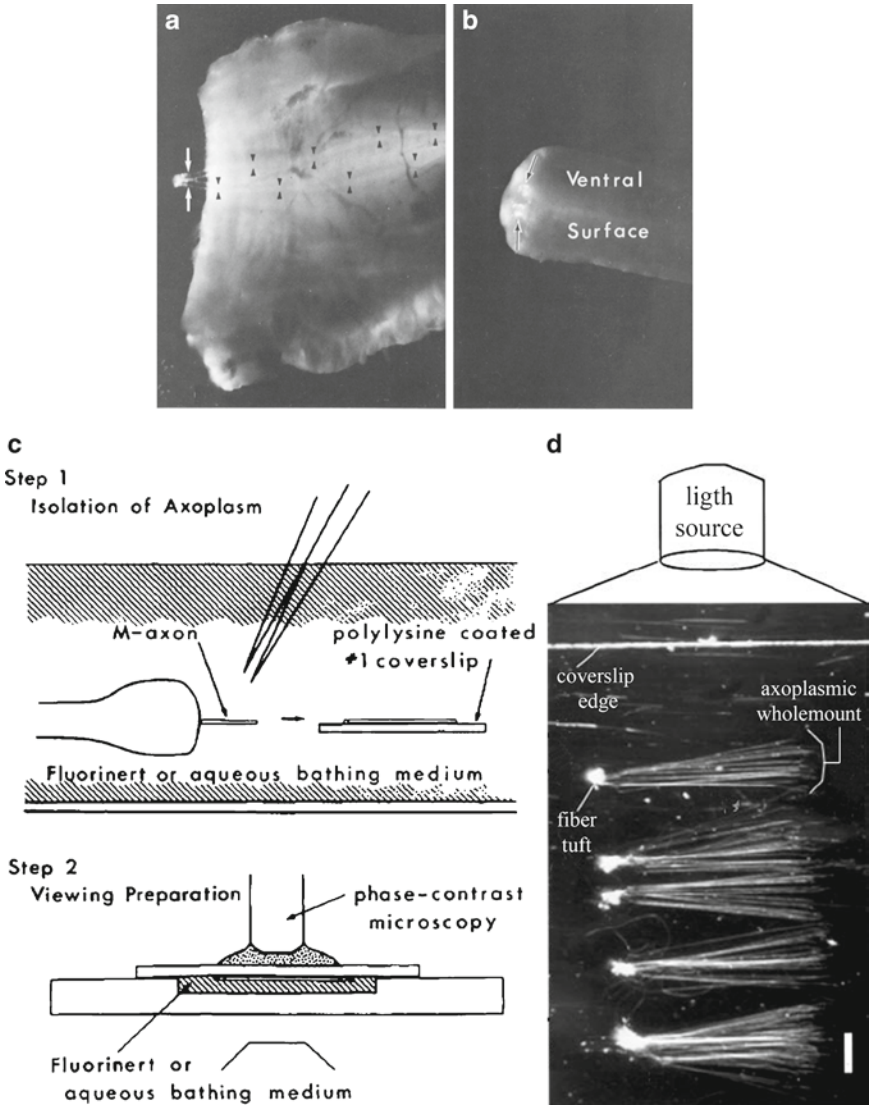

Fig. 1. Locating M-cell axons in the brainstem and spinal cord. (**a**) An isolated brainstem after trimming, showing two ensheathed M-cell axons, partially translated out of their in situ location. Axons lie superficially in the floor of the fourth ventricle and can be visualized in a dissecting microscope with reflected or transilluminated light. (**b**) M-cell axons assume a position in the ventral quadrant of the spinal cord, and can be made to protrude from the cut surface by slight compression applied to the lateral surfaces of the cord stump. Two ensheathed M-cell axons are shown protruding (*arrows*). (**c**) Diagrammatic description of the isolation of M-cell axons in preparation for viewing. Step 1: M-cell axons are translated out of their in situ locations with a pair of no. 5 watchmaker's tweezers in an appropriate bathing medium, and deposited fully extended on a polylysine-coated coverslip with the aid of an eyebrow hair. Step 2: after axons are attached to the coverslip, the coverslip is removed, the bottom surface is wiped, and it is inverted over the well of a chamber, whereupon the space is filled with the appropriate bathing medium. The chamber is made from two glass histological slides cemented together (courtesy of Dr. Edward Koenig, modified from Brain Research (19)). (**d**) A dark-field view through a dissecting microscope of five axon sprays isolated from rabbit ventral nerve root fibers that were attached to a coverslip surface. A spray is defined as multiple isolated axoplasmic whole mounts originating in a nerve fiber tuft remnant that was used to grasp the spray. *Scale bar*, 1 mm (courtesy of Dr. Edward Koenig, modified from *Journal of Neuroscience* (18)).

(see Note 6). Different concentrations of axon pulling solution should be tested for optimal recovery of cortical axoplasm (see Note 7). Once the best recovery is assessed it's possible to pull out axoplasm from the remaining segments with at least 50% chances of success with respect of cortical located structures.

4. Once the axon is out of the spinal cord, it should be moved to the coverslip surface with the aid of an eyebrow tool to attach first the end and then the middle segment of the axon (Fig. 1c).

3.2.3. Isolation of Axoplasmic Whole-Mounts from Mammalian Myelinated Spinal Root Fibers

1. Dissect lumbar spinal nerve roots from either euthanized rat, mice, or rabbit depending on the model you consider using.
2. Suspend the tissues (several nerve root/rootlet) in ice-cold Cortland solution.
3. A nerve root/rootlet, 3–5 mm, is immersed in denaturing solution for 10 min.
4. Then the tissue is placed in a 35-mm plastic culture dish containing 2 mL pulling solution and a #1 coverslip previously coated with 1% 3-aminopropyltriethoxysilane.
5. Grasp a small portion of the tip of the ventral root with #5 forceps (while holding the other end with another forceps) and pool out to obtain a spray of axons attached to a nerve fiber tuft (whole mounts). Attach isolated axoplasmic whole-mounts with the aid of eyebrow hair tools to #1 coverslips (Fig. 1d).

3.2.4. YOYO-1 and POPO-1 Staining of Axoplasmic Whole-Mounts

1. Recovery of PARPs (see Note 8) can be assessed by staining of the wholemounts with YOYO-1 iodide (491/509) (see Note 9).
2. One microliter of a 1:10 stock solution of YOYO-1 or POPO-1 in DMSO was added to 2 mL of the pulling medium for 15 min.
3. YOYO-1 or POPO-1 were washed out by brief immersion in 0.15 M ammonium acetate and 0.01% Tween 20, NaN_3 5 mM.
4. For fluorescence microscopy the coverslip with axoplasmic sprays was mounted on a flow-through chamber filled with 0.15 M ammonium acetate solution (see Note 10).
5. After verifying the presence or absence of YOYO-1 staining (epifluorescence or confocal microscope) the coverslips are returned to the Petri dishes and stored at 4°C to be used shortly thereafter for ISH.

3.3. In Situ Hybridization (see Note 11)

1. Fix isolated Zn-denatured axoplasmic whole-mounts in 3.75% paraformaldehyde buffered with PBS with 0.1% Tween 20, or if no salts are preferred, use 0.1 mol/L sodium diethylmalonate buffer at pH 7.0, with 0.1% Tween 20, for 3 h at 20°C (see Note 12).

2. Wash twice for 10 min with ammonium acetate solution at room temperature.
3. Dehydrate in 70, 95, and 100% alcohols and air dry.
4. Pre-incubate specimens in hybridization solution (i.e., 4× SSC, 500 µg/µL of salmon sperm DNA, 250 µg/µL of yeast tRNA, 1× Denhardt, and 10% (w/v) dextran sulfate) for 15 min at 42°C in a humid chamber.
5. Denature sense or antisense RNA probe and mix it with hybridization solution at a final concentration of 2 ng/µL and incubate for 3 h at 42°C in humid chamber (longer incubation time will affect PARP structures).
6. Wash coverslips once in 4× SSC for 20 min, at room temperature.
7. Wash two times with 0.2× SSC and 0.2% bovine serum albumin, at 50°C with agitation.

3.4. Detection by Tyramide Amplification

1. Quench endogenous peroxidase using 0.3% H_2O_2 in PBS for 10 min.
2. Block coverslips with 100–300 µL of TNB Buffer in a humidified chamber for 30 min at room temperature.
3. Incubate coverslips for 30 min at room temperature in a humidified chamber 1/500 of anti-DIG-HRP conjugated antibody. Using 100–300 µL of antidigoxigenin-HRP diluted in TNB Buffer.
4. Wash the slides three times for 5 min each in TNT Buffer at room temperature with agitation.
5. TSA Plus Fluorescence Systems Amplification. Pipet 100–300 µL of the Fluorophore Tyramide Working Solution onto each slide. Incubate the slides at room temperature for 3–10 min.
6. Wash the slides three times for 5 min each in TNT Buffer at room temperature with agitation in the presence of 10% of dextran sulfate to improve localization of tyramide (28).
7. Follow desired fluorescence observation by mounting the coverslip on the flow through chamber (see Subheading 3.2.2) or by mounting the coverslip upside down on a slide containing a small drop of ProLong antifade (Invitrogen). Results of ISH and detection of RNA binding proteins in axonal wholemounts can be seen in Figs. 2 and 3.

4. Notes

1. Solutions used in direct contact with axonal wholemounts should be filtered (0.45 µm) to avoid adhesion of fine particulate material.

2. To avoid precipitation caused by spermidine, reagents must be at room temperature before starting.
3. Do not use water treated with DEPC, since small traces of it will inhibit RNA polymerases, resulting in low yields of labeled transcripts.
4. Quantification of the labeled probe could be carried out by dot blots of serial dilutions (provided in the kit) or by capillary gel electrophoresis on Bioanalyzers (Agilent).
5. This extra precipitation step helps to decrease background because it improves removal of unincorporated DIG-nucleotides.
6. In the spinal cord, the axons are located in the ventral quadrants and can frequently be made to protrude by gentle compression (using number 5 forceps) of the spinal cord stump. This is accomplished by grasping the exposed cut ends of the axons with the tweezers and pulling them out in a deliberate fashion. Experience will aid in determining an optimum rate for pulling. Once the tips of the axons are visible, one can hold and later pull out the protruding end of the axon with the aid of forceps. Use extreme caution to avoid bending of the tips of forceps, since this will reduce the ability to grasp the axons.
7. It is imperative to use different concentrations of pulling solutions (30–50 mM aspartate) to establish a critical permissive concentration. This concentration is empirically defined as the one at which PARPs, PARP markers, and/or YOYO-1 staining is optimized (18), since PARPs are not always recovered at the same aspartate concentration.
8. The integrity of PARP domains and the presence of nucleic acids in the isolated axons can be verified by phase contrast and fluorescence microscopy (see Figs. 2 and 3). When preservation of PARPs is optimal, it is possible to observe phase-dense regions, which can be used as landmarks to find PARP domains after ISH development (Fig. 2). Do not stain with YOYO-1 after ISH, because hybridization buffers include blocking nonspecific probe binding with an excess of nucleic acids. Instead, detect ribosomes to observe PARP distribution. It is of special value to validate a particular mRNA localization to localize an RNA-binding protein known to bind the mRNA being assessed. That can be seen in Fig. 3 in which ZBP1, a known binding partner of beta-actin mRNA (9), was localized to PARP domains in which the same message was observed by ISH (Fig. 2).
9. If one wishes to detect nucleic acids at a different wavelength, it is possible to use POPO-1 iodide (434/456), although it fades more rapidly than YOYO-1.
10. The chamber was constructed by inverting the coverslip over spacers (0.5–1 mm thick) made of Silastic elastomer (Dow

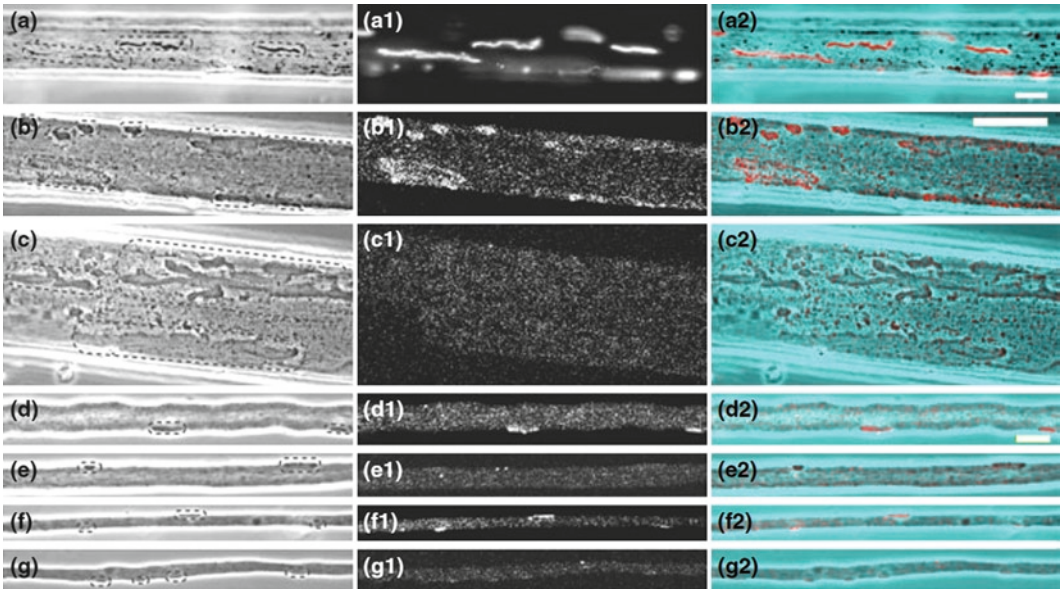

Fig. 2. Localization of β-actin mRNA by in situ hybridization (ISH) in periaxoplasmic ribosomal plaque (PARP) domains, identified by phase structural correlates (outlined by *green dash ovals*). (**a**) Structural correlates of PARP formations are revealed in a phase micrograph of an isolated goldfish Mauthner axoplasmic whole-mount. (**a1**) RNA labeled with YOYO-1, a high affinity RNA binding fluorescent dye, shows a discrete localization and distribution along the length of the whole-mount. (**a2**) A merge of RGB-rendered phase and fluorescence images in (**a**) and (**a1**) confirms that RNA fluorescence localizes in PARP formations identified by phase correlates. Representative examples of ISH labeling in axoplasmic whole-mounts isolated from (**b–b2** and **c–c2**) Mauthner, (**d–d2** and **e–e2**) rabbit, and (**f–f2** and **g–g2**) rat nerve fibers. The size and morphology of PARPs in Mauthner axons are highly variable, in contrast to the unremarkable simple morphology of PARPs in rabbit and rat whole-mounts. The b-actin mRNA antisense probe is localized in delimited domains in (**b1**) Mauthner, (**d1**) rabbit, and (**f1**) rat whole-mount ISH images. In contrast, the sense probe ISH yields diffuse background in (**c1**) Mauthner, (**e1**) rabbit, and (**g1**) rat whole-mounts. Merges of RGB-rendered phase images in (**b–g**) and corresponding (**b1–g1**) ISH images in (**b2–g2**), respectively, show that there is a close correspondence between PARP structural correlates and the localization and distribution density of antisense β-actin mRNA ISH signals. *Grayscale* images shown in (**a–g**) and (**a1–g1**) were assigned *blue-green* and *red* colors, respectively, from a lookup table to highlight correspondence (**a2**, **b2**, **d2**, and **f2**), or no correspondence (**c2**, **e2**, and **g2**) in merged images, using NIH ImageJ. *Calibration bars*: **a–c2**, 50 μm and **d–g2**, 10 μm, see Sotelo-Silveira et al. (9), with permission of the *Journal of Neurochemistry* (*Wiley-Blackwell*).

Corning, Midland, MI) attached to a large glass coverslip (35 × 50 mm) taped to a thin, U-shaped metal plate.

11. Effectiveness of the probes in detecting message can be assessed in parallel using positive control tissues (prepared by cryotomy) in which neuronal cell bodies are abundant and mRNA concentration is high (e.g., motor neurons in spinal cord).

12. Since PARP domains are exposed directly to hybridization solutions, different fixing times and hybridization length were tested to avoid PARP removal/destruction during hybridization. A combination of 3 h fixation and 3 h hybridization was determined by following YOYO-1 staining in the presence of 50% formamide, 4× SSC.

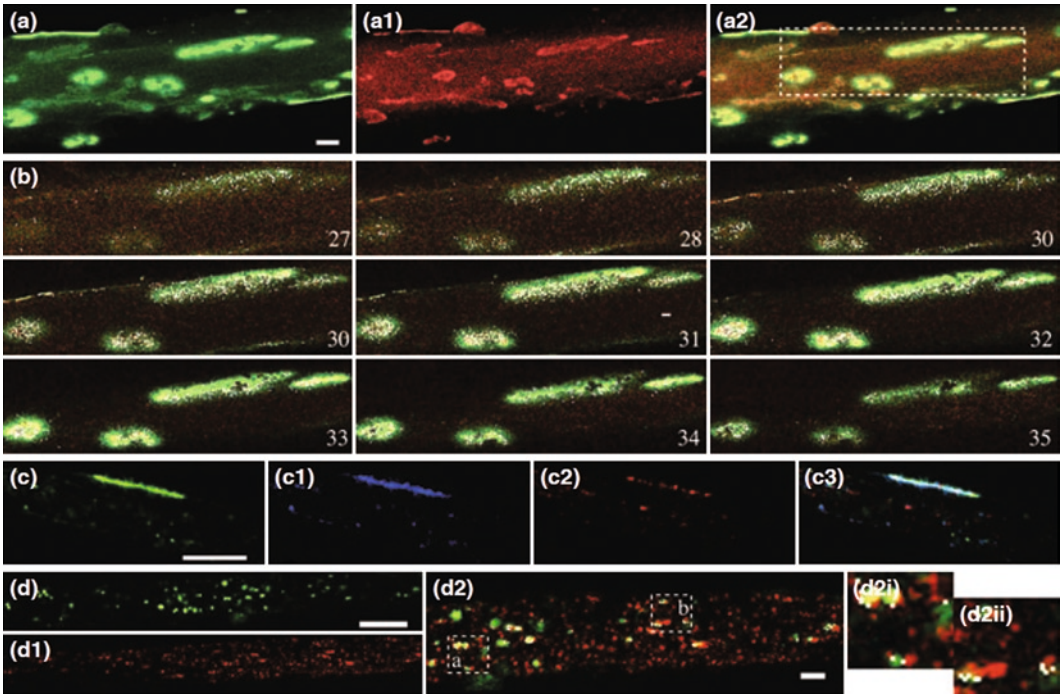

Fig. 3. Confocal microscopic evaluation of PARP-containing RNA and ZBP-1 in axoplasmic whole-mounts isolated from Mauthner and rat ventral root fibers. (**a–a2**) Low magnification (×20) merges of 39 optical slices (1.45 μm) of a Mauthner whole-mount (~55 μm in diameter), in which (**a**) RNA fluorescence labeling of PARPs with YOYO-1 in the *green* channel and (**a1**) ZBP-1 immunofluorescence in the *red* channel are shown localized in PARP formations (**a2**). A merged image of (**a**) and (**a1**) reveals co-distributions of PARP RNA fluorescence and ZBP-1 immunofluorescence. (**b**) NIH ImageJ software was used to analyze a series of nine consecutively numbered slices (b27–35) in a region outlined in (**a2**) from the outer one-third of the whole-mount in order to evaluate co-localization of RNA and ZBP-1 fluorochrome pixels. Apparent co-localization is indicated by *bright* signals, in which the intensity ratio of YOYO-1 and anti-ZBP-1 fluorochromes is ≥80%, and the overlap ratio is >0.9. Note that while inspection of (**a–a2**) indicates considerable overlap of YOYO-1 fluorescence and ZBP-1 immunofluorescence in PARPs, co-localization signals are not uniformly distributed within PARP domains. Rather, colocalization signals tend to distribute outside of the compact portions of the PARP domain. (**c–c3**) Co-distribution of (**c**) RNA (*green*), labeled by YOYO-1, (**c1**) ribosomes (*blue*), labeled with ribosome anti-P protein, and (**c2**) immunofluorescence of anti-ZBP-1 (*red*) in a surface PARP of an axoplasmic whole-mount from a rat ventral root fiber; (**c3**) a merged image of (**c–c2**). Putative "in-transit" RNA/ZBP-1-containing "particles" within the axoplasmic core of a whole-mount from a rat ventral root fiber is suggested from inspection of (**d**) RNA (*green*) (**d1**) anti-ZBP-1 immunofluorescence (*red*), and (**d2**), an enlarged merged image, which shows occasional areas containing co-localization signals (see *dash rectangles*) that are further enlarged in (**d2i** and **d2ii**). *Calibration bars*: **a–a2**, 12.2 μm and **c–d1**, 10 μm, see Sotelo-Silveira et al. (9), with permission of the *Journal of Neurochemistry* (*Wiley-Blackwell*).

Acknowledgments

The authors thank John Mercer for a critical reading of this manuscript and Edward Koenig for the use of figures presented in Fig. 1. This project was partially funded by CSIC, PEDECIBA, ANII, MEyC, PEW fellowship to JRSS, NIH grant #1R03 TW007220-01A2.

References

1. John H.A., Birnstiel M.L. Jones K.W. (1969). RNA-DNA hybrids at the cytological level. *Nature* **223**, 582–7.
2. Gall J.G., Pardue M.L. (1969). Formation and detection of RNA-DNA hybrid molecules in cytological preparations. *Proc. Natl. Acad. Sci. USA* **63**, 378–83.
3. Femino A.M., Fay F.S., Fogarty, K., Singer, R.H. (1998). Visualization of single RNA transcripts in situ. *Science* **280**, 585–90.
4. Craig A.M., Banker, G. (1994). Neuronal polarity. *Annu. Rev. Neurosci.* **17**, 267–310.
5. Sotelo-Silveira J.R., Calliari, A., Kun, A., Koenig, E., Sotelo, J.R. (2006). RNA trafficking in axons. *Traffic* **7**, 508–15.
6. Giuditta, A., Kaplan, B.B., van Minnen, J., Alvarez, J., Koenig, E. (2002). Axonal and presynaptic protein synthesis: new insights into the biology of the neuron. *Trends Neurosci.* **25**, 400–4.
7. Giuditta, A., Menechini, E., Perrone, Capano. C., Langella, M., Castigli, E., Kaplan BB. (1991). Active polysomes in the axoplasms of the squid giant axon. *J. Neurosci. Res.* **28**, 18–28.
8. Sotelo-Silveira J.R., Calliari, A., Kun, A., Benech, J.C., Sanguinetti, C, Chalar, C., Sotelo J.R. (2000). Neurofilament mRNAs are present and translated in the normal and severed sciatic nerve. *J. Neurosci. Res.* **62**, 65–74.
9. Sotelo-Siveira, J.R., Crispino, M., Puppo, A., Sotelo, J.R., Koenig, E. (2008). Myelinated axons contain beta-actin mRNA and ZBP-1 in periaxoplasmic ribosomal plaques and depend on cyclic AMP and F-actin integrity for in vitro translation. *J. Neurochem.* **104**, 545–57.
10. Koenig E. (2009). Organized ribosome-containing structural domains in axons. *Results Prob. Cell Differ.* **48**, 173–91.
11. Kun, A., Otero, L., Sotelo-Silveira, J.R., Sotelo, J.R. (2007). Ribosomal distributions in axons of mammalian myelinated fibers. *J. Neurosci. Res.* **85**, 2087–98.
12. Mohr, E., Richter, D. (1993). Complexity of mRNAs in axons of rat hypothalamic magnocellular neurons. *Ann NY Acad Sci* **689**, 564–6.
13. Vassar, R., Chao, S.K., Sitcheran, R., Nunes, J.M., Vosshall, L.B., Axel, R. (1994). Topographic organization of sensory projections to the olfactory bulb. *Cell* **79**, 981–91.
14. Eng, H., Lund, K., Campenot, R.B. (1999). Synthesis of beta-tubulin, actin, and other proteins in axons of sympathetic neurons in compartmented cultures. *J. Neurosci.* **19**, 1–9.
15. Zheng, J.Q., Kelly, T.K., Chang, B., Ryazantsev, S., Rajasekaran, A.K., Martin, K.C., Twiss, J.L. (2001). A functional role for intra-axonal protein synthesis during axonal regeneration from adult sensory neurons. *J. Neurosci.* **21**, 9291–303.
16. Kiebler, M.A., Bassell, G.J. (2006). Neuronal RNA granules: movers and makers. *Neuron* **51**, 685–90.
17. Bassell, G.J., Zhang, H., Byrd, A.L., Femino, A.M., Singer, R.H., Taneja, K.L., Lifshitz, L.M., Herman, I.M., Kosik, K.S. (1998). Sorting of beta-actin mRNA and protein to neurites and growth cones in culture. i. **18**, 251–65.
18. Koenig, E., Martin, R., Titmus, M., Sotelo-Silveira, J.R. (2000). Cryptic peripheral ribosomal domains distributed intermittently along mammalian myelinated axons. *J. Neurosci.* **20**, 8390–400.
19. Koenig E. (1986). Isolation of native Mauthner cell axoplasm and an analysis of organelle movement in non-aqueous and aqueous media. *Brain Res.* **398**, 288–97.
20. Koenig, E, Martin R. (1996). Cortical plaque-like structures identify ribosome-containing domains in the Mauthner cell axon. *J. Neurosci.***16**, 1400–11.
21. Koenig, E., Repasky E. (1985). A rational analysis of alpha-spectrin in the isolated Mauthner neuron and isolated axons of the goldfish and rabbit. *J. Neurosci.* **5**, 705–14.
22. Koenig E. (1979). Ribosomal RNA in Mauthner axon: implications for a protein synthesizing machinery in the myelinated axon. *Brain Res.***174**, 95–107.
23. Sotelo-Silveira, J.R., Calliari, A., Cárdenas, M., Koenig, E., Sotelo, J.R. (2004). Myosin Va and kinesin II motor proteins are concentrated in ribosomal domains (periaxoplasmic ribosomal plaques) of myelinated axons. *J. Neurobiol.* **60**, 187–96.
24. Muslimov, I.A., Titmus, M., Koenig, E., Tiedge, H. (2002). Transport of neuronal BC1 RNA in Mauthner axons. *J Neurosci.* **22**, 4293–301.
25. Yoon, B.C., Zivraj, K.H., Holt, C.E. (2009). Local translation and mRNA trafficking in axon pathfinding. *Results Prob. Cell Differ.* **48**, 269–88.
26. Willis, D., Li, K.W., Zheng, J.Q., Chang, J.H., Smit, A., Kelly, T., Merianda, T.T., Sylvester,

J.,van Minnen, J.,Twiss, J.L. (2005). Differential transport and local translation of cytoskeletal, injury-response, and neurodegeneration protein mRNAs in axons. *J. Neurosci.* **25**, 778–91.

27. Hanz, S., Perlson, E., Willis, D., Zheng, J.Q., Massarwa, R., Huerta, J.J., Koltzenburg, M., Kohler, M., van-Minnen, J., Twiss, J.L., Fainzilber, M. (2003). Axoplasmic importins enable retrograde injury signaling in lesioned nerve. *Neuron* **40**, 1095–104.
28. van Gijlswijk, R.P., Zijlmans, H.J., Wieganet, J., Bobrow, M.N., Erickson, T.J., Adler, K.E., Tanke, H.J., Raap, A.K. (1997). Fluorochrome-labeled tyramide: use in immunocytochemistry and fluorescence in situ hybridization. *J. Histochem. Cytochem.* **45**, 375–82.